



**Test anti-senescence interventions to  
postpone or reverse skin ageing**

**Evon Low**

A thesis submitted for Doctor of Philosophy

Institute for cell and molecular biosciences

November 2023

## Abstract

While the role of cell senescence is well-established as a main driver of ageing in various tissues, the impact in human skin ageing remains unclear. Many studies predominantly focused on specific skin compartments or cell types foregoing the importance of cellular crosstalk. This makes cross-model comparisons challenging due to variation in the causes and effects of senescence. Consequently, the existing data do not conclusively establish whether senescence of skin cells is the primary contributor to skin ageing.

This study aims to evaluate the role of senescence in skin ageing by assessing changes in morphology during skin ageing in various mammalian models, including human skin biopsies from donors of different ages, mice, therapy-induced premature-ageing mice, and senolytic/senostatic treated mice. We also tested a range of natural compounds and compared their senolytic efficacy against skin fibroblasts with published data. As there was no consensus on which senescent marker best distinguishes senescent cells in the skin, this study was designed to validate as many senescence markers as possible in both *in vitro* dermal fibroblasts and keratinocytes and *in vivo* ageing human skin. We also created 3D bioengineered skin equivalents to study the crosstalk between skin layers by incorporating different frequencies of senescent fibroblasts in the dermis.

This study showed that senolytic or senostatic did not improve extrinsic skin ageing characteristic in therapy-induced premature -ageing mice. Natural compounds with reported 'anti-ageing' activity showed no senolytic efficacy against skin fibroblasts. Senescence markers were well detected *in vitro*, but they were not as sensitive in *in vivo* skin samples. Some senescence markers were found to be cell-type specific and could vary over the course of senescence development. However, the enlargement of cell size has shown reliability as a senescence marker in both *in vitro* and 3D model, potentially *in vivo* if we have better quality samples. In comparison to published results, 3D skin models revealed effects of senescent dermal fibroblasts onto the epidermis are largely matrix dependent.

## Acknowledgements

I would like to extend my deepest gratitude to my dedicated and insightful supervisors, Professor Thomas von Zglinicki and Doctor Satomi Miwa, for giving me this golden opportunity. Their guidance, unwavering support, and wealth of knowledge have been invaluable throughout this research journey. I am truly fortunate to have had such mentors.

I am also profoundly thankful to Durham University for their invaluable collaboration on this project, particularly Doctor Lucy Smith. Her expertise and dedication significantly enriched the depth and scope of this study.

To my family, whose boundless love, unwavering belief in me, and financial support provided the foundation for this achievement, I am forever indebted. Your sacrifices and contributions have been my pillar of strength.

Lastly, I want to take a moment to thank myself. The countless hours of hard work, determination, and perseverance have been the driving force behind this achievement. This journey has been a testament to my own dedication, and for that, I am proud.

## Contents

Abstract.....	1
Acknowledgements .....	2
List of Figures .....	6
List of tables.....	8
Chapter I - Introduction.....	9
1.0 Skin structure and function .....	9
1.1 Characteristics of intrinsic and extrinsic skin ageing.....	11
1.2 Molecular mechanisms of skin ageing.....	14
1.3 Cellular senescence .....	17
1.4 Detection of senescence markers in skin ageing ( <i>in vivo</i> ).....	20
1.5 3D skin equivalents to study skin ageing.....	24
1.6 Effects of senolytics and senostatic on skin ageing.....	26
1.7 Aims.....	28
Chapter II – Materials and Methods .....	29
2.0 Cell Types .....	29
2.1 Retroviral transduction of human dermal fibroblasts (HDFn) .....	29
2.2 Induction of cellular senescence .....	31
2.3 Tissue Samples.....	32
2.3.1 Animals .....	32
2.3.2 Irradiation and drug treatments .....	32
2.3.3 Human skin samples.....	35
In this study, skin samples were obtained from donors aged 20 years old (young) and 60 years old (elderly). Both paraffin-embedded and frozen skin samples were provided by P&G as part of the BBSRC IPA grant BH190685. The arm (sun-exposed) and buttock (sun-protected) skin samples were collected from these age groups.....	35
2.4 3D skin equivalents.....	35
2.4.1 Full thickness 3D Collagen gel skin equivalents .....	35
2.4.2 Full thickness Alvetex 3D skin equivalents .....	37
2.4.3 Alvetex 3D dermal skin equivalents .....	39
2.5 2D Drug screening assay.....	40
2.6 Histology and Immunofluorescence staining methods.....	42
2.6.1 General deparaffinise and antigen retrieval methods .....	42
2.6.2 Haematoxylin and Eosin staining .....	43
2.6.3 Picro-Sirius Red and Fast Green staining .....	43
2.6.4 Immunofluorescence staining.....	44
2.6.5 Sen- $\beta$ -gal staining .....	45
2.6.6 Crystal Violet staining.....	46

2.7 Operationalisation of measurement between observers for 3D Alvetex models .....	46
2.7.1 Epidermal thickness measurement.....	47
2.7.2 Basal cells size and nuclear size measurement .....	48
2.7.3 Semi-quantitative analysis of fluorescent staining .....	49
Chapter III – Changes of skin morphology with age, irradiation, and the effect of intervention on skin .....	51
3.0 Introduction .....	51
3.1 Thinning in epidermal thickness with age in mice skin tissue .....	53
3.2 Effect of irradiation on epidermal thickness in mouse models .....	54
3.3. Senolytic and senostatic treatments have no effect on epidermal thickness in irradiated mice .....	56
3.4 No change in epidermal thickness with age in arm and buttock human skin samples .....	59
3.5 Changes in epidermal thickness compared between region: sun-exposed (arm) and sun-protected (buttock) skin samples in human .....	60
3.6 Discussion .....	62
Chapter IV 2D drug screening to test the effect of senolytics in dermal fibroblasts viability .....	64
4.0 Introduction .....	64
4.1 Screening of natural compounds for their possible senolytic effects on skin fibroblasts .....	65
4.2 Screening of the mixture of natural compounds for their possible synergisms of senolytic effects on skin fibroblasts.....	69
4.3 Further assessment of senolytic and senostatic activity of NOVOS Boost in co-culture assay .....	71
4.4 Discussion .....	74
Chapter V Characterisation of senescence markers <i>in vitro</i> and <i>in vivo</i> .....	80
5.0 Introduction .....	80
5.1 Characterisation of senescence markers <i>in vitro</i> .....	82
5.1.1 Ki-67 reduction in HDFn and HEKn cells post-irradiation.....	82
5.1.2 LaminB1 reduction in HDFn and HEKn cells post-irradiation.....	83
5.1.3 HMGB1 reduction in HDFn and HEKn cells post-irradiation .....	84
5.1.4 $\gamma$ H2A.x DNA damage foci increased in HEKn post-irradiation but not in HDFn cells .....	86
5.1.5 No change in p21WAF1/CIP1 expression in HEKn and HDFn cells post-irradiation.....	87
5.1.6 Elevation of P16INK4a expression in HEKn post-irradiation but not in HDFn cells.....	88
5.1.7 Enlargement in nuclear size in HEKn and HDFn cells post-irradiation.....	89
5.1.8 Increased in Senescence-associated $\beta$ -galactosidase (Sen- $\beta$ -Gal) activity in HDFn cells post-H <sub>2</sub> O <sub>2</sub> treatment.....	90
5.1.9 Decreased LaminB1 expression in HDFn cells post-H <sub>2</sub> O <sub>2</sub> treatment .....	91
5.1.10 Reduction of Ki-67 accompanied by an increase in $\gamma$ H2A.x in HDFn cells post- H <sub>2</sub> O <sub>2</sub> treatment.....	92
5.1.11 Enlargement in nuclear size in HDFn cells post-H <sub>2</sub> O <sub>2</sub> treatment .....	93

5.1.12 Reduction in LaminB1 expression observed in both HDFn and HEKn cells from day 0 to day 10 post-irradiation .....	94
5.1.13 Reduction in Ki-67 accompanied by an increase in $\gamma$ H2A.x observed in HDFn and HEKn cells from day 0 to day 10 post-irradiation.....	95
5.1.14 No change in p21WAF1/CIP1 observed in HDFn and HEKn cells from day 0 to day 10 post-irradiation .....	97
5.1.15 No change in P16INK4a observed in HDFn and HEKn cells from day 0 to day 10 post-irradiation .....	98
5.1.16 Enlargement in nuclear size in HDFn and HEKn from day 0 to day 10 post-irradiation...	99
5.2 Characterisation of senescence markers <i>in vivo</i> .....	100
5.2.1 Changes in Lamin B1 compared between different age groups in human skin samples.	100
5.2.2 Changes in Lamin B1 compared between different regions in human skin samples.....	101
5.2.3 Changes in p16INK4a compared between different age groups in human skin samples	102
5.2.4 Changes in p16INK4a compared between different regions in human skin samples .....	104
5.2.5 Changes in HMGB1 compared between different age groups in human skin samples ...	105
5.2.6 Changes in HMGB1 compared between different regions in human skin samples .....	106
5.2.7 Changes in nuclear size compared between different age groups in human skin samples .....	108
5.2.8 Changes in nuclear size compared between different regions in human skin samples ..	109
5.2.9 Measurement of nuclear size in basal and suprabasal cells using skin differentiation marker.....	111
5.2.10 Changes in basal and suprabasal nuclear size in human skin with age .....	112
5.2.11 Changes in basal and suprabasal nuclear size compared between regions in human skin samples .....	113
5.2.12 Senescence-associated $\beta$ -galactosidase (Sen- $\beta$ -Gal) in human tissue.....	115
5.3 Discussion .....	116
Chapter VI Addressing the effects of senescent fibroblasts in the full thickness Alvetex 3D skin equivalents.....	122
6.0 Introduction .....	122
6.1 Full thickness 3D collagen gel and 3D Alvetex skin equivalent.....	125
6.2 Senescent dermal fibroblasts caused basal cells hypertrophy in the epidermis. ....	126
6.3 Frequencies of senescent fibroblasts in the dermal skin models are low .....	130
6.4 Discussion .....	133
Chapter VII General Discussion .....	137
Bibliography.....	148
Appendices.....	168

## List of Figures

Figure 1 Skin structure. ....	10
Figure 2 Characteristics of intrinsic and extrinsic skin ageing. ....	13
Figure 3 Breakdown of senescence markers in different skin layers (in vivo). ....	23
Figure 4 Retroviral transfection with acGFP in human dermal fibroblasts (HDFn). ....	29
Figure 5 Mice treatment and study plans ....	33
Figure 6 Flowchart of the development of 3D collagen gel skin equivalent. ....	35
Figure 7 Flowchart of the development of Alvetex 3D skin equivalent. ....	37
Figure 8 Illustration of 3D Alvetex dermal model ....	39
Figure 9 Example colour differences between the Ethanol and H2O stock preparations. ....	42
Figure 10 Example of epidermal thickness measurement. ....	47
Figure 11 Example of Basal cells size and nuclear size measurement. ....	48
Figure 12 Example of senescence markers quantification. ....	49
Figure 13 Change in epidermal thickness between age differences. ....	53
Figure 14 Change in epidermal thickness before and after irradiation. ....	55
Figure 15 The change in epidermal thickness compared between non-treated and senolytic or senostatic -treated in irradiated mice. ....	57
Figure 16 The change in epidermal thickness with age compared between arm and buttock human skin samples. ....	59
Figure 17 The change in epidermal thickness compared between arm and buttock human skin samples. ....	61
Figure 18 Individual natural compound senolytic efficacy test on cell viability of senescent and proliferating human skin fibroblasts. ....	69
Figure 19 Mixture of natural compound senolytic efficacy test on cell viability of senescent and proliferating human skin fibroblasts. ....	70
Figure 20 Dose response curves using water solvent stock. ....	72
Figure 21 Dose response curves using ethanol solvent stock. ....	73
Figure 22 Comparison of the changes of Ki-67 in young and senescent cells in HDFn and HEKn. ....	83
Figure 23 Comparison of changes of LaminB1 in young and senescent cells in HDFn and HEKn. ....	84
Figure 24 Comparison of changes of HMGB1 in young and senescent cells in HDFn and HEKn. ....	85
Figure 25 Comparison of changes of $\gamma$ H2A.x in young and senescent cells in HDFn and HEKn. ....	87
Figure 26 Comparison of changes of p21WAF1/CIP1 in young and senescent cells in HDFn and HEKn. ....	88
Figure 27 Comparison of changes of p16INK4a in young and senescent cells in HDFn and HEKn. ....	89
Figure 28 Comparison of changes of nuclear size in young and senescent cells in HDFn and HEKn. ....	90
Figure 29 Comparison of changes of Sen- $\beta$ -Gal in young and senescent cells in HDFn after H <sub>2</sub> O <sub>2</sub> treatment. ....	91
Figure 30 Comparison of changes of LaminB1 in young and senescent cells in HDFn after H <sub>2</sub> O <sub>2</sub> treatment. ....	92
Figure 31 Comparison of changes of Ki-67 and $\gamma$ H2A.x in young and senescent cells in HDFn after H <sub>2</sub> O <sub>2</sub> treatment. ....	93
Figure 32 Comparison of changes in nuclear size in young and senescent cells in HDFn after H <sub>2</sub> O <sub>2</sub> treatment. ....	94
Figure 33 The development of LaminB1 from day 0 to day 10 after irradiation. ....	95
Figure 34 The development of Ki-67 and $\gamma$ H2A.x from day0 to day 10 after irradiation. ....	96
Figure 35 The development of p21WAF1/CIP1 from day0 to day 10 after irradiation. ....	97
Figure 36 The development of P16INK4a from day 0 to day 10 after irradiation. ....	98
Figure 37 The changes in nuclear size from day 0 to day 10 after irradiation. ....	99
Figure 38 Changes in Lamin B1 compared between ages in human skin samples. ....	101

Figure 39 Changes in Lamin B1 compared between arm and buttock regions in human skin samples. ....	102
Figure 40 Changes in p16INK4a compared between ages in human skin samples. ....	103
Figure 41 Changes in p16INK4a compared between arm and buttock regions in human skin samples. ....	105
Figure 42 Changes in HMGB1 compared between ages in human skin samples. ....	106
Figure 43 Changes in HMGB1 compared between arm and buttock regions in human skin samples. ....	107
Figure 44 Changes in nuclear size compared between ages in human skin samples. ....	109
Figure 45 Changes in nuclear size compared between arm and buttock regions in human skin samples. ....	110
Figure 46 Abnormality resembling nodular melanoma was found in human epidermal samples. ....	112
Figure 47 The comparison of basal and suprabasal nuclear size in young and old arm skin samples. ....	113
Figure 48 The comparison of basal and suprabasal nuclear size in young and old buttock skin samples. ....	114
Figure 49 Sen- $\beta$ -Gal staining in human arm skin sample. ....	115
Figure 50 Full thickness 3D collagen gel and 3D Alvetex skin equivalent. ....	125
Figure 51 Representative immunofluorescence micrographs of full thickness models ....	127
Figure 52 Effect of increasing frequencies of senescent dermal fibroblasts onto the epidermal compartment measured by two independent observers. ....	128
Figure 53 Observer bias in the assessment of increasing frequencies of senescent dermal fibroblasts onto the epidermal compartment. ....	129
Figure 54 Senescent fibroblast densities within the dermal equivalent. ....	132



## List of tables

Table 1 List of compounds tested and concentration range.....	40
Table 2 Information of antibodies used and concentration ranges for Immunofluorescence staining.....	44
Table 3 Concentration ranges for Sen- $\beta$ -gal staining solution. ....	45
Table 4 Concentration ranges for Crystal Violet staining.....	46
Table 5 Changes of senescence phenotypes in vitro. ....	116
Table 6 Summary of the changes in senescence phenotypes in vivo. ....	118
Table 7 Summary of two-way-ANOVA p values for untransformed and normalised data.....	133

## Chapter I - Introduction

### 1.0 Skin structure and function

The skin is the body's largest organ, covering approximately 1.5–2 m<sup>2</sup> of surface area. It consists of three complex layers: the epidermis, dermis, and hypodermis, each with specific functions. The epidermis primarily comprises keratinocytes, alongside other cell types such as Merkel cells (Merkel, 1875), Langerhans cells (Streilein & Bergstresser, 1984) and melanocytes. The epidermis is divided into four layers, beginning with the epidermal stem cells located at the *stratum basale*. These epidermal stem cells gradually migrate towards the outer layer, forming the *stratum spinosum*, *stratum granulosum* and *stratum corneum* (Eckert & Rorke, 1989).

As keratinocytes mature during differentiation, they undergo changes, including the loss of intracellular organelles and flattening of their structure. The expression of keratin also transitions from keratin 5/14 into keratin 1/10 as the cells move into the *stratum spinosum* (Blanpain & Fuchs, 2009). In *stratum granulosum*, keratinocytes become granular cells containing keratohyalin granules enriched with histidine- and cysteine-rich proteins such as profilaggrin (Fukuyama & Epstein, 1975). The formation of lamellar granules serves as a water barrier in *stratum granulosum*.

During terminal differentiation, corneocytes are encased within a lipid lamellae matrix (Verdier-Sévrain & Bonté, 2007) and gain a cornified envelope of protein cross-linked by calcium-dependent transglutaminases (Candi, Schmidt, & Melino, 2005; Verdier-Sévrain & Bonté, 2007) to serve the skin barrier function. The epidermis is tightly bound to the dermis through the dermo-epidermal junction (DEJ). The DEJ strengthens the mechanical connection between epidermis and dermis, facilitates the exchange of substances, and aids in the polarization of the basal keratinocytes (Briggaman & Wheeler, 1975).

The dermis exhibits a complex architecture, maintained through dynamic interactions between dermal-resident cells and a composite extracellular matrix network. The dermis is rich in collagen and can be further divided into two morphologically distinct layers: the papillary dermis and the reticular dermis. The papillary dermis contains fine and sparsely arranged collagen, oxytalan and elaunin fibres with a perpendicular orientation to the DEJ (Cotta-Pereira, Guerra Rodrigo, & Bittencourt-Sampaio, 1976). In contrast, the reticular dermis harbours a dense network of collagen and elastic fibres embedded within a non-fibrous ground substance composed of glycoproteins, proteoglycans and glycosaminoglycans. The

primary collagen types in the dermis are type I and type III, accounting for 85% and 15% of total skin collagen, respectively (Veysey & Finlay, 2010). Elastic fibres are responsible for the skin's elasticity and extensibility, complementing the tensile strength provided by the collagen (Cotta-Pereira, Guerra Rodrigo, & Bittencourt-Sampaio, 1976). The hydrophilic nature of the ground substance creates an osmotically active space and forms a hydrated gel-like substance, providing turgidity and viscoelasticity to withstand external compression forces (Papakonstantinou, Roth, & Karakiulakis, 2012).

Beneath the dermis lies the hypodermis, which connects the skin to the underlying fascia. Comprising lobules of adipocytes separated by the connective tissue septae, the hypodermis serves as a thermal insulator and assists in shock absorption (Khavkin & Ellis, 2011).

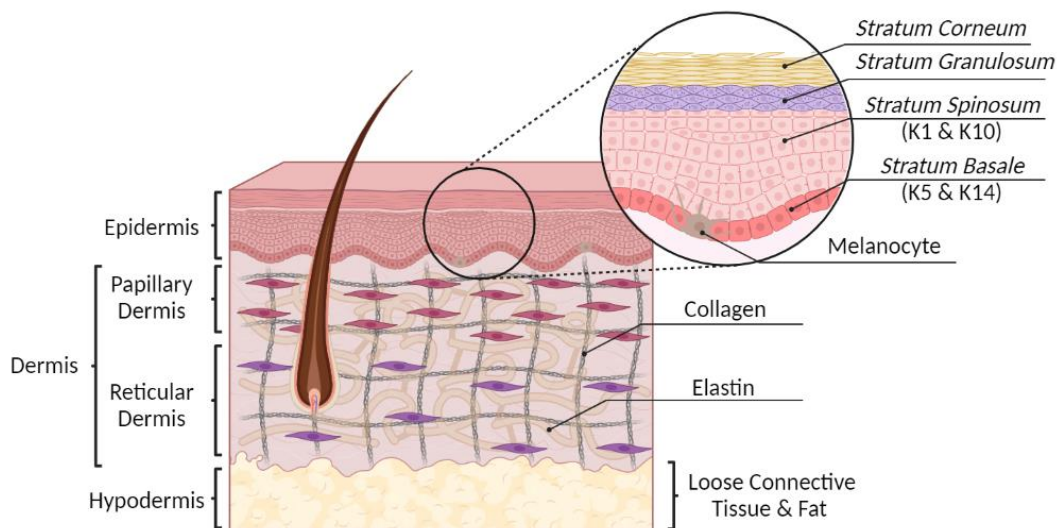


Figure 1 Skin structure.

The epidermis layer is separated from the underlying dermis by the dermal-epidermal junction, also known as the basement membrane. The epidermis is predominantly composed of keratinocytes that are mainly responsible for protecting against penetration by microorganisms and regulating water loss from the body. During cell differentiation, new cells become flatter, associated with the thickening of cell membranes as they are pushed superficially towards the *stratum corneum*. Each stage of differentiation is characterised by the expression and translation of specific factors, as listed above. In the *stratum granulosum*, cells containing small dark purple dots represent the lamellar granulosum that serves as a water barrier. Melanocytes located within the *stratum basale* of the epidermis provide skin colour and protection from UV damage. The dermis is a fibrous layer rich in collagen and elastin, which is divided into two morphologically distinct layers, including the papillary and reticular dermis, which contribute to the elasticity and extensibility of the skin. The hypodermis is the deepest layer of the skin that is made up of loose connective tissue and fat and acts as padding to protect internal organs and regulate body temperature. Image modified from (Dijkhoff, et al., 2020)

## 1.1 Characteristics of intrinsic and extrinsic skin ageing

The skin, being in direct contact with the external environment, is constantly exposed to both intrinsic and extrinsic factors that can lead to a progressive loss of structural integrity and physiological function (Friedman, 2005). The ageing process is accompanied by not only phenotypic changes in cutaneous cells, but also structural and functional alterations in extracellular matrix components, including collagens, elastin, and proteoglycans. These components are crucial for providing the skin with tensile strength, elasticity, and hydration (Mora Huertas, Schmelzer, Hoehenwarter, Heyroth, & Heinz, 2016).

Intrinsic skin ageing primarily results from natural physiological changes over time. These include hormonal imbalance, decreased ability to repair skin damage, and increased production of reactive oxygen species (ROS) (Farage, Miller, & Maibach, 2008). The most remarkable changes in intrinsic skin ageing include skin thinning (Maibach & Waller, 2005), followed by visible signs of wrinkles, reduced skin elasticity, hyperpigmentation, and hair greying. Although the epidermal strata remain unchanged during the skin ageing process, the thickness of the epidermis decreases, along with a reduction in epidermal turnover and associated structural changes (Grove & Kligman, 1983; Branchet, Boisnic, Frances, & Robert, 1990). The most remarkable histological changes in the epidermis occur within the basal cell layer, including a reduced proliferative capacity of basal keratinocytes (Rübe, et al., 2021), diminished height of basal keratinocytes (Sauermann, et al., 2002), enlarged size of basal keratinocytes and nuclei (Liao, et al., 2013), as well as a decreased number of melanocytes (Gilchrest, Blog, & Szabo, 1979). All of these factors can result in an altered balance between differentiation and proliferation of basal keratinocytes, leading to a reduced maintenance of stratified layers (Charruyer, et al., 2021; Rorteau, Chevalier, Fromy, & Lamartine, 2020) and an overall thinning of the epidermis (Gilhar, et al., 2004).

In dermal ageing, the most noticeable changes involve a reduction in elasticity, decreased extensibility, and increased skin laxity. These changes occur primarily due to a decline in collagen content, accompanied by an upregulation of collagen-degrading enzymes, such as matrix metalloproteinase (MMPs) (Rittié & Fisher, 2002), and a decelerated collagen synthesis (Shuster, Black, & McVitie, 1975) with age. Consequently, the distance within the dermo-epidermal junction diminishes, leading to insufficient nutrition supply to the epidermis, and ultimately reducing the ability of basal cell proliferation (Moragas, Castells, & Sans, 1993; Makrantonaki & Zouboulis, 2007).

Morphologically, intrinsically aged dermis exhibits a decrease in the number of mast cells, fibroblasts, collagen fibres and elastic fibres in intrinsically aged dermis decreases compared to the young dermis. Additionally, the superficial dermis thins with age due to the gradual lysis of connective tissues, with the thinnest fibres deteriorating first, leaving thicker collagen fibres in the deep dermis. This process eventually weakens resistance at the skin's surface (Bonta, Daina, & Muşiu, 2013). The age-related loss of subcutaneous fat from the hypodermis contributes to the wrinkling and sagging of ageing skin.

Unlike intrinsic skin ageing, which is primarily driven by natural physiological changes, extrinsic skin ageing is largely influenced by lifestyle and environmental factors, such as exposure to ultraviolet radiation (UV), smoking, and environmental pollution. Common signs of extrinsic ageing include the development of deep wrinkles, increased skin laxity, roughness, alterations in pigmentation and the visible appearance of blood vessels under the skin surface (Telangiectasias/ the 'spider veins') (Wlaschek, et al., 2001). In contrast to the characteristic of intrinsic skin ageing, extrinsic ageing particularly due to UV-radiation, leads to thickening of the epidermis, prevalently shown in the *stratum corneum* (Kligman L. H., 1989). This thickening occurs because the corneocyte desmosomes fail to degrade effectively in responses to UV exposure.

UV exposure also significantly reduces the expression of basal cell  $\beta$ 1-integrin, impairing keratinocyte differentiation (Bosset, et al., 2003; Makrantonaki & Zouboulis, 2007). Healthy skin features densely packed and well-organized elastin and collagen fibres, but not in extrinsically aged skin (Duncan & Leffell, 1997; Quan & Fisher, 2015; Yasui, et al., 2012). Increased expression of Matrix metalloproteinases (MMPs) in extrinsic skin ageing disrupts the balance between type 1 collagen and type 3 collagen (Lovell, et al., 1987), and also alters the frequency of type 7 collagen, contributing to the formation of wrinkles (Contet-Audonneau, Jeanmaire, & Pauly, 1999). In addition, the loss of functional melanocytes in extrinsic ageing impairs the protective barrier function against UV radiation (Brenner & Hearing, 2008), further affecting trans-epidermal water loss (TEWL) (Choi, 2019).

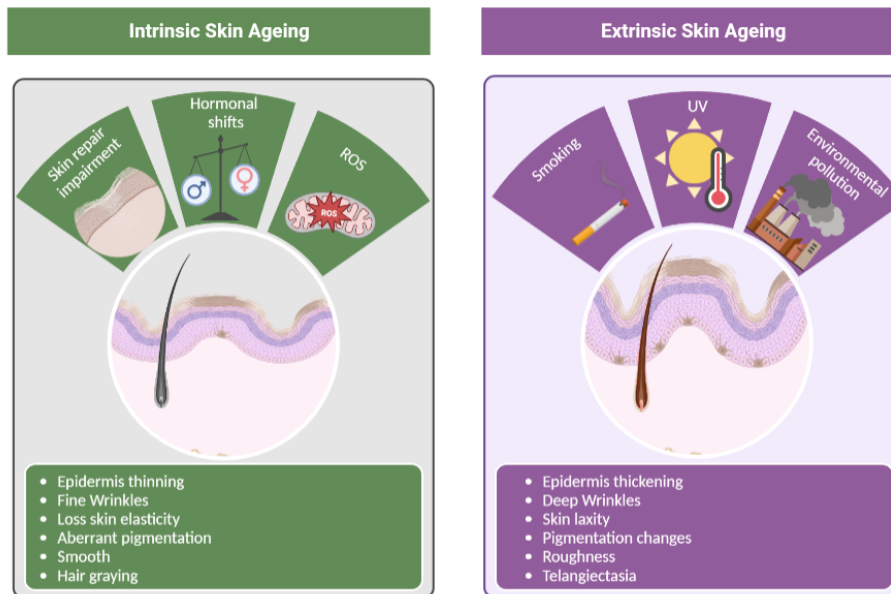


Figure 2 Characteristics of intrinsic and extrinsic skin ageing.

Skin ageing is a complex process influenced by both intrinsic factors, such as reactive oxygen species (ROS), impaired skin repair mechanisms, and hormonal changes, as well as extrinsic factors, including exposure to UV radiation, smoking, and environmental pollution. These factors can lead to distinct ageing phenotypes in the skin. Intrinsic aging is characterized by features such as epidermal thinning, the development of fine wrinkles, loss of elasticity, irregular pigmentation, hair greying, and a generally smoother appearance. In contrast, extrinsic ageing, often driven by factors like UV exposure, cigarette smoke and environmental pollutants, results in thickened and rough skin texture. Extrinsic aging is associated with the development of coarse wrinkles, increased skin laxity, changes in pigmentation, and the visible appearance of blood vessels under the skin surface, known as telangiectasia.

## 1.2 Molecular mechanisms of skin ageing

Oxidative stress is a critical factor contributing to both intrinsic (Zouboulis & Makrantonaki, 2011) and extrinsic skin ageing in humans (Gonzaga , 2009; Kammeyer & Luiten, 2015; Natarajan, Ganju, Ramkumar, Grover, & Gokhale, 2014; Rittié & Fisher, 2002). One of the primary contributors of oxidative stress is mitochondria, which continuously produce reactive oxygen species (ROS) as by-products during the electron transport process of aerobic respiration. Electrons transport through complex I (via NADH) and into complex II (via FADH<sub>2</sub>), followed by complex III and IV to eventually produce molecular oxygen. However, electrons can prematurely leak at complexes I and III, leading to the formation of superoxide instead of water. The excessive accumulation of superoxide, a key component of ROS, over time can cause damage to macromolecular such as lipids, DNA and proteins, ultimately resulting in cellular dysfunction.

The contribution of ROS production from mitochondria mainly affects the basal cells in the epidermis. These cells actively undergo the cornification process and gradually lose intracellular organelles, including the nucleus, mitochondria, peroxisomes, and the endoplasmic reticulum (Holbrook , 1989; Jeon, Djian, & Green, 1998). UV exposure further intensifies ROS production, leading to mitochondrial DNA mutations, including deletions and point mutations of mtDNA. Such mtDNA damage creates a positive feedback loop, exacerbating mitochondrial ROS production and contributing to premature ageing in mammals (Kujoth, et al., 2005; Trifunovic, et al., 2004).

The increased production of reactive oxygen species (ROS) triggers the activation of mitogen-activated protein kinase (MAPK) pathway, which subsequently activates nuclear factor- $\kappa$ B (NF- $\kappa$ B) and transcription factor activator protein-1 (AP-1). Both NF- $\kappa$ B and AP-1 play crucial roles in regulating matrix metalloproteinases (MMPs), which are responsible for shaping the composition of the extracellular matrix (ECM) in the dermis. Collagens, vital components of the ECM, are cleaved by MMP-1 and further degraded by MMP-3 and MMP-9. During the skin ageing process, there is a substantial increase in the expression of MMPs, coupled with a downregulation of tissue inhibitors of metalloproteinases (TIMPs), which inhibits MMPs. In intrinsic ageing, collagen turnover is mainly mediated by MMP-1, MMP-8, MMP-13, and MMP-14. However, MMP-1 contributes the most significant role in the fragmentation and disorganisation of collagen fibres in the dermis (Varani J. , et al., 2000; Fisher, G. J., et al., 2002). Similar to intrinsic ageing, in response to UV exposure, only MMP-1 among the three

collagenolytic MMPs in human skin, which include MMP-1, MMP-8, and MMP-13, is induced (Fisher, et al., 2001; Brennan, et al., 2007).

Telomere attrition is another critical factor driving skin ageing. Telomeres serve as protective caps that shield the ends of chromosomes from degradation and from being recognized as a double-strand break (DSB). To maintain telomere length, the telomerase enzyme complex can add TTAGGG sequences to the ends of the chromosomes. The stability in dynamics between telomere length and telomerase activity is crucial for limiting cellular lifespan and preventing uncontrolled cell growth, such as cancer. In skin ageing, telomeres naturally shorten over time, causing the ends of chromosomes to be recognized as double-strand breaks (DSB). This triggers a persistent DNA damage response (DDR) at these locations, eventually leading to cellular senescence. Additionally, extrinsic factors such as ultraviolet (UV) exposure can accelerate telomere shortening in the basal cells of human skin (Ikeda, et al., 2014). Interestingly, in sun-protected areas of the human epidermis, there is little or no telomere loss with age (Kronic, et al., 2009; Victorelli, et al., 2019). This phenomenon may be attributed to the active shredding and regeneration of the epidermis from the basal stem cells, which possess telomerase activity (Härle-Bachor & Boukamp, 1996; Kronic, et al., 2009).

Another mechanism driving skin ageing is 'Inflammaging'. During the ageing process of the skin, the cytokine signalling pathway becomes activated, leading to imbalances in the production of proinflammatory factors such as tumour necrosis factor (TNF- $\alpha$ ) and interleukins. UV exposure further elevates TNF- $\alpha$  and the production of interleukins, including IL-1, IL6, IL-8, IL-10, and IL-15, in the epidermis (Enk, Sredni, Blauvelt, & Katz, 1995) and dermal fibroblasts (de Kossodo, et al., 1995). UV radiation induces the production of reactive oxygen species (ROS) in the epidermis, causing cellular damage and oxidised lipids. These oxidised lipids and oxidation-specific epitopes on damaged cells trigger 'Inflammaging', which, in turn, activates macrophages to remove the damaged cells and oxidised lipids (Takahara, et al., 2003; Yoshida, et al., 1998). Activated macrophages then release matrix metalloproteinases (MMPs) to degrade the extracellular matrix. Advanced glycation end products (AGE) also play a role in activating cytokine signalling pathways. AGEs are formed during nonenzymatic glycation when proteins, lipids, and nucleic acids covalently bond with reducing sugars such as glucose or fructose (Ahmed, 2005). AGEs accumulate in both keratinocytes (Kawabata, et al., 2011) and fibroblasts (Kueper, et al., 2007) in aged skin, as well as in photoaged skin (Jeanmaire, Danoux, & Pauly, 2001). Glycated collagens are highly resistant to degradation by MMPs, leading to



their buildup in the collagen and elastin of connective tissue. This accumulation ultimately results in stiffening and a loss of skin elasticity (Bucala & Cerami, 1992).

### 1.3 Cellular senescence

Cellular senescence, originally described as a phenomenon in which cells cease proliferating after reaching a limited capacity to divide (Hayflick & Moorhead, 1961). Later, replicative senescence was linked to the shortening of the telomeres with each cell division (Harley, Futcher, & Greider, 1990). Senescence encompasses more than just persistent cell cycle arrest and the senescence-associated secretory phenotype (SASP); it also leads to various phenotypic changes. These changes are driven by several key factors, including telomere attrition, mitochondrial dysfunction, autophagy dysfunction, nutrient signalling alteration and the production of SASP (von Zglinicki, Wan, & Miwa, 2021).

In replicative senescence, telomeres shorten in each cell division (Harley, Futcher, & Greider, 1990) until they reach a minimal critical length, causing the DNA ends to be recognised as double-strand breaks (DSB). This triggers the activation of the DNA damage response (DDR), ultimately contributing to cellular senescence (d'Adda di Fagagna, et al., 2003). Non-telomeric DNA damage can be repaired over time. However, DNA damage located within the telomere, known as telomere-associated foci (TAF), is repaired less efficiently or may even be irreparable, leading to the persistent activation of DDR (P A Kruk, Kruk, Rampino, & Bohr, 1995; Fumagalli, et al., 2012; Hewitt, et al., 2012). Telomeric damage can occur irrespective of telomere length via stress-induced senescence (Hewitt, et al., 2012). Oxidative stress, for example, induces single strand breaks in telomeric DNA, accelerating the rate of telomere shortening (von Zglinicki , 2000). Thus, in turn, contributes to the ageing process and senescence.

Dysfunctional cellular organelles such as mitochondria and lysosomes, are typically targeted for degradation through the process of autophagy (Doherty & Baehrecke, 2018). However, in senescent cells, there is often a notable increase in mitochondrial mass, as observed in replicative senescence (Passos, et al., 2007) and exposure to genotoxic stress such as X-ray radiation in MRC5 fibroblasts (Correia-Melo, et al., 2016; Dalle Pezze, et al., 2014). This increase in mitochondrial mass is accompanied by a decrease in mitochondrial membrane potential ( $\psi_m$ ) and an elevation in reactive oxygen species (ROS) production, which are influenced by the signalling pathways downstream of CDKN1A and mTOR (Passos, et al., 2007). This increase in mitochondrial mass may result from a failure in the degradation of mitochondria through mitophagy, a selective form of autophagy targeting mitochondria (Korolchuk, Miwa, Carroll, & von Zglinicki, 2017). The accumulation of these defective

mitochondria can result in further damage to mitochondria DNA and overproduction of reactive oxygen species (ROS). Excessive ROS production induces mitochondrial dysfunction, triggering a persistent activation of the DNA damage response (DDR) pathway through p38MAPK and TGF- $\beta$ 1 (Transforming growth factor-beta 1), creating a positive feedback loop that stabilises senescence (Korolchuk, Miwa, Carroll, & von Zglinicki, 2017). Senescence can also be induced by mitochondrial dysfunction without the involvement of ROS, resulting in a lower level of SASP production (Wiley, et al., 2016). Similarly, impaired autophagy activity in senescent cells hinders the elimination of the damaged macromolecules and organelles. Autophagy normally serves as a critical cellular mechanism for degrading and recycling damaged or dysfunctional cellular components, including proteins and organelles. However, in senescent cells, this process become less efficient, leading to the accumulation of cellular debris and impaired removal of damaged molecules. This accumulation causes a build-up of cellular lysosomal content, as the undegraded material is stored within the lysosomes. The increase lysosomal content is associated with a higher level of  $\beta$ -galactosidase (Kurz, Decary, Hong, & Erusalimsky, 2000), which serves as a marker of senescent cells.

The nutrient sensing pathway is closely intertwined with autophagy activity with the mechanistic target of rapamycin (mTOR) serving as the central regulator of cell growth. mTOR maintains the balance between mRNA translation, ribosome biogenesis, autophagy, and metabolism (Guertin & Sabatini, 2005; Wullschleger, Loewith, & Hall, 2006) through its two multiprotein signalling complexes: mammalian target of rapamycin complex 1 (mTORC1) and mammalian target of rapamycin complex 2 (mTORC2). While mTORC1 primarily regulates cellular growth by coordinating protein anabolism (Averous & Proud, 2006; Ma & Blenis, 2009), nucleotide biosynthesis (Ben-Sahra, Howell, Asara, & Manning, 2013; Robitaille, et al., 2013), lipogenesis (Lamming & Sabatini, 2013; Ricoult & Manning, 2013), glycolysis (Laplante & Sabatini, 2012; Laplante & Sabatini, 2008), mitochondrial biogenesis (Laplante & Sabatini, 2013), and autophagy (Hosokawa, et al., 2009; Ganley, et al., 2009). mTORC2 is involved in regulating the cytoskeleton, cellular metabolism, cell survival and cellular response to insulin (Cybulski & Hall, 2009; Oh & Jacinto, 2011). Together these complexes form a sophisticated signalling network that integrates extracellular signals with intracellular processes to maintain cellular homeostasis and coordinate cellular responses to environmental changes.

Amino acids play an important role in the activation of mTORC and the initiation of its signalling cascade. Their presence alone is sufficient to stimulate mTORC1 activation, a process

further enhanced by the presence of growth factors (Hara, et al., 1998; Long, Ortiz-Vega, Lin, & Avruch, 2005; Carroll, et al., 2016). Growth factors, such as insulin, transmit signals through the PI3K/Akt pathway and the tuberous sclerosis complex (TSC1/2), ultimately leading the activation of Rheb, a key activator of mTORC1 (Dibble & Cantley, 2015). Rheb's activity is regulated by the availability of growth factors and specific amino acids, particularly arginine (Demetriades, Doumpas, & Teleman, 2014; Carroll, et al., 2016; Menon, et al., 2014), which modulate mTORC1 activity by regulating its lysosomal localization through the Regulator complex and Rag GTPases signalling pathway (Laplante & Sabatini, 2012). Under conditions of growth factor or amino acid deprivation, mTORC1 activity is repressed, prompting the activation of autophagy as a cellular response mechanism (Carroll, Korolchuk, & Sarkar, 2015). However, in senescent cells, there is a persistent activation of mTORC1, specifically due to deficiencies in starvation-induced primary cilia growth (Bishop, et al., 2010; Breslin, Prosser, Cuffe, & Morrison, 2014), which consequently impair their ability to regulate Akt and mTORC1 signalling in response to serum and amino acid starvation (Boehlke, et al., 2010; Wang, Livingston, Su, & Dong, 2015).

Another vital building block of cellular senescence is the senescence-associated secretory phenotypes (SASP). Despite their inability to divide, senescent cells remain biologically active and release a large number of proinflammatory cytokines/chemokines, growth factors and matrix metalloproteinases (MMPs) (Coppé, et al., 2008). The activation of several damage-sensing signalling pathways, including nuclear factor (NFkB) and CCAAT/enhancer-binding protein-B (C/EBPβ), p38MAPK and mammalian target of rapamycin (mTOR) signalling, regulates the production of SASP in response to the activation of the DNA damage response (DDR). The primary purpose of SASP is to signal the immune system to eliminate senescent cells. For instance, chemokines (CXCL and CCL) and proinflammatory cytokines (IL-6 and IL-8) play a role in recruiting immune cells (macrophages, neutrophils, and natural killer T cells) to eliminate transient senescent cells (Kang, et al., 2011). However, because senescent cells are resistant to apoptosis (Wang E. , 1995), the accumulation of SASP over time has a bystander effect on the neighbouring cells. This effect can contribute to various age-related diseases associated with senescence.

Lastly, another significant event during senescence is the formation of facultative heterochromatin structures known as senescence-associated heterochromatin foci (SAHF). Activation of the DNA damage response (DDR) pathway induces the formation of SAHF,

allowing senescent cells to evade apoptosis (Di Micco, et al., 2011). SAHF formation is associated with the recruitment of retinoblastoma (RB), which represses E2F genes that are essential for the cell cycle progression (Pagano, Dürst, Joswig, Draetta, & Jansen-Dürr, 1992). Inactivation of the RB pathway thus inhibits cell cycle progression. SAHF formation can be detected using general DNA staining with DAPI (Narita, et al., 2003).

#### **1.4 Detection of senescence markers in skin ageing (*in vivo*)**

There is compelling evidence demonstrating the accumulation of senescent cells in all skin compartments, regardless of exposure to UV radiation. The very first organs where the existence of senescent cells was discovered was in the skin of baboons (Herbig, Ferreira, Condel, Carey, & Sedivy, 2006). In the epidermis, keratinocytes undergo terminal differentiation from the *stratum basale* to the *stratum corneum* every 3 to 6 weeks, allowing for the elimination of damaged macromolecules. This process may explain the relatively low accumulation of senescent cells in aged keratinocytes (Ho & Dreesen, 2021). However, the frequency and intensity of Sen- $\beta$ -Gal, a marker of senescence, have still been reported to increase with age in the basal cells of keratinocytes and fibroblasts in human skin (Dimri, et al., 1995). Lysosomal  $\beta$ -Galactosidase plays a crucial role in degrading damaged organelles, protein, and intracellular waste at a range of pH4 through macroautophagy. However, in senescent cells, the lysosomal function is altered, resulting in alkaline conditions that compromises the efficiency of this enzyme in eliminating cellular waste. This alteration leads to an increase of lysosomal mass in senescent cells, along with higher lysosomal  $\beta$ -galactosidase activity, which can be detected at pH6, a.k.a. the senescence-associated  $\beta$ -galactosidase (Sen-  $\beta$ -Gal) (Dimri, et al., 1995; Kurz, Decary, Hong, & Erusalimsky, Senescence-associated (beta)-galactosidase reflects an increase in lysosomal mass during replicative ageing of human endothelial cells, 2000). The limitation of this assay is that lysosomal  $\beta$ -galactosidase activity is retained only in fresh tissue sample and is often lost in paraffin or cryopreserved tissues (Severino, Allen, Balin, Balin, & Cristofalo, 2000).

p16INK4a, p21WAF1/CIP1 and P53 are associated with cellular aging and plays a role in regulating cell proliferation and senescence. Thus, they are widely used to detect the presence of senescent cells. P16INK4a, an inhibitor of cyclin-dependent kinases (CDK4 and CDK6), is upregulated with chronological ageing of human skin in both epidermis and dermis compartments (Ressler, et al., 2006). In the aged epidermis's *stratum basale*, increased expression of p16INK4a is often accompanied by the accumulation of lipofuscin (Rübe, et al.,

2021), another hallmark of senescence (Dodig, Čepelak, & Pavić, 2019). In skin ageing, the increase of p16INK4a with age in the epidermis, primarily identified in melanocytes (Waaiker, et al., 2016; Victorelli, et al., 2019) and dermis, contributes to the formation of facial wrinkles and morphological changes in elastic fibre (Waaiker, et al., 2016). Skin wrinkling is primarily a result of the breakdown of collagen and elastin fibres in the dermis which are responsible for skin elasticity and firmness (Lovell, et al., 1987). While P16INK4a itself does not directly cause skin wrinkles, the effects of senescence associated secretory phenotypes such as metalloproteinases (MMPs), which remodel the extracellular matrix (ECM) by degrading collagen and elastin fibres, leading to wrinkles over time (Fisher, et al., 2009; Xia, et al., 2013).

Melanocytes release melanin to repress high intracellular ROS to protect themselves and the adjacent keratinocytes from UV radiation which explains why melanocytes express higher p16INK4A than keratinocytes (Jenkins & Grossman, 2013; Jenkins, et al., 2011). P21WAF1/CIP1 expression also increases with age, particularly in the *stratum granulosum* of the epidermis (Victorelli, et al., 2019). In the skin-specific p53 activation mouse model, elevated P53 expression led to skin thinning and a loss of subdermal fat, resulting in dry skin due to reduced sebaceous gland activity (Kim, et al., 2014).

Cellular senescence is initiated through the persistent activation of DNA damage pathways and can be identified by the presence of specific markers such as phosphorylated H2A.x ( $\gamma$ H2A.x) (d'Adda di Fagagna, et al., 2003) and H2A.J (Rübe, et al., 2021). In mice skin, the proportion of  $\gamma$ H2A.x-positive fibroblasts increases with age (Wang, et al., 2009) while the frequency of H2A.J accumulation rises with age in the human epidermis, especially in the *stratum spinosum* and *stratum granulosum* accompanied by a decline in Ki-67 (Rübe, et al., 2021). However, detecting DNA damage alone is not specific enough to identify telomeric DNA damage resulting from replicative senescence. Therefore, researchers have established telomere-associated DNA damage foci (TAF) as a marker, characterized by the colocalization of  $\gamma$ H2A.x, and telomeres (immunoFISH). This specific marker allows for the detection of persistent telomeric DNA damage (Herbig, Ferreira, Condel, Carey, & Sedivy, 2006; Hewitt, et al., 2012). The frequency of telomeric immunoFISH assay to detect telomere dysfunction foci (TIF) increases with age in baboon dermal fibroblast (Jeyapalan, Ferreira, Sedivy, & Herbig, 2007); as well as in melanocytes and keratinocytes of the human epidermis (Victorelli, et al., 2019).

A relatively straightforward method for detecting senescent cells involves examining their morphological characteristics. Senescent cells often exhibit larger cell sizes, along with an increase in nuclear and nucleolar size. By using nuclear morphology as an indicator of senescence, the proportion of senescent cells in aged papillary dermis increases from approximately 25% to almost 60% (Lewis, Travers, Machado, Somani, & Spandau, 2011). In senescent nuclei, the reorganisation of chromatin structure causes transcriptional silencing of growth-promoting genes in heterochromatin to condense and form senescence-associated heterochromatin foci (SAHF) (Narita, et al., 2003). SAHF can be easily visualised through staining with 4', 6-diamidino-2-phenylindole (DAPI), which reveals darker fluorescent spots within the nucleus of senescent cells (Aravinthan, 2015). The detection of SAHF is less frequently used in skin ageing, but compared to non-senescent melanocytes and keratinocytes, nevus melanocytes showed less histone content (Ivanov, et al., 2013), confirming the drastic changes of chromatin in senescent cells. The existence of SAHF is also implicated with the loss of LaminB1 (Hernandez-Segura, Nehme, & Demaria, 2018; Salama, Sadaie, Hoare, & Narita, 2014), a structural component of the nuclear envelope that provides strength and stability to the cells. LaminB1 reduces with age in human epidermis (Dreesen, et al., 2013).

High mobility group box 1 (HMGB1) is a nuclear protein that serves dual functions. Within the cells, HMGB1 play a crucial role in regulating DNA transcription and organising chromatin structure. However, when released from the cells, HMGB1 acts as an inflammatory mediator in response to cellular damage. This is why, in the context of senescent cells, HMGB1 tends to translocate from the cell nuclei to the extracellular environment as individuals age, releasing proinflammatory SASP factors such as IL-1 $\beta$ , IL-6 and MMP3 (Davalos, et al., 2013; Biran, et al., 2017). While there is still a limited amount of evidence regarding the expression of HMGB1 in skin ageing *in vivo*, studies have shown that UV exposure significantly reduces the number of HMGB1 nuclei-positive cells in mouse skin keratinocytes (Johnson, Wulff, Oberyszyn, & Wilgus, 2013). In various cell types, the proportion of HMGB1 nuclei-positive cells also decreases in aged melanocytes (Vitorelli, et al., 2019). The levels of MMPs such as MMP-1, -2 and -9 elevated in the dermis as individuals age (Varani J., et al., 2000), often accompanied by a reduction in tissue inhibitors of metalloproteinases (TIMPs) (Ashcroft, et al., 1997).

There has yet to be a consensus on which marker or how many markers are required to detect senescent cells specifically. Various senescence markers have been used individually or in

combination to improve detection reliability. However, the skin consists of numerous cell types, and each may manifest the consequences of skin ageing differently. As a result, the search for cell-type specific senescence markers in skin ageing requires further characterization.

In general, different studies were conducted using different biological models such as *in vivo* (mice, baboon, and human), *in vitro* (keratinocytes, fibroblasts) and 3D skin models and mainly focused on a specific skin compartment/ cell type. However, it is challenging to directly compare results from different models due to variation in the causes and effects of senescence. Consequently, existing data do not conclusively establish whether senescence of skin cells is the primary contributor to skin ageing. Furthermore, none of these studies have simultaneously examined changes in senescence phenotypes both *in vivo* and *in vitro* as they could present differently. To truly understand the role of senescence in skin ageing, it is essential to correlate findings from various models and cell types, enabling a clearer distinction of the impact of senescence on skin ageing.

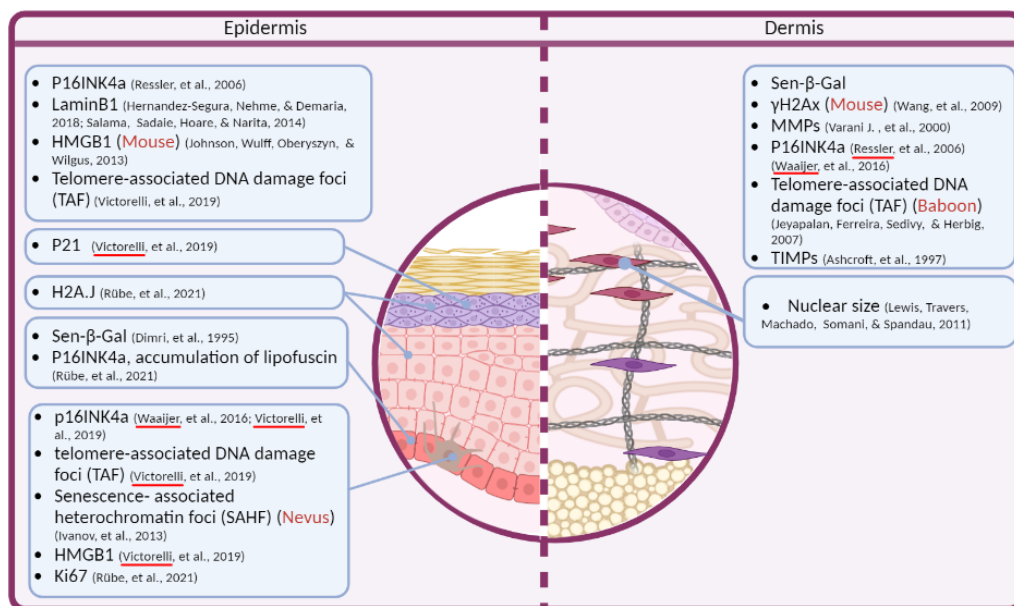


Figure 3 Breakdown of senescence markers in different skin layers (*in vivo*).

The illustration is divided into two parts; the left side represents the epidermis, while the right side represents the dermis. Each side of the illustration displays various senescence markers corresponding to the respective skin layer. Senescent cells are characterised by a) elevation of P16INK4a, b) reduction of LaminB1, c) increased proportion of HMGB1 translocation into extracellular space, d) increased telomere-associated DNA damage foci (TAF), e) increased appearance of senescence-associated heterochromatin foci (SAHF) f) increased H2A.J, g) reduction of Ki-67 positive cells, h) increased activity of Sen-β-Gal, i) accumulation of lipofuscin, j) enlargement of nuclear, k) increased expression of MMPs. Different cell types within the skin could express the consequences of skin ageing differently. Therefore, cell-type specific senescence markers in skin ageing still require further characterization.



### 1.5 3D skin equivalents to study skin ageing

Two-dimensional (2D) cell culture has largely been used to study drug toxicity, cellular morphology, and molecular signalling. However, not all the results provided are translatable into a physiological system (Duval, et al., 2017; Langhans, 2018). Moreover, 2D monolayers lack the structural complexity required to study the crosstalk between different cell types or layers of the skin associated with the *in vivo* microenvironment. For instance, 2D cell culture cannot be used to study the pattern of cell proliferation, migration, and differentiation as well as the morphological changes affected by cellular responses at the 3D interfaces. In addition, due to the prohibition on the use of animals for testing active compounds for cosmetics (Cosmetics regulation EC No 1223/2009), alternative methods such as three-dimensional (3D) skin models have become a fundamental tool in academic research, industry, and clinical applications.

Unlike 2D cell culture, fibroblasts grow in three dimensions within an organized extracellular matrix (ECM), mimicking some aspects of the multicellular and multi-layered complexity of human skin. These models primarily focus on the co-culture of the main cell types in the skin, including dermal fibroblasts, keratinocytes, and less frequently, hair follicles (Abaci, et al., 2018), melanocytes (Zoio, Ventura, Leite, & Oliva, 2021; Victorelli, et al., 2019), subcutaneous fat layer (Bellas, Seiberg, Garlick, & Kaplan, 2012), nerves and immune cells (Vidal, et al., 2019). 3D *in vitro* human skin models offer a reproducible and scalable approach to studying fundamental skin biology, with diverse technologies offering different options depending on the aims of experimental work. Popular methodologies include hydrogels and solid scaffolds, both natural and synthetic (Weinmüllner, et al., 2020; Roger, et al., 2019).

So far, the features of the ageing phenotypes have been recreated using senescent fibroblasts or melanocytes in 3D skin model. However, they lack the physiological complexity of aged human skin. For example, there are a few ageing 3D skin models developed using fully senescence dermal layer. Fully senescence dermal layer is not as representative of human skin because only 5% - 50% of the fibroblasts were identified as senescent in aged human skin (Dimri, et al., 1995; Lewis, Travers, Machado, Somani, & Spandau, 2011). Additionally, the methods used to accelerate premature ageing in cells and the protocol used to create 3D skin model were varied. These studies mainly focus on a specific skin compartment, foregoing the importance of the intercellular crosstalk between the different cell types in the human skin.

Furthermore, the experimental outputs varied. Taken together, the existing data were insufficient to conclude whether cellular senescence is the major cause of skin ageing.

A 3D model incorporating late-passage fibroblasts shows a thinner dermal layer compared to early-passage fibroblasts. The thinning of dermis has been associated with an increase in the expression of the matrix-degrading enzyme (MMP1) and the expression of keratin 6 but lower expression of keratin 10, which alters the differentiation of keratinocytes in the epidermis (Janson, Rietveld, Mahé, Saintigny, & El Ghalbzouri, 2017). Mitomycin-C (MMC) induced senescent fibroblasts in the dermal layer elevated MMP1 expression, resulting in less collagen content, including collagen I and III. Additionally, the upper epidermis was also altered with lower expression of filaggrin (Diekmann, et al., 2016). Instead of introducing senescent fibroblasts in the dermal layer in 3D model, UV-induced senescent melanocytes in the epidermis can decelerate the proliferative rate of neighbouring keratinocytes, resulting in a thinner epidermis (Vicarelli, et al., 2019).

To obtain a more physiologically relevant ageing 3D skin model, modifiable proportion of oxidative stress-induced or doxorubicin-induced senescent cells in the dermal layer was introduced to uncover the crosstalk between epidermis and dermis of the skin (Weinmüller, et al., 2020). This method produced alterations in keratinocyte differentiation and barrier function in the model, with decreased keratin 10 and filaggrin expression associated with a partial impairment of barrier integrity, as measured by biotin permeability assay (Weinmüller, et al., 2020).

To summarise, numerous studies have used 3D skin models to investigate the connection between skin ageing and senescence. Nevertheless, only one study has integrated a variable proportion of oxidative stress-induced or doxorubicin-induced senescent cells into the dermal layer, constructed from a collagen gel matrix, to explore the crosstalk between the epidermis and dermis in the skin (Weinmüller, et al., 2020). It is important to determine whether scaffold-supported 3D skin models could replicate the findings from the collagen gel data.

## 1.6 Effects of senolytics and senostatic on skin ageing

Senescent cells were first discovered to be resistant to apoptosis (Wang E. , 1995) due to the activation of the senescent cell anti-apoptotic pathway (SCAP), which allows senescent cells to survive despite their SASP (Zhu, et al., 2015). Senolytic drugs specifically target the SCAP pathway and selectively induce cell death or apoptosis of senescent cells. The first-generation senolytics, ABT-737, acts as a BCL-2 inhibitor. ABT-737 effectively eliminates senescent cells by inhibiting apoptosis, resulting in increased proliferation of hair-follicle stem cell proliferation (Yosef, et al., 2016). It reverses hyperplasia and diminishes the activation of WNT pathway and decreases the number of p16INK4A-positive cells in transgenic mice (Azazmeh, et al., 2020). In a clinical study, a combination of Dasatinib and Quercetin (D+Q) reduced the abundance of senescent cell in human epidermal basal cells by downregulation of P16INK4A and p21WAF1/CIP1 expression (Hickson, et al., 2020). Topical application of Fisetin shows photoprotective activity, inhibiting the production of AP-1, reducing the expression MMPs, and increasing the expression of filaggrin to protect the barrier function. AS a result, Fisetin improves trans-epidermal water loss (TEWL) and reduces inflammation in UV-irradiated hairless mice (Wu, et al., 2017).

Unlike senolytics, senostatic drugs do not kill senescent cells but suppress SASP by targeting their upstream signalling cascades, including NF- $\kappa$ B or p38-MAPK pathway. Metformin and Rapamycin are popular senostatics. Topical application of 0.6% Metformin cream is sufficient to improve skin damage in UV-induced skin damage in mice and reduces the production of SASP in UV-radiated keratinocytes *in vitro* (Xiao, et al., 2021). In senescence, the activity of the kinase complex remains constantly high because mTORC1 fails to react to nutrient starvation. Rapamycin, also known as a caloric restriction mimetic, suppresses mTORC1 in senescence to prevent the production of SASP (IL-6 and IL-1 $\alpha$ ) and further reduce other SASP by suppressing NF- $\kappa$ B activity in *in vitro* human fibroblasts (Laberge, et al., 2016). Other than that, topical application of Rapamycin improves skin photoaging, including reduced fine wrinkles, increased dermal volume, brightened skin tone, and reduced sagging in human skin. The improvement of photoaging skin is accompanied by a reduction of p16INK4a in the epidermis and increased collagen VII, which plays a vital role in skin barrier function (Chung, et al., 2019).

To study the contribution of senescence to the ageing phenotype *in vitro*, many have developed tissue-engineered 3D skin models that incorporate modifiable frequencies of senescent cells (Janson, Rietveld, Willemze, & El Ghalbzouri, 2013; Diekmann, et al., 2016;

Lämmermann, et al., 2018; Weinmüllner, et al., 2020). 3D models mimic the complex multi-layered microenvironment of human skin *in vitro*, allowing for the study of the interaction between cell types. ABT-737 treatment shows promising results in removing senescent melanocytes and increasing epidermal thickness in a 3D skin model containing UV-induced senescent melanocytes. One of the SASP inhibitors, mitochondria-targeted antioxidant MitoQ, shows a similar result using the same 3D skin model, in agreement with a causal role for oxidative stress in UV-induced senescence of melanocytes (Vitorelli, et al., 2019). From a different aspect of drug intervention, a natural plant extract from Goldenrod (*Solidago Virgaurea*) exhibited weak senolytic activity, suppressing SASP production *in vitro* and enhancing the papillary phenotype of fibroblasts in the dermal layer and improving differentiation in the epidermis (Lämmermann, et al., 2018).

So far, only one study has shown an increase in epidermal thickness resulting from high dose X-ray irradiation (14-17 Gy) accompanied by increased senescence markers such as p21WAF1/CIP1, p15INK4b, Interleukin-1 $\beta$ , -8 and ROS in the skin of c57BL/6 mice (McCart, et al., 2017). No other study has used the same mouse models to study the effect on the skin using low or moderate X-ray irradiation. In addition, none have tested whether these compounds can rescue skin damage from X-ray induction in the c57BL/6 mice model. Thus, I aim to validate if these compounds can rescue skin damage.

## 1.7 Aims

This project aims to evaluate the role of senescence in skin ageing through the following objectives:

1. Evaluate morphology during skin ageing in various mammalian models, including human skin biopsies from donors of different ages, mice, therapy-induced premature-ageing mice, and senolytic/senostatic treated mice.
2. Screen a range of natural compounds with reported 'anti-ageing' activity for their senolytic activity against skin fibroblasts.
3. Validate senescence markers in both *in vitro* skin fibroblast and keratinocyte and *in vivo* ageing human skin.
4. Assess the impact of experimental variation (especially inter-observer variation) on the determination of senescent cell frequencies in human 3D skin equivalents.

## Chapter II – Materials and Methods

### 2.0 Cell Types

Human dermal fibroblasts neonatal (HDFn) were cultured in Dulbecco's modified Eagle's medium (DMEM), supplemented with 5ml of L-Glutamine (G7513-100ML), 5ml Penicillin streptomycin (PS) and 50ml Foetal Bovine Serum (FBS) Sigma (F9665-500ML) at a 37°C humidified atmosphere with 5% CO<sub>2</sub>.

Human Epidermal Keratinocytes neonatal (HEKn) were routinely cultured in keratinocytes basal medium 2 (KBM-2) supplemented with KGM-2 SingleQuot kit (LONZA, Cat #CC-3107) at a 37°C humidified atmosphere with 5% CO<sub>2</sub>. To subculture HEKn, 0.25% trypsin/EDTA was diluted 1:10 with Versene solution (Thermofisher 15040066). 5ml of the solution was applied to the cells for 10-15 minutes until the cells detached from the flask, followed by the addition of 5ml of Trypsin neutralising solution (Lonza, Cat #CC-5002). The cells were then transferred to a 15 ml falcon tube and centrifuge at 800 rpm for 4 minutes. The supernatant was then discarded. Cells were resuspended in 10 ml of KGM-2 and count was determined by taking 20 µl and placed on a hemacytometer. The number of +cells per 4 large squares were counted, then multiplied by 10<sup>5</sup>, and multiplied by the volume of cells. The cells were then prepared for downstream usage.

### 2.1 Retroviral transduction of human dermal fibroblasts (HDFn)

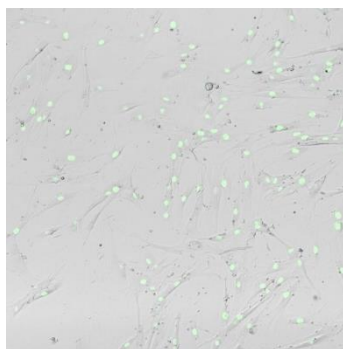


*Figure 4 Retroviral transfection with acGFP in human dermal fibroblasts (HDFn).*

Retroviral transduction of human dermal fibroblasts (HDFn) was performed by Dr. Edward Fielder. Early passage HDFn cells were transduced with acGFP1 using rLV-EF1a-AcGFP1-Nuc-IRES-Puro-WPRE Vector (Takara bio, #0016VCT) according to manufacturer's instructions at an MOI of 20. Cells were cultured in DMEM, supplemented with L-Glutamine and Pen-Strep

as above, and were selected under 1 $\mu$ g/ml puromycin. Sensitivity to selection was confirmed using cell viability by crystal violet staining (section 2.6.6) after 7 days of treatment. The expression of nuclear located acGFP1 protein, with transfection efficacy reaching 90% after selection, and which remained after senescence induction (86%) using 20Gy X-ray irradiation, as determined by Leica DMI8 using GFP cube and analysed manually using the Fiji ImageJ distribution.

For MCherry HDFn, early passage cells were transduced with mCherry encoding virus (mCherry was a gift from Rob Parton (Addgene plasmid # 176016) (Lo, et al., 2021) to generate HDF-mCherry (Red, mCherry). Plasmid DNA was extracted from E. Coli culture under ampicillin selection using the Invitrogen PureLink HiPure Plasmid Maxiprep Kit (K210006), according to manufacturer's instructions. DNA concentration was determined using a nanodrop spectrophotometer (ND-1000), and plasmid DNA was stored at 1 $\mu$ g/ $\mu$ l in 1X Tris-EDTA (TE) buffer at -20°C.

Restriction digests were performed to confirm the isolated plasmids using BAMHI, Sall and XbaI in NEBuffer 3.1 #B7203S (New England Biolabs), PstI and HindIII in NEBuffer Blue #B7002S (New England Biolabs) and EcoRI in Cut Smart Green #B7204S (New England Biolabs), with 5% enzyme concentration, with 5% plasmid DNA. The digests were carried out at 37°C using a thermal cycler (Veriti, ThermoFisher Scientific) for 3 hours, and confirmed with gel electrophoresis on a 0.8% agarose gel containing 0.005% cyber green peak green DNA binder (Peolab, 37- 5099).

Hek 293T packaging cells were cultured and transfected with 12 $\mu$ g of equimolar plasmid DNA using the Lipofectamine 3000 reagent kit (Invitrogen, L3000001). 6% Lipofectamine 3000 in serum-free DMEM media was mixed 1:1 with diluted plasmid DNA (serum free media with 2% plasmid DNA and 4% P3000 reagent). The generated virus from Hek 293T cells was supplemented with 6 $\mu$ g/ml polybrene and added to the target cells for 12 hours at 37°C.

## 2.2 Induction of cellular senescence

Different methods were used to accelerate the development of senescence phenotypes in cells based on the availability of equipment used. To induce cellular senescence, fibroblasts or dermal models were subject to either 20 Gy ionising X ray radiation or were treated with a final concentration of 2 uM Doxorubicin in serum free media for 4 hours. Cells were then maintained for at least 10 days to allow the senescent phenotype to develop, before use in experiments (Passos, et al., 2010).

For H<sub>2</sub>O<sub>2</sub> treatment, fibroblasts were treated with a final concentration of 300 µM H<sub>2</sub>O<sub>2</sub> in serum free media for 45 minutes followed by a fully supplemented media change. Senescence was verified by Sen-β-gal staining, as well as a combination of Ki-67 and γH2A.x and LaminB1 on day 7 and day 10 after H<sub>2</sub>O<sub>2</sub> treatment.

Preparation as below (To make 10ml of 300 µM H<sub>2</sub>O<sub>2</sub>):

- For 5 ml stock, add 5ul H<sub>2</sub>O<sub>2</sub> (1:1000) to 5 ml serum free medium =9.8mM
- $300\mu\text{M}/9.8\text{mM} \times 10\text{ml} = 0.3\text{mM}/9.8\text{mM} \times 10\text{ml} = 300\text{ul}$
- 300ul of 9.8mM stock into 10ml serum free media = 300 uM

For 3D skin model dermal fibroblasts or dermal models were subject to either 20Gy ionizing X-ray radiation or treated with a final concentration of 2uM Doxorubicin in serum free media for 4 hours. Cells were then maintained for at least 10 days to allow the senescent phenotype to develop, before use in experiments. Senescence was confirmed through growth arrest and changes in the expression of senescence associated markers.



## 2.3 Tissue Samples

Various mammalian tissue samples were obtained based on the requirements of specific experiments.

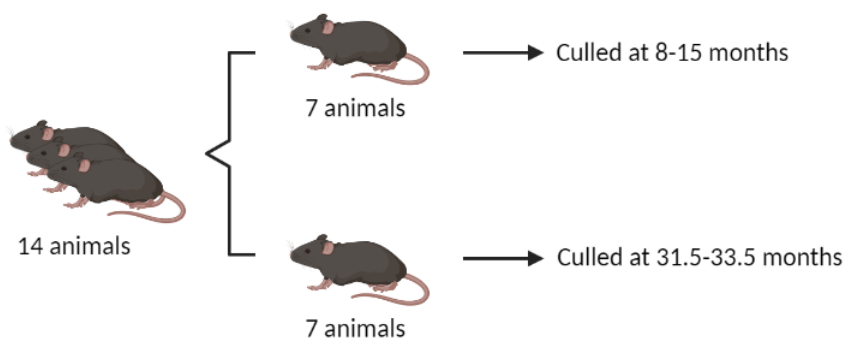
### 2.3.1 Animals

Male C57BL/6 mice (DOB: 22 February 2017) were purchased from Charles River. Mice were subjected to a group of 6 per cage (Cameron , Miwa, Walker , & von Zglinicki , 2012). Most of the mice were fed with standard pelletized food such as CRM-P formulation rodent or SDS diets; the remaining mice were fed either gavage-fed for two weeks or given soaked food similar to above from 1 month after irradiation. The work was licensed by the UK Home Office (PB048F3A0) and complied with the guiding principles for the care and use of laboratory animals. Animal and skin sample preparation was performed by Dr Satomi Miwa and Dr Edward Fiedler as a part of a previous CRUK-funded project.

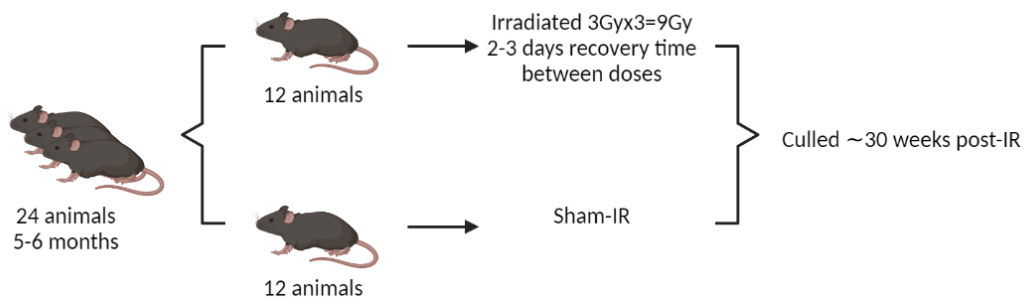
### 2.3.2 Irradiation and drug treatments

At 5 months of age, mice were sublethally irradiated thrice (NDT320, 225kV) with 3 Gy of X-ray irradiation, with two days of recovery between each dose, as described (Fielder, et al., 2019). Mice received 1% Baytril solution in drinking water for 2 days before, and for 14 days after, to the start and end of irradiation, respectively. Mice were orally gavaged with either 5 mg/kg/day Dasatinib and 50 mg/kg/day quercetin or with 5 mg/kg/day Navitoclax for 10 days total (5 days, 2 days recovery, and 5 days). Compounds were prepared for oral gavage in 10% polyethylene glycol (PEG400). Control mice were gavaged with PEG400 only. Dasatinib (CDS023389), quercetin (1592409), and PEG400 (8074851000) were purchased from Sigma-Aldrich (now Merck). Navitoclax (285063-USB) was purchased from Stratech (Fielder, et al., 2022).

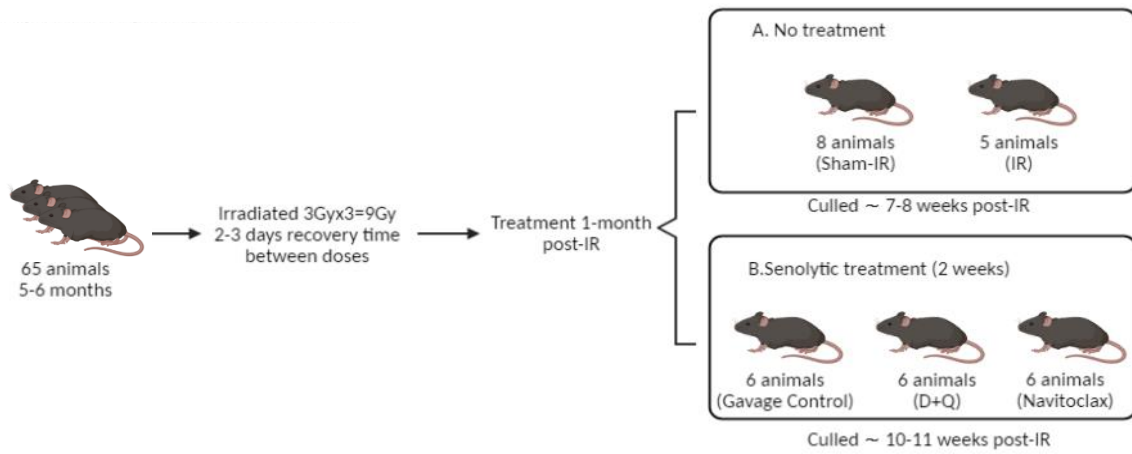
Cohort 1



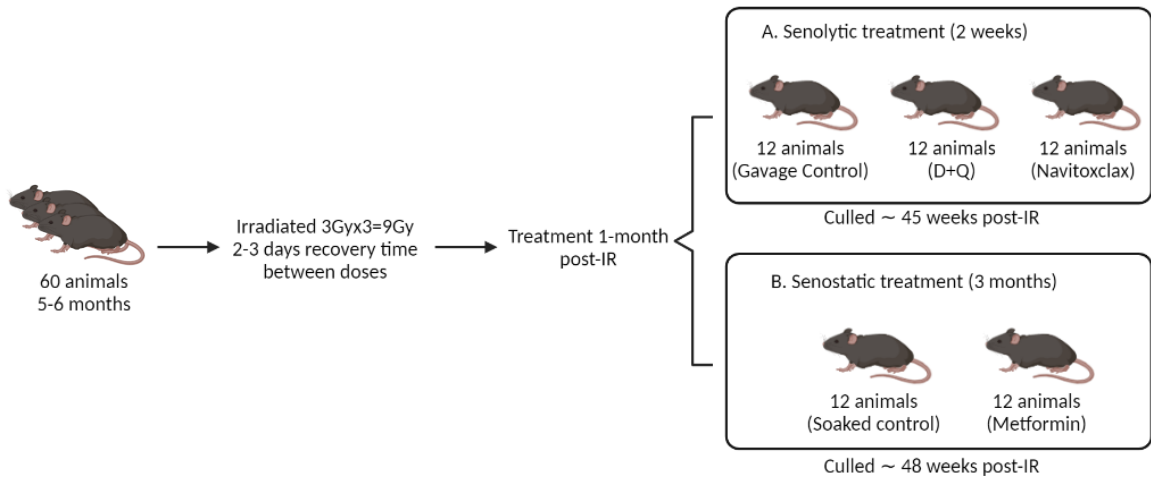
## Cohort 2



## Cohort 3



## Cohort 4



## Cohort 5



Figure 5 Mice treatment and study plans

The animal was divided into the 5 different cohorts as below:

**Cohort 1 (young VS old):** Mice were divided into 2 groups without treatment and were culled at the young age of 8-15 months and the age of 31.5-33.5 months.

Mice from cohorts 1 to 5 were subjected to receive sub-lethally irradiated (NDT 320 or X-RAD225, 225 kV) with 3 Gy of X-ray irradiation to accelerate premature ageing. Irradiation was given three times, with a total of 9 Gy, and two days of recovery time were given between doses at the age of 5-6 months.

**Cohort 2 (Sham-irradiated VS irradiated):** Half of the mice underwent Sham irradiation, while the other half underwent sub-lethal irradiation. Mice were culled approximately 30 weeks post-irradiation at the age of 12 months.

**Cohort 3 (Immediate effect after treatment):** Mice were divided into 2 groups. Group A was culled approximately 7-8 weeks after irradiation at 7 months without any treatment. Group B were orally gavaged with senolytic treatment (Dasatinib+Quercetin (D+Q) or Navitoclax) for 2 weeks and was culled 10-11 weeks after irradiation at the age of 8 months.

**Cohort 4 (Long-term effect after early treatment):** Mice were divided into 2 groups to receive senolytic (Dasatinib+Quercetin (D+Q) or Navitoclax) or senostatic drug (Metformin). All the treatments were given one-month post-irradiation; treatment for the senolytic group lasted for two weeks, while the senostatic group lasted for three months. Animals were culled at the age of 17 months.

**Cohort 5 (Effect of late treatment):** Mice were given senolytic (Dasatinib+Quercetin (D+Q) or Navitoclax) 8 months after irradiation that lasted for 2 weeks. Mice were culled at the age of 17 months.

### 2.3.3 Human skin samples

In this study, skin samples were obtained from donors aged 20 years old (young) and 60 years old (elderly). Both paraffin-embedded and frozen skin samples were provided by P&G as part of the BBSRC IPA grant BH190685. The arm (sun-exposed) and buttock (sun-protected) skin samples were collected from these age groups.

### 2.4 3D skin equivalents

The 3D skin equivalents were developed to investigate the skin microenvironment and the interactions among different cell types within the skin. These equivalents can accurately replicate the complex, multilayered structure of human skin by co-culturing essential cell types, such as dermal fibroblasts and keratinocytes. Both collagen gel and Alvetex skin models were utilized to achieve complete epidermal formation with distinct keratinocyte sublayers. However, it was observed that the Alvetex skin models exhibited superior reproducibility. As a result, it was decided to proceed with further experiments using the Alvetex platform, primarily due to the significant shrinkage observed during the formation of the collagen gel 3D model.

#### 2.4.1 Full thickness 3D Collagen gel skin equivalents

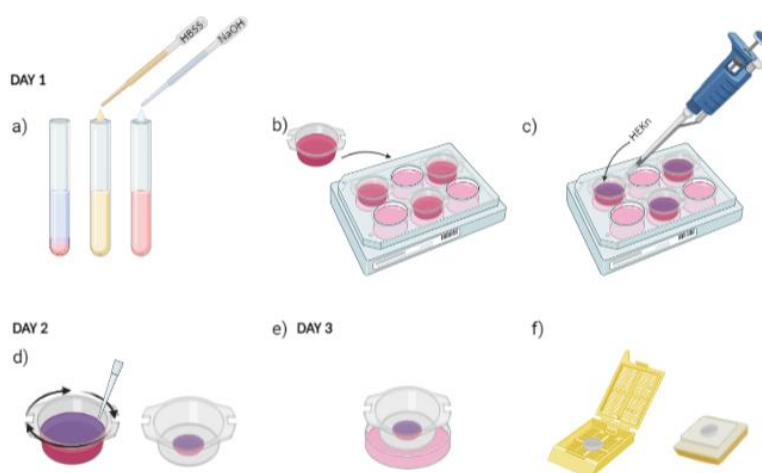


*Figure 6 Flowchart of the development of 3D collagen gel skin equivalent.*

Full thickness 3D human collagen gel skin equivalents were generated as described in (Weinmüller, et al., 2020). Inserts (3.0  $\mu\text{m}$  pore size, 6-well format; Falcon, Cat# 353092) were placed into deep well plates (6-well plate; BD Biosciences, Cat# 355467 (Lot# 54227).

- a)  $2.5 \times 10^5$  human dermal fibroblasts (HDFn) were suspended in 1 part of foetal bovine serum (FBS) and seeded in collagen gel made up of 1 part of 10x Hanks' balanced Salt solution (HBSS, with Phenol red, Gibco, cat #14060-040) and 8 parts of Collagen G (0.4% Collagen solution in HCL, Type I, 4mg/ml, Biochrom, Cat#L7213). 10x HBSS was added dropwise into the collagen matrix while mixing until the yellow colour was achieved, followed by dropwise addition of 1M NaOH until the mixture turned pink again.
- b) The collagen matrices were transferred into the inserts quickly while the temperature remained cold with 2.5ml per insert. The inserts were incubated for 2 hours at 37°C without CO<sup>2</sup> until solidified.
- c) Keratinocytes basal medium 2 (KBM-2) (LONZA, Cat# CC-3107) supplemented with KGM-2 SingleQuot kit (LONZA, Cat #CC-4152) was added into the wells followed by a keratinocyte overlay of  $1 \times 10^6$  cells. Keratinocytes were let settled overnight in the incubator.
- d) On day 2, the skin models were carefully loosened around the outer wall of the insert by using a 200µl pipette tip. The models should shrink approximately 30-50% once loosened from the insert.
- e) On day 3, the skin equivalents were lifted to the air-liquid interface (ALI). The existing media were then replaced by differentiation media (LONZA, Cat #CC-3111) supplemented with all components of the KGM BulletKit (LONZA, #CC-4131), except for bovine pituitary extract. In addition, 1.15 mM CaCl<sub>2</sub>, 50 µg/ml L-ascorbic acid, 0.1% bovine serum albumin, and 10 µg/ml transferrin were added. The differentiation media was replaced every other day throughout the whole differentiation process from day 3 to 10. On the 10<sup>th</sup> day, the skin equivalents were harvested.
- f) Skin models were rinsed with PBS and incubated in 4% PFA for 2 hours at room temperature. The models were then dehydrated in graded ethanol (EtOH) series for 15 minutes each (30%, 50%, 70%, 80%, 90%, 95%, and 100%).
- g) Models were transferred to cassette and immersed in HistoClear for 15 minutes followed by a mixture of HistoClear and melted wax with (1:1 ratio) for 30 minutes in the 60°C oven. Then, models were moved to full melted wax for 1 hour before fully embedded in wax.
- h) After embedded in paraffin wax, samples were sectioned with a thickness of 3 µm.

## 2.4.2 Full thickness Alvetex 3D skin equivalents

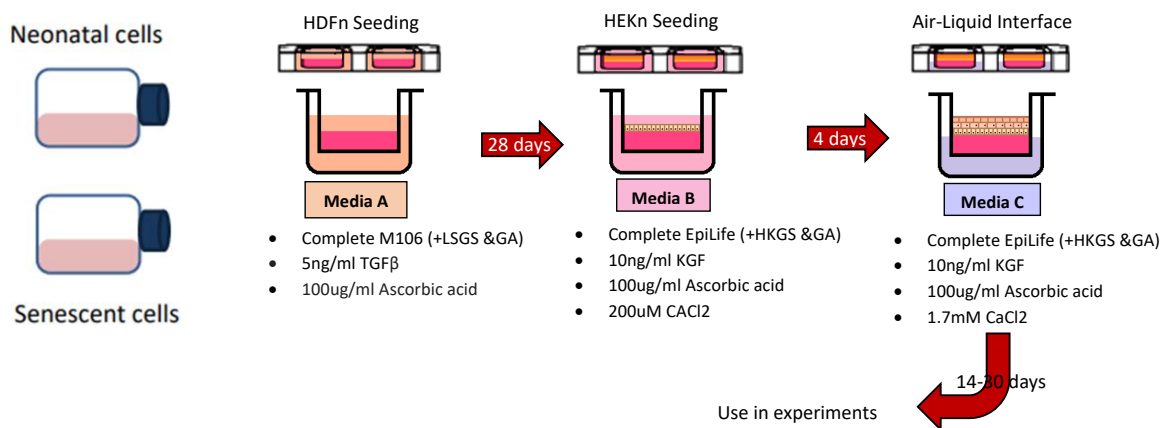


Figure 7 Flowchart of the development of Alvetex 3D skin equivalent.

Performed by Dr. Lucy Smith

Full thickness 3D human Alvetex skin equivalents were generated as described in (Roger, et al., 2019), with some minor with some minor modifications to the protocol to incorporate senescent cells into the dermal compartment. The standard 12 well format as described was used, as was the smaller 24 well format, with cell seeding densities for both HDFn and HEKn scaled down accordingly.

1. 12-well Alvetex Scaffold inserts (Reinnervate AVP005) were first treated in 70% Ethanol and rinsed with PBS in a petri dish. Inserts were then transferred into 6 well plate and immersed in M106 media.
2.  $5 \times 10^5$  dermal fibroblasts were suspended in M106 media and seeded onto scaffolds in a dropwise manner. The inserts were then incubated for a minimum of 2 hours at 37°C with 5% CO<sub>2</sub>. Senescent cells were treated in 2uM Doxorubicin in serum-free media for 4 hours and change to Media A.
3. Media A was prepared by adding Low Serum Growth Supplement (Life Tech S-003-10) and Gentamicin/Amphotericin Solution (Life Tech R-015-10), with addition of 5ng/ml TGFβ<sub>1</sub> (Life Tech PHG9214) and 100 µg/ml of ascorbic acid (Sigma A4544) into complete M106 media.
4. M106 media was replaced with Media A into the outer compartment of the well until the media was touching the bottom of the scaffold. 0.5ml of media A were then added to fill up the outer compartment to a maximum level. The plate was incubated at 37°C with 5% CO<sub>2</sub> for 28 days with media changes every 3-4 days.

5. Media B was prepared by adding 10ng/ml keratinocyte growth factor (KGF) (diluted to 10 µg/mL in 1X DPBS) (Life Tech PHG0094), 100µg/ml Ascorbic acid (Sigma A4544) and 200uM of CaCl<sub>2</sub> (2 M Stock) into complete EpiLife media (Life Tech M-EPI-500). 1.3x10<sup>6</sup> keratinocytes were suspended in Media B and seeded onto the dermal layer. Inserts were kept in a 37°c incubator (5% CO<sub>2</sub>, 95% relative humidity) and cells were allowed to attach for 2 hours. Each insert was filled with 10ml of media and incubated at 37° c, 5% CO<sub>2</sub> and 95% relative humidity for 48 hours.
6. Media C was prepared by adding 10ng/ml keratinocyte growth factor (KGF) (diluted to 10 ug/mL in 1X DPBS) (Life Tech PHG0094), 100µg/ml Ascorbic acid (Sigma A4544) and 1.7mM of CaCl<sub>2</sub> (2 M Stock) into complete EpiLife media (Life Tech M-EPI-500).
7. The inserts were transferred into a Reinnervate deep dish (Reinnervate AVP015-2) with an Alvetex holder. 35ml of media C was added into each dish where the media only touches the bottom of the model (air-liquid interface), incubated at 37°C with 5% CO<sub>2</sub> for 2 weeks. Media was replaced twice a week until epidermis was fully formed.
8. Harvested skin models were rinsed with PBS and incubated in 4% PFA for 2 hours at room temperature. The models were then dehydrated in graded ethanol series for 15 minutes each (30%, 50%, 70%, 80%, 90%, 95%, and 100%). Models were transferred to plastic cassettes and immersed in HistoClear for 30 minutes followed by a mixture of HistoClear and melted wax with (1:1 ratio) for 30 minutes in the 60°C oven. Then, models were moved to full melted wax for 60 minutes before being fully embedded in wax in moulds.
9. After embedded in paraffin wax, samples were sectioned with a thickness of 3 µm.

### 2.4.3 Alvetex 3D dermal skin equivalents

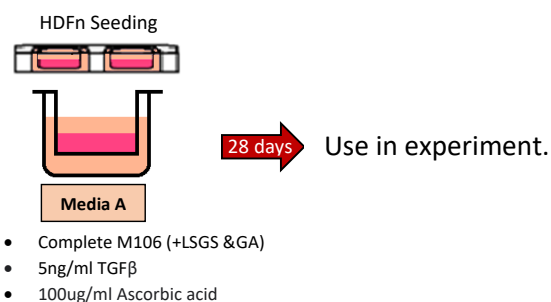
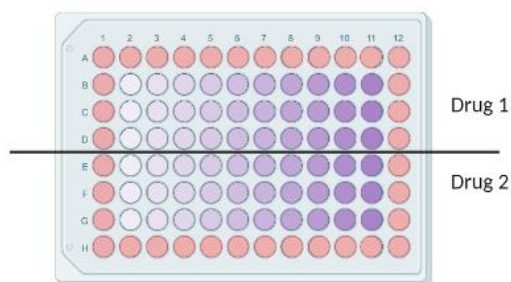


Figure 8 Illustration of 3D Alvetex dermal model

1. 12-well Alvetex Scaffold inserts (Reinnervate AVP005) were first treated in 70% Ethanol and rinsed with PBS in a petri dish. Inserts were then transferred into 6 well plate and immersed in M106 media.
2.  $5 \times 10^5$  dermal fibroblasts were suspended in M106 media and seeded onto scaffolds in a dropwise manner. The inserts were then incubated for a minimum of 2 hours at 37°C with 5% CO $_2$ . Senescent cells were either treated in 2uM Doxorubicin in serum-free media for 4 hours and change to Media A or exposed to 20 Gy irradiation on Day 10.
3. Media A was prepared by adding Low Serum Growth Supplement (Life Tech S-003-10) and Gentamicin/Amphotericin Solution (Life Tech R-015-10), with addition of 5ng/ml TGF $\beta$ 1 (Life Tech PHG9214) and 100  $\mu$ g/ml of ascorbic acid (Sigma A4544) into complete M106 media.
4. M106 media was replaced with Media A into the outer compartment of the well until the media was touching the bottom of the scaffold. 0.5ml of media A were then added to fill up the outer compartment to a maximum level. The plate was incubated at 37°C with 5% CO $_2$  for 28 days with media changes every 3-4 days.
5. Harvested skin models were rinsed with PBS and incubated in 4% PFA for 2 hours at room temperature. The models were then dehydrated in graded ethanol (EtOH) series for 15 minutes each (30%, 50%, 70%, 80%, 90%, 95%, and 100%). Models were transferred to cassette and immersed in HistoClear for 30 minutes followed by a mixture of HistoClear and melted wax with (1:1 ratio) for 30 minutes in the 60°C oven. Then, models were moved to full melted wax for 1 hour before fully embedded in wax.
6. After embedded in paraffin wax, samples were sectioned with a thickness of 3  $\mu$ m.



## 2.5 2D Drug screening assay



*Table 1 List of compounds tested and concentration range.*

In this table, "Stock Concentration" refers to the concentration of the compound in the stock solution, "Solvent" indicates the solvent used to dissolve the compound, and "Maximum Tested Concentration" denotes the highest concentration of the compound tested in the experiment. All concentrations are expressed in millimolar (mM) or micrograms per milliliter ( $\mu\text{g}/\text{ml}$ ) as appropriate.

Drugs	Stock concentration	solvent	Maximum tested concentration
NOVOS Core	0.5 mg/ml	DMSO: H <sub>2</sub> O	4 $\mu\text{g}/\text{ml}$
NOVOS Core + NMN (NOVOS Boost)	0.5 mg/ml	DMSO: H <sub>2</sub> O	4 $\mu\text{g}/\text{ml}$
<i>Rhodiola Rosea</i>	500 mM	H <sub>2</sub> O	2mM
Fisetin	100 mM	H <sub>2</sub> O	0.4 mM
Lithium Orotate	25 mM	DMSO	0.1 mM
Glucosamine Sulfate	500 mM	DMSO	1 mM
Gingerols	100 mM	DMSO	0.4 mM
Pterostilbene	50 mM	EtOH	0.2 mM
L-Theanine	250 mM	H <sub>2</sub> O	0.5 mM
Glycine	30 mM	Media	3 mM
Ascorbic Acid	100 mM	H <sub>2</sub> O	0.2 mM

Human embryonic skin fibroblasts were rendered senescent by irradiation with 20Gy and subsequent culture for 10 days. On the 7<sup>th</sup> days of senescence development, young cells were plated into a different 96-well plate as control. The outer wells were left with no cells but filled with media to prevent media loss in the seeded wells. Both irradiated and young plates were then treated with a graded concentration series of the compounds in triplicate fashion on the

same day. This treatment lasted for 3 days; the cells were stained with crystal violet. The plate was then placed in the Omega machine to measure the absorbance of each well at 570 nm. Non-irradiated cells with a population doubling level below 30 were used as controls. Percent viability is reported relative to the absorbance of untreated control cells at day 3. Between 2 and 4 independent experiments were conducted. The data is presented as titration curves with moving averages, and SEM of the experiments is indicated.

The solubility tests for NOVOS Boost were conducted by Dr. Edward Fiedler. The primary stock was prepared in water or ethanol and subsequently mixed with media as described below.

**Water:**

1. 1 sachet of NOVOS Core and 2 pills of NMN Boost (2x 125mg) were added to 1 litre of distilled (MilliQ) H<sub>2</sub>O and mixed at room temperature, with agitation.
2. The supernatant was drawn off and filtered through a cell-strainer (45µm mesh) to remove large debris to give the stock solution.
3. This highest concentration final solution was prepared by adding 1 part stock solution to 3 parts x4 concentrated high glucose DMEM tissue culture media with L-Glutamine, 10% foetal bovine serum, and 1% penicillin G & streptomycin. This gives 67.6% stock solution in x1 high glucose DMEM media.

This highest concentration final solution was prepared by adding 1 part stock solution to 3 parts x4 concentrated high glucose DMEM tissue culture media with L-Glutamine, 10% foetal bovine serum, and 1% penicillin G & streptomycin. This gives 67.6% stock solution in x1 high glucose DMEM media.

**Ethanol:**

1. 1 sachet of NOVOS Core and 2 pills of NMN Boost (2x 125mg) were added to 150ml of 99.8% analytical grade Ethanol and mixed at room temperature, with agitation.
2. The supernatant was drawn off and filter-sterilised to give the stock solution, as a smaller volume was required to prepare the final solution added to cells. T
3. This highest concentration final solution was prepared by adding 2% of the ethanol stock solution to high glucose DMEM media (2% Ethanol was used in the controls). Magnesium Malate, Glycine, L-Theanine, Hyaluronic acid and b-nicotinamide mononucleotide are likely not soluble in ethanol according to the available literature. This highest concentration final solution was prepared by adding 2% of the ethanol stock solution to high glucose DMEM media (2% Ethanol was used in the controls).

A dose-response series was then tested on a combination of young proliferating HDFs and deeply senescent HDFs using sequential  $\frac{1}{2}$  concentrations. The highest concentrations from the water-dissolved stock solution (67.6% solution in media) led to some deposition of unidentified material (Figure 8A). This was visible in the same channel (red) as our proliferating cells, so we cannot discount whether this is an alteration in cell morphology of young cells or due to not filter sterilising this solution, given to the higher volumes required. Ethanol stock exhibits a significantly more yellow colour, likely due to increased solubility of Fisetin. Heat and agitation of the H<sub>2</sub>O stock preparation was attempted, but without a significant change in colour (Figure 8B).

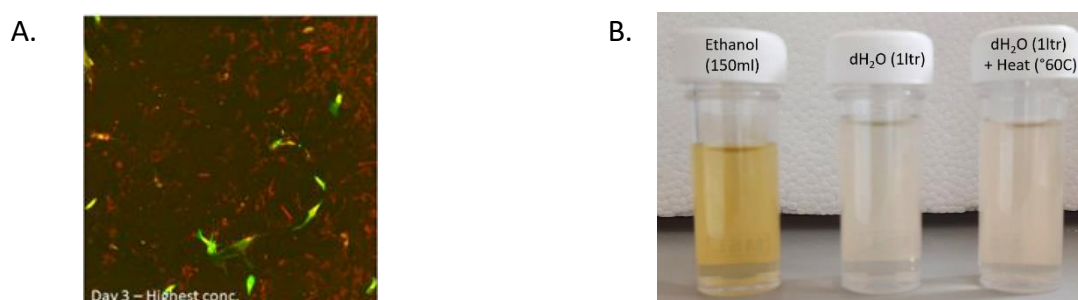


*Figure 9 Example colour differences between the Ethanol and H<sub>2</sub>O stock preparations.*

A. Example of unidentified deposition shown as the same colour as the young proliferative cells (Red). B. Example of colour differences between the Ethanol and H<sub>2</sub>O stock preparations.

## **2.6 Histology and Immunofluorescence staining methods**

Different staining techniques were performed based on the requirements of specific experiments.

### **2.6.1 General deparaffinise and antigen retrieval methods**

Paraffin-embedded sections were placed in a rack and baked in a 60°C oven for 20 minutes to melt the paraffin before deparaffinisation and rehydration. Sections were transferred to two changes of HistoClear for 5 minutes each after being taken out from the oven. Samples were rehydrated in descending grades of Ethanol (100%, 100%, 90%, 90% and 70%) for 5 minutes each. After rehydration, the samples were washed in distilled water twice for 5 minutes on an orbital shaker plate with gentle agitation. Antigen retrieval was then performed by microwaving the samples in a citric acid buffer (10mM sodium citrate, pH6) for 4 minutes at high power and 10 minutes at medium-low power. Samples were cooled in an ice bath before proceeding with epitope blocking solution.

### **2.6.2 Haematoxylin and Eosin staining**

Following deparaffinisation and antigen retrieval steps, the samples were sequentially treated with haematoxylin for 3 minutes, acid alcohol for 10 seconds, warm water for 30 seconds and eosin solution for 30 seconds. Sections were rinsed in tap water for 5 minutes between each step. Samples were then dehydrated using the same ethanol concentration in ascending order (70%, 90, 90%, 100%, and 100%) for 30 seconds each. After drying, slides were mounted using DPX and imaged using a Nikon E800 microscope at 200x magnification.

### **2.6.3 Picro-Sirius Red and Fast Green staining**

Following deparaffinisation and antigen retrieval, paraffin tissue samples were rinsed in distilled water and PBS. After washing, the sections were marked using an immune-blocker pen to create a hydrophobic barrier around the specimen on the slides. The sections were stained with haematoxylin for 8 minutes, followed by washing under running tap water. The tissues were incubated in Picro-Sirius red solution for 60 minutes, then rinsed quickly in 2 changes of Acetic acid solution. The sections were incubated in 0.04% Fast Green for 15 minutes (0.1g in 250ml) and rinsed in distilled water using a pipette. The sections were dehydrated in 3 changes of ethanol (95%, 100%, and 100%) for one minute in each stage, then cleared in Histoclear twice for 5 minutes each before being mounted in DPX.

## 2.6.4 Immunofluorescence staining

*Table 2 Information of antibodies used and concentration ranges for Immunofluorescence staining.*

In this table, "Host" refers to the host species of the primary antibody, "Catalog Number" is the unique identifier for the antibody, "Dilution" indicates the dilution ratio used for both primary and secondary antibodies. The dilution ratio for primary antibodies is specified for cells and tissue separately where applicable. The dilution ratio for the secondary antibody is constant for all cases.

Primary antibody		Host	Primary antibody	Dilution	Secondary antibody	Dilution	VECTASHIELD® Antifade Mounting Medium with DAPI (H-1200-10). VECTASHIELD® Antifade Mounting Medium with DAPI (H-1200-10).
p16INK4a	Abcam	Rabbit	Ab94619	1:250(cells) 1:200 (tissue)	Alexa Fluor 488 goat anti rabbit	1:1000	
p21WAF1/CIP1	Abcam	Rabbit	Ab109520	1:250	Alexa Fluor 488 goat anti rabbit	1:1000	
Ki-67	Abcam	Rabbit	Ab15580	1:250	Alexa Fluor 488 goat anti rabbit	1:1000	
LaminB1	Abcam	Rabbit	Ab16048	1:250(cells) 1:200 (tissue)	Alexa Fluor 488 goat anti rabbit	1:1000	
HMGB1	Abcam	Rabbit	Ab79823	1:250(cells) 1:200 (tissue)	Alexa Fluor 488 goat anti rabbit	1:1000	
Phospho-Histone H2A.X (Ser139)	Cell signalling	Mouse	D7T2V #80312	1:250	Alexa Fluor 488 goat anti mouse	1:1000	
P63	Abcam	Rabbit	Ab124762	1:250	Alexa Fluor 488 goat anti rabbit	1:1000	
Cytokeratin 14	Abcam	Mouse	Ab7800	1:200	Alexa Fluor 488 goat anti mouse	1:1000	
Cytokeratin 10	Abcam	Rabbit	Ab766318	1:250	Alexa Fluor 594 goat anti rabbit	1:1000	
Collagen-1	Abcam	Rabbit	Ab34710	1:100	Alexa Fluor 488 goat anti rabbit	1:1000	
MMP-1	Protein-Tech	Rabbit	10371-2-AP	1:100	Alexa Fluor 488 goat anti rabbit	1:1000	
Living Colors full-length GFP polyclonal antibody	Takara	Rabbit	632592	1:100	Alexa Fluor 488 goat anti rabbit	1:1000	

Cells were seeded onto 19mm round glass coverslips in 12-well plates and cultured as described, cells were treated with X-ray irradiation and subsequent culture for 10 days. Young

cells were seeded into the plate 2 days before the senescent cells were ready. On the day 10, the cells were fixed with 2% PFA and rinsed with PBS for 3 times with 5 minutes each.

For paraffin samples, the samples underwent deparaffinisation and antigen retrieval steps, rinsed in distilled water and PBS. After washing, the sections were marked using an immune-blocker pen to create a hydrophobic barrier around the specimen on the slides.

Cells/ paraffin samples were incubated in blocking solution; 1:60 [Normal Goat Serum]: [0.1% BSA/PBS] for 1 hour at room temperature followed by incubation of primary antibody. The samples were washed in PBS 3 times for 5 minutes each followed by another hour of secondary antibody incubation at room temperature. Once the samples were washed, they were mounted onto microscope slides with VECTASHIELD® Antifade Mounting Medium with DAPI (H-1200-10).

### 2.6.5 Sen-β-gal staining

*Table 3 Concentration ranges for Sen-β-gal staining solution.*

This table presents the protocol for preparing the Sen-β-gal staining solution. For the Sodium Phosphate solution, the 0.1M concentration should be prepared by adjusting the pH of 0.1M sodium phosphate dibasic to pH6 by gradually adding 0.1M sodium phosphate monobasic. The base solution is ensured to achieve the desired pH of 6.

Solution	Concentration	Volume
NaCl	1M	1.5ml
MgCl	1M	20ul
Citric Acid	0.5M	800ul
Sodium Phosphate	0.1M	1.2ml
Solution	Concentration	volume
Base solution		8.8ml
Potassium ferrol-cyanide (Iron Bru)		1ml
X-gal	200mg/ml in dimethylformamide	200ul

Cells were seeded onto 19mm round glass coverslips in 12-well plates and cultured as described, cells were treated with X-ray irradiation and subsequent culture for 10 days. Young cells were seeded into the plate 2 days before the senescent cells were ready. On the day 10, the cells were fixed with 2% PFA and rinsed with PBS for 3 times with 5 minutes each.

Frozen sections were taken out from the -80°C freezer and allowed to thaw at room temperature for 10-20 minutes. Excess condensation and OCT were carefully removed with a blue roll. The sections were fixed with 4% paraformaldehyde (PFA) for 20 minutes at room temperature. PFA was removed, and sections were washed in PBS for 5 minutes. Samples were circled using a liquid blocker pen and washed briefly with PBS.

The base solution was prepared as described. Sections/coverslips were rinsed with PBS using a pipette and incubated in a staining solution for at least 2 days at 37°C. Wash the sections with PBS and mount them with VECTASHIELD® Antifade Mounting Medium with DAPI (H-1200-10).

### 2.6.6 Crystal Violet staining

*Table 4 Concentration ranges for Crystal Violet staining.*

This table outlines the concentration ranges for Crystal Violet staining. To prepare the staining solution, Crystal Violet (Sigma-Aldrich C0775) is dissolved in a specified volume of Ethanol and dH<sub>2</sub>O as follows: 1g of Crystal Violet is dissolved in 10ml of Ethanol, and then the total volume is adjusted to 500ml with dH<sub>2</sub>O.

Reagent	Mass	Volume
Crystal violet (Sigma-Aldrich C0775)	1g	
Ethanol		10ml
dH <sub>2</sub> O		490ml

Cells were then washed with PBS and stained with 50ul of 0.2% Crystal violet/1% Ethanol solution for 10 minutes. Plates were then washed twice by immersion in a basin of tap water and dried. Once dry, 100ul of 1% SDS was added to the plate to solubilize the stain for 1 hour on an orbital shaker until the colour was uniform with no areas of dense colouration at the bottom of the wells. The plate was placed in the Omega machine to read the absorbance of each well at 570 nm.

### 2.7 Operationalisation of measurement between observers for 3D Alvetex models

All staining and measurements were performed independently by two observers using separate sections from the same skin equivalent. Observer 2 was fully blinded to the senescent fibroblast density in the model. Pilot experiments showed a high degree of variation between estimates by independent observers.

### 2.7.1 Epidermal thickness measurement

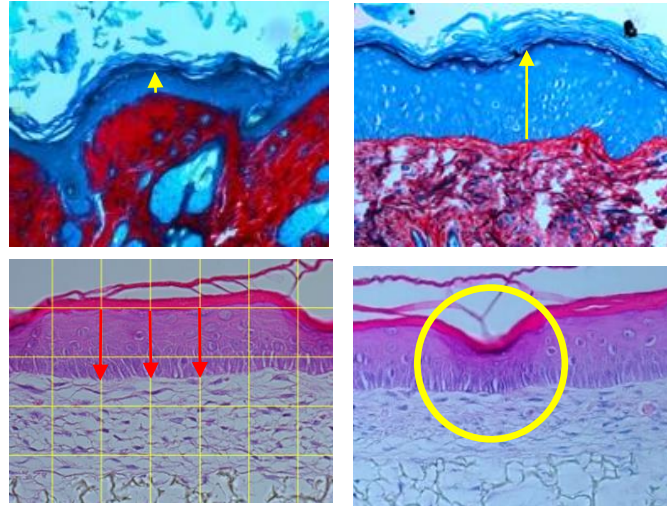


*Figure 10 Example of epidermal thickness measurement.*

The figure in the top row shows an example of Picro-Sirius red/fast green stained sample. The one on the left represents the mouse skin sample, and the one on the right represents the human skin sample. The thickness of the epidermis was measured from the bottom of the basal cells to the bottom of the stratum corneum (indicated by yellow arrows). The figure in the bottom row shows an example of Haematoxylin and Eosin staining on full thickness 3D skin model. The thickness of the epidermis was measured from the bottom of the basal cells to the bottom of the stratum corneum (indicated by red arrows). Abnormal regions were excluded from the measurement (indicated by the yellow circle).

Mouse and human skin samples were subjected to Picro-Sirius red/fast green staining, a histochemical technique utilized for detecting collagen fibres. This method relies on the distinct contrast between collagenous fibres (appearing red) and non-collagenous components (appearing green/blue). Given that the dermal layer primarily consists of collagen, the epidermal layer (green/blue) stands out against the red-coloured collagen components. Images were captured at 200x magnification using a Nikon E800 light microscope. Three images were taken for each sample. Using the straight-line tool in ImageJ software, the length of 25 regions in each image was measured, and the average length from the three images was recorded.

3D Alvetex skin samples, they were stained with Haematoxylin and Eosin. Images were acquired using a 20x objective on a Nikon E800 light microscope. A grid was overlaid onto the images at regular 50  $\mu\text{m}$  intervals, and the length of epidermal thickness was measured using the straight-line tool in ImageJ. A total of 300 measurements were made across the entire length of the model. The mean length of the viable cell layers, measured from the bottom of the basal cells to the bottom of the stratum corneum in each image, was measured (indicated



by the yellow arrow). The effects of variable seeding densities of senescent cells were assessed by 1-way ANOVA and by linear regression on data that were normalised to the zero senescent cell controls for each experiment, with equal weights given to the results from both observers. To assess inter-observer variability, 2-way ANOVA was carried out on both raw and normalised data sets.

### 2.7.2 Basal cells size and nuclear size measurement

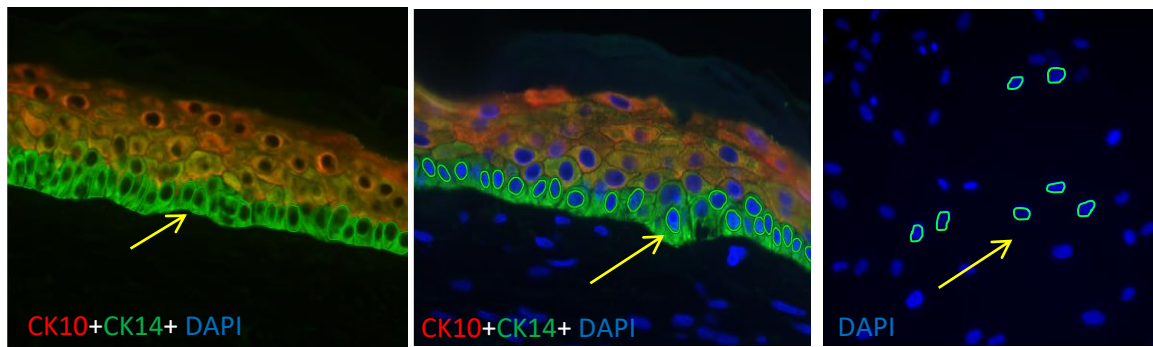


Figure 11 Example of Basal cells size and nuclear size measurement.

Basal cell and nuclear size were measured by manually drawing around each cell or nucleus (green).

Co-staining of CK10 and CK14 was used to determine the location of basal cell layer. CK14 is restricted to the basal layer (keratinocytes stem cells) and CK10 stained in early differentiated cells at the spinous layer and is remains detectable across all differentiated layers. Thus, cells that were in the green layer are considered as basal cells and were assessed for their size, and the DAPI-stained nuclei (blue) within these basal cells were measured for nuclear size. Only the cells that touches the basal membrane and with clearly identifiable and non-overlapping cells were included in the measurement. Images were taken using a 20x objective on a DM18 microscope, with 10 images were taken for each condition. The basal cells and nuclear size were assessed by measuring the area ( $\mu\text{m}^2$ ) of each cell, which was manually outlined (in green) using the ICY polygon tool. The mean area of an average of 300 cells was measured for each sample. Statistical analysis was performed using 1-way ANOVA and by linear regression on data that were normalised to the zero senescent cell controls for each experiment, with equal weights given to the results from both observers. To assess inter-observer variability, 2-way ANOVA was carried out on both raw and normalised data sets.

On the right, a similar approach was applied for *in vitro* cells. After fluorescent staining with DAPI, the size of each nucleus was manually measured as area ( $\mu\text{m}^2$ ) by outlining each cell

using the polygon tool in ICY. The mean diameter of 400-500 cells was measured, and statistical analysis was carried out using a T-test.

### 2.7.3 Semi-quantitative analysis of fluorescent staining

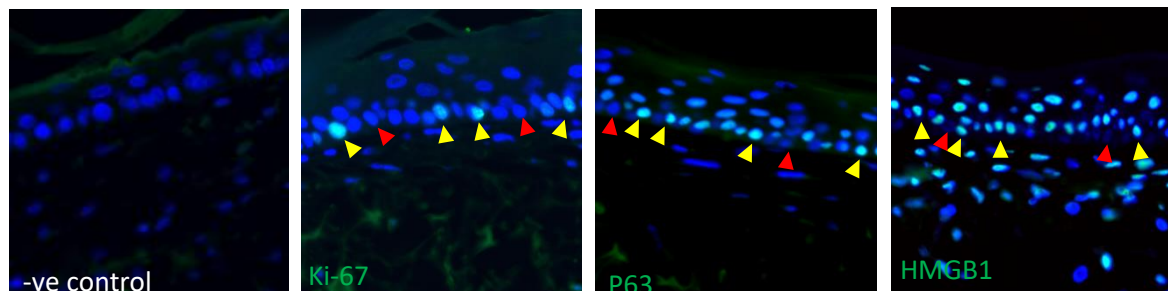


*Figure 12 Example of senescence markers quantification.*

A. The figure shows an example of negative control. B.-E. Target markers were stained in green, including Ki-67, P63 and HMGB1. Yellow arrows indicate some of the examples of cell positivity with the stained marker, while red arrows indicate absence of staining.

A semi-quantitative evaluation was performed by counting the frequencies of target marker-positive cells. 3D skin samples were subjected to fluorescent staining, including markers for cell proliferation (Ki-67), keratinocytes stem cells (P63) and senescence (HMGB1). All the samples were counterstained with nuclear DAPI (stained in blue). Staining and quantification were carried out separately by two individuals, observer 1 (non-blinded) and 2 (blinded). Stained samples were compared to the negative control sample as reference to distinguish positively stained cells. For Ki-67, P63 and HMGB1 analysis, the background intensity was adjusted to the lowest setting, and nuclei with strong staining were considered as positively stained cells (indicated by yellow arrows). The images were analysed iteratively between the two observers to standardise the quantification method and establish a consensus subjective threshold of positive cell counts for each marker. This consensus was then applied to quantify all images across each relevant marker. For example, quantify cells with more than half of the area is stained, count only those cells that entirely identifiable, and avoid counting overlapping cells. For P63, only the bottom layer of the cells was quantified. While staining was done independently, protocols were homogenized as much as possible. Specifically, the same antibodies from the same companies were used at equal dilution, same time, and temperature by both observers. All the samples were imaged using a 20x objective on a DMI8 microscope. 10 images were captured, with an average of 300 cells measured for each condition. To assess the percentage of marker-positive cells, manual quantification was performed using the cell counter plugin in ImageJ. The effects of variable seeding densities of senescent cells were

assessed by 1-way ANOVA and by linear regression on data that were normalised to the zero senescent cell controls for each experiment, with equal weights given to the results from both observers. To assess inter-observer variability, 2-way ANOVA was carried out on both raw and normalised data sets.

## Chapter III – Changes of skin morphology with age, irradiation, and the effect of intervention on skin

### 3.0 Introduction

Cancer has become a curable disease with high survivorship via radiotherapy treatment. However, 95% of cancer patients experience radiation-induced skin injuries during their treatment (McQuestion, 2011; Salvo, et al., 2010). Radiation can cause immediate damage to the skin by destroying parts of the basal keratinocytes, leading to failure in epidermal renewal (McQuestion, 2011). With repeated exposure to radiation, it slows down or prevents the reparation of DNA damage caused by the radiation. Subsequently, this accelerates premature ageing and triggers the DNA-damaging pathway by initiating persistent cell cycle arrest leading to cellular senescence. Senescent cells accumulate in cancer survivors over time and produce a large amount of senescence-associated secretory phenotype (SASP), spreading senescence towards their neighbouring cells (Nelson, et al., 2012). The overproduction of SASP could cause a relapse of cancer and even secondary cancers with a poorer prognosis (Jena, Das, Bharadwaj, & Mandal, 2020; Saleh, Tyutyunyk-Massey, & Gewirtz, 2019). Therefore, sub-lethal whole-body irradiated mouse models were developed to accelerate premature ageing, mimicking the side effects of post-cancer therapy (Fielder, et al., 2019).

Much evidence has shown that senescent cells accumulate in many organs and tissue during ageing. The existence of senescence plays a major causal role in mediating age-related deterioration, including osteoporosis (Farr, et al., 2017), frailty, cardiovascular diseases (Erusalimsky & Kurz, 2005), osteoarthritis (Martin & Buckwalter, 2003), chronic lung disease (Nouredine, et al., 2011), renal diseases (Valentijn, Falke, Nguyen, & Goldschmeding, 2018), neurodegenerative diseases (Si, Sun, & Wang, 2021), hepatic steatosis (Ogrodnik, et al., 2017), precancerous lesions (Collado, Blasco, & Serrano, 2007) and obesity-induced anxiety (Ogrodnik, et al., 2019). It was clearly shown that the abundance of senescent cells could vary across tissue samples within one animal. Similar to skin, well-documented evidence shows an increased proportion of senescent cells with age. However, the results varied widely among studies depending on the observed models or cell types. The knowledge about senescence accumulation during ageing in the primary skin cell types has yet to be fully understood.

Elimination of senescent cells could improve and delay age-associated deterioration. Eliminating senescent cells via gene-mediated ablation of P16INK4a-overexpressing cells in INK-AATAC mice showed positive effects in delaying age-related diseases and improving health

span (Baker, et al., 2011). The application of senolytics in clearing senescent cells is also reported to postpone age-associated functional loss and deterioration in multiple organ systems, including muscle, liver, lung, bone, the cardiovascular system, and the brain (Robbins, et al., 2021). In contrast, transplanting as few as 0.03% of senescent cells in young mice could lead to onset symptoms like age-associated deterioration, which can be rescued by the treatment of senolytic (Xu, et al., 2018; Xu, et al., 2017). The percentage of senescent cells *in vivo* is relatively small; a complete clearance of senescent cells is unnecessary, as removing as few as 30% of cells can lead to positive impacts (Li, et al., 2019). These studies confirm the importance of senescence as a causal role of ageing. Unfortunately, only a few studies have tested the effects of senolytics or senostatic in skin ageing. Whether senescent cells are causally implicated in skin ageing and whether their removal is beneficial remained unknown. Using the same batch of therapy-induced mice model (Fielder, et al., 2019), this study focuses on the changes in skin morphology by looking at the most frequently quantified skin ageing characteristic, i.e., changes in epidermal thickness. The experiment first compared the skin morphology between age differences, followed by the effect of X-ray radiation (therapy-induced). Then, to study the effects of senolytic or senostatic treatment on epidermal thickness at different time points, the skin samples were culled and collected 3 and 12 months after irradiation.

There are significant morphological differences between mammalian models for skin ageing where mice epidermis has 2-3 cell layers thick, a higher density of hair follicles, absence of rete ridges and a thinner epidermis. In addition, normal mice with fur were not an appropriate model for human responses to UV irradiation, which might not be relevant to compare to the skin ageing process in humans. Therefore, this study looked at skin ageing characteristics in age differences in human skin samples, i.e., changes in epidermal thickness. Human skin samples obtained from sun-exposed and sun-protected areas were observed to compare the characteristics of intrinsic and extrinsic skin ageing.

### 3.1 Thinning in epidermal thickness with age in mice skin tissue

This experiment aimed to investigate the change in epidermal thickness during skin ageing in male C57BL/6 mice. Two age groups were compared: adult mice aged 8-15 months and old mice group aged 31.5-33.5 months. Epidermal thickness was assessed using picro-sirius red/fast green staining and reported as length in perimeter ( $\mu\text{m}$ ).

The results showed a significant reduction in epidermal thickness with increasing age. Specifically, the epidermal thickness decreased from  $8.698\mu\text{m} \pm 0.9992 \text{ SEM}$  ( $n=7$ ) in adult mice to  $6.186\mu\text{m} \pm 0.2110 \text{ SEM}$  ( $n=7$ ) in old mice ( $p<0.05$ ). this represented a 30% reduction in skin thickness (Figure 13B).

These findings suggest that epidermal thinning is a characteristic feature of skin ageing in male C57BL/6 mice, mirroring observations in human skin ageing.

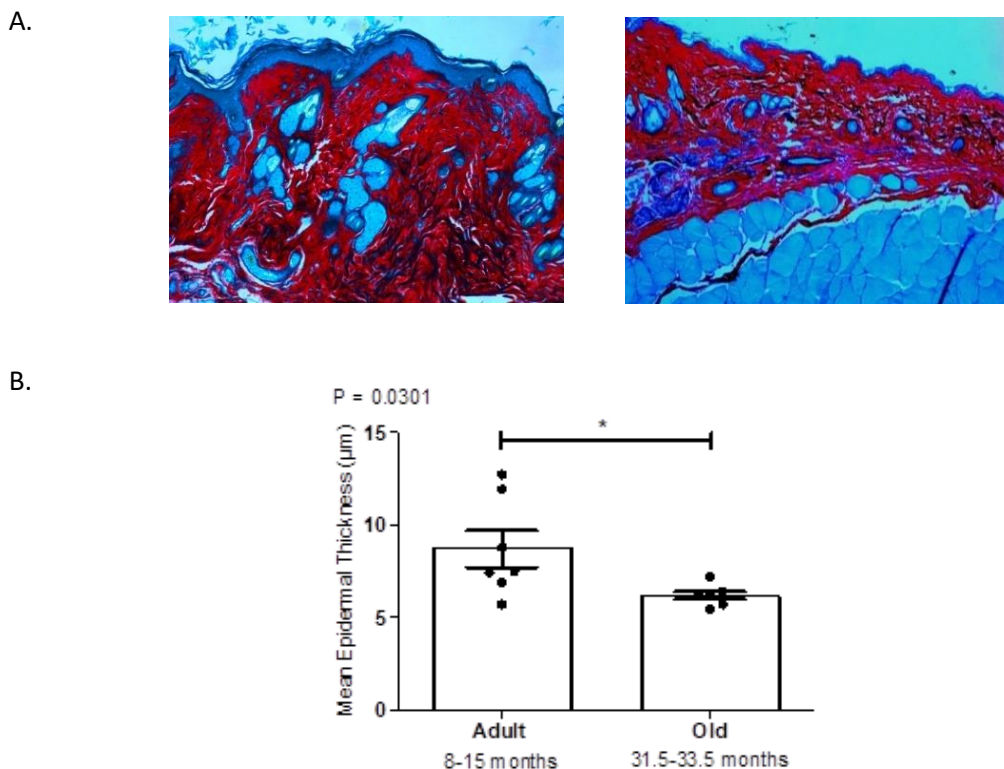


Figure 13 Change in epidermal thickness between age differences.

**A.** Representative images of adult mice skin (left) and old mice skin (right) stained with picro-sirius red. Images were captured at 200x magnification using a DMI8 microscope.

**B.** The graph shows the comparison of epidermal thickness between adult (8-15 months) and old (31.5-33.5 months) mice skin. Thinning of the epidermis with increasing age was observed. Data were analysed by unpaired t-test; each graph represents the mean of 7 mice per age group with error bars indicating the standard error of the mean (SEM), and each dot represents one sample. Significant differences are denoted by \* for  $p<0.05$  with a p-value of 0.0301\*.

### 3.2 Effect of irradiation on epidermal thickness in mouse models

This experiment aims to investigate the effect of irradiation on epidermal thickness in mice. Cohort 1, consisting of 24 mouse samples, was divided into two groups, each containing 12 animals. One group received Sham-IR as the control, while the other group received three doses of 3Gy of X-ray irradiation (totalling 9Gy) at the age of 5-6 months. The mice were culled approximately 30 weeks post-IR at 12 months. Epidermal thickness was assessed using picro-sirius red/fast green staining and reported as length in perimeter ( $\mu\text{m}$ ).

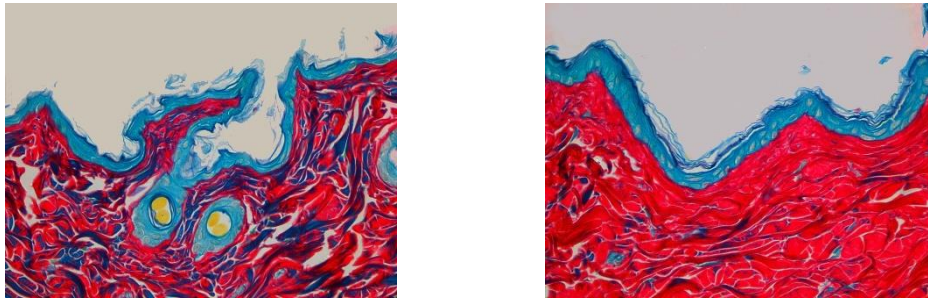
The results revealed a significant increase in epidermal thickness in the irradiated group compared to the control group. Specifically, the thickness of the epidermis significantly increased from  $6.298\mu\text{m} \pm 0.3051 \text{ SEM}$  ( $n=11$ ) in the control group to  $9.929\mu\text{m} \pm 1.104 \text{ SEM}$  ( $n=9$ ) in the irradiated group ( $p < 0.01$ ). This corresponds to a 57% increase in skin thickness, as illustrated in Figure 14B.

To assess the immediate effect of irradiation on epidermal thickness, cohort 2 was divided into two groups. Four mice received sham-IR as the control group, while the remaining eight animals received three doses of 3Gy of X-ray irradiation (totalling 9Gy) at 5-6 months. The mice were culled approximately 7-8 weeks post-IR at 7-8 months. Epidermal thickness was assessed using picro-sirius red/fast green staining.

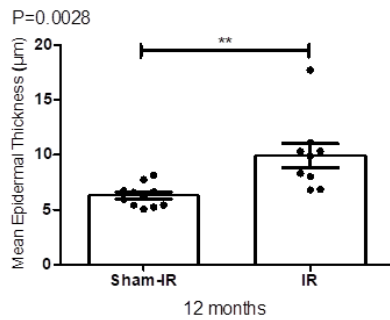
The result showed no significant change in epidermal thickness observed in mice 2 months post-irradiation. The thickness of the epidermis remained relatively similar, with measurements of  $10.69 \mu\text{m} \pm 0.8313 \text{ SEM}$  ( $n=8$ ) in the control group and  $10.91\mu\text{m} \pm 0.2395 \text{ SEM}$  ( $n=4$ ) in the irradiated group (Figure 14C).

Notably, the control group mice in cohort 2 exhibited epidermal thickness comparable to that of the IR-treated mice group in cohort 1. This observation suggests that factors other than irradiation may contribute to variations in epidermal thickness between different experimental cohorts.

A.



B.



C.

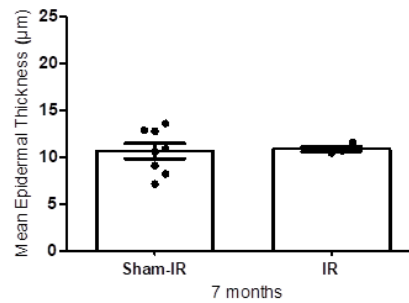


*Figure 14 Change in epidermal thickness before and after irradiation.*

**A.** Representative images of epidermis thickness in mice skin samples. The left image shows a control sample (sham-IR), while the right image shows a sample from the treated group after receiving three doses of 3Gy X-ray irradiation, totalling 9Gy. The mice were culled at the age of 12 months. The samples were stained with picrosirius red. Images were captured at 400X magnification using a DMI8 microscope.

**B.** Thickening of the epidermis resulting from irradiation was observed. The graph above shows the change in epidermal thickness compared between control (Sham-IR) and irradiated (IR) mice. The mice were culled at the age of 12 months. Data were analysed by unpaired t-test; the bar on the left (Sham-IR) represents the mean of 11 mice, and the bar on the right (IR) shows the mean of 9 mice with error bars representing the standard error of the mean (SEM), and each dot represents one sample. Significant differences are denoted by\*\* for  $p < 0.01$  with a p-value of 0.00258.

**C.** The graph shows the comparison between control (Sham-IR) mice (left) and irradiated (IR) mice (right). The mice were culled at the age of 7 months to observe the immediate effect of irradiation. No changes in epidermal thickness were observed. Data were analysed by unpaired t-test; the bar on the left (Sham-IR) shows the mean of 8 mice, while the bar on the right (IR) shows the mean of 4 mice, with error bars representing the standard error of the mean (SEM), and each dot represents one sample. No significant difference was observed, with a p-value of 0.8596.



### 3.3. Senolytic and senostatic treatments have no effect on epidermal thickness in irradiated mice

This study aimed to assess the effect of senolytic and senostatic treatment on epidermal thickness at different time points following irradiation in mice. Dasatinib+Quercetin (D+Q) or Navitoclax were administered as senolytic treatments, and Metformin served as a senostatic treatment. The treatments were initiated one-month post-irradiation and lasted for 2 weeks and 3 months, respectively. Skin samples were collected from irradiated mice at 3- and 12-months post-irradiation, with epidermal thickness evaluated using picro-sirius red/fast green staining, reported as length in perimeter ( $\mu\text{m}$ ).

At 3 months post-irradiation, neither Dasatinib+Quercetin (D+Q) nor Navitoclax induced significant changes in epidermal thickness compared to the gavage control group (D+Q:  $11.80 \mu\text{m} \pm 0.7002 \text{ SEM}$  (n=6) to  $11.30 \mu\text{m} \pm 0.5497 \text{ SEM}$  (n=6); Navitoclax:  $11.80 \mu\text{m} \pm 0.7002 \text{ SEM}$  (n=6) to  $10.16 \mu\text{m} \pm 0.2709 \text{ SEM}$  (n=5)) (Figure 15A).

Similar results were observed at 12 months post-irradiation, with neither with neither D+Q nor Navitoclax inducing significant alterations in epidermal thickness compared to the gavage control group (D+Q:  $11.06 \mu\text{m} \pm 0.8378 \text{ SEM}$  (n=7) to  $12.35 \mu\text{m} \pm 1.555 \text{ SEM}$  (n=8); Navitoclax:  $11.06 \mu\text{m} \pm 0.8378 \text{ SEM}$  (n=7) to  $13.77 \mu\text{m} \pm 1.529 \text{ SEM}$  (n=6)) (Figure 15B). There was also no change in epidermal thickness in the Metformin-treated group ( $10.38 \mu\text{m} \pm 0.6627 \text{ SEM}$  to  $8.393 \mu\text{m} \pm 0.9420 \text{ SEM}$ ) (n=5)) compared the soaked control (Figure 15C).

To test the effect of late senolytic treatment on irradiated mice epidermis, irradiated mice were subjected to senolytic (Dasatinib+Quercetin (D+Q) or Navitoclax) at 8 months after irradiation. The treatments were given and lasted for 2 weeks. Animals were culled at the age of 17 months. The epidermal thickness was analysed on picro-sirius red/fast green stained samples and reported as length in perimeter ( $\mu\text{m}$ ). Neither D+Q treatment ( $8.437 \mu\text{m} \pm 0.5160 \text{ SEM}$  (n=8) to  $9.900 \mu\text{m} \pm 0.7573 \text{ SEM}$  (n=9)), nor Navitoclax treatment ( $8.437 \mu\text{m} \pm 0.5160 \text{ SEM}$  (n=8) to  $8.850 \mu\text{m} \pm 0.4685 \text{ SEM}$  (n=12)) induced a change in epidermal thickness (Figure 15D).

These findings suggest that neither senolytic nor senostatic treatments significantly affected epidermal thickness in irradiated mice at different time points post-irradiation.

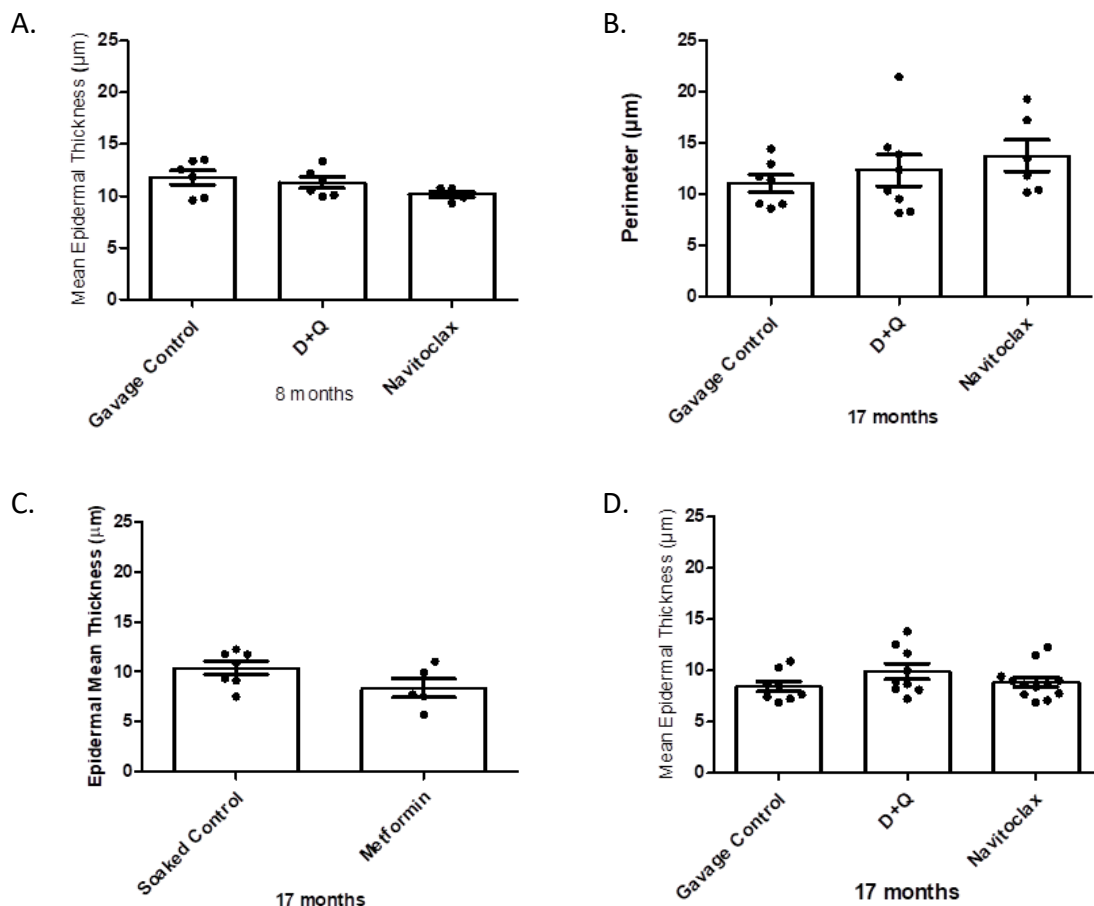


Figure 15 The change in epidermal thickness compared between non-treated and senolytic or senostatic -treated in irradiated mice.

**A.** The graph presents a comparison of epidermal thickness among three groups of mice: gavage control, Dasatinib+Quercetin (D+Q) treatment, and Navitoclax treatment. Mice were irradiated at 5-6 months of age and culled at 8 months. The treatments were administered one-month post-irradiation and lasted for two weeks. The data shows no significant change in epidermal thickness after senolytic treatment. Data were analysed using unpaired t-test, with each group (Gavage control; D+Q; Navitoclax) representing the mean of 6 mice. Error bars denote the standard error of the mean (SEM), and each dot represents one sample. No significant difference was observed between the gavage control group ( $p = 0.5901$ ), nor between the Navitoclax-treated group compared to the gavage control ( $p=0.0742$ ).

**B.** The graph presents a comparison of epidermal thickness among three groups of mice: gavage control, Dasatinib+Quercetin (D+Q) treatment, and Navitoclax treatment. Mice were irradiated at 5-6 months of age and culled at 17 months. The treatments were administered one-month post-irradiation and lasted for two weeks. Data were analysed by unpaired t-test. Gavage control (left) shows the mean of 7 mice, D+Q (middle) 8 mice and Navitoclax (right) 6 mice in SEM, with each dot represents one sample. No significant difference was observed between the gavage control and D+Q treated group, with a p-value of 0.4958; similarly, no significant difference was observed between the gavage control and Navitoclax-treated group, with a p-value of 0.1339.

**C.** The graph shows the comparison between control and Metformin-treated mice in term of epidermal thickness. The mice were irradiated at the age of 5-6 months and culled at 17 months. The treatment was administered a month after irradiation and lasted for three months. The soaked control group (left) illustrates the mean epidermal thickness of 7 mice, while the Metformin-treated group (right) represents the mean of 5 mice. Error bars indicate the standard error of the mean (SEM). Each dot on the graph represents one sample. Data were analysed using unpaired t-test, revealing no significant difference between the soaked control and Metformin-treated groups ( $p = 0.1046$ ).

**D.** The graph shows the comparison of epidermal thickness in three groups of mice samples: gavage control (left), D+Q-treated (middle) and Navitoclax-treated (right). The mice were irradiated at the age of 5-6 months and treatment were administered 8 months post-irradiation; The mice were culled at the age of 17 month to assess the late effects of senolytic treatment on epidermal thickness. The data shows no significant change in epidermal thickness following senolytic treatment with either D+Q or Navitoclax compared to the gavage control group. Each bar represents the mean epidermal thickness, with error bars indicating standard error of the mean (SEM). Data analysis was performed using unpaired t-test, showing no significant difference between the gavage control and D+Q-treated groups ( $p=0.1407$ ); no significant difference was observed between the gavage control and navitoclax-treated groups ( $p= 0.5701$ ). The number of mice per group were as follows: gavage control ( $n = 8$ ), D+Q-treated ( $n = 9$ ), and Navitoclax-treated ( $n = 12$ ).

### 3.4 No change in epidermal thickness with age in arm and buttock human skin samples

This experiment investigate the morphological changes associated with ageing in human skin samples obtained from both the arm and buttock regions. Samples were stained with picro-sirius red/fast green stained samples and reported as length in perimeter ( $\mu\text{m}$ ). Although not statistically significant, the data showed consistent trend towards reduction in epidermal thickness with increasing age in both the arm and buttock regions.

In the arm region, epidermal thickness decreased from  $63.51\mu\text{m} \pm 5.172 \text{ SEM}$  ( $n=5$ ) in young individuals to  $56.60\mu\text{m} \pm 1.831 \text{ SEM}$  ( $n=5$ ) in older individuals. Similarly, in the buttock region, epidermal thickness showed a decline from  $73.28 \mu\text{m} \pm 4.045 \text{ SEM}$  ( $n=5$ ) in young individuals to  $63.96 \mu\text{m} \pm 0.5346 \text{ SEM}$  ( $n=3$ ) in older group.

These findings collectively provide robust evidence of age-related changes in epidermal thickness, suggesting a consistent pattern of reduction across different anatomical regions of the body.

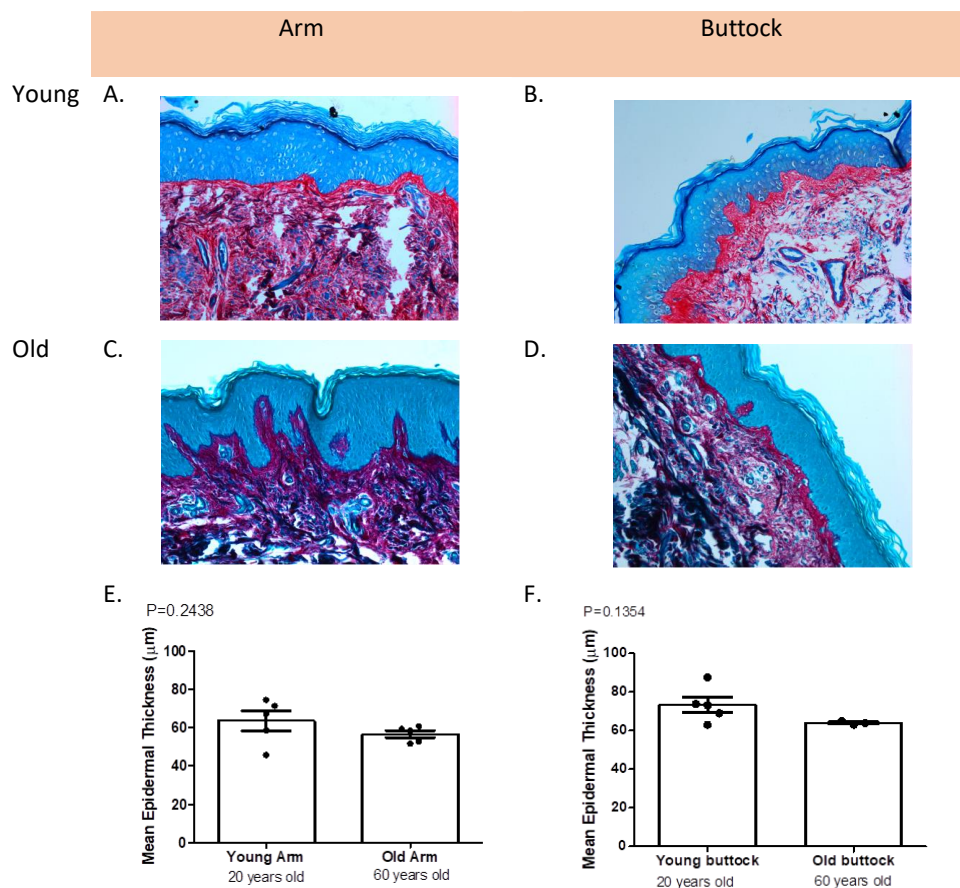


Figure 16 The change in epidermal thickness with age compared between arm and buttock human skin samples.

**A-D** Representative images of young (20 years old, A&B) and old (60 years old, C&D) human skin samples obtained from both arm (A & C) and buttock (B & D) regions. The samples were stained with picro-sirius red for enhanced visualisation and imaged at 200x magnification using a DMI8 microscope.

**E.** The graph presents the comparison of epidermal thickness between young (20 years old) and old (60 years old) human arm skin samples. Data analysis was performed using a unpaired t-test. Each bar represents the mean epidermal thickness of 5 individuals per age group, with error bars indicating the standard error of the mean (SEM). No significant change in epidermal thickness was observed, with a trend towards epidermal thinning observed with increasing age in arm.

**F.** The graph presents a comparison of epidermal thickness between young (20 years old) and old (60 years old) human buttock skin samples. Young buttock samples comprised 5 individuals, while old buttock samples comprised 3 individuals. Data analysis, performed using an unpaired t-test, revealed no significant difference in epidermal thickness between young and old buttock skin samples, with p-values of 0.2438 and 0.1354, respectively.

### **3.5 Changes in epidermal thickness compared between region: sun-exposed (arm) and sun-protected (buttock) skin samples in human**

This study investigate the regional variation in epidermal thickness within different age groups of human skin samples obtained from the arm and buttock regions. Skin samples were collected from individuals aged between 20 and 60 years old and compared between sun-exposed (arm) and sun-protected (buttock) conditions. The epidermal thickness was analysed on picro-sirius red/fast green stained samples and reported as length in perimeter ( $\mu\text{m}$ ).

In the comparison of epidermal thickness between young arm and young buttock skin samples (Figure A), there was no significant change observed. Data analysis, utilizing unpaired t-tests, revealed similar epidermal thickness between the buttock epidermis ( $73.28 \mu\text{m} \pm 4.045 \text{ SEM}$ ,  $n=5$ ) and the arm epidermis ( $63.51 \mu\text{m} \pm 5.172 \text{ SEM}$ ,  $n=5$ ) in younger donors.

However, skin samples from the older donors showed a thicker epidermis in the buttock region ( $63.96 \mu\text{m} \pm 0.5346 \text{ SEM}$ ,  $n=3$ ) compared to the arm region ( $56.60 \mu\text{m} \pm 1.831 \text{ SEM}$ ,  $n=5$ ) (p-value  $<0.05$ ) (Figure 17 B). The significance of this finding may be influenced by the smaller sample size of old buttock samples, indicating the need for further investigation with a larger sample size to validate these results.

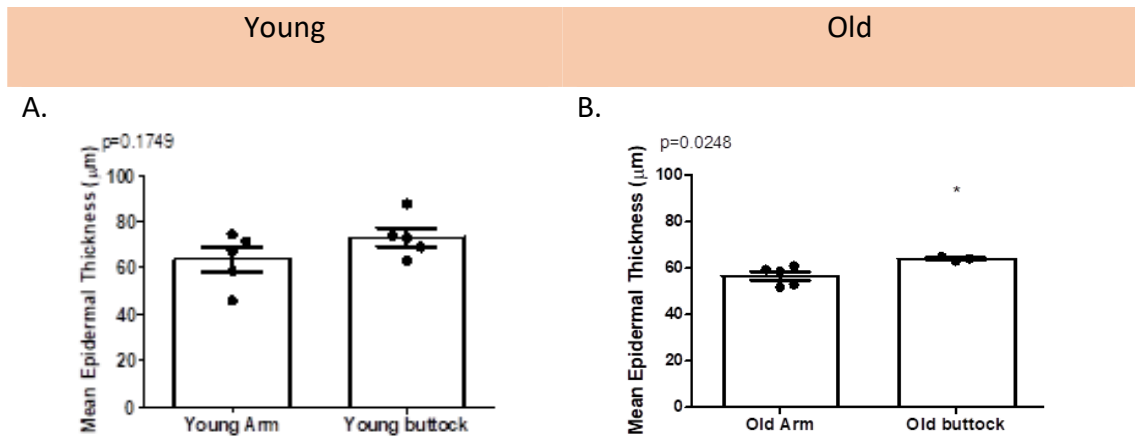


Figure 17 The change in epidermal thickness compared between arm and buttock human skin samples.

**A.** The graph shows the comparison of epidermal thickness between young arm and young buttock skin samples to investigate regional variation within the same age group and assess potential effects of sun exposure. Data analysis was performed using unpaired t-test, with each bar representing the mean of 5 individuals per age group with standard error of the mean (SEM). No significant difference was observed between the two groups, with a p-value of 0.175.

**B.** The graph compares epidermal thickness between old arm and old buttock skin samples. The arm group comprises 5 samples, while the buttock group consists of 3 samples. Data analysis was performed using unpaired t-tests, with standard error of the mean (SEM) represented. A significant difference was found, with the older buttock group exhibiting thicker epidermal thickness compared to the older arm group (p-value = 0.025).

### 3.6 Discussion

At present, there is limited literature demonstrating changes in mice's skin epidermal thickness with age. However, in humans, epidermal thinning occurs over time as a result of decreased proliferation and renewal capacity of basal keratinocytes, along with a reduced number of epidermal stem cells (Kligman A. , 1979; Montagna & Carlisle, 1979; Mimeault & Batra, 2010; Dreesen, et al., 2013; López-Otín, Blasco, Partridge, Serrano, & Kroemer, 2013). This experiment has shown that like in humans, mice's epidermis, too, showed a 30% notable attrition of epidermal thickness with age. Although therapy-induced mouse models show signs of premature ageing in different tissues with higher frequencies of senescent cells in the liver and hippocampus as well as higher SASP production (Fielder, et al., 2019), in the skin, it showed approximately a 57% increase in epidermal thickness 6 months- post- irradiation. Short-term effects might differ but were not assessed.

To test the hypothesis regarding the potential of anti-senescence intervention in mitigating therapy-induced skin ageing by targeting senescent cells, irradiated mouse models treated with either senolytic (Dasatinib+Quercetin (D+Q) or Navitoclax) or senostatic (Metformin) and compared to non-treated groups. The data indicates that neither D+Q nor Navitoclax reduced epidermal thickness at the different treatment timepoints. In the second set of experiments (Figure 14C), the epidermal thickness in the non-irradiated control group was found to be similar to that observed in the irradiated mice from the first experiments (Figure 14B). One potential explanation for the observed differences could be the technical variability in sample collection and processing. Differences in the angle of incidence during the collection of full-thickness cross-sections or variations in the embedding process might have contributed to discrepancies in epidermal thickness measurements between the two cohorts. Additionally, the fact that skin samples from Cohort 1 were collected in 2018, while those from Cohort 2 were collected in 2019 and handled by different technicians, introduces the possibility of inter-laboratory variability. The age at the time of sample collection and environmental influences may have influenced the skin phenotype and contributed to the differences observed between cohorts. It's worth noting that our lab procedure is standardized for housing conditions, ensuring consistency in factors such as cage size and the number of mice in each cage. However, factors that could not be controlled, such as mouse behaviour (including activity levels, grooming behaviour, and stress responses), may also influence skin physiology and

epidermal thickness. Additionally, the smaller sample size in Cohort 2 compared to Cohort 1 could have impacted the statistical power and precision of the results.

Early treatment of senostatic (Metformin) demonstrated a trend towards a reduction in signs of epidermal thickness. In a previous study, epidermal thinning was found in aged mice compared to young mice, and Navitoclax (ABT-263 and ABT737) was effective in rescuing epidermal thickness (Kim, et al., 2022). It is likely that there are distinct molecular mechanisms underlying natural and stress-induced skin ageing. Further work is required to determine the causes of heterogeneity between these models, and the effects of senolytic treatments.

In human, no significant change, but rather a trend toward epidermal thinning, was observed with age in both sun-exposed and sun-protected area. Region comparisons were performed between sun-exposed (arm) and sun-protected (buttock) area. However, it is important to note that the comparison between regions may not be entirely accurate, as epidermal thickness varies across different body sites. For instance, the thickness of epidermal layer in the buttock region is influenced not primarily by UV damage, but by factors such as blood content, which can be quantified using a skin reflectance meter (quantification of light absorption) (Sandby-Møller, Poulsen, & Wulf, 2003). Therefore, a more precise measure for assessing skin ageing would be comparing samples from the same region, but on opposite sides of a tan line. For example, comparing the upper arm, which is frequently covered by clothing sleeves, with a lower region that is not covered.



## Chapter IV 2D drug screening to test the effect of senolytics in dermal fibroblasts viability

### 4.0 Introduction

In this set of experiments, various compounds were received from a pharmaceutical client company (NOVOS) to assess the anti-senescence effects of the active compounds in their core product. NOVOS is a nutraceutical company that specialises on developing science-based nutraceuticals to slow down ageing and improve longevity. There were two main formulas of the supplemental drink provided by the pharmaceutical client company known as NOVOS Core and NOVOS Boost (NOVOS Core+ NMN). The Novos Core consists of several natural ingredients, including Fisetin, Magnesium, Glycine, Glucosamine Sulfate, Pterostilbene, Hyaluronic Acid, Rhodiola Rose, L-Theanine, Lithium Aspartate, Ascorbic acid, Malate, Gingerol, and Calcium Alpha-Ketoglutarate. NOVOS Boost contained all the ingredients in NOVOS core with an addition of nicotinamide mononucleotide (NMN). While some of these compounds, such as Glycine and Ascorbic acid, can be synthesized or obtained through diet, others like Fisetin and Pterostilbene are naturally occurring substances found in select foods or plants. Their levels in the body may not necessarily diminish with age as they depend on factors like dietary habits and lifestyle choices.

Research has demonstrated the accumulation of senescent cells in various tissues, contributing to the ageing processes. Longevity-promoting compounds have been shown to impact senescent cells by either preferentially killing senescent cells (senolytic) or by suppressing the senescent phenotypes (senostatics or senomorphic). This potentially includes Fisetin, pterostilbene, *Rhodiola rosea*, alpha-ketoglutarate and gingerols, all which are present in the provided product.

Dr. Edward Fiedler assessed the solubility of the core products in two different solvents: water and ethanol. A dose-response series was then applied to a combination of young proliferating HDFs and deep-senescent HDFs, where serial half dilutions of NOVOS Boost were tested for 3 days, cell numbers and size were recorded. In parallel, I evaluated the senolytic activity of the 9 individual ingredients from the product, followed by NOVOS Core and NOVOS Boost over a wide concentration range on both young and senescent human skin fibroblasts. However, some ingredients, including Magnesium, Hyaluronic acid, and Malate, were not provided for testing from the company, and thus, were not included in this experiment. Additionally, Calcium Alpha-Ketoglutarate was excluded due to solubility issues.

#### 4.1 Screening of natural compounds for their possible senolytic effects on skin fibroblasts

In this experiment, senolytic activity of several compounds with reported 'anti-ageing' properties on dermal fibroblasts were assessed.

The first compound tested was *Rhodiola rosea* which contains salidroside, flavonoids, terpenoids, sterols, tannins and many other compounds that work together, providing antioxidant, anti-inflammation, anti-fatigue, and antidepressant effects. Numerous studies have demonstrated the therapeutic effect of *Rhodiola rosea* in a variety of age-related diseases, including Alzheimer's disease (AD), Parkinson's disease (PD), cerebrovascular disease, diabetes, and cardiovascular disease (CVD) (for references, see (Zhuang, et al., 2019)). In this experiment, the maximum concentration of *Rhodiola rosea* tested was 2 mM. Our finding showed no senolytic effect in skin fibroblasts, but the treatment of *Rhodiola rosea* dramatically reduced viability of proliferating cells at 0.2mM, while only reducing viability of the senescent cells by 10% at 0.5 mM (Figure 18A).

Fisetin, a bioactive flavonol molecule typically found in fruits and vegetables at a concentration of 2-160 µg/g (Arai, et al., 2000). The average daily intake of Fisetin is recommended at about 100-500 mg. It can effectively scavenge free radicals, which contribute to oxidative stress, and has been shown to improve lifespan and reduce age-related pathology in mice. It also exhibits senolytic activity in endothelial cells (Zhu, et al., 2017). However, there are contradictory results regarding its senolytic activity in fibroblasts (Zhu, et al., 2017), (Yousefzadeh, et al., 2018). Our findings demonstrate that Fisetin ultimately led to the elimination of proliferating cells at 0.1 mM when tested at doses ranging from 0.01 mM to 0.4 mM. However, its effective dose for senescent cells was higher, indicating no specific senolytic activity for human dermal fibroblasts (Figure 18B).

Lithium, a trace mineral that can be found in grains and vegetables (Schrauzer , 2002), has been acknowledged as one of the most promising senolytic compounds. It has been demonstrated potential in reducing cellular senescence in human astrocytes by inhibiting SASP production (Viel, et al., 2020). In this experiment, a clear senolytic effect was observed within a specific dosage range of 0.003 mM to 0.1mM, with no significant impact on proliferating cells (Figure 18C).

Glucosamine sulfate (GS) plays an essential role in the biosynthesis of glycolipids, glycoproteins, glycosaminoglycans (GAGs), hyaluronate, and proteoglycans which are essential in maintaining skin ageing. The maximum concentration of Glucosamine sulphate (GS) tested was 1 mM. The data showed GS has no significant senolytic effect but a trend towards reduction in senescent cells within a very narrow window dosage range, specifically 0.1mM (Figure 18D).

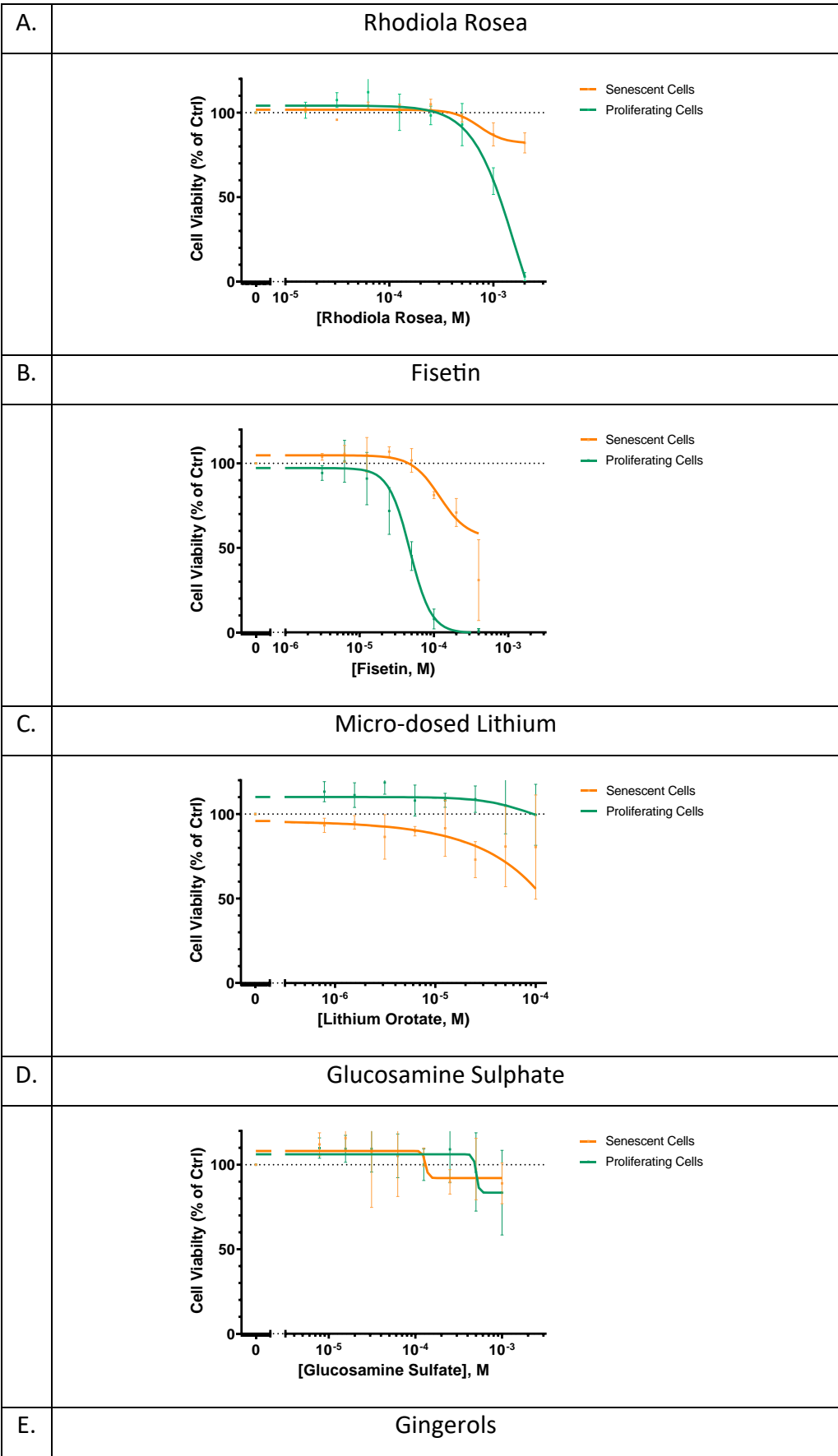
Gingerols, phenolic phytochemical compounds found in fresh ginger, inhibit proinflammatory cytokines such as IL-1, IL-8, and TNF- $\alpha$  (Nair, Gopi, & Jacob, 2021). Our findings show that Gingerol showed no significant senolytic effect but a trend towards 30% reduction in senescent cells at 0.1 mM, while the reduction in proliferating cells occurred at a slower rate as the dosage increased (Figure 18E).

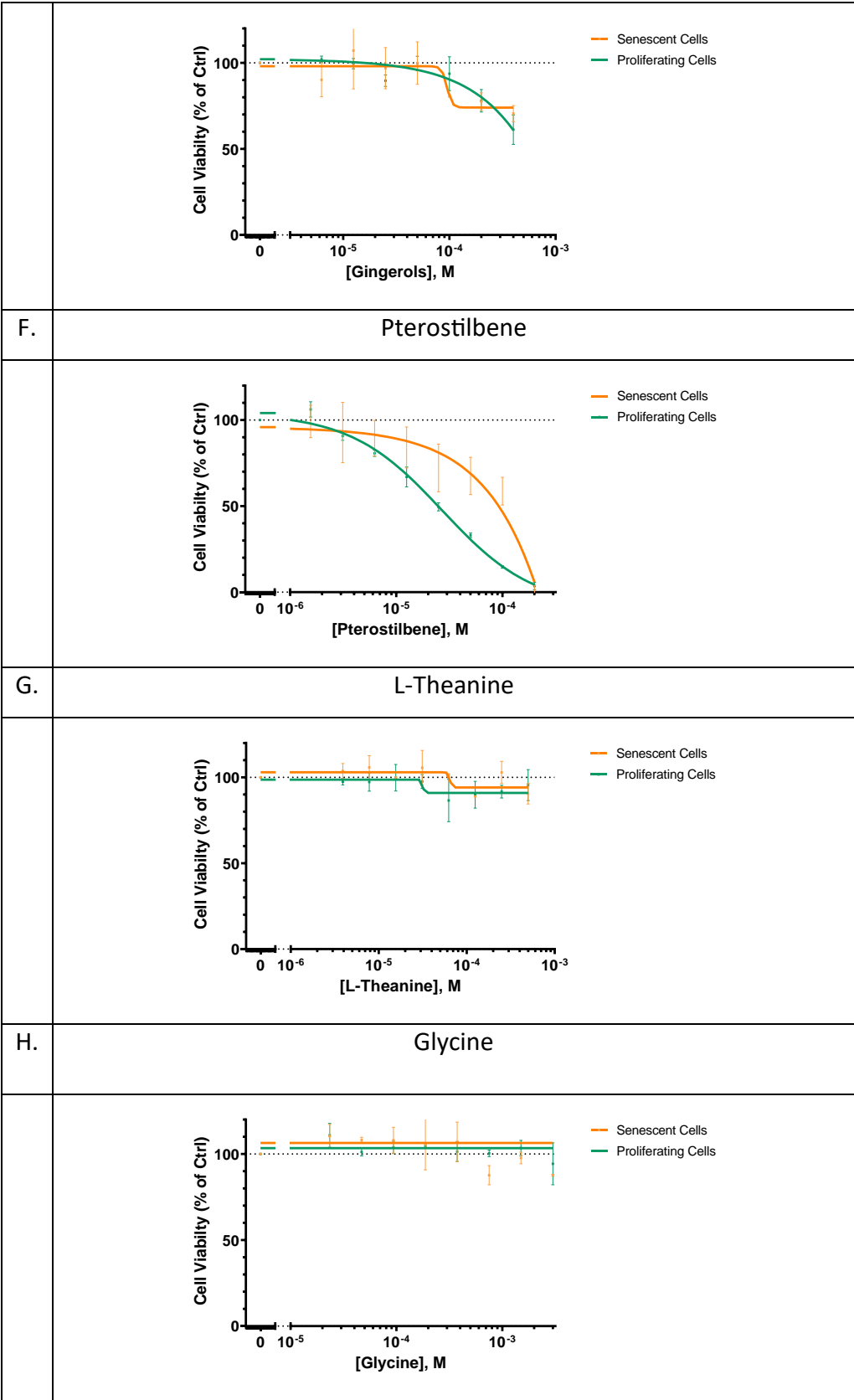
Pterostilbene (PTS), a naturally demethylated analogue of resveratrol is primarily found in blueberries. It has been reported that daily consumption of 100 or 250mg of PTS is able to lower high cholesterol level. Our data showed that treatment with PTS in the 10 -100 mM range removed proliferating cells quicker than the senescent cells (Figure 18F).

L-theanine is a non-protein amino acid derived from green tea (Sharma, Joshi, & Gulati, 2018) and has been reported to effectively inhibit the formation of advanced glycation end products (AGEs) (Culetu, Fernandez-Gomez, Ullate, del Castillo, & Andlauer, 2016). Our finding showed very little effect on cell viability for proliferating and senescent cells up to almost 1 mM (Figure 18G).

Glycine is the most abundant amino acid in collagen and one of the essential amino acids in the body for synthesising the antioxidant glutathione. The human body can produce glycine naturally, but it can also be derived from high protein intake. In this experiment, glycine showed no effect on cell viability in both proliferating and senescent cells within the tested dosage ranging from 0.01 mM to 3 mM (Figure 18H).

Ascorbic acid, or Vitamin C, can be found in fruits and vegetables. Similar to glycine, ascorbic acid did not have a negative effect on cell viability in both proliferating and senescent cells, even at dosages ranging from 0.001 mM to 0.2 mM (Figure 18).





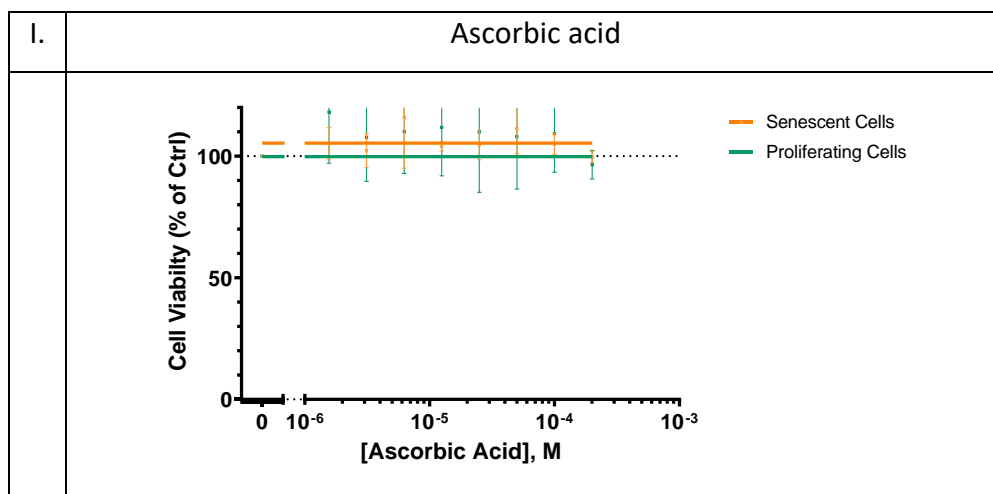


Figure 18 Individual natural compound senolytic efficacy test on cell viability of senescent and proliferating human skin fibroblasts.

**A.-I.** The graphs above show the concentration range of the compounds tested and their impact on cell viability. The orange line represents senescent cells, while the green line represents proliferating cells. The cells were exposed to the compound for 3 days, followed by crystal violet staining. The viability percentage presented relative to the absorbance of untreated control cells at day 3. Between 2 and 4 independent experiments were conducted. Data is presented as titration curves with moving averages, and the standard error of the mean (SEM) for the experiments is indicated.

#### 4.2 Screening of the mixture of natural compounds for their possible synergisms of senolytic effects on skin fibroblasts

After conducting individual tests for each compound, the combination of all the active compounds (NOVOS Core) and NOVOS Boost (NOVOS Core +NMN) was evaluated for potential synergistic senolytic effects on skin fibroblasts. A mixture of half DMSO and half H<sub>2</sub>O served as the solvent for dissolve the formula.

NOVOS Core comprises various natural ingredients, including Fisetin (100mg), Magnesium (304mg), Glycine (2000mg), Glucosamine Sulfate (1000mg), Pterostilbene (50mg), Hyaluronic Acid (100mg), Rhodiola Rose (300mg), L-Theanine (150mg), Lithium Aspartate (20mg), Ascorbic acid (100mg), Malate (1700mg), Gingerol (100mg), and Calcium Alpha-Ketoglutarate (231mg). The highest tested concentration was 4 ug/ml. The results show a possible reduction of senescent fibroblast viability at a dosage of 0.8ug/ml, however, viability of proliferating cells was very similarly reduced (Fig. 19A).

The second compound tested was the combination of NOVOS Core with a boost of nicotinamide mononucleotide (NMN) (250mg), denoted as NOVOS Boost. Variants of NOVOS Boost were tested with sequential half dilutions of NMM. NOVOS Boost exhibited a gradual reduction of senescent cells within a dose range of 1 ug/ml to 2.5 ug/ml. Proliferating cells, on the other hand, showed a sharp 20% reduction at 2ug/ml (Figure 19B).

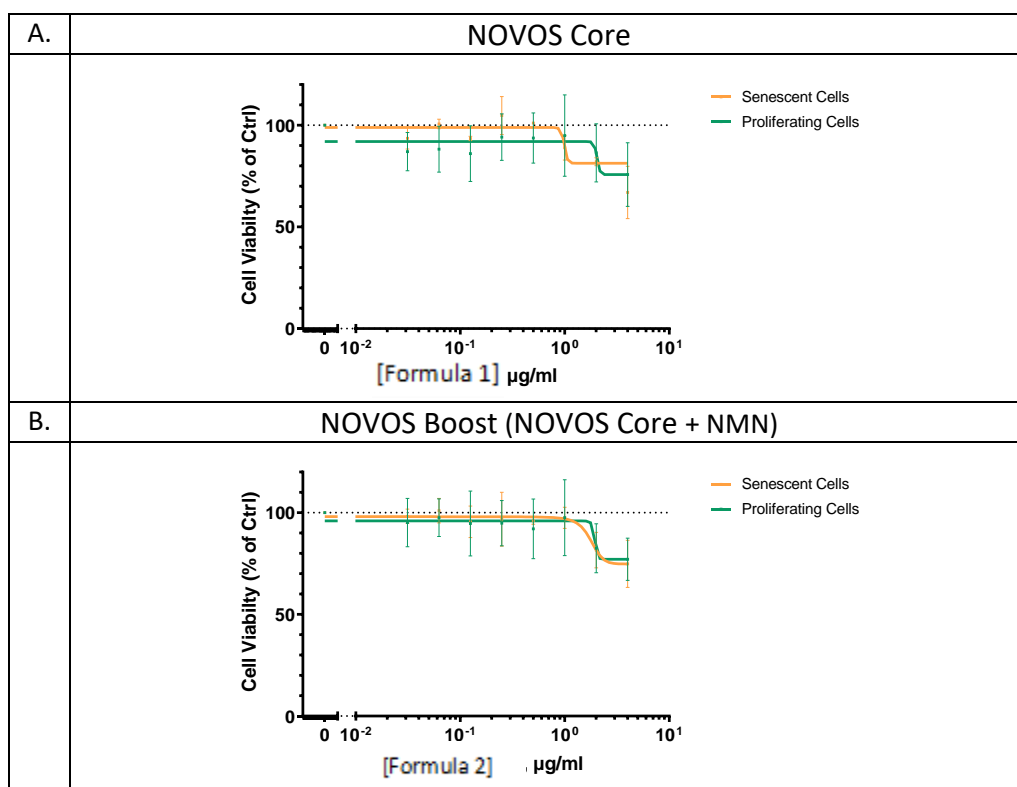


Figure 19 Mixture of natural compound senolytic efficacy test on cell viability of senescent and proliferating human skin fibroblasts.

**A.-B.** The graphs above show the concentration range of the compounds tested and their impact on cell viability. The orange line corresponds to senescent cells, and the green line represents proliferating cells. Cells were subjected to the respective compound for a duration of 3 days, followed by crystal violet staining. The viability percentage is presented relative to the absorbance of untreated control cells at day 3. Between 2 and 4 independent experiments were carried out. Data is presented as titration curves with moving averages, and the standard error of the mean (SEM) for the experiments is indicated.

### 4.3 Further assessment of senolytic and senostatic activity of NOVOS Boost in co-culture assay

The following experiments were conducted by Dr. Edward Fiedler. This assay combines proliferating young cells with cells that have undergone stress-induced senescence in a single well, mimicking the situation *in vivo* where non-senescent and senescent cells coexist.

In this assay, senescent cells, induced by high-dose X-ray radiation, were labelled in green, while proliferative young cells were labelled in red. After allowing senescent phenotypes to develop over a period of 10 days, young cells were subsequently added to the well. The primary objective of these experiments was to assess the senolytic and senostatic potential of compounds.

Both populations were tracked using fluorescent markers to assess the changes in cell number and morphology over time. The result shows a reduction in proliferation of young cells with increasing concentration of the stock solution, while no reduction was observed in senescent cells, indicating no senolytic response (Figure 20b). However, a reduction in the size of senescent cells was noted at higher concentration, suggestive of a senostatic response (Figure 20c). These findings were further validated through manual analysis of the images (Figure 20d-e).

The highest concentrations of the ethanol-dissolved stock solution (2% solution in media) lead to a reduction in cell size of senescent cells (Figure 21a). Reductions in size in a selection of individual senescent cells are shown (Figure 21b). No significant change in senescent cell number was observed with increasing concentration, although a drop in young cell proliferation was seen by automated analysis (Figure 21c). Higher concentrations of the stock solution resulted in a dose-dependent reduction in the size of senescent cells (Figure 21d) as confirmed manual analysis (Figure 21e-f).



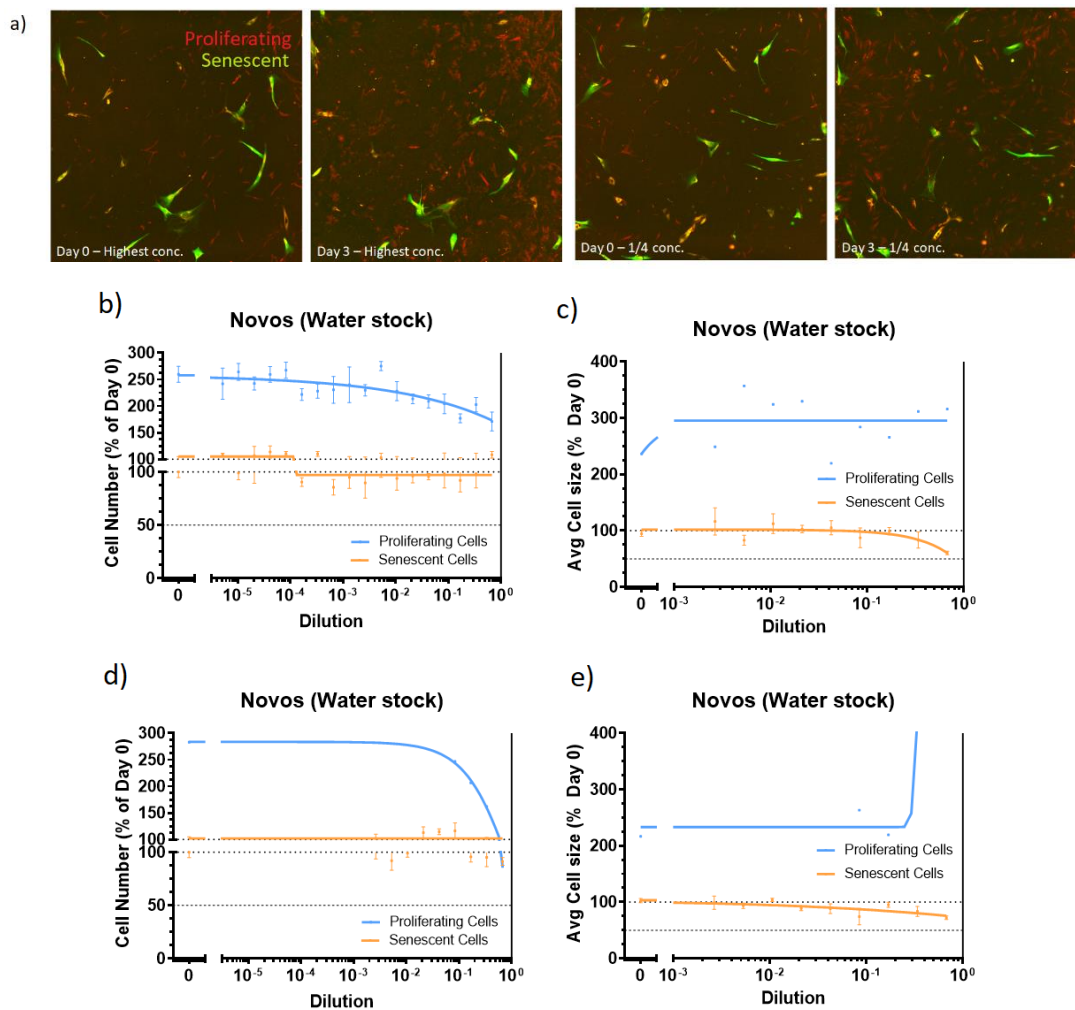


Figure 20 Dose response curves using water solvent stock.

Experiment conducted by Dr. Edward Fiedler involving the treatment of cells with different concentrations of a water-based stock solution.

**A.** Example images were captured before and after 3 days of treatment with 67.6% water stock in media, and a  $\frac{1}{4}$  of this dose. Notably, there was a deposition of material observed in the highest concentration, potentially due to lack of filter sterilisation. Green-labelled cells represent senescent cells and red-labelled cells represent young proliferative cells. In the images, green-labelled cells represent senescent cells, while red-labelled cells represent young proliferative cells. **B.** Automated analysis of cell number change for proliferating and senescent cells. **C.** Automated analysis of the change in average cell size for proliferating and senescent cells. **D-E.** manually performed quantification of the images used for b-c.

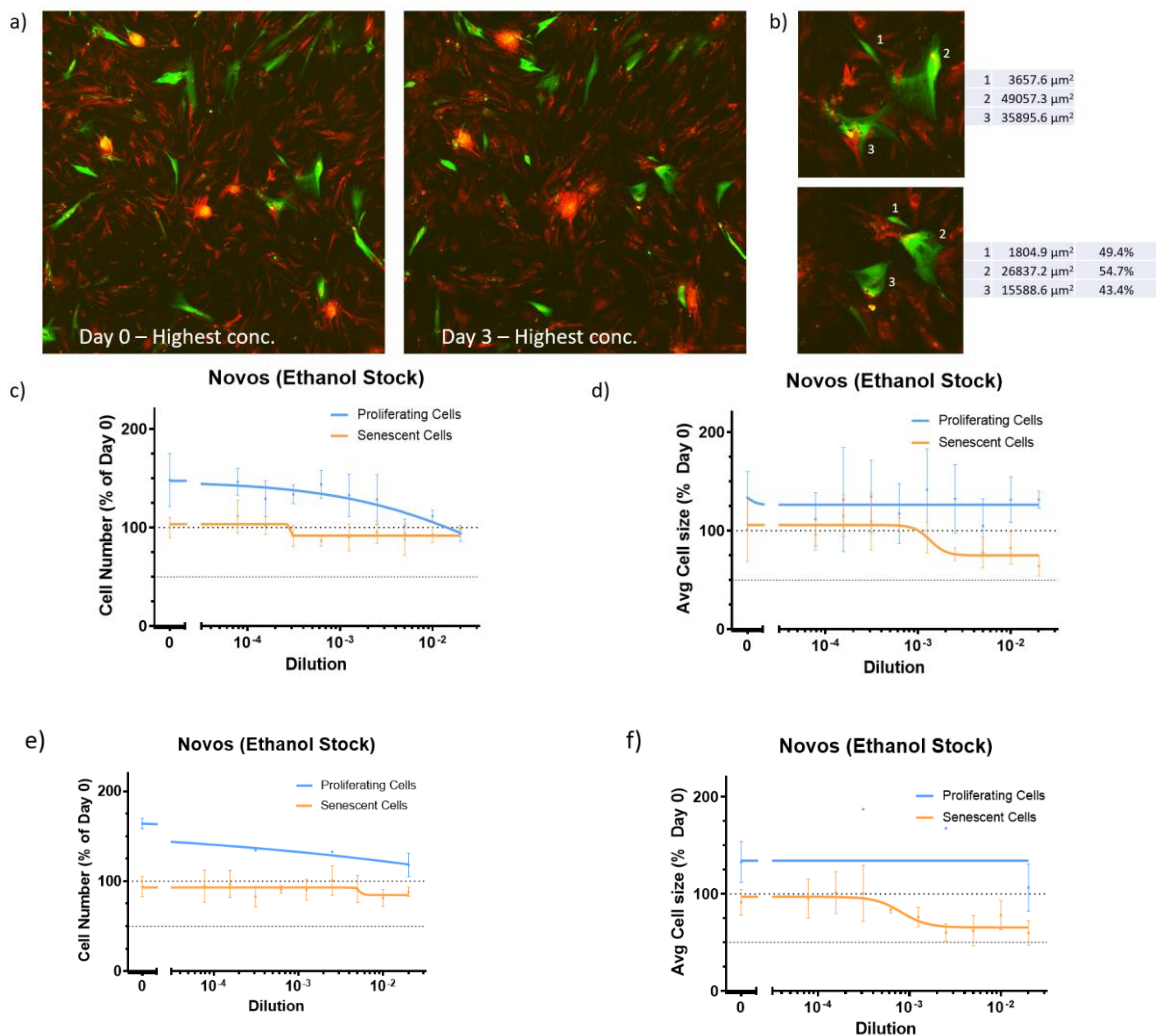


Figure 21 Dose response curves using ethanol solvent stock.

Experiment conducted by Dr. Edward Fiedler involving the treatment of cells with a 2% Ethanol stock solution in media.

**A.** Example images were captured before and after 3 days of treatment to observe the effects on cell behaviour. **B.** Changes in individual senescent cells on day 0 (top) and day3 (bottom) were recorded, cells labelled 1-3 along with their individual cell size in  $\mu\text{m}^2$  and percentage change. **C.** Automated analysis of cell number change for proliferating and senescent cells. **D.** Automated analysis of the change in average cell size for proliferating and senescent cells. **E-F.** manually performed quantification of the images used for c-d.

#### 4.4 Discussion

This experiment aimed to validate the effects of various compounds against the previous studies and assess their senolytic efficacy. Each ingredient was individually tested across a wide concentration range on both young and senescent human skin fibroblasts. Senescent cells were used in this experiment because they represent a biologically relevant model for studying ageing. As mentioned in section 3.0, senescent cells accumulate over time due to factors such as ageing and DNA damage, contributing to various age-related deteriorations. Unlike quiescent cells, which enter a reversible growth arrest state due to lack of nutrition and growth factors, senescent cells undergo irreversible growth arrest. This characteristic makes senescent cells particularly suitable for studying the long-term effects of cellular senescence and investigating interventions targeting senescent cells. Additionally, we explored whether these ingredients exhibited synergistic senolytic effects. Some compounds such as Glucosamine sulphate, gingerols, micro-dose of lithium and L-Theanine demonstrated a small potential therapeutic window of senolytic activity at specified dosages.

*Rhodiola rosea*, while known for its various therapeutic effects, did not exhibit a senolytic effect on skin fibroblasts. Instead, we observed some degree detrimental effect on cell viability at the dosage of 0.2mM. Our finding shows that 0.1 mM of Fisetin ultimately killed off proliferating fibroblasts but not the senescent cells. Instead, the number of senescent cells gradually reduce at a dosage of 0.05 mM in dermal fibroblasts. A previous study demonstrated that treatment with 0.01mM Fisetin for 3 days can effectively eliminate senescent HUVECs by inducing apoptosis. The same effect does not present in IMR90 cells or human preadipocytes (Zhu, et al., 2017). (Yousefzadeh, et al., 2018) then confirmed that 0.005 mM Fisetin treatment is able to reduce senescence in murine embryonic fibroblasts (MEFs) and IMR90 cells in a dose-dependent manner without affecting proliferating cells. Fisetin induces apoptosis, as measured by caspase 3/7 activity, but in MEFs, Fisetin suppressed markers of senescence (Sen- $\beta$ -gal). This suggests that Fisetin's senolytic effect may be specific to certain cell types targeting different senescence pathways.

While high doses of lithium can have detrimental effects to cell viability, microdoses of this mineral have demonstrated remarkable benefits, including lifespan extension in various model organisms such as flies and *C. elegans* (Castillo-Quan, et al., 2016; McColl, et al., 2008). In *C.elegans*, 0.01mM of Lithium led to a reduction in mortality, while 0.001mM showed no

effect; additionally, in a human study involving 1 million individuals, long-term consumption of lithium in drinking water ranging from 0.7 (0.1 $\mu$ M) to 59  $\mu$ g/L (8.5 $\mu$ M) reduced overall mortality (Zarse, et al., 2011). Our data showed a clear senolytic effect within a specific dosage range of 0.003 mM to 0.1mM without significant impact on proliferating cells. The upper range of Lithium observed in the human and *C. elegans* study falls within the range of the concentrations tested in our experiments, while the lower end concentrations in our study falls within the observed range in (Zarse, et al., 2011). This significant overlap strongly implies that Lithium may have a senolytic effect.

Glucosamine is an amino sugar synthesized from glucose and glutamine, existing in two primary forms: glucosamine hydrochloride (GHCL) and glucosamine sulphate (GS). Both forms are readily absorbed through oral administration. However, GS must be stabilised with salt with salt resulting in 74% purity as compared to the more stable GHCL at 99% purity (Owens, Wagner, & Vangsness, 2004). There are several clinical studies have shown GS's positive impact on osteoarthritis (Reginster, et al., 2001) and skin ageing (Bissett , 2006) by the stimulation of hyaluronic acid synthesis. However, none has shown the effects of GS on skin fibroblast. In human chondrocytes *in vitro* studies, GS treatment ranging from 0.05mM to 10mM significantly increased protein synthesis (Piperno, et al., 2000), inhibit NF- $\kappa$ B activation (Largo, et al., 2003) and oxidative stress (Calamia, et al., 2010) when stimulated with IL-1  $\beta$ . Our study showed a subtle but not significant senolytic effect albeit within a very narrow dosage range. This effect may be differed to certain cell types.

Gingerols are polyphenolic compounds found in fresh ginger. The major gingerols include 6-gingerol, 8-gingerol, and 10-gingerol. With heat treatment or long-time storage, gingerols can be transformed into shogaols, which are the dehydrated forms of gingerols. While there was limited evidence suggesting that gingerol acts as a senolytic, the dehydrated form of gingerols, shogaol, has demonstrated cytoprotective, anti-apoptotic, and antioxidant effects in HDFn. The treatment of shogaol showed no negative effect to cell viability to HDFn at concentration of 0.005, 0.01, 0.02, and 0.04mM. In UVA-induced senescent HDFn, cell viability increased upon shogaol treatment in a dose-dependent manner up to 0.02mM (Han, et al., 2018). In our study, we further study the dosage range up to a maximum of 0.4mM. Similarly, no detrimental effect on cell viability was observed within the tested range. While no significant senolytic effect was observed, there was a trend towards reduction in senescent cells at a

higher dose of 0.1mM. Proliferating cells gradually reduced in a dose-dependent manner from 0.1mM to 0.4mM.

Pterostilbene (PTS) has been identified as a potential senolytics due to its ability to modulate various hallmarks of ageing, such as oxidative stress, inflammation, telomere attrition and cellular senescence (Li, Li, & Lin, 2018). PTS is structurally similar to resveratrol but exhibits better bioavailability due to the presence of two methoxy groups. This increased lipophilicity, improves oral absorption, potential for cellular uptake, and a longer half-life compared to resveratrol (McCormack & McFadden, 2012). *In vivo* study using rat models have demonstrated that pterostilbene has an 80% bioavailability while resveratrol has a lower bioavailability of 20% via oral administration (Kapetanovic, Muzzio, Huang, Thompson, & McCormick, 2011). In experiments involving HaCaT keratinocytes, treatment with 0.02mM of PTS did not affect cell viability. Additionally, it significantly reduced particulate matter (PM)-induced intracellular ROS production, inhibited PM-induced Mitogen Activated Protein Kinases (MAPKs), inflammation (COX-2), and aging (MMP-9), and rescued moisturizing protein expression (AQP-3) (Teng, Huang, Wang, Tseng, & Yen, 2021). However, in our study, at a lower concentration of 0.002 mM, PTS reduces cell viability to proliferating cells more rapidly than the senescent cells.

L-theanine is a non-protein, water soluble amino acid found in tea plants (Saeed, et al., 2020). It is renowned for its health benefits *in vivo*, including antioxidant effects (Tsai, et al., 2019; Deng, et al., 2016), anti-inflammatory effects in conditions such as osteoarthritis (Bai, et al., 2020), inflammatory bowel disease (Chen, et al., 2020) and acute liver injury (Wang, et al., 2018)., Additionally, it provides neuroprotective effects (Takeshima, Miyazaki, Murakami, Kita, & Asanuma, 2016), anticancer (Fan, et al., 2021; Liu, et al., 2016), immune regulatory effects (Li, et al., 2016), and anti-obesity effects (He, et al., 2021). In *in vitro* studies, treatment with 0.05mM L-theanine led to an increase in cell proliferation and glucose consumption in human Sertoli cells (hSCs), thereby improving mitochondrial membrane potential and balancing the prooxidant -antioxidant state (Dias, et al., 2019). Additionally, exposure to 2 or 3 days of 0.25mM of theanine treatment reduced the migration ratio by 44% in Human cervical cancer cell lines (HeLa), associated with increased apoptosis (Liu, et al., 2016). So far, there is no evidence of detrimental effect on cell viability associated with L-theanine in mammalian system, suggesting its general tolerance. In our study, we found that L-theanine showed no beneficial or detrimental effects up to 0.5mM. Further assessment with higher dosages of L-

theanine treatment should be conducted to investigate its impact on both young and senescent dermal fibroblasts cells.

Glycine supplementation has been shown to extend the lifespan in various organisms, including mice (Miller, et al., 2019) and *C. elegans* (Liu, et al., 2019). Studies have demonstrated that defects in glycine metabolism in the mitochondria lead to downregulating the SHMT2 and GCAT expressions, which are essential for the mitochondrial translation activity, resulting in age-associated respiration defects (Hayashi, et al., 1994; Locasale, 2013; Edgar & Polak, 2000). Administration of 0.14mM glycine for 10 days to the culture medium of 97-year-old human diploid fibroblast cell line restored the respiratory function (Hashizume, et al., 2015). In our experiment, glycine showed no effect on cell viability in both proliferating and senescent cells within the tested dosage ranging from 0.01 mM to 3 mM. The differences of the cell type used, and the duration of the treatment could account for variations in the data. However, this suggests that glycine has no negative effect on cell viability.

Studies have reported that ascorbic acids (AA) is protective against senescence via ROS scavenging in mesenchymal stem cells (Yang, et al., 2018), protection against apoptosis in skin and hair (Wakame, et al., 2017), chondrocytes (Chang, Huo, Li, Wu, & Zhang, 2015) and fibroblasts (Kashino, et al., 2003). *In vitro*, ascorbic acid is widely used as a supplement in the culture media, acting as a growth factor as well as having antioxidant properties to suppress the generation of ROS, promoting cell growth. However, high dose of ascorbic could result in increased intracellular ROS levels via the production of hydrogen peroxide  $H_2O_2$  (Uetaki, Tabata, Nakasuka, Soga, & Tomita, 2015; Clément, Ramalingam, Long, & Halliwell, 2001). On the other hand, treatment with a range of AA concentrations from 0.5mM to 4mM for an hour can variably induce 50% cell death (e.g. 0.5mM for Lymphoma (JLP119); 2.5mM for breast (MCF7); 7mM for breast (MB231); and 20mM for breast (Hs587t)), while normal cells remained unaffected at 20mM (Chen, et al., 2005). In our study, ascorbic acid did not exhibit any effects on cell viability for both proliferating and senescent cells within the tested dosage range of 0.001 mM to 0.2 mM. Based on the literature, our tested dosage is relatively low, and it was clear that the senolytic efficacy varies depending on the specific cell type. Assessing the long-term effect would be beneficial.

NOVOS Core and NOVOS Boost were also tested for the viability of both young and senescent human skin fibroblasts. According to a clinical study conducted by the company, 6 months of

daily use of NOVOS Core improved an average skin firmness by an average of 22%, as measured by an indentometer (Scientific evidence behind Novos' best-in-class longevity formulas , 2022). Another clinical study demonstrated that 6 months of daily use of NOVOS Core and 2 significantly reduced the biological pace of ageing using an epigenetic test kit (Scientific evidence behind Novos' best-in-class longevity formulas , 2022). However, both were small pilot studies with only 4 and 12 patients.

*In vitro* studies showed that HUVEC (human umbilical vein endothelial cells) treated with NOVOS Core prior to irradiation exhibited protective effects against DNA damage, with 68% lesser DNA damage compared to the untreated control (Scientific evidence behind Novos' best-in-class longevity formulas , 2022). In our study, no significant senolytic efficacy was observed. From the co-culture assay conducted by Dr Edward Fiedler, solubility of the ingredients was solvent specific. For example, the water-dissolved stock likely had low levels of Glycine, Fisetin and Pterostilbene while the Ethanol dissolved stock likely had low levels of Magnesium malate, glycine, L-Theanine, Hyaluronic acid and b-nicotinamide mononucleotide. Consequently, a water-dissolved stock is expected to present weaker senolytic effects. Our data confirms this; while no significant senolytic effect was observed in the water stock, the effect on senescent cell size reduction was more pronounced with the 2% ethanol-dissolved stocks. This suggests that the compounds crucial for driving this effect are preferably dissolved in Ethanol. However, the effect of ethanol itself to cell size was not assessed, as literature has shown that exposure to 1% ethanol leads to cell shrinking in NIH 3T3 (mouse embryonic fibroblasts) (Kar & Bellare, 2021).

Given that the compounds were received from a pharmaceutical client company, the primary focus of the study was to investigate the anti-senescence effects of the active compound in their core product. However, the absence of compound stability testing poses a limitation in this study's ability to fully assess the compounds efficacy and safety. Stability tests are important in monitoring and evaluating the quality of Active Pharmaceutical Ingredients (API) and Finished Pharmaceutical Products (FPP) throughout their shelf life. Stability testing helps ensure that pharmaceutical formulations maintain their potency, efficacy, and safety under various environmental conditions and storage durations. Environmental factors such as temperature, humidity, and light exposure can significantly impact the stability of pharmaceutical formulations. Compounds may degrade or lose potency under these conditions, leading to changes in their chemical, physical, microbiological, therapeutic, and

toxicological properties. For instance, glycerol are prone to degradation during repeated use or improper storage, potentially leading to the generation of impurities that can affect the stability of the drug product (Sun, et al., 2022).

Moreover, the choice of solvent can also influence compound stability. While some compounds may fully or partially dissolve in solvents, others may be sensitive to hydrolysis or other degradation mechanisms, making them unsuitable candidates for liquid dosage forms. For example, our study observed differences in stability of compounds dissolved in water versus ethanol, highlighting the importance of solvent selection in pharmaceutical formulations. Ethanol's ability to improve the absorption of lipophilic substances may lead to synergistic effects when combined with certain ingredients. By enhancing the solubility and absorption of co-administered compounds, ethanol could potentiate their individual effects, resulting in enhanced therapeutic activity.

Furthermore, the lack of assessment of absorption, distribution, metabolism, and excretion (ADME) properties of the compounds further complicates the interpretation of results. Understanding the pharmacokinetics of compounded preparations is crucial for evaluating their bioavailability, distribution in the body, metabolism, and elimination. Without these assessments, it is difficult to assess whether the ingredients are adequately absorbed by consumers or if they undergo changes that affect their pharmacokinetics and pharmacodynamics.



## Chapter V Characterisation of senescence markers *in vitro* and *in vivo*

### 5.0 Introduction

As mentioned, there is no single universal marker for senescent cells and yet to have a complete consensus on which marker combination might be the best to detect their presence. The combination of various senescent markers such as p16INK4a, p21WAF1/CIP1 (Beauséjour, et al., 2003), Sen-  $\beta$ -Gal (Kurz, Decary, Hong, & Erusalimsky, Senescence-associated (beta)-galactosidase reflects an increase in lysosomal mass during replicative ageing of human endothelial cells, 2000), LaminB1 (Dreesen, et al., 2013; Wang, Ong, Chojnowski, Clavel, & Dreesen, 2017), HMGB1 (Biran, et al., 2017) and colocalization of DNA damage foci (detect by  $\gamma$ H2A.x) and telomeres by immunoFISH (telomere-associated foci, TAF) (Herbig, Ferreira, Condel, Carey, & Sedivy, 2006; Hewitt, et al., 2012) is now a standard requirement to increase the confidence in detection of senescent cells (Gorgoulis, et al., 2019). As the skin is a complex organ consisting of multiple cell types, many studies only observed senescence markers in specific models, skin compartment layers, or certain cell types in the skin (Figure 3). There is no confirmation on which markers work specifically on each cell type.

Therefore, these experiments aimed to test as many senescence markers as possible in different mammalian skin models, including *in vitro* (fibroblasts and keratinocytes) and *in vivo* (human skin tissue). This experiment hypothesised senescence markers such as p16INK4a, p21WAF1/CIP1,  $\gamma$ H2A.x, senescence-associated- $\beta$ -galactosidase (Sen- $\beta$ -gal) and nuclear size to increase with age while HMGB1, LaminB1 and Ki-67, were expected to decrease with age. Prior to testing the senescence markers (Ki-67, HMGB1, LaminB1, p16INK4a, p21WAF1/CIP1 and  $\gamma$ H2A.x) *in vivo*, they were validated *in vitro* using human dermal fibroblasts (HDFn) and human epidermal keratinocytes (HEKn). It is essential to characterise the markers in these skin component cell types as they could present differently in the different cell types.

For the characterisation of senescence markers, the HDFn and HEKn were subjected to 20 Gy irradiation to induce premature ageing and settled for 10 days until a senescence phenotype

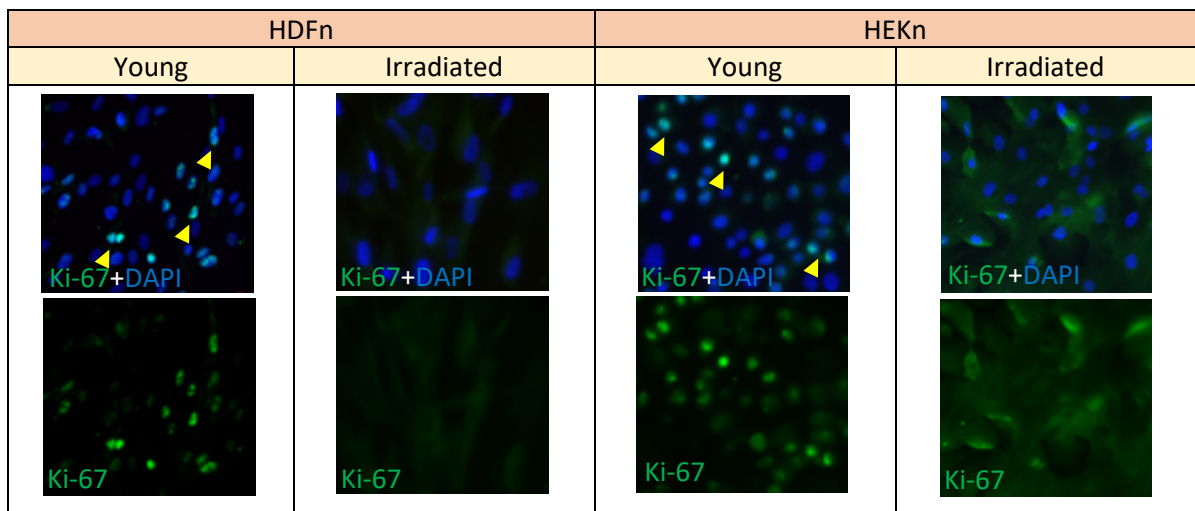
developed. Then, the senescence markers, including Ki-67, LaminB1, HMGB1, p16INK4a, p21WAF1/CIP1,  $\gamma$ H2A.x and nuclear size were tested individually and compared between young and irradiated senescent cells. A time course test to study the development of senescence phenotypes in HDFn and HEKn from day 0 to day 10 post-IR was performed at one-day intervals. The development of senescence was verified by the staining of LaminB1, P16INK4a, p21WAF1/CIP1, the combination of Ki-67 and  $\gamma$ H2A.x and nuclear size. Due to unforeseen circumstances, the X-ray irradiation machine was unavailable for an extended period. A substitution method to induce premature ageing in cells was used. However, only human dermal fibroblasts were tested in this experiment due to insufficient keratinocytes. HDFn was treated with 300  $\mu$ M H<sub>2</sub>O<sub>2</sub> to induce senescence. The development of senescence was verified by SA- $\beta$ -gal staining, the combination of Ki67 and  $\gamma$ H2A.x and LaminB1 on day 7 and day 10 after H<sub>2</sub>O<sub>2</sub> treatment.

The same markers were then characterised in the *in vivo* samples. *In vivo* samples were obtained from young individuals (20 years old) and older individuals (60 years old) for both sun-exposed (Arm) and sun-protected areas (buttock). Similar to the experiments *in vitro*, this set of experiments hypothesised senescence markers such as p16INK4a, p21WAF1/CIP1,  $\gamma$ H2A.x, senescence-associated- $\beta$ -galactosidase (Sen- $\beta$ -gal) and nuclear size to increase with age while HMGB1, LaminB1 and Ki-67, should decrease with age. The alternative hypothesis for this experiment is that skin samples from the arm region show more senescence markers than the buttock region due to greater sun exposure. To distinguish between skin sublayers, skin differentiation markers such as Cytokeratin 10 (K10) and Cytokeratin 14 (K14) were used to distinguish skin sublayers, and the nuclear size was recorded.

## 5.1 Characterisation of senescence markers in *in vitro*

### 5.1.1 Ki-67 reduction in HDFn and HEKn cells post-irradiation

Ki-67 is a proliferative marker that can detect anywhere from G1 through the end of mitosis, but it is not present in cells in the G0 resting phase. Since senescent cells permanently exit from the cell cycle, they should not express Ki-67. Therefore, Ki-67 serves as an excellent marker to identify whether cells have undergone cell cycle arrest. In this study, HDFn and HEKn were subjected to 20 Gy irradiation to induce premature ageing and allowed to settle for 10 days until a senescence phenotype developed. The changes in Ki-67 expression were observed in young and senescent cells (HDFn and HEKn) by quantifying the number of Ki-67 nuclear-positive cells. Ki-67 was indicated by immunofluorescence staining and reported as a percentage (%). The percentage of Ki-67 nuclear-positive cells in HDFn significantly decreased from 48.08%  $\pm$  6.696 SEM to 0.6667%  $\pm$  0.4216 SEM ( $p < 0.001$ ). The percentage of Ki-67 nuclear-positive cells in HEKn significantly decreased from 35.00%  $\pm$  2.266 SEM to 4.333%  $\pm$  1.085 SEM ( $p < 0.001$ ).



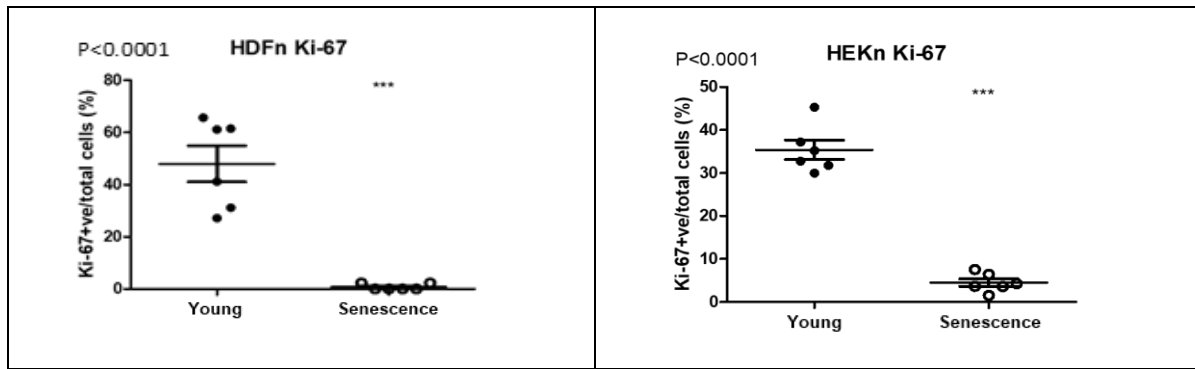


Figure 22 Comparison of the changes of Ki-67 in young and senescent cells in HDFn and HEKn.

Immunofluorescence staining of dermal fibroblasts (HDFn) and keratinocytes (HEKn) with Ki-67 (green) and DAPI (blue) was performed to assess the percentage of Ki-67-positive cells in young and senescent populations. Representative images show a decrease in the frequency of Ki-67-positive cells (indicated by full or partial nuclear stain, yellow arrows) after induction of senescence. The graph on the left compares Ki-67 positivity between young and senescent HDFn, while the graph on the right compares young and senescent HEKn. Data were analyzed using unpaired t-tests. Each data point represents one image, with both young and senescent cells displaying the mean of 6 images. Error bars represent the standard error of the mean (SEM). Significance was denoted by  $p < 0.0001$  for both cell types.

### 5.1.2 LaminB1 reduction in HDFn and HEKn cells post-irradiation

Nuclear lamina LaminB1 is a major structural component of the nuclear envelope that contributes to the nucleus size, shape and stability (Bridger, Foeger, Kill, & Herrmann, 2007) (Dechat, et al., 2008). The loss of LaminB1 is considered as one of the hallmarks of senescence.

HDFn and HEKn were subjected to 20 Gy irradiation to induce premature ageing and left to settle for 10 days until a senescence phenotype developed. The changes of LaminB1 were observed in young and senescent cells (HDFn and HEKn) by quantifying the number of LaminB1-positive cells. The alterations in LaminB1 were indicated by immunofluorescence staining and reported as a percentage (%). The percentage of LaminB1-positive cells in HDFn significantly decreased from  $50.66\% \pm 3.160$  SEM to  $20.77\% \pm 1.279$  SEM ( $p < 0.001$ ). The percentage of LaminB1-positive cells in HEKn also significantly reduced from  $47.83\% \pm 4.574$  SEM to  $16.99\% \pm 4.251$  SEM ( $p < 0.001$ ).

HDFn		HEKn	
Young	Irradiated	Young	Irradiated

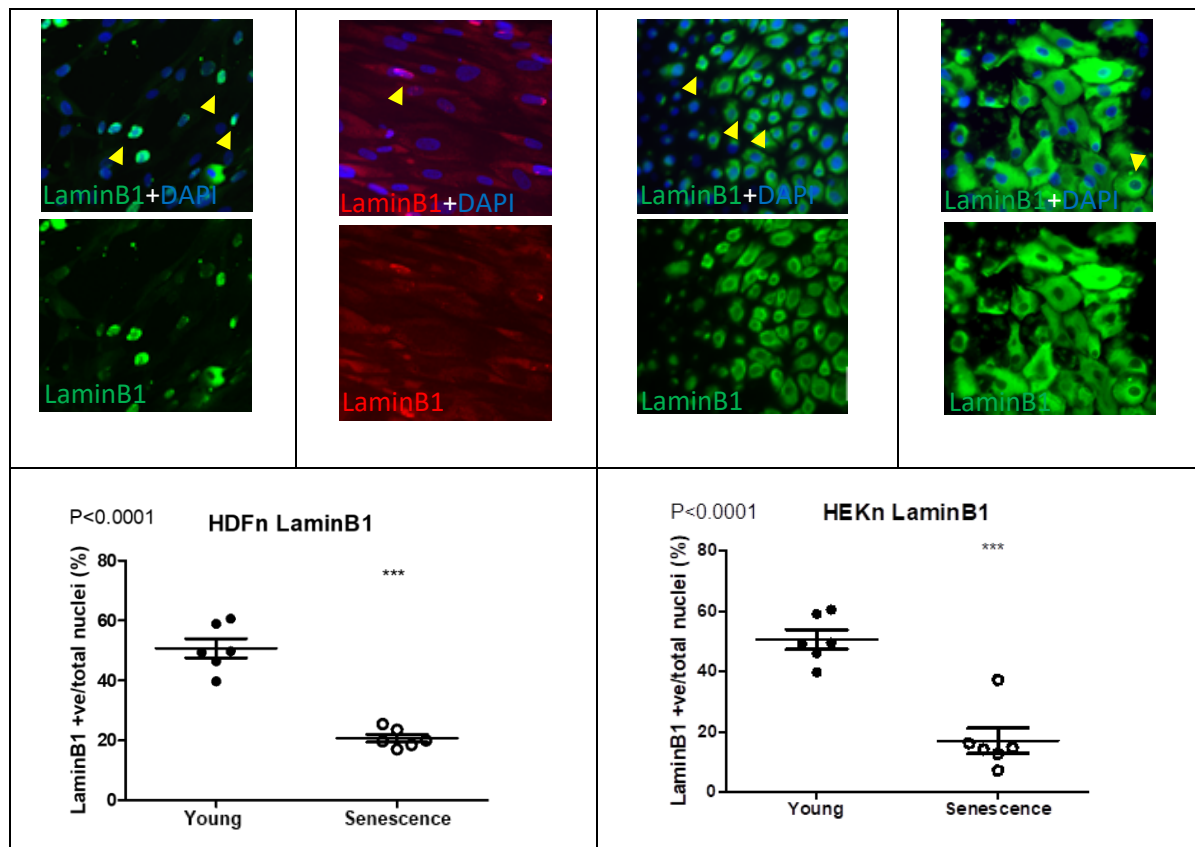


Figure 23 Comparison of changes of LaminB1 in young and senescent cells in HDFn and HEKn.

Immunofluorescence staining of dermal fibroblasts (HDFn) and keratinocytes (HEKn) with LaminB1 was performed to assess changes in nuclear lamina structure between young and senescent cells. LaminB1 cell positivity characterized by ring-like staining around the nuclear lamina (as indicated by yellow arrows), was assessed. Irradiated HDFn were stained in red due to insufficient amount of secondary antibody during the staining process. However, this discrepancy is not expected to affect the quantification. Statistical analysis using unpaired t-tests revealed significant reductions in LaminB1 positivity in both HDFn ( $p < 0.0001$ ) and HEKn ( $p < 0.0001$ ). Each data point represents one image, with the mean positivity calculated from 6 images for both young and senescent cells. Error bars indicate the standard error of the mean (SEM). The graph on the left shows the comparison between young HDFn and senescent HDFn, while the graph on the right shows the comparison between young HEKn and senescent HEKn.

### 5.1.3 HMGB1 reduction in HDFn and HEKn cells post-irradiation

High mobility group box 1 (HMGB1) is a nuclear protein that binds to DNA, contributing to chromatin structure. In young proliferating cells, HMGB1 localises in the nucleus but translocate to the cytoplasm as an inflammatory mediator when cells are damaged (Bianchi & Manfredi, 2007; Yamada & Maruyama, 2007), which in turn facilitates the release of other SASP factors such as IL-1 $\beta$ , IL-6 and MMP3 (Biran, et al., 2017; Davalos, et al., 2013). The loss of nuclear HMGB1 is known as one of the characteristics of senescence.

HDFn and HEKn were subjected to 20 Gy irradiation to induce premature ageing and settled for 10 days until a senescence phenotype developed. The changes in HMGB1 were observed in young and senescent cells (HDFn and HEKn) by quantifying the number of HMGB1 nuclear-positive cells. The translocation of HMGB1 from nuclear to extracellular space was analysed by immunofluorescence staining and reported as a percentage (%). The percentage of HMGB1 nuclear-positive cells in HDFn significantly reduced from 44.89 %  $\pm$  3.760 SEM to 20.44%  $\pm$  2.090 SEM ( $p < 0.001$ ). The percentage of HMGB1 nuclear-positive cells in HEKn significantly reduced from 58.62%  $\pm$  4.622 SEM to 39.33%  $\pm$  4.873 SEM ( $p < 0.05$ ).

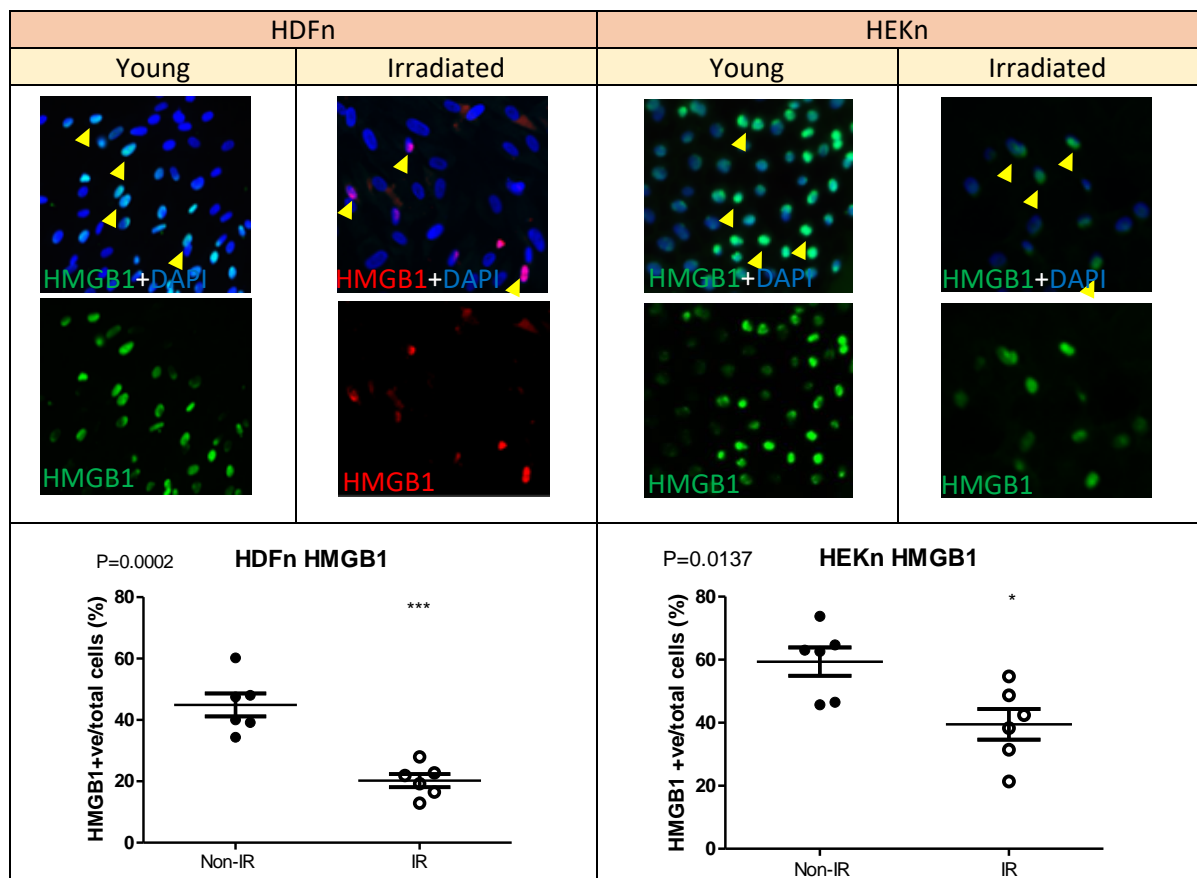


Figure 24 Comparison of changes of HMGB1 in young and senescent cells in HDFn and HEKn.

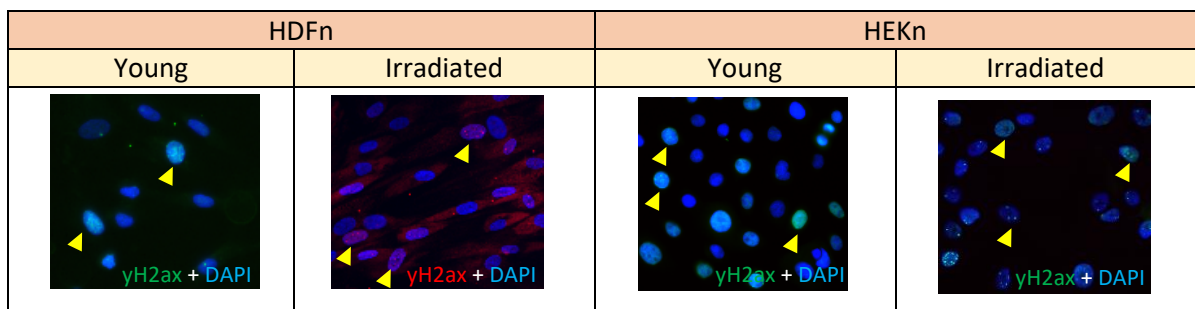
Immunofluorescence staining of dermal fibroblasts (HDFn) and keratinocytes (HEKn) for HMGB1 was conducted to assess the changes in nuclear HMGB1 expression between young and senescent cells. HMGB1 nuclear positivity, indicated by a fully nuclear stain (as highlighted by yellow arrows), was assessed. Irradiated HDFn were stained in red due to insufficient amount of secondary antibody during the staining process. However, this discrepancy is not expected to affect the quantification. Statistical analysis via unpaired t-tests revealed a significant decrease in HMGB1 nuclear positivity in both HDFn ( $p = 0.0002$ ) and HEKn ( $p = 0.0137$ ). Each data point represents one image, with the mean calculated from 6 images for both young and senescent cells. Error bars represent the standard error of the mean (SEM). The left graph compares young HDFn and senescent HDFn, while the right graph compares young HEKn and senescent HEKn.

#### 5.1.4 $\gamma$ H2A.x DNA damage foci increased in HEK293 cells post-irradiation but not in HDFn cells

The phosphorylated form of histone variant H2AX ( $\gamma$ H2A.x) is crucial in the recruitment of DNA repair and checkpoint proteins to the sites of DNA damage. Cellular senescence is initiated by the activation of a persistent DNA damage pathway and can be identified by the presence of phosphorylated H2A.x ( $\gamma$ H2A.x) (d'Adda di Fagagna, et al., 2003).

HDFn and HEK293 cells were subjected to 20 Gy irradiation to induce premature ageing and settled for 10 days until a senescence phenotype developed. The formation of DNA damage foci was observed in young and senescent cells (HDFn and HEK293) by quantifying the number of  $\gamma$ H2A.x nuclear-positive cells. A cell with more than 3 foci in the nucleus was quantified as a  $\gamma$ H2A.x nuclear-positive cell.

The amount of  $\gamma$ H2A.x was analysed by the staining of immunofluorescence reported as percentage (%). The percentage of  $\gamma$ H2A.x nuclear-positive cells in HDFn showed a trend to decrease from 42.78%  $\pm$  5.376 SEM to 28.36%  $\pm$  3.281 SEM. The number of  $\gamma$ H2A.x nuclear-positive cells in HEK293 significantly increased from 69.42%  $\pm$  2.638 SEM to 98.36%  $\pm$  3.281 SEM ( $p < 0.001$ ).



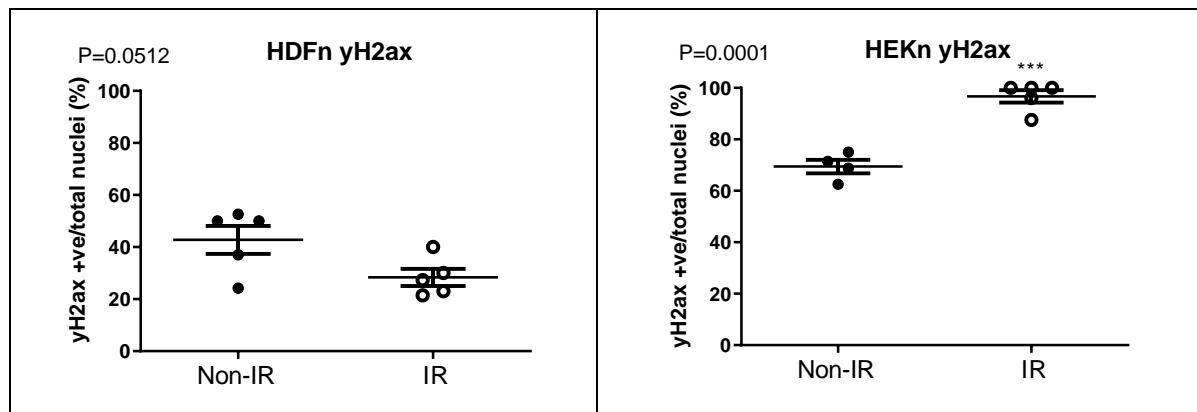


Figure 25 Comparison of changes of  $\gamma$ H2A.x in young and senescent cells in HDFn and HEKn.

The frequency of  $\gamma$ H2A.x nuclear-positive cells (indicated by more than 3 foci in the nucleus, as shown by yellow arrows) increased in HEKn after irradiation. Irradiated HDFn were stained in red due to insufficient amount of secondary antibody during the staining process. However, this discrepancy is not expected to affect the quantification. The graph on the left shows the comparison of young HDFn and senescent HDFn; the graph on the right shows the comparison of young HEKn and senescent HEKn. Data were analysed by unpaired-t-test; both young and senescent cells show the mean of 5 images taken and measured in SEM with each dot represents one image. No significant difference was observed in HDFn with a p-value of 0.0512; a significant difference in HEKn presented with a p-value <0.001\*\*\*.

### 5.1.5 No change in p21WAF1/CIP1 expression in HEKn and HDFn cells post-irradiation

p21WAF1/CIP1 is a cyclin-dependent kinase (CDK) inhibitor that triggers cell cycle arrest associated with senescence and damage response. Increase of p21WAF1/CIP1 is known as a phenotypic feature of senescence.

HDFn and HEKn were subjected to 20 Gy irradiation to induce premature ageing and settled for 10 days until a senescence phenotype developed. The changes in p21WAF1/CIP1 were observed in young and senescent cells (HDFn and HEKn) by quantifying the number of p21WAF1/CIP1 nuclear-positive cells. The amount of p21WAF1/CIP1 was analysed by the staining of immunofluorescence staining reported as percentage (%). There was no change of the percentage of p21WAF1/CIP1 -nuclear-positive cells in HDFn (35.31%  $\pm$  3.480 SEM to 33.74%  $\pm$  2.873 SEM). No p21WAF1/CIP1 nuclear-positive cells were found in HEKn.

HDFn		HEKn	
Young	Irradiated	Young	Irradiated



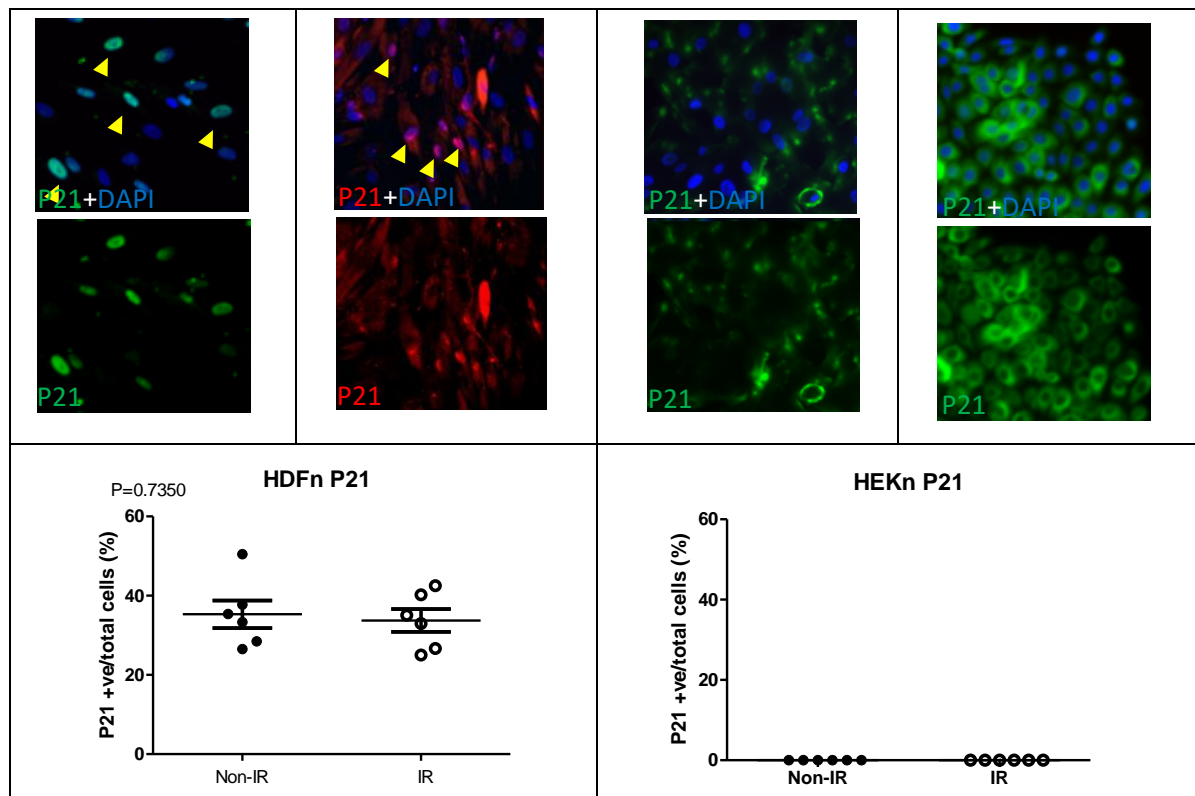


Figure 26 Comparison of changes of p21WAF1/CIP1 in young and senescent cells in HDFn and HEKn.

The frequency of p21WAF1/CIP1 nuclear-positive cells (indicated by a fully nuclear stain, as shown by yellow arrows) showed no change after irradiation. Irradiated HDFn were stained in red due to insufficient amount of secondary antibody during the staining process. However, this discrepancy is not expected to affect the quantification. The graph on the left shows the comparison of young HDFn and senescent HDFn; the graph on the right shows the comparison of young HEKn and senescent HEKn. Data were analysed by unpaired-t-test; both young and senescent cells show the mean of 6 images taken and measured in SEM with each dot represents one image. No significant difference was observed in HDFn with a p-value of 0.7350; no p21WAF1/CIP1 nuclear-positive cells were seen in HEKn.

### 5.1.6 Elevation of P16INK4a expression in HEKn post-irradiation but not in HDFn cells

Similar to p21WAF1/CIP1, p16INK4a is also a tumour suppressor protein that is a cyclin-dependent kinase inhibitor and is essential in regulating the cell cycle. Increased p16INK4a is known as a phenotypic feature of senescence.

HDFn and HEKn were subjected to 20 Gy irradiation to induce premature ageing and settled for 10 days until a senescence phenotype developed. The changes in p16INK4a in young and senescent cells (HDFn and HEKn) were quantified as change in p16INK4a nuclear-positive cells. The amount of p16INK4a was analysed by the staining of immunofluorescence staining reported as percentage (%). The percentage of p16INK4a nuclear-positive cells in HEKn

significantly increased from  $9.919 \pm 1.579$  SEM to  $32.45 \pm 1.179$  SEM ( $p < 0.001$ ). No p16INK4a nuclear-positive cells were found in HDFn.

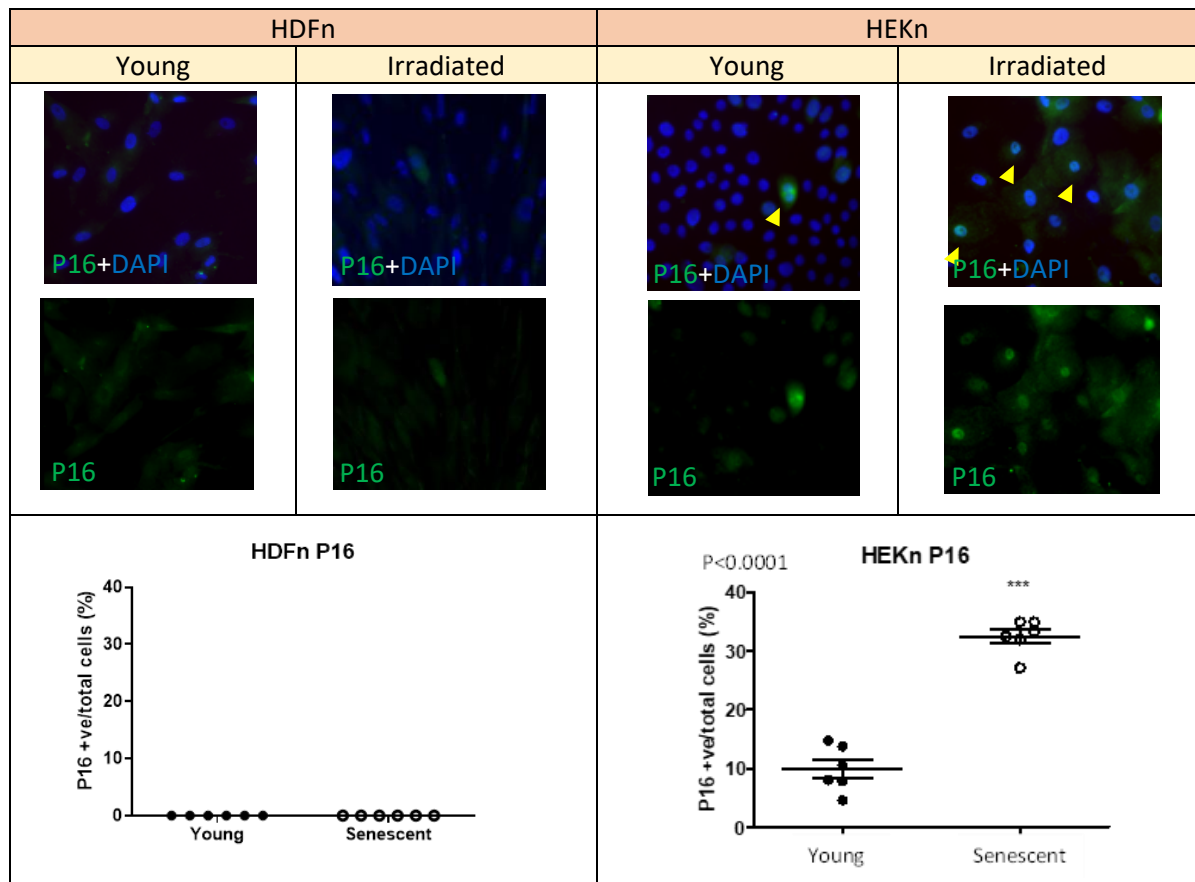


Figure 27 Comparison of changes of p16INK4a in young and senescent cells in HDFn and HEKn.

The frequency of p16INK4a nuclear-positive cells (indicated by a fully nuclear stain, as shown by yellow arrows) increased in HEKn after irradiation. The graph on the left shows the comparison of young HDFn and senescent HDFn; the graph on the right shows the comparison of young HEKn and senescent HEKn. Data were analysed by unpaired-t-test; both young and senescent cells show the mean of 6 images taken and measured in SEM with each dot represents one image. A significant difference in HEKn presented with a p-value  $< 0.0001^{***}$ ; no p16INK4a nuclear-positive cells were seen in HDFn.

### 5.1.7 Enlargement in nuclear size in HEKn and HDFn cells post-irradiation

The change in nuclear morphology is one of the characteristics of senescent cells. The enlargement of cellular size is often accompanied by a ‘flattened’ appearance and enlargement of nuclear and nucleolar size. Measurement of nuclear size is the most straightforward assay to determine senescent cells.

HDFn and HEKn were subjected to 20 Gy irradiation to induce premature ageing and settled for 10 days until a senescence phenotype developed. Nuclear sizes were measured as area ( $\mu\text{m}^2$ ) by manually drawing each cell around using the ICY polygon tool. Therapy-induced

senescence in HDFn showed a significant increase in nuclear size area ( $\mu\text{m}^2$ ) ( $305.1 \pm 4.567$ ) compared to young cells ( $187.0 \pm 3.591$ ) ( $p < 0.001$ ). Therapy-induced senescence in HEKn showed a significant increase in nuclear size area ( $\mu\text{m}^2$ ) ( $312.8 \pm 6.144$ ) compared to young cells ( $144.3 \pm 2.357$ ) ( $p < 0.001$ ).

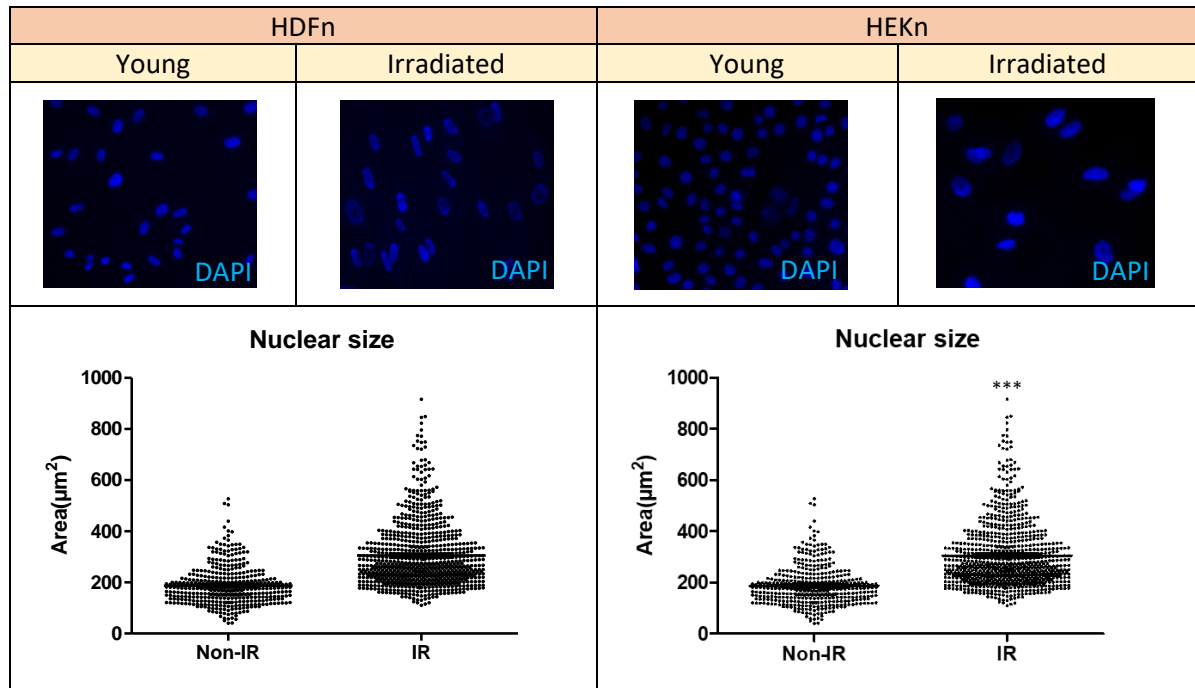


Figure 28 Comparison of changes of nuclear size in young and senescent cells in HDFn and HEKn.

Nuclear sizes were measured as area ( $\mu\text{m}^2$ ) and significantly increased after irradiation. The graph on the left shows the comparison of young HDFn and senescent HDFn; the graph on the right shows the comparison of young HEKn and senescent HEKn. The data were analysed by unpaired-t-test; both young and senescent cells show the mean of total cells taken and measured in SEM with each dot representing one cell. A significant difference was observed in HDFn with a p-value  $< 0.0001^{***}$ ; a significant difference was also observed in HEKn with a p-value  $< 0.0001^{***}$ .

### 5.1.8 Increased in Senescence-associated $\beta$ -galactosidase (Sen- $\beta$ -Gal) activity in HDFn cells post- $\text{H}_2\text{O}_2$ treatment

The increased lysosomal mass in senescent cells is associated with a higher lysosomal  $\beta$ -galactosidase activity which can be detected at pH6, a.k.a. the senescence-associated  $\beta$ -galactosidase (Sen- $\beta$ -Gal) (Dimri, et al., 1995; Kurz, Decary, Hong, & Erusalimsky, Senescence-associated (beta)-galactosidase reflects an increase in lysosomal mass during replicative ageing of human endothelial cells, 2000).

An increase in Sen-β-Gal was observed after H<sub>2</sub>O<sub>2</sub> treatment. Changes in Sen- β-Gal was observed in young and senescent cells (HDFn) on day 7 and day 10 by quantifying the number of Sen-β-Gal -positive cells. The amount of Sen-β-Gal was analysed by the staining of immunofluorescence, staining reported as percentage (%). The percentage of Sen- β-Gal positive cells in HDFn gradually increased from 0% to 51% on day 7 to 61% on day 10.

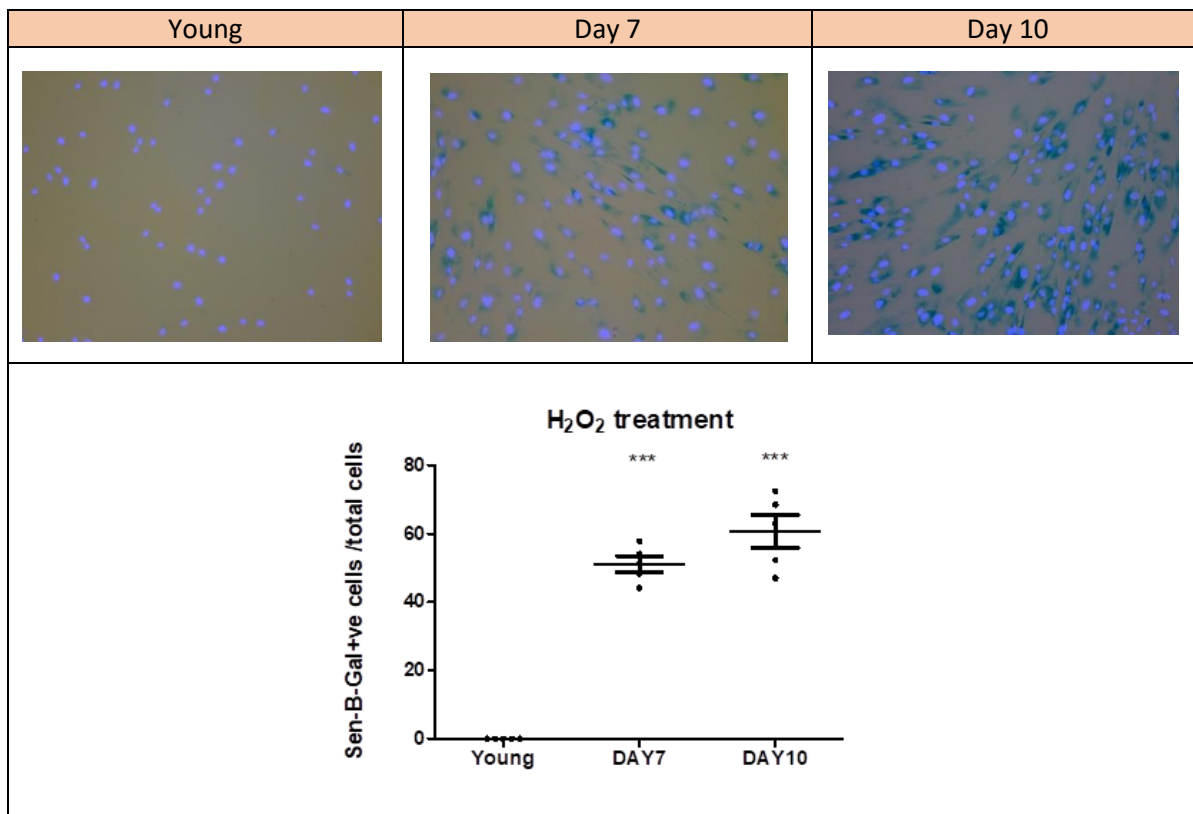


Figure 29 Comparison of changes of Sen- β-Gal in young and senescent cells in HDFn after H<sub>2</sub>O<sub>2</sub> treatment.

The graph shows the comparison of young HDFn and senescent HDFn. Data were analysed by One-way ANOVA and Bonferroni’s multiple comparison test.; both young and senescent cells show the mean of 5 images taken and measured in SEM, with each dot represents one image. The increase in Sen- β-Gal – positive cell frequency was presented with a significant <0.05 on day 7\*\*\*and day 10\*\*\*.

### 5.1.9 Decreased LaminB1 expression in HDFn cells post-H<sub>2</sub>O<sub>2</sub> treatment

A decrease in LaminB1 was observed after H<sub>2</sub>O<sub>2</sub> treatment. Changes of LaminB1was observed in young and senescent cells (HDFn) on day 7 and day 10 by quantifying the number of LaminB1-positive cells. The amount of LaminB1 was analysed by immunofluorescence staining, and staining was reported as percentage (%). The percentage of LaminB1-positive cells in HDFn gradually decreased from 44% to 22% on day 7 to 6% on day 10.

Young	Day 7	Day 10
-------	-------	--------

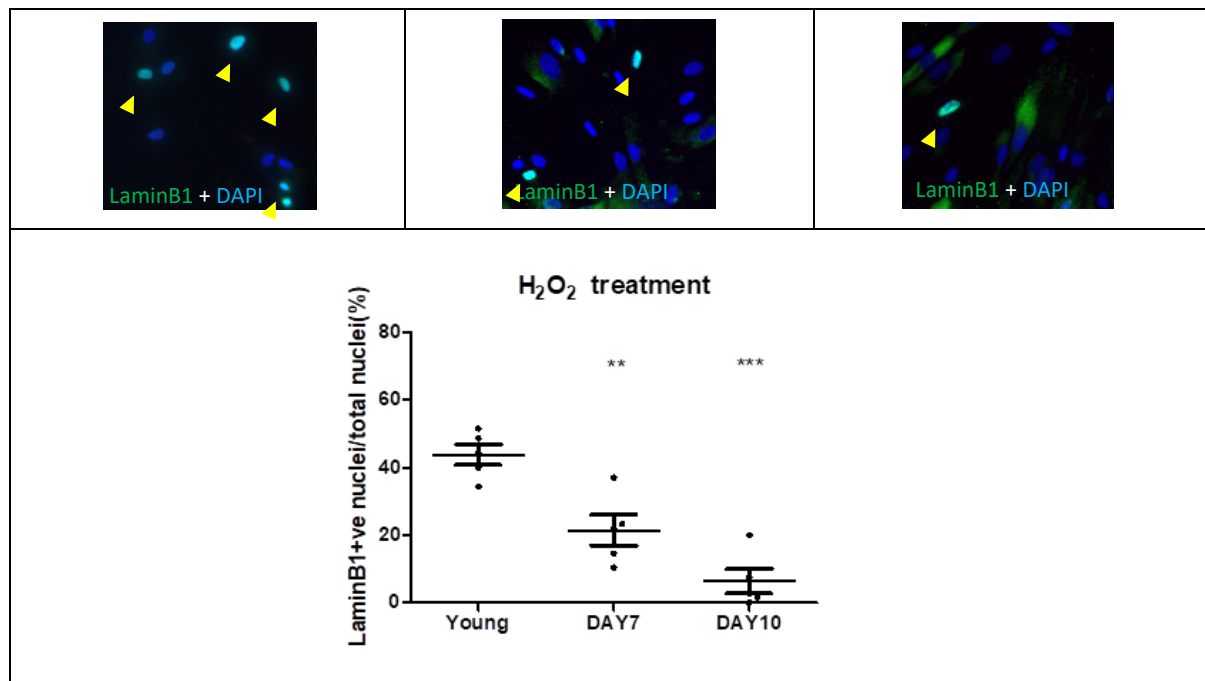


Figure 30 Comparison of changes of LaminB1 in young and senescent cells in HDFn after  $H_2O_2$  treatment.

The frequency of LaminB1-positive cells (indicated by ring-like staining around the nuclear lamina, as shown by yellow arrows) decreases after induction of senescence. The graph shows the comparison of young HDFn and senescent HDFn. Data were analysed by One-way ANOVA and Bonferroni's multiple comparison test.; both young and senescent cells show the mean of 5 images taken and measured in SEM, with each dot represents one image. The decrease in LaminB1-positive cell frequency was significant on day 7\*\* and day 10\*\*\* with p-values < 0.05 and < 0.001, respectively.

#### 5.1.10 Reduction of Ki-67 accompanied by an increase in $\gamma$ H2A.x in HDFn cells post- $H_2O_2$ treatment

Ki-67 is commonly used as a proliferation marker. A hallmark of senescent cells is a permanent exit from the cell cycle; thus, senescent cells do not express Ki-67.  $\gamma$ H2A.x is the early sign of the double strand break in senescence. An increase of  $\gamma$ H2A.x also can be seen in young cells due to the phosphorylation during cell proliferation. Therefore, a combination of Ki-67 and  $\gamma$ H2A.x was done to avoid counting  $\gamma$ H2A.x in young proliferative cells for a robust comparison.

A decrease in Ki-67, accompanied by an increase in  $\gamma$ H2A.x, was observed after  $H_2O_2$  treatment. The combination of Ki-67 and  $\gamma$ H2A.x was observed in young and senescent cells (HDFn) on day 7 and day 10 by quantifying the number of Ki67 or  $\gamma$ H2A.x-positive cells. The amount of Ki67 or  $\gamma$ H2A.x was analysed by the immunofluorescence staining, and staining was reported as percentage (%). The percentage of Ki67-positive cells in HDFn gradually decreased

from 30 % to 0 % on day 7 to 1 % on day 10. The percentage of  $\gamma$ H2A.x-positive cells in HDFn gradually increased from 20 % to 67 % on day 7 and recovered to 49 % on day 10.

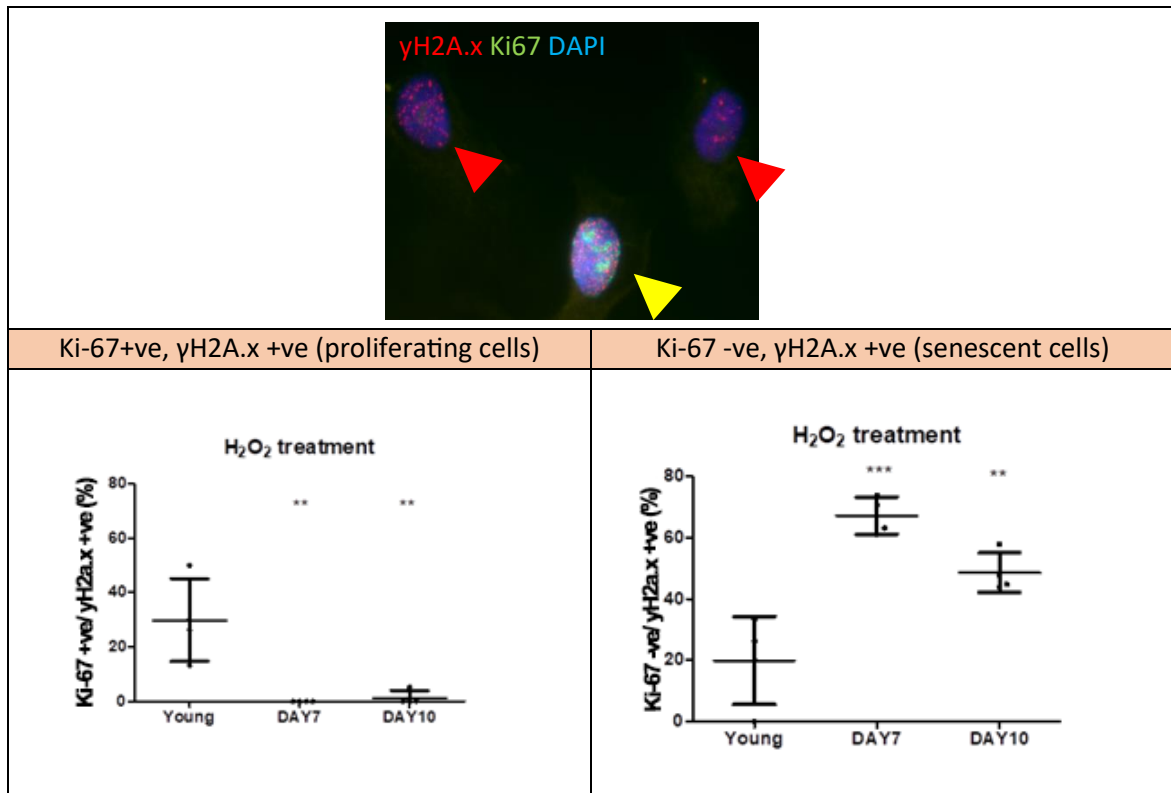
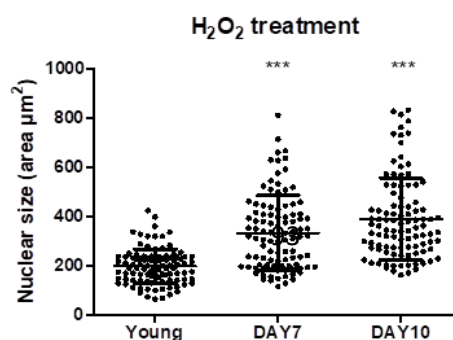


Figure 31 Comparison of changes of Ki-67 and  $\gamma$ H2A.x in young and senescent cells in HDFn after H<sub>2</sub>O<sub>2</sub> treatment.

The figure shows the combination of Ki67(green) and  $\gamma$ H2A.x (red) staining to distinguish young proliferative cells (indicated by yellow arrow). Sole  $\gamma$ H2A.x (red) staining is used to identify senescent cells (indicated by red arrows), with a counterstained of DAPI to determine the nucleus. Data were analysed by One-way ANOVA and Bonferroni's multiple comparison test.; both young and senescent cells show the mean of 5 images taken and measured in SEM, with each dot represents one image. A decrease in proliferative cell frequency was observed, presenting significance on day 7\*\* and day 10\*\* (p < 0.05). An increase in  $\gamma$ H2A.x-positive cell frequency was also noted, showing significance on day 7\*\*\* and day 10\*\* (p < 0.05).

### 5.1.11 Enlargement in nuclear size in HDFn cells post-H<sub>2</sub>O<sub>2</sub> treatment

An increase in nuclear size was observed after H<sub>2</sub>O<sub>2</sub> treatment. Nuclear sizes were measured as area ( $\mu$ m<sup>2</sup>) by manually drawing each cell around using the ICY polygon tool. The nuclear size area ( $\mu$ m<sup>2</sup>) gradually increased from 197.9  $\pm$  7.077 (N=101) to 334.9  $\pm$  14.95 (N=101) on day 7 and to 391.7  $\pm$  16.498 SEM (N=101) on day 10.



*Figure 32 Comparison of changes in nuclear size in young and senescent cells in HDFn after H<sub>2</sub>O<sub>2</sub> treatment.*

Nuclear sizes were measured as area ( $\mu\text{m}^2$ ) and showed a significant increase after H<sub>2</sub>O<sub>2</sub> treatment. The data were analysed by unpaired-t-test; each dot represents one cell. The enlargement of nuclear size was significant with a p-value of  $P < 0.0001^{***}$  on Day 7 and Day 10.

#### **5.1.12 Reduction in LaminB1 expression observed in both HDFn and HEKn cells from day 0 to day 10 post-irradiation**

This time-course experiment aims to observe the changes in senescence phenotypes from day 0 to day 10 post-IR at one-day intervals. It was conducted based on previous experiments that compared young (day 0) and senescent (day 10) cells, where the results showed that p21WAF1/CIP1 is only present in HDFn but not HEKn, whereas the opposite is true for P16INK4a. Additionally,  $\gamma\text{H2a.x}$  showed no change in HDFn after irradiation. This set of experiments seeks to validate whether the hypothesis is indeed true.

HDFn and HEKn were subjected to 20 Gy irradiation to induce premature ageing and settled for 10 days until a senescence phenotype developed. The changes in LaminB1 from day 0 to day 10 post-IR at one-day intervals were observed in young and senescent cells (HDFn and HEKn) by quantifying the number of LaminB1-positive cells. The LaminB1 was analysed by immunofluorescence staining and reported as a percentage (%). The percentage of LaminB1-positive cells in HDFn gradually reduced after irradiation from 96.5 % on day 0 to 17 % on day 5 and slowly recovered on day 6 with 51.7 % until it reached a plateau. The percentage of LaminB1-positive cells in HEKn reduced from 70.7 % to 0% on day 10.

HDFn	HEKn
------	------

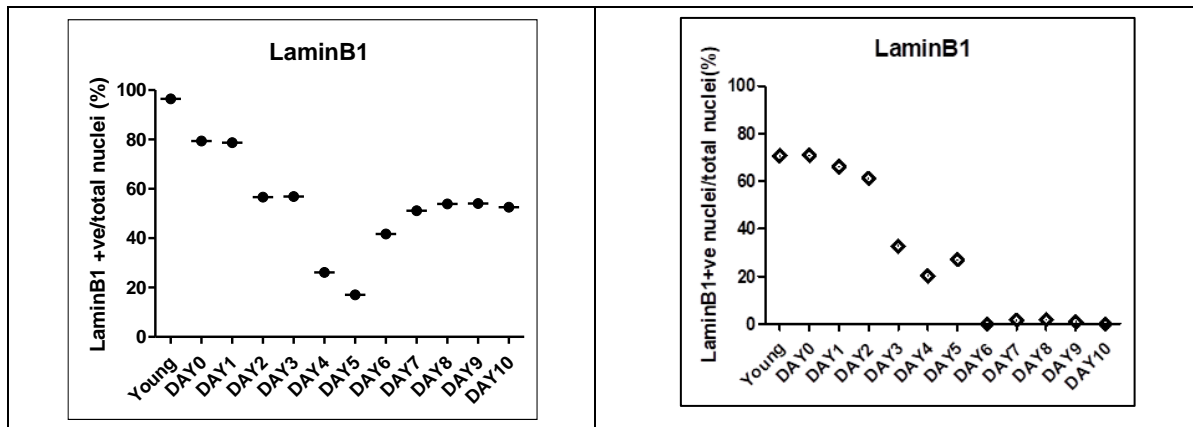


Figure 33 The development of LaminB1 from day 0 to day 10 after irradiation.

The graph on the left shows the comparison of young HDFn and senescent HDFn; the graph on the right shows the comparison of young HEKn and senescent HEKn. The % of LaminB1-positive cells was collected from Day 0 to Day 10 post-irradiation at one-day intervals, with each point representing the average percentage of five images.

### 5.1.13 Reduction in Ki-67 accompanied by an increase in $\gamma$ H2A.x observed in HDFn and HEKn cells from day 0 to day 10 post-irradiation

This experiment aim to evaluate the changes in Ki-67 and  $\gamma$ H2A.x expression following irradiation-induced premature aging in human dermal fibroblasts (HDFn) and human epidermal keratinocytes (HEKn) over a 10-day period. Notably, a decrease in Ki-67 expression, accompanied by an increase in  $\gamma$ H2A.x, was observed post-irradiation.

HDFn and HEKn were subjected to 20 Gy irradiation to induce premature ageing and settled for 10 days until a senescence phenotype developed. The changes in Ki-67 and  $\gamma$ H2A.x from day 0 to day10 post-IR at one-day intervals were observed in young and senescent cells (HDFn and HEKn) by quantifying the number of proliferative cells (Ki-67+ve and  $\gamma$ H2A.x +ve), or senescent cells (Ki-67 -ve and  $\gamma$ H2A.x +ve) reported as percentage (%).

The percentage of proliferative cells indicated by (Ki-67+ve and  $\gamma$ H2A.x +ve) in HDFn significantly reduced from 78.9 % on Day 1 to 5.7 % on day 2, then remained at 0-4 % until day 10. The percentage of senescent cells indicated by (Ki-67 -ve and  $\gamma$ H2A.x +ve) in HDFn dramatically increased to 88.6 % on Day 2, remained high until day 9 and recovered to 50 % on day 10.

The percentage of proliferative cells indicated by (Ki-67+ve and  $\gamma$ H2A.x +ve) in HEKn slowly decreased from 50 % on day 2 and remained at 0 % until day 9, with a slight recovery on Day



10 with 6.2 %. The percentage of senescent cells indicated by (Ki-67 -ve and  $\gamma$ H2A.x +ve) in HEKn gradually increases from 27.3 % on day 2 to 88.9 % on day 9, with a slight recovery on day 10 with 78.1 %.

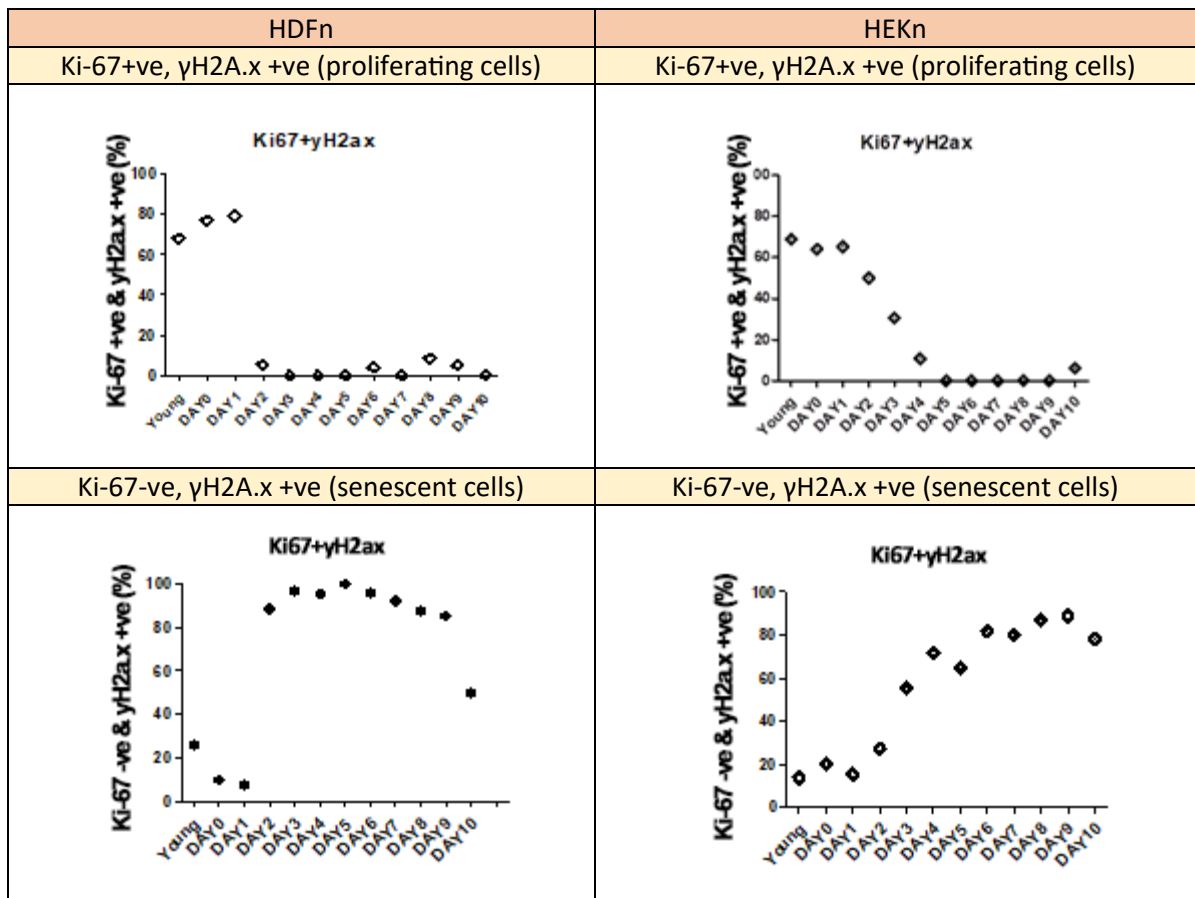


Figure 34 The development of Ki-67 and  $\gamma$ H2A.x from day0 to day 10 after irradiation.

The graph show temporal dynamics of senescent cell development in dermal fibroblasts (HDFn) and keratinocytes (HEKn) following irradiation with 20 Gy of X-rays. Presented over a

ten-day period, the data showcase the fluctuations in proliferating and senescent cell populations, quantified by Ki-67 (top row) and  $\gamma$ H2AX (bottom row) positivity, respectively.

### 5.1.14 No change in p21WAF1/CIP1 observed in HDFn and HEKn cells from day 0 to day 10 post-irradiation

HDFn and HEKn were subjected to 20 Gy irradiation to induce premature ageing and settled for 10 days until a senescence phenotype developed. The changes in p21WAF1/CIP1 from day 0 to day 10 post-IR at one-day intervals were observed in young and senescent cells (HDFn and HEKn) by quantifying the number of p21WAF1/CIP1-positive cells. The p21WAF1/CIP1 was analysed by immunofluorescence staining and reported as a percentage (%). The percentage of p21WAF1/CIP1 -positive cells in HDFn shows a trend towards reduction and increased from 45.0 % on day 5 to 69.4 % on day 6. No p21WAF1/CIP1-positive cells observed in HEKn.

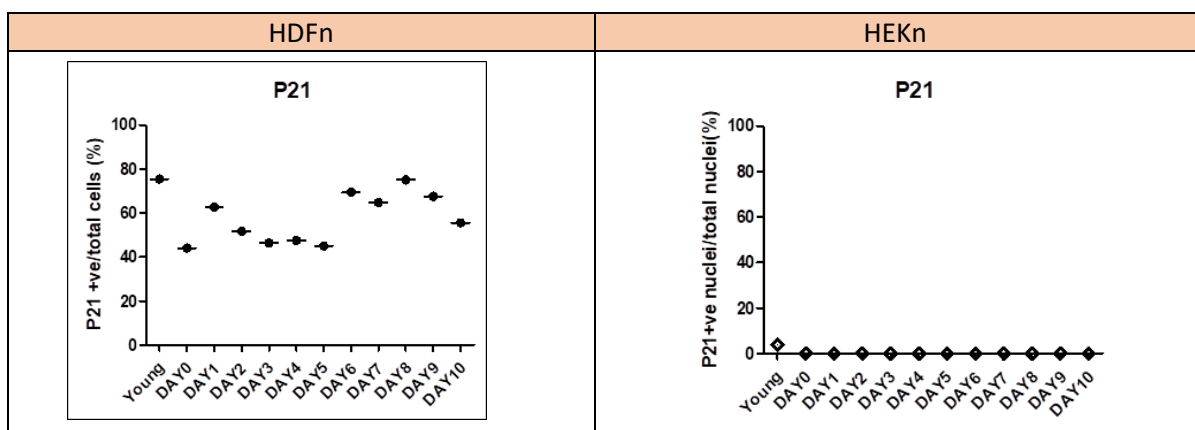


Figure 35 The development of p21WAF1/CIP1 from day0 to day 10 after irradiation.

The graph on the left compares young HDFn and senescent HDFn; while the graph on the right shows the comparison of young HEKn and senescent HEKn. The percentage of p21WAF1/CIP1

-positive cells was collected from day 0 to day 10 post-irradiation at one-day intervals, with each point representing the average percentage of five images.

### 5.1.15 No change in P16INK4a observed in HDFn and HEKn cells from day 0 to day 10 post-irradiation

HDFn and HEKn were subjected to 20 Gy irradiation to induce premature ageing and settled for 10 days until a senescence phenotype developed. The changes in P16INK4a from day 0 to day 10 post-IR at one-day intervals were observed in young and senescent cells (HDFn and HEKn) by quantifying the number of P16INK4a-positive cells. The P16INK4a was analysed by immunofluorescence staining and reported as a percentage (%). The percentage of P16INK4a-positive cells in HDFn was relatively low, ranging from 0-18 %. No P16INK4a-positive cells observed in HDFn.

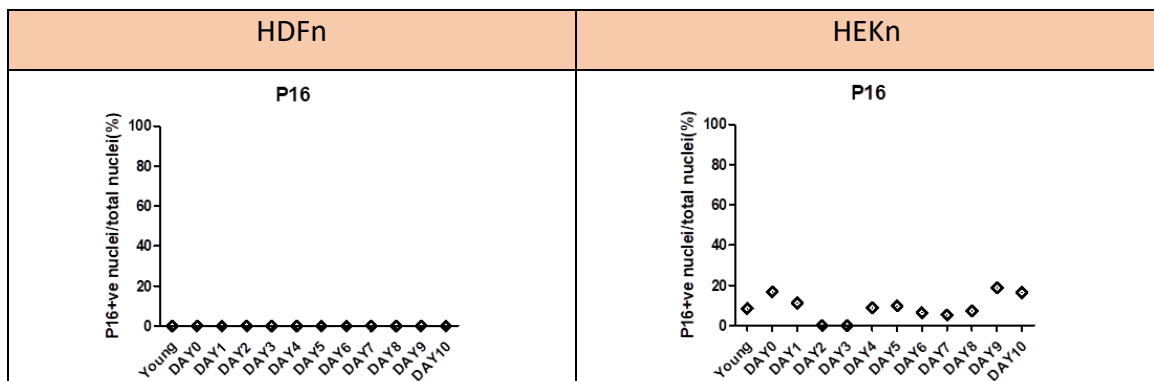


Figure 36 The development of P16INK4a from day 0 to day 10 after irradiation.

The graph on the left shows the comparison of young HDFn and senescent HDFn; the graph on the right shows the comparison of young HEKn and senescent HEKn. The percentage of P16INK4a -positive cells was collected from day 0 to day 10 post-irradiation at one-day intervals, with each point representing the average percentage of five images.

### 5.1.16 Enlargement in nuclear size in HDFn and HEKn from day 0 to day 10 post-irradiation

An increase in nuclear size was observed after irradiation. The changes in nuclear size was recorded from day 0 to day 10 post-IR at one-day intervals in young and senescent cells (HDFn and HEKn). The nuclear size was measured as area ( $\mu\text{m}^2$ ) by manually drawing each cell around using the ICY polygon tool. The average size of nuclei in HDFn increases from  $142.9 \pm 7.654$  to  $478.0 \pm 26.45$  on day 10. Similarly, the average size of nuclear in HEKn increases from  $108.6 \pm 8.015$  to  $391.4 \pm 150.41$  on day 10.

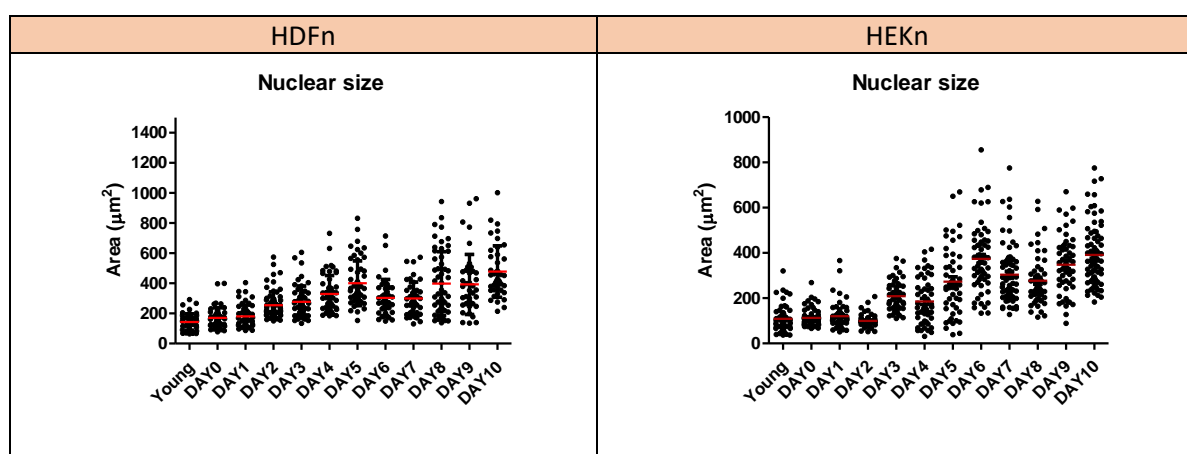


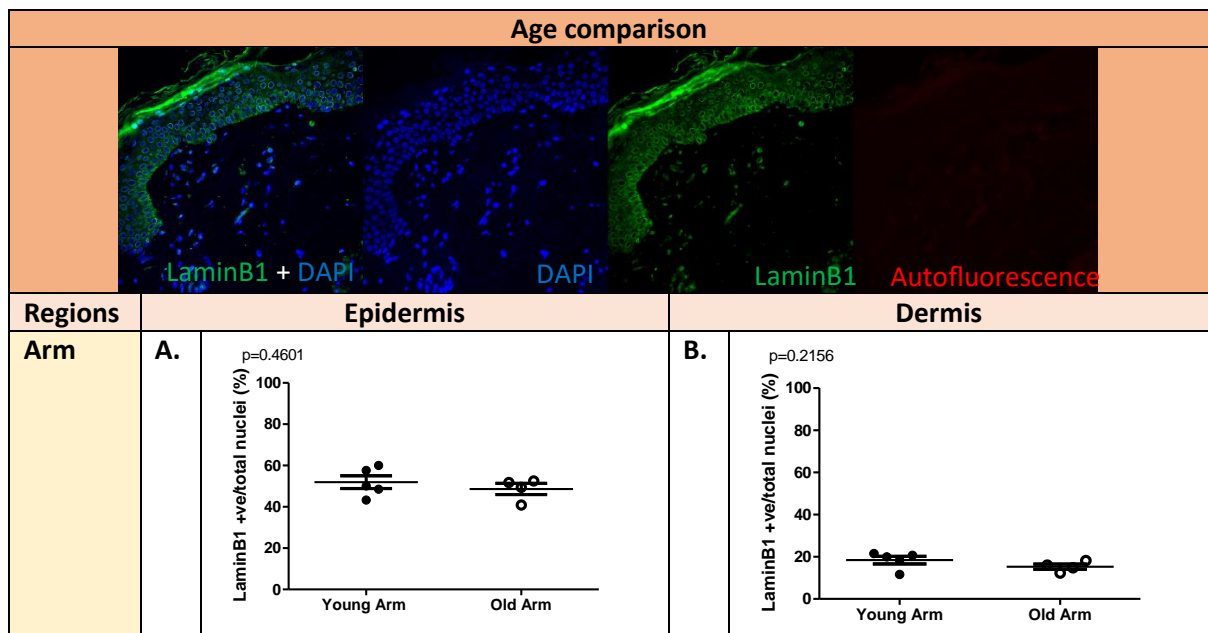
Figure 37 The changes in nuclear size from day 0 to day 10 after irradiation.

The graph on the left shows the comparison of young HDFn and senescent HDFn; the graph on the right shows the comparison of young HEKn and senescent HEKn. The changes in nuclear size were collected from day 0 to day 10 post-irradiation at one-day intervals, with each point representing the average percentage of five images. Both young and senescent cells show the mean of total cells taken and measured in SEM with each dot represents one cell. Enlargement of nuclear size was noted after irradiation

## 5.2 Characterisation of senescence markers *in vivo*

### 5.2.1 Changes in Lamin B1 compared between different age groups in human skin samples

Skin samples from individuals aged between 20- and 60-years old were obtained and compared the change of Lamin B1 in both compartments of the skin (epidermis and dermis). The Lamin B1 was analysed by immunofluorescence staining and reported as a percentage (%). LaminB1 showed no change in the arm epidermis compared between the young ( $51.94 \pm 3.070$  n=5) and old ( $48.66 \pm 2.681$  n=4) donors. There was no change in LaminB1 in the arm dermis compared between the young ( $18.44 \pm 1.778$  n=5) and old donors ( $15.32 \pm 1.242$  n=4). There was no change in LaminB1 in the buttock epidermis compared between young donors ( $45.86 \pm 2.909$  n=5) and old donors ( $47.92 \pm 2.126$  n=4). The percentage of LaminB1-positive cells in the buttock dermis showed no change with age (young  $20.90 \pm 2.079$  n=5 vs old  $24.13 \pm 1.984$  n=4).



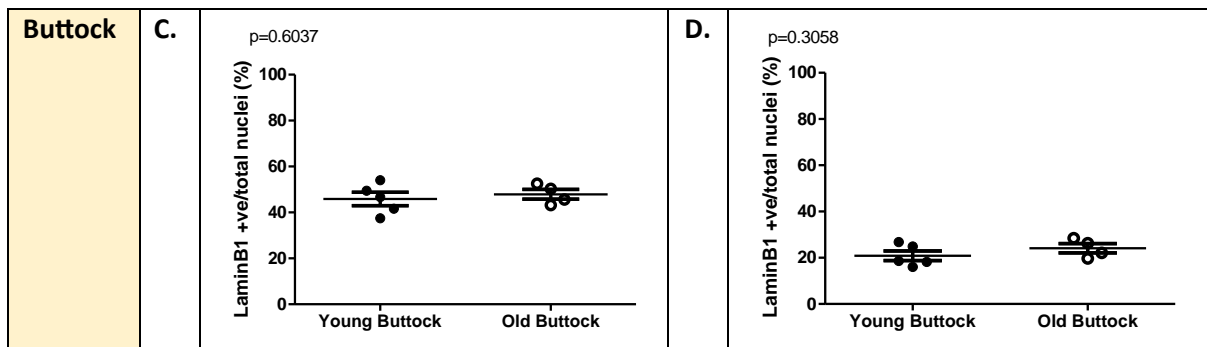


Figure 38 Changes in Lamin B1 compared between ages in human skin samples.

Immunofluorescence staining was conducted on skin tissue samples obtained from two different age groups: 20 years old (young) and 60-year-old (old) individuals. Tissue samples were stained with LaminB1 (green) alongside DAPI (blue) for nuclear visualization. LaminB1 and DAPI staining facilitated the visualization of cellular structures, with cell positivity indicated by ring-like fluorescence surrounding the cells. The sample size comprised n=5 for young subjects and n=4 for old subjects, with each dot representing one individual. Data were analysed using unpaired t-tests with standard error of the mean (SEM). **A.** Comparison of LaminB1 cell positivity in the epidermis of the arm between young and old individuals revealed no significant differences between the two age groups, with a p-value of 0.4601. **B.** The graph illustrates the comparison of LaminB1 cell positivity in the dermis of the arm between young and old individuals. No significant difference was observed, as indicated by a p-value of 0.2156. **C.** Comparison of LaminB1 cell positivity in the buttock epidermis between young and old individuals showed no significant difference in LaminB1 cell positivity between the two age groups, with a calculated p-value of 0.6037. **D.** The analysis of LaminB1 cell positivity in the buttock dermis between young and old individuals revealed no significant difference, with a p-value of 0.3058.

### 5.2.2 Changes in Lamin B1 compared between different regions in human skin samples

The change of Lamin B1 was observed in both compartments of the skin (epidermis and dermis) comparing between skin regions. The Lamin B1 was analysed by immunofluorescence staining and reported as a percentage (%). Lamin B1 showed no difference in the epidermis compared between sun-exposed (arm) ( $51.94 \pm 3.070$  n=5) and sun-protected (buttock) ( $45.86 \pm 2.909$  n=5) regions in younger donor. No change of Lamin B1 in the dermis compared between arm ( $18.44 \pm 1.778$  n=5) and buttock ( $20.90 \pm 2.079$  N=5) region in younger donor. There was no difference in Lamin B1 in the epidermis compared between arm ( $48.66 \pm 2.681$  n=4) and buttock ( $47.92 \pm 2.126$  n=4) region in older donor. Buttock dermis showed a higher percentage of Lamin B1- positive cells ( $24.13 \pm 1.984$  n=4) compared to the arm region ( $15.32 \pm 1.242$  n=4) from the older group.

**Region comparison**

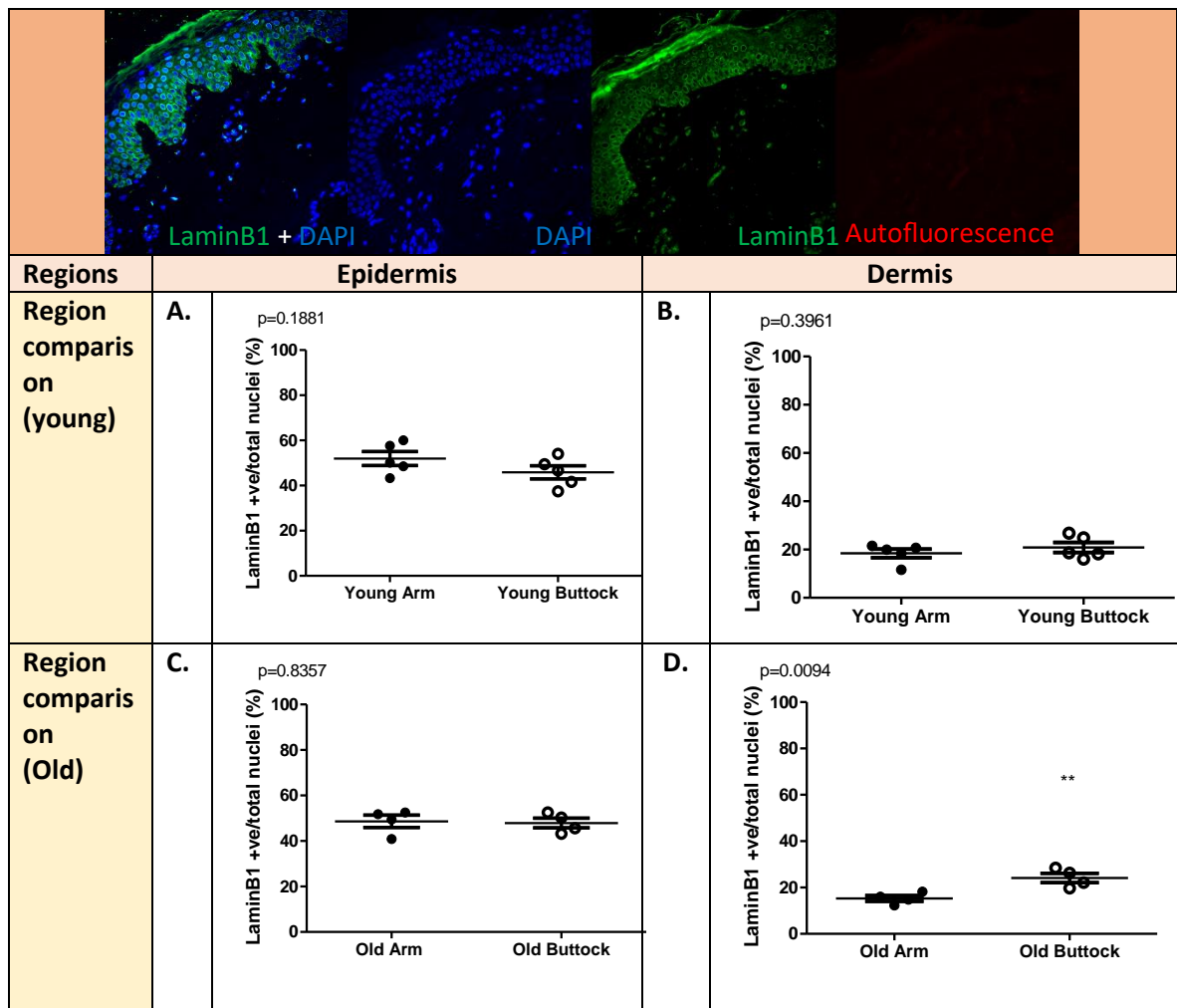


Figure 39 Changes in Lamin B1 compared between arm and buttock regions in human skin samples.

**A.** The comparison of Lamin B1 between arm and buttock epidermis from young donors. No significant difference was observed with a p-value of 0.1881. **B.** The comparison of Lamin B1 compared between arm and buttock dermis from young donors. No significant difference was observed with a p-value of 0.3961. **C.** The comparison of Lamin B1 compared between arm and buttock epidermis from old donors. No significant difference was observed with a p-value of 0.8357. **D.** The comparison of Lamin B1 compared between arm and buttock dermis from old donors. A significant difference was presented with a p-value <0.01\*\*. Data were analysed by unpaired-t-test; Young samples (arm and buttock) show the mean of 5 individuals, and old samples (arm and buttock) show the mean of 4 individuals, with each dot represents one individual.

### 5.2.3 Changes in p16INK4a compared between different age groups in human skin samples

The change of p16INK4a was observed in both compartments of the skin (epidermis and dermis) comparing between ages. The p16INK4a was analysed by immunofluorescence staining and reported as a percentage (%). p16INK4a in the arm epidermis significantly increased with age (young  $10.17 \pm 0.6842$  n=5 vs old  $18.62 \pm 1.153$  n=4). There was no change

in p16INK4a in the arm dermis compared between the young ( $5.997 \pm 0.9741$  n=5) and old donors ( $6.771 \pm 1.023$  n=5). There was a significant increase in p16INK4a in the buttock epidermis compared between young ( $12.74 \pm 0.4481$  n=5) and old donors ( $15.77 \pm 0.2443$  n=4). The percentage of p16INK4a nuclear-positive cells in the buttock dermis significantly increased with age (young  $3.900 \pm 0.7411$  n=5 vs old  $11.39 \pm 1.341$  n=5).

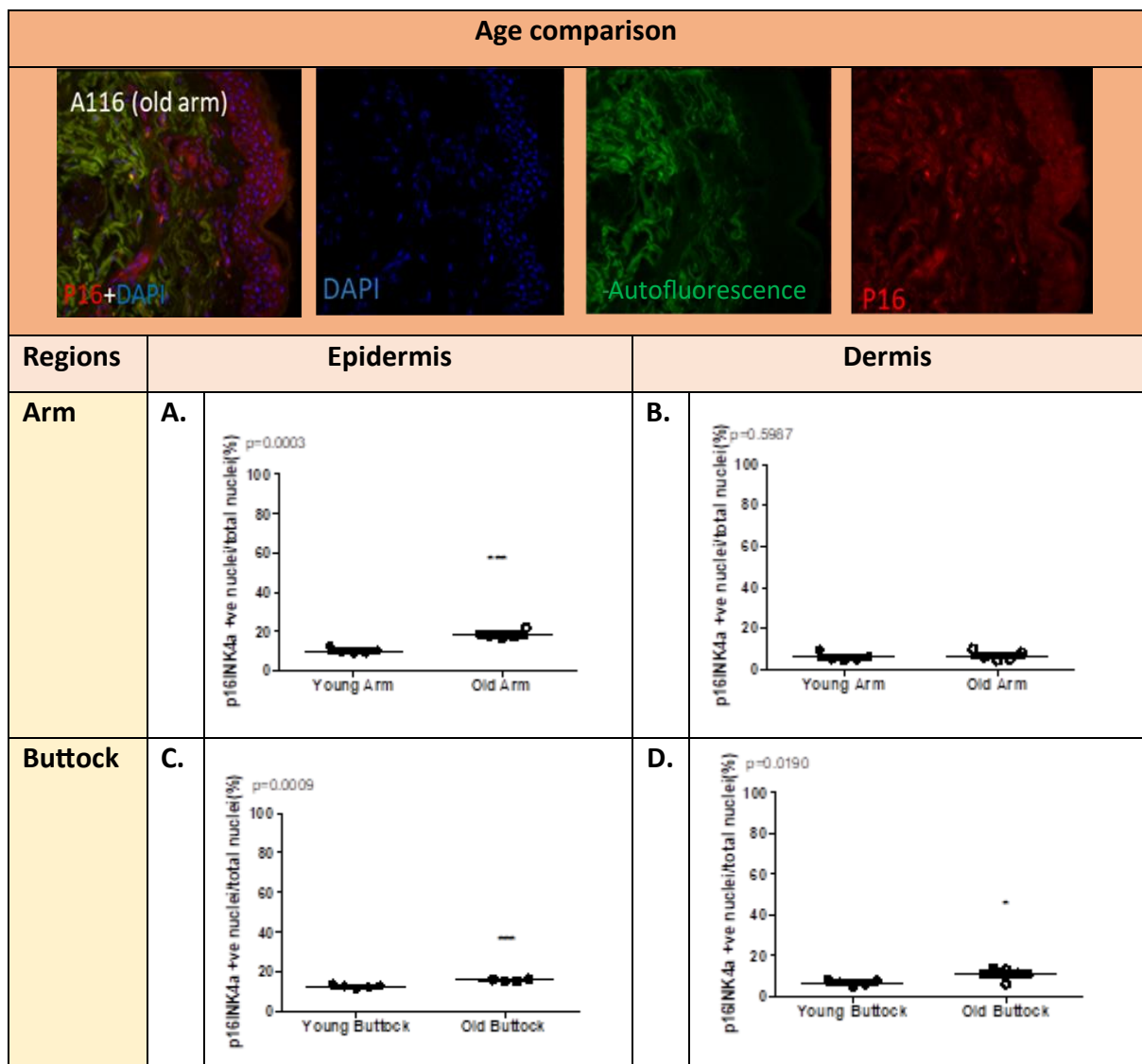


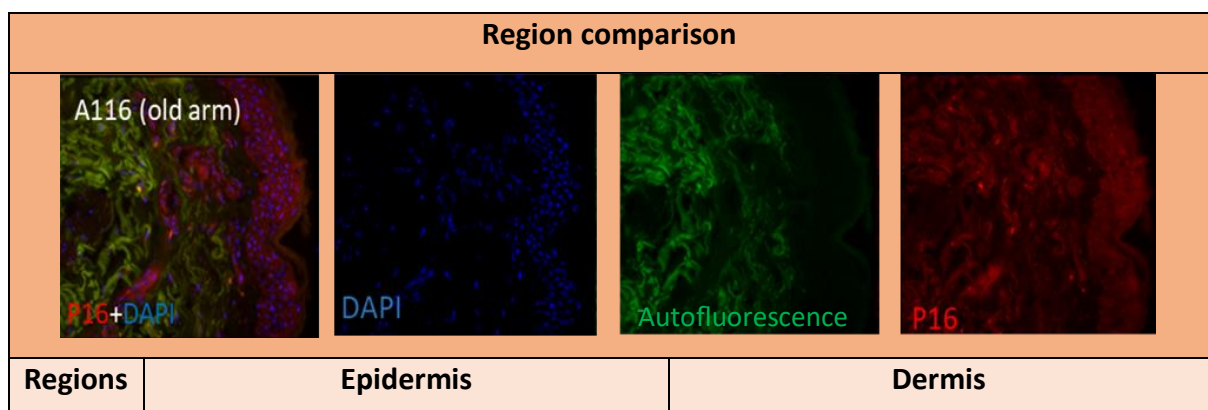
Figure 40 Changes in p16INK4a compared between ages in human skin samples.



**A.** The change of p16INK4a compared between young and old arm epidermis. A significant difference was presented with a p-value <0.001\*\*\*. **B.** The change of p16INK4a compared between young and old arm dermis. No significant difference was observed with a p-value of 0.5987. **C.** The change of p16INK4a compared between young and old buttock epidermis. A significant difference was presented with a p-value <0.001\*\*\*. **D.** The change of p16INK4a compared between young and old buttock dermis. A significant difference was presented with a p-value <0.01\*. Data were analysed by unpaired-t-test; Young and old samples (arm and buttock) show the mean of 5 individuals, except old arm and buttock epidermis (A & C) show the mean of 4 individuals, with each dot represents one individual.

#### 5.2.4 Changes in p16INK4a compared between different regions in human skin samples

The change of p16INK4a was observed in both compartments of the skin (epidermis and dermis) comparing between skin regions. The Lamin B1 was analysed by immunofluorescence staining and reported as a percentage (%). P16INK4a showed no difference in the epidermis compared between sun-exposed (arm) ( $10.17 \pm 0.6842$  n=5) and sun-protected (buttock) ( $12.74 \pm 0.4481$  n=5) regions in younger donors. No change of P16INK4a in the dermis compared between arm ( $18.44 \pm 1.778$  n=5) and buttock ( $20.90 \pm 2.079$  N=5) region in younger donors. There was no change in p16INK4a in the epidermis compared between arm ( $18.62 \pm 1.153$  n=4) and buttock ( $15.77 \pm 0.2443$  n=4) region in older donors. Buttock dermis showed a higher percentage of P16INK4a- positive cells ( $11.39 \pm 1.341$  n=5) compared to the arm region ( $6.771 \pm 1.023$  n=5) from the older group.



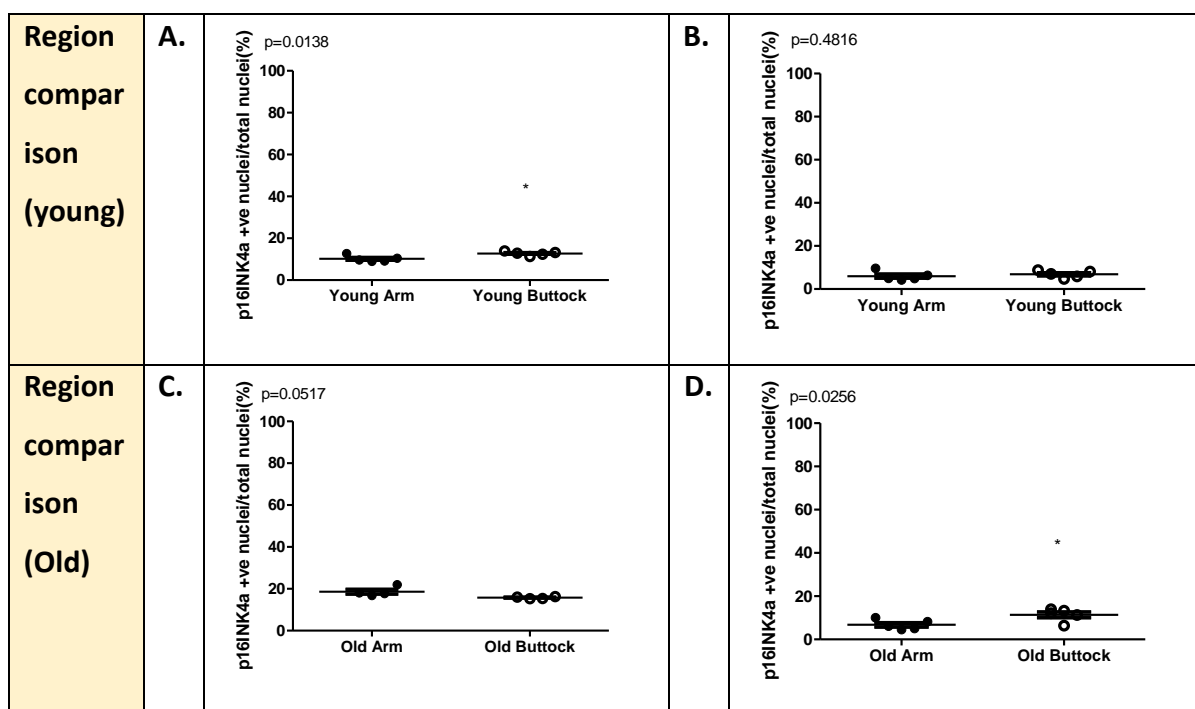


Figure 41 Changes in p16INK4a compared between arm and buttock regions in human skin samples.

**A.** The comparison of p16INK4a compared between arm and buttock epidermis from young donors. A significant difference was presented with a p-value  $<0.05^*$ . **B.** The comparison of p16INK4a compared between arm and buttock dermis from young donors. No significant difference was observed with a p-value of 0.4816. **C.** The comparison of p16INK4a between arm and buttock epidermis from old donors. No significant difference was observed with a p-value of 0.0517. **D.** The comparison of p16INK4a compared between arm and buttock dermis from old donors. A significant difference was presented with a p-value  $<0.05^*$ . Data were analysed by unpaired-t-test; Young samples (arm and buttock) show the mean of 5 individuals, and old samples (arm and buttock) show the mean of 4 individuals, with each dot represents one individual.

### 5.2.5 Changes in HMGB1 compared between different age groups in human skin samples

The change of HMGB1 was observed in both compartments of the skin (epidermis and dermis) comparing between ages. The HMGB1 was analysed by immunofluorescence staining and reported as a percentage (%). HMGB1 significantly decreased in the arm epidermis compared between the young ( $45.07 \pm 2.531$  n=5) and old ( $30.02 \pm 1.160$  n=4) donors. There was no change in HMGB1 in the arm dermis compared between the young ( $11.78 \pm 0.7992$  n=5) and old donors ( $11.00 \pm 1.825$  n=4). There was no change in HMGB1 in the buttock epidermis compared between young ( $39.28 \pm 2.643$  n=5) and old donors ( $32.08 \pm 2.587$  n=5). The percentage of HMGB1 nuclear-positive cells in the buttock dermis showed no change with age (young  $10.64 \pm 1.835$  n=4 vs old  $15.14 \pm 1.185$  N=5).

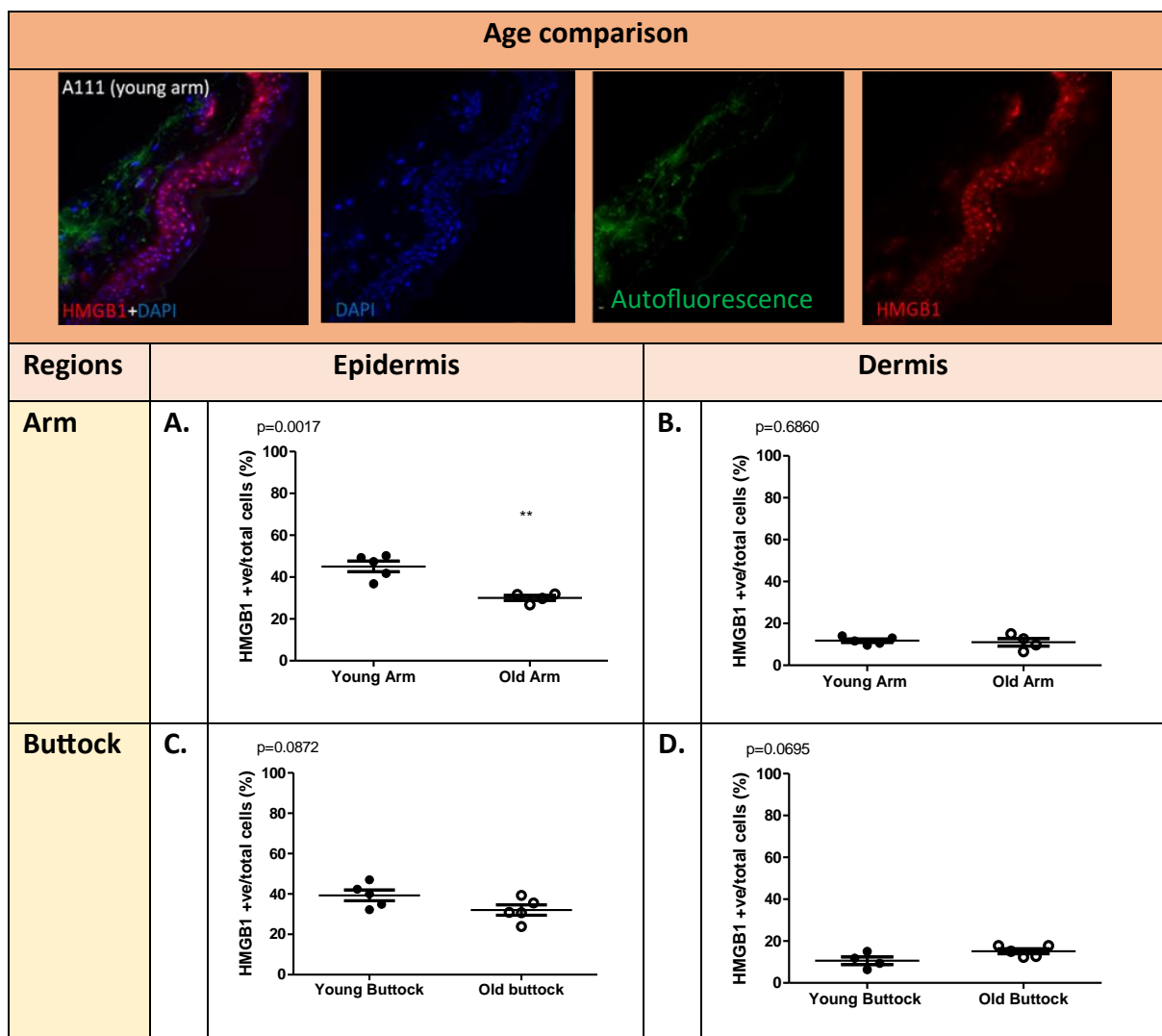


Figure 42 Changes in HMGB1 compared between ages in human skin samples.

**A.** The change of HMGB1 compared between young and old arm epidermis. A significant difference was presented with a p-value  $<0.01^{**}$ . **B.** The change of HMGB1 compared between young and old arm dermis. No significant difference was observed with a p-value of 0.6860. **C.** The change of HMGB1 compared between young and old buttock epidermis. No significant difference was observed with a p-value of 0.0872. **D.** The change of HMGB1 compared between young and old buttock dermis. No significant difference was observed with a p-value of 0.0695. Data were analysed by unpaired-t-test; Young and old samples (arm and buttock) show the mean of 5 individuals, except old arm and young buttock dermis (B & D) show the mean of 4 individuals, with each dot represents one individual.

### 5.2.6 Changes in HMGB1 compared between different regions in human skin samples

The change of HMGB1 was observed in both compartments of the skin (epidermis and dermis) comparing between skin regions. The Lamin B1 was analysed by immunofluorescence staining and reported as a percentage (%). HMGB1 showed no difference in the epidermis compared between sun-exposed (arm) ( $45.07 \pm 2.531$  n=5) and sun-protected (buttock) ( $39.28 \pm 2.643$  n=5) regions in younger donors. No change of HMGB1 in the dermis compared between arm

( $11.78 \pm 0.7992$  n=5) and buttock ( $10.64 \pm 1.835$  n=4) region in younger donors. There was no change in HMGB1 in the epidermis compared between arm ( $30.02 \pm 1.160$  n=4) and buttock ( $32.08 \pm 2.587$  n=5) region in older donors. Buttock dermis showed a higher percentage of HMGB1- positive cells ( $11.00 \pm 1.825$  n=4) compared to the arm region ( $15.14 \pm 1.185$  n=5) from the older group.

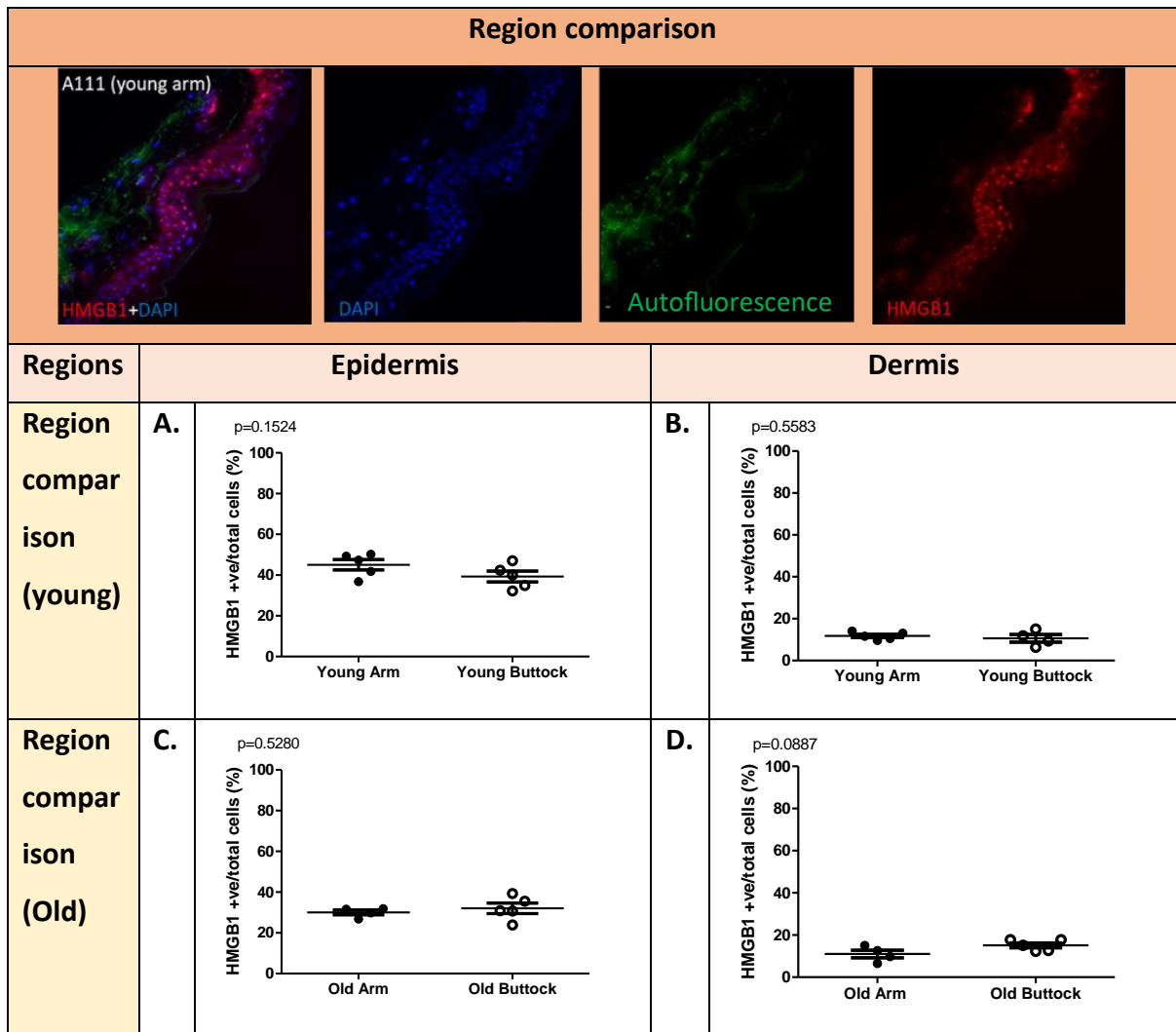


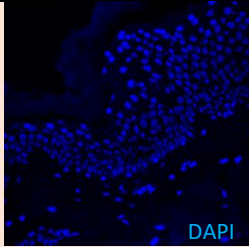
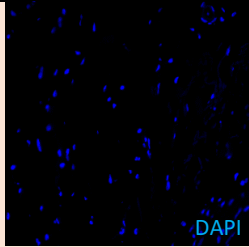
Figure 43 Changes in HMGB1 compared between arm and buttock regions in human skin samples.

**A.** The change of HMGB1 compared between arm and buttock epidermis from young donors. No significant difference was observed with a p-value of 0.1524. **B.** The change of HMGB1 compared between arm and buttock dermis from young donors. No significant difference was observed with a p-value of 0.5583. **C.** The change of HMGB1 compared between arm and buttock epidermis from old donors. No significant difference was observed with a p-value of 0.5280. **D.** The change of HMGB1 compared between arm and buttock dermis from old donors. No significant difference was observed with a p-value of 0.0887. Data were analysed by unpaired-t-test; Young and old samples (arm and buttock) show the mean of 5 individuals, except old arm epidermis and dermis (C & D) show the mean of 4 individuals, with each dot represents one individual.

### 5.2.7 Changes in nuclear size compared between different age groups in human skin samples

The change of nuclear size was observed in both compartments of the skin (epidermis and dermis) when comparing different age groups. The nuclear size was analysed using immunofluorescence staining and measured as area ( $\mu\text{m}^2$ ) by manually outlining each cell using the ICY polygon tool. In the arm epidermis, the nuclear size significantly decreased in older donors ( $26.51 \pm 0.3098$ ,  $n=1090$ ) compared to younger donors ( $30.85 \pm 0.2720$ ,  $n=1764$ ). Similarly, there was a decrease in nuclear size in the arm dermis for older donors ( $16.88 \pm 0.4239$ ,  $n=697$ ) compared to younger donors ( $18.51 \pm 0.1645$ ,  $n=635$ ).

Conversely, in the buttock epidermis, the nuclei significantly increased in size for older donors ( $31.71 \pm 0.3198$ ,  $n=1088$ ) compared to younger donors ( $28.35 \pm 0.2120$ ,  $n=1925$ ). Additionally, the area of nuclear size in the buttock dermis significantly increased with age (young:  $17.02 \pm 0.4544$ ,  $n=464$ ; old:  $19.20 \pm 0.5079$ ,  $n=532$ ).

Age comparison		
		
Regions	Epidermis	Dermis

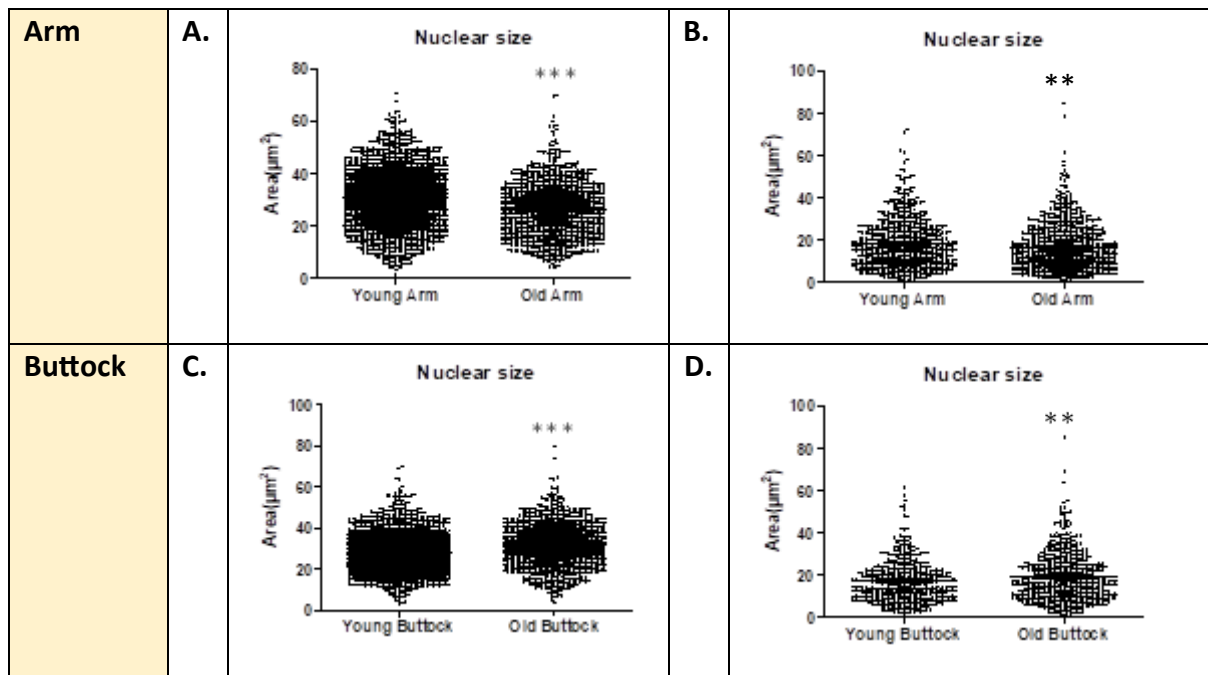


Figure 44 Changes in nuclear size compared between ages in human skin samples.

**A.** The change of nuclear size compared between young and old arm epidermis. A significant difference was presented with a p-value  $<0.001^{***}$ . **B.** The change of nuclear size compared between young and old arm dermis. A significant difference was presented with a p-value  $<0.05^{**}$ . **C.** The change of nuclear size compared between young and old buttock epidermis. A significant difference was presented with a p-value  $<0.001^{***}$ . **D.** The change of nuclear size compared between young and old buttock dermis. A significant difference was presented with a p-value  $<0.05^{**}$ . Data were analysed by unpaired-t-test with each dot represents one nucleus.

### 5.2.8 Changes in nuclear size compared between different regions in human skin samples

The change in nuclear size was observed in both compartments of the skin (epidermis and dermis) comparing between different regions. Nuclear size was analysed through immunofluorescence staining and was measured as area ( $\mu\text{m}^2$ ) by manually outlining each cell using the ICY polygon tool.

In younger donors, the sun-exposed (arm) region showed larger nuclear sizes in the epidermis ( $30.85 \pm 0.2720$ ,  $N=1764$ ) compared to the sun-protected (buttock) region ( $28.35 \pm 0.2120$ ,  $N=1925$ ). Similarly, in the dermis, the arm region showed larger nuclei sizes ( $18.51 \pm 0.4645$ ,  $N=635$ ) compared to the buttock region ( $17.02 \pm 0.4544$ ,  $N=464$ ).

Among the older group, the buttock epidermis showed larger nuclear sizes ( $31.71 \pm 0.3198$ ,  $N=1088$ ) compared to the arm ( $26.51 \pm 0.3098$ ,  $N=1090$ ). Additionally, the buttock dermis

showed larger nuclear sizes ( $19.20 \pm 0.5079$ , N=532) compared to the arm region ( $16.88 \pm 0.4239$ , N=697).

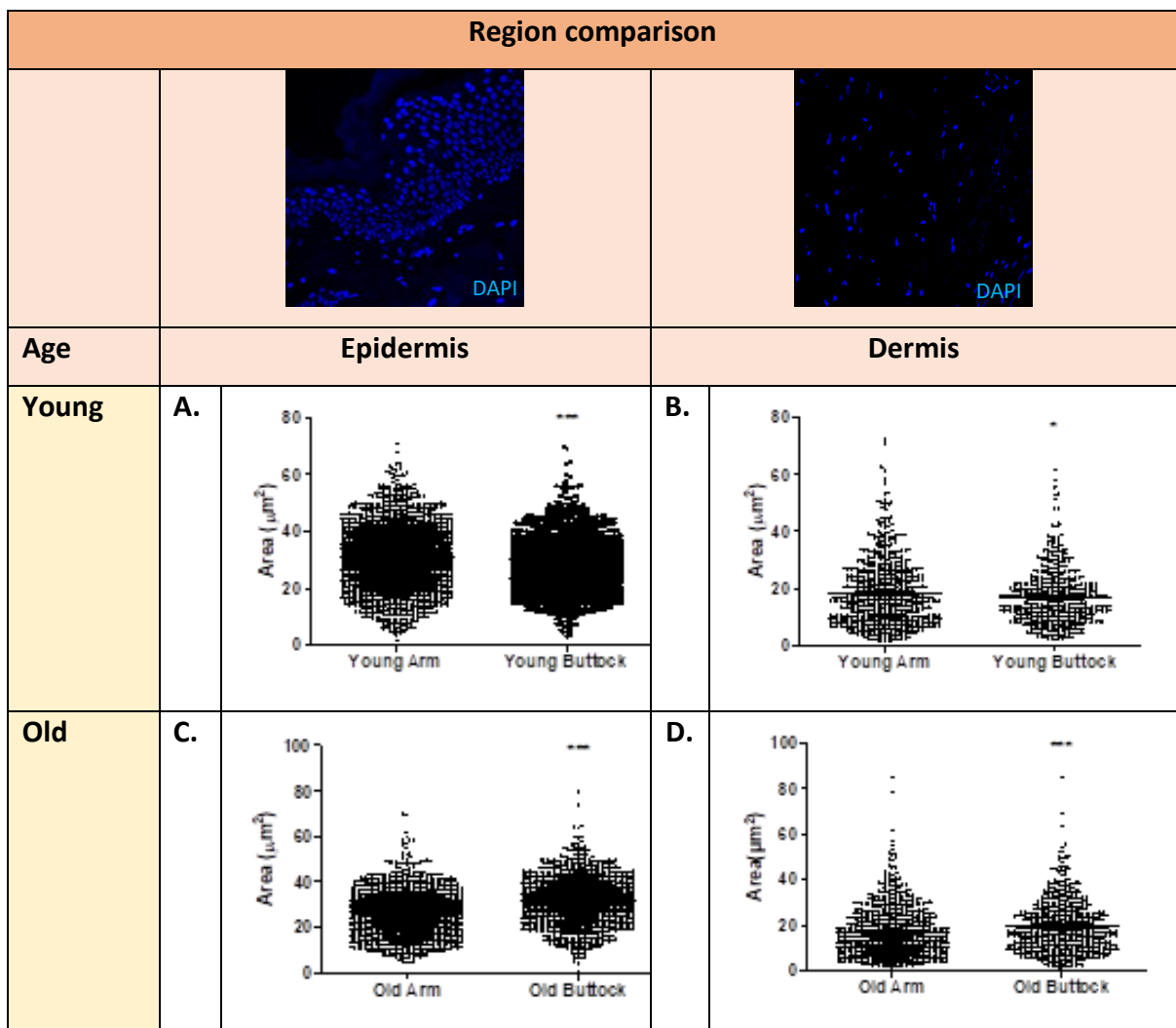


Figure 45 Changes in nuclear size compared between arm and buttock regions in human skin samples.

**A.** The change of nuclear size compared between arm and buttock epidermis from young donors. A significant difference was presented with a p-value <0.0001\*\*\*. **B.** The change of nuclear size compared between arm and buttock dermis from young donors. A significant difference was presented with a p-value 0.0259\*. **C.** The change of nuclear size compared between arm and buttock epidermis from old donors. A significant difference was presented with a p-value <0.0001\*\*\*. **D.** The change of nuclear size compared between arm and buttock dermis from old donors. A significant difference was presented with a p-value 0.0004 \*\*\*. Data were analysed by unpaired-t-test with each dot represents one nucleus.

### 5.2.9 Measurement of nuclear size in basal and suprabasal cells using skin differentiation marker

In the previous results, we anticipated observing larger nuclear sizes in the sun-exposed area (arm) due to UV exposure accelerating skin aging. However, the findings showed a significant increase in nuclear size with age only in the buttock area, in both the epidermis and dermis. The earlier results quantified nuclear size across the entire epidermal layer, without distinguishing between different cell types within it. Literature suggests that the most substantial changes during skin aging occur in the basal layer of the epidermis. Therefore, to ascertain if the expected changes could be identified, the tissues were subcategorized into basal and suprabasal layers with the staining of skin differentiation markers, Cytokeratin 10 (CK-10) and cytokeratin 14 (CK-14), to differentiate between basal and suprabasal cells. During the staining process with CK-10 and CK-14, we observed potential artifact regions (Figure 46), such as abnormalities resembling nodular melanoma, revealing pseudoepitheliomatous hyperplasia with high expression of K14 (Kodet, et al., 2015). These abnormalities were excluded from the measurements.

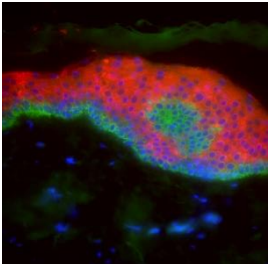
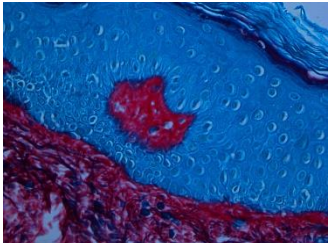
CK10 & CK14	Picro-sirus red and fast green staining
	



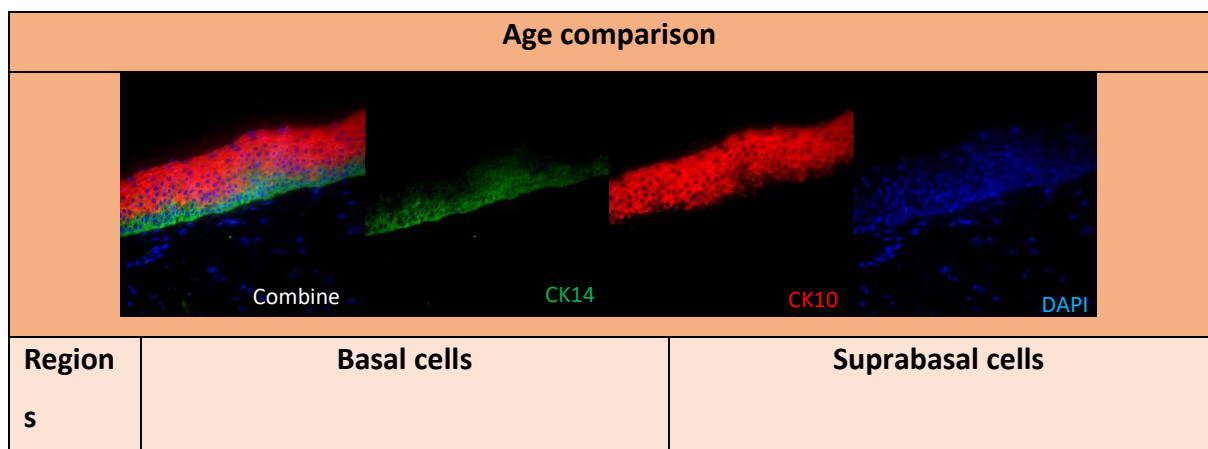
Figure 46 Abnormality resembling nodular melanoma was found in human epidermal samples.

The figure above depicts abnormalities in the epidermis of human skin samples, exhibiting similarities to nodular melanoma through the staining of CK-10 (red) and CK-14 (green). There is a hyperexpression of CK-14 evident in the suprabasal region

### 5.2.10 Changes in basal and suprabasal nuclear size in human skin with age

Nuclear sizes were measured as area ( $\mu\text{m}^2$ ) by manually outlining each cell using the ICY polygon tool. Basal cells were identified through Cytokeratin 14 staining, and nuclei within the green area were measured. The basal nuclear size area ( $\mu\text{m}^2$ ) was significantly reduced in the old arm ( $30.94 \pm 0.3650$ ,  $n=783$ ) compared to the young arm ( $34.12 \pm 0.3647$ ,  $n=1060$ ) (Figure 47A). Suprabasal cells were identified through Cytokeratin 10 staining, and nuclei within the red area were measured. The suprabasal nuclear size area ( $\mu\text{m}^2$ ) showed a significant reduction in the old arm ( $32.79 \pm 0.3132$ ,  $n=970$ ) compared to the young arm ( $35.08 \pm 0.2602$ ,  $n=1357$ ) (Figure 47B).

In the buttock region, there was no change of basal nuclear size area ( $\mu\text{m}^2$ ) with old buttock ( $31.67 \pm 0.4043$ ,  $n=845$ ) compared to the young buttock ( $32.07 \pm 0.2907$ ,  $n=1266$ ) (Figure 47C). The suprabasal nuclear area ( $\mu\text{m}^2$ ) showed a significant reduction in the old buttock ( $29.58 \pm 0.2599$ ,  $n=1242$ ) compared to the young buttock ( $33.18 \pm 0.2121$ ,  $n=1557$ ) (Figure 47D).



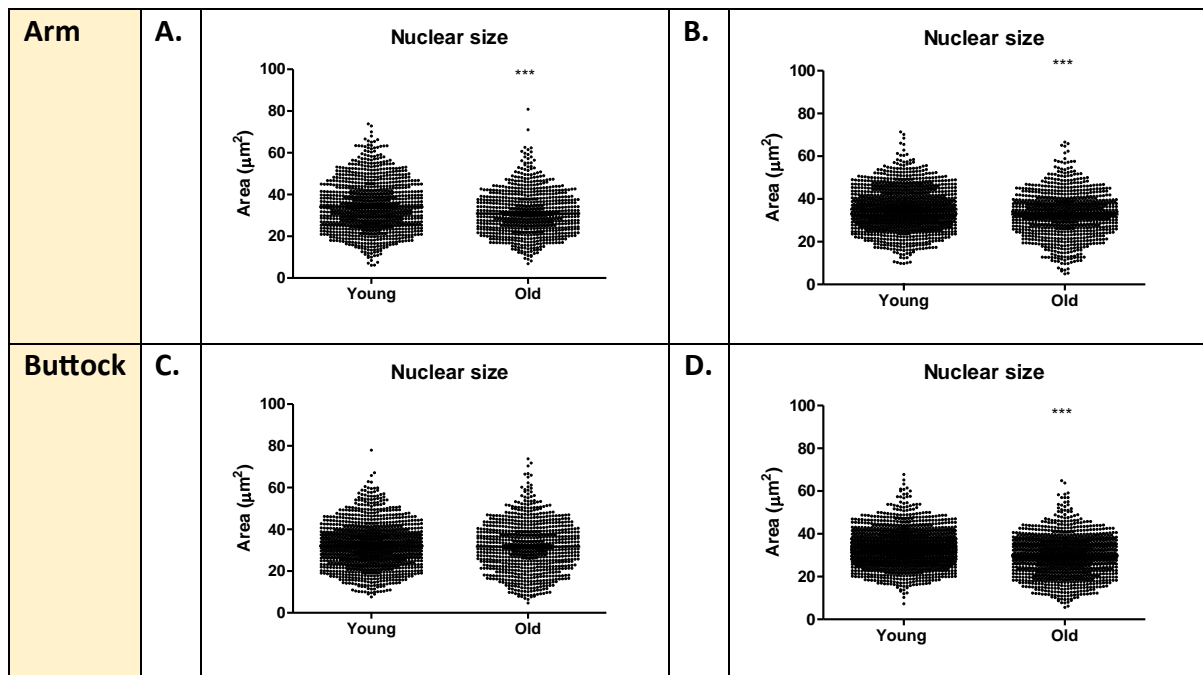


Figure 47 The comparison of basal and suprabasal nuclear size in young and old arm skin samples.

**A.** Comparison of nuclear size between young and old arm epidermis basal cells, identified by Cytokeratin 14 (green). A significant difference was observed with a p-value of  $<0.001^{***}$ . **B.** Comparison of nuclear size between young and old arm epidermis suprabasal cells, identified by Cytokeratin 10 (red). A significant difference was noted with a p-value of  $<0.001^{***}$ . **C.** Comparison of nuclear size between young and old buttock epidermis basal cells, identified by Cytokeratin 14. No significant difference was observed, with a p-value of 0.4039. **D.** Comparison of nuclear size between young and old buttock epidermis suprabasal cells, identified by Cytokeratin 10. A significant difference was observed with a p-value of  $<0.001^{***}$ .

### 5.2.11 Changes in basal and suprabasal nuclear size compared between regions in human skin samples

Nuclear sizes were measured in terms of area ( $\mu\text{m}^2$ ) by manually outlining each cell using the ICY polygon tool. Basal cells were identified through Cytokeratin 14 staining, and nuclei within the green area were measured. In younger donors, the basal nuclear size area ( $\mu\text{m}^2$ ) was larger in the arm ( $34.12 \pm 0.3647$ ,  $n=1060$ ) than in the buttock ( $32.07 \pm 0.2907$ ,  $n=1266$ ) regions (Figure 48A). Suprabasal cells were determined by Cytokeratin 10 staining. Nuclei stained within the red area were measured. The suprabasal nuclear size area ( $\mu\text{m}^2$ ) was larger in the arm ( $35.08 \pm 0.2602$ ,  $n=1357$ ) than in the buttock ( $33.18 \pm 0.2121$ ,  $n=1557$ ) regions in the younger donors (Figure 48B).

In older donors, there was no change in basal nuclear size area ( $\mu\text{m}^2$ ) between the old arm ( $31.67 \pm 0.4043$ ,  $n=845$ ) and old buttock ( $30.94 \pm 0.3650$ ,  $n=783$ ) (Figure 48C). However, the

suprabasal nuclear area ( $\mu\text{m}^2$ ) was significantly larger in the old buttock ( $33.18 \pm 0.2121$ ,  $n=1557$ ) compared to the arm (Figure 48D).

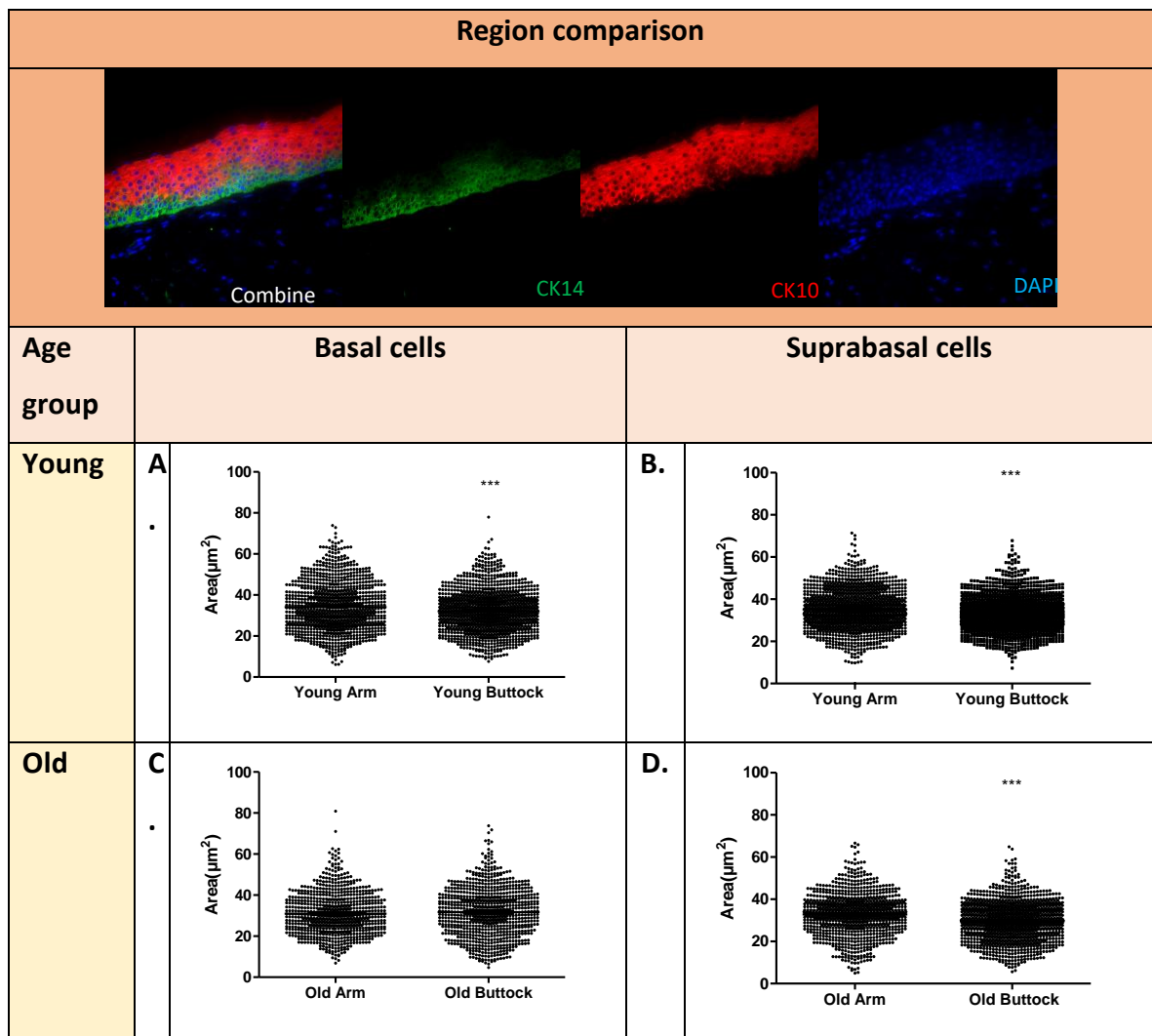


Figure 48 The comparison of basal and suprabasal nuclear size in young and old buttock skin samples.

**A.** Comparison of nuclear size between young arm and buttock epidermis basal cells, identified by Cytokeratin 14 (green). A significant difference was observed with a p-value of  $<0.001^{***}$ . **B.** Comparison of nuclear size between young arm and buttock epidermis suprabasal cells, identified by Cytokeratin 10 (red). A significant difference was observed with a p-value of  $<0.001^{***}$ . **C.** Comparison of nuclear size between old arm and buttock epidermis basal cells, identified by Cytokeratin 14. No significant difference was found, with a p-value of 0.1826. **D.** Comparison of nuclear size between old arm and buttock epidermis suprabasal cells, identified by Cytokeratin 10. A significant difference was observed with a p-value of  $<0.001^{***}$ . The data were analyzed using an unpaired t-test, with each dot representing one nucleus.

#### 5.2.12 Senescence-associated $\beta$ -galactosidase (Sen- $\beta$ -Gal) in human tissue

There was a faint staining of Sen- $\beta$ -Gal observed in the *stratum corneum* region, no staining was found in other parts of the epidermis and dermis. However, the presence of clear cell melanisation in the *stratum basale* indicates sun-damage.

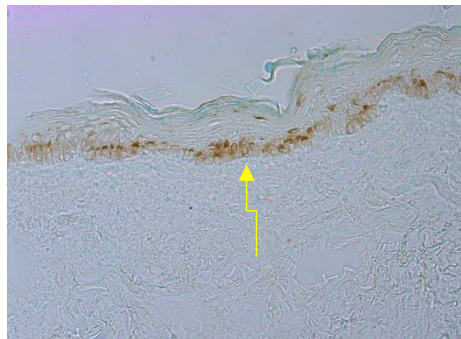


Figure 49 Sen- $\beta$ -Gal staining in human arm skin sample.

The figure above shows Sen- $\beta$ -Gal staining in human arm skin samples. No Sen- $\beta$ -Gal staining (blue) seen in either epidermis or dermis. However, cell melanisation (brown) (shown by yellow arrows), was visible in the basal epidermal layer, indicating sun-damaged skin (Dimri, et al., 1995).

### 5.3 Discussion

Table 5 Changes of senescence phenotypes *in vitro*.

This table illustrates the changes in senescence phenotypes *in vitro* under various conditions. Biomarkers such as LaminB1, Ki67,  $\gamma$ H2A.x, P16INK4a, p21WAF1/CIP1, HMGB1, Sen- $\beta$ -Gal, and nuclear size are compared between young cells and cells induced to senescence by IR or H<sub>2</sub>O<sub>2</sub> treatment over specific time intervals. The colour coding table helps visually represent the changes in senescence biomarkers across different experimental conditions in Table 5.

Biomarker	Young VS IR-induced senescent (Day 10)		Young VS H2O2-induced senescent (Day 7 & 10)	Young VS IR-induced senescent (Day 0-Day 10)	
	HDFn	HEKn	HDFn	HDFn	HEKn
LaminB1	↓***	↓***	↓***	↓***	↓***
Ki67	↓***	↓***	↓***	↓***	↓***
yHY2A.x	No change	↑***	↑***	↑***	↑***
P16INK4a	-	↑***	NA	-	No change
p21WAF1/CIP1	No change	-	NA	No change	-
HMGB1	↓***	↓*	NA	NA	NA
Sen- $\beta$ -Gal	NA	NA	↑***	NA	NA
Nuclear size	↑***	↑***	↑***	↑***	↑***

Colour Coding	Indication
	Decrease
	No change
	Increase
	Not found
	Not Available (NA)

In this experiment, senescence markers were validated across various mammalian models, starting with *in vitro* studies involving fibroblasts and keratinocytes, followed by *in vivo* experiments using human skin tissue. The first experiment involved the comparison between young and senescent cells (10 days post IR) in neonatal human dermal fibroblasts (HDFn) and neonatal human epidermal keratinocytes (HEKn). Overall, the results for all the senescence markers aligned with our hypotheses, where Ki-67, HMGB1 and LaminB1 were significantly reduced in senescent cells in both HDFn and HEKn.

In section 5.1.4, it was observed that  $\gamma$ H2A.x significantly increased in senescent HEKn but showed no change in the HDFn cells. The increase in  $\gamma$ H2A.x in young cells could be due to the phosphorylation during cell proliferation. Therefore, relying solely on  $\gamma$ H2A.x staining might not accurately distinguish senescent cells. This is why the dual staining of Ki-67 and  $\gamma$ H2A.x is considered a superior method for identifying senescent cells as senescent cells stopped proliferating, allowing us to easily exclude the young proliferative cells that are positive for both Ki-67 and  $\gamma$ H2A.x (Ki-67 +ve / $\gamma$ H2A.x +ve). This leaves us the cells that are Ki-67 negative and only positive for  $\gamma$ H2A.x (Ki-67 -ve / $\gamma$ H2A.x +ve), serving as a clear indicator of senescent cells. However, while p21WAF1/CIP1 is only present in HDFn but not HEKn, the opposite is true for P16INK4a. The absence of P16INK4a, p21WAF1/CIP1 and no change of  $\gamma$ H2A.x in senescent cells could have been repaired or recovered during the 10 days of resting while waiting for the senescence phenotypes to develop.

A time course test was conducted to examine whether the hypothesis was supported by observing the change of senescence phenotypes in HDFn and HEKn. Initially, H<sub>2</sub>O<sub>2</sub> treatment was used to induce senescence in HDFn, and the changes in senescence phenotypes were observed on days 0, 7 and 10. Sen-  $\beta$ -Gal significantly increased sharply on day 7 and even further on day 10, while Ki-67 and Lamin B1- positive cells showed a dramatic reduction after H<sub>2</sub>O<sub>2</sub> treatment. Since the previous  $\gamma$ H2A.x staining alone did not yield the expected results, subsequent experiments involved co-stained with Ki-67 to identify senescent cells more distinctly. As expected, senescent cells (Ki-67 -ve / $\gamma$ H2A.x +ve) significantly increased after 7 days of H<sub>2</sub>O<sub>2</sub> treatment, but a slight recovery was observed on day 10.

A similar experiment was duplicated using IR-induced senescent cells. This time, the change of senescence phenotypes was observed from day 0 to day 10 post-IR at one-day intervals. In HDFn, LaminB1 gradually reduced after irradiation and recovered until it reached a plateau. On the other hand, HEKn proved more sensitive to irradiation, displaying the loss of LaminB1

with no recovery. When Ki-67 and  $\gamma$ H2A.x were combined to detect young proliferative cells, the data showed that young cells (Ki-67 +ve / $\gamma$ H2A.x +ve) decreased sharply after irradiation and remained constant through day 10. A similar trend was observed in HEK293T but it occurred gradually. In contrast, the trend for senescent cells (Ki-67 -ve / $\gamma$ H2A.x +ve) was opposite. These time course experiments have conclusively demonstrated that  $\gamma$ H2A.x significantly increased after the induction of senescence by both irradiation and H<sub>2</sub>O<sub>2</sub> treatment. However, a slight drop in  $\gamma$ H2A.x was observed from day 7 to day 10. This decrease of  $\gamma$ H2A.x suggests that some  $\gamma$ H2A.x recovered on day 10 after irradiation. It also raises the possibility that relying solely on  $\gamma$ H2A.x staining may not be entirely reliable. However, it could still possibly be due to experiment-to-experiment variation in the assignment of cells as positive or negative as each experiment was conducted at a different time using different batches of antibodies, cells or even variations in intensity between images, which might lead to a subjective definition of senescent cells. Additionally, there was a change in the color of the secondary antibody due to insufficient secondary antibody during the staining process. However, this change is unlikely to affect quantification. The data also confirmed that p21WAF1/CIP1 is only present in HDFn but not HEK293T; the opposite holds true for P16INK4a.

The enlargement of nuclear size was observed in all three experiments involving IR and H<sub>2</sub>O<sub>2</sub>-induced senescent cells. The enlargement in nuclear size represents the most straightforward assay for identifying senescent cells.

*Table 6 Summary of the changes in senescence phenotypes in vivo.*

This table illustrates the comparison of various parameters including LaminB1, P16INK4a, HMGB1, Sen- $\beta$ -Gal, and nuclear size in human skin tissue samples, both in terms of age and regional differences. The colour coding facilitates the interpretation of the data.

Human skin tissue sample (Age Comparison)				
	Epidermis		Dermis	
	Arm	Buttock	Arm	Buttock
P16INK4a	↑***	↑***	No change	↑***
LaminB1	No change	No change	No change	No change
HMGB1	↓**	No change	No change	No change
Sen- $\beta$ -Gal	-	-	-	-
Human skin tissue sample (Regional Comparison)				
P16INK4a	No change	↑*	No change	↑*
LaminB1	No change	No change	No change	↑**
HMGB1	No change	No change	No change	No change
Sen- $\beta$ -Gal	-	-	-	-

Nuclear size ( $\mu\text{m}^2$ ) (all cells in epidermis) (Age comparison)				
	Epidermis		Dermis	
Arm	↓***		↓**	
Buttock	↑***		↑**	
Nuclear size ( $\mu\text{m}^2$ ) (all cells in epidermis) (Regional comparison)				
	Epidermis		Dermis	
	Arm	Buttock	Arm	Buttock
Young	Larger***	No change	Larger*	No change
Old	No change	Larger***	No change	Larger***
Nuclear size ( $\mu\text{m}^2$ ) (CK14+CK10) (Age comparison)				
	Basal cells		Suprabasal cells	
Arm	↓***		↓**	
Buttock	No change		↓**	
Nuclear size ( $\mu\text{m}^2$ ) (CK14+CK10) (Regional comparison)				
	Basal cells		Suprabasal cells	
	Arm	Buttock	Arm	Buttock
Young	Larger***	No change	Larger***	No change
Old	No change	No change	No change	Larger***

Colour Coding	Indication
	Decrease
	No change
	Increase/larger
	Not found

A parallel experiment was conducted using *in vivo* models aimed to corroborate the observed senescence markers in a more physiologically relevant context. This study involved skin samples from individuals aged between 20- and 60-years old obtained from arm and buttock regions to represent sun-exposed and sun-protective areas, respectively. The staining methodology applied *in vitro* for senescence markers was replicated in the *in vivo* setting.

Overall, no significant change was found with age except for p16INK4a. The finding shows that p16INK4a is the only marker showing a significant increase with age in both the epidermis in arm and buttock regions. This indicated a potential role of p16INK4a in age-related changes in skin. However, it is worth noting that the frequency of p16INK4a-positive cells remains relatively low, accounting for less than 20% in both skin compartments. A previous study has demonstrated that in the epidermis, cells positive for p16INK4a or p21 increased with age, accounting 4% and 6% of total cells in older individuals, respectively. Meanwhile in the dermis, while p21 showed an increase with age, p16 was undetectable (Idda, et al., 2020). Reduction of HMGB1 was observed in arm epidermis with age. This raises the question of whether it is



true that almost all the cells expressing high levels of p16INK4a were melanocytes (Waaijer, et al., 2016; Victorelli, et al., 2019) since the density of melanocytes in the human epidermal basal layer is most often referred to as 5- 10% (Chung, Suh, Han, & Oh, 2011; Burns & Rook , 2004)

Similarly, Sen- $\beta$ -Gal staining, while accurately for determining senescence in Human dermal fibroblasts cells (HDFn), did not yield conclusive results *in vivo*. Sen- $\beta$ -Gal staining only present in the *stratum corneum* region and was absent in the epidermis and dermis. While Sen- $\beta$ -Gal is a well-established method for identifying senescent *in vivo*, it is important to note that it is most effective with freshly obtained tissue samples.

Since nuclear enlargement was observed in all the *in vitro* experiments, we attempted to use the standard measurement of nuclear size to identify senescent cells. Our results showed that nuclear enlargement only present in the buttock region when comparing two different age groups. In the regional comparisons, young donors showed larger nuclear size in arm region, potentially due to greater outdoor activities. In contrast, in the older group, nuclear size was larger in the buttock region, possibly linked to ageing. However, this observation may be related to blood content, as measured by skin reflectance meter (quantification of light absorption) (Sandby-Møller, Poulsen, & Wulf, 2003). To further distinguish the sublayers within the epidermis, we utilized skin differentiation markers Cytokeratin 14 (CK-14) and Cytokeratin 10 (CK-10). The nuclear size of both basal and suprabasal cells was separately, excluding the abnormalities present in the epidermis (Figure 46). Similarly, young donors showed larger nuclear size in the arm region.

This set of experiments underscore that senescence phenotypes can vary significantly depending on cell types, methodological issues with marker sensitivity, or even time points over senescence phenotype development. When different markers are required to identify senescence, inconsistency of biomarkers application and various combinations of biomarkers can be individually nonspecific (Sharpless & Sherr, 2015). Our data supports the hypothesis that age comparisons hold true for *in vitro* studies but not *in vivo*. The alternative hypothesis was inconclusive, as no difference were found between spectated regions.

However, there were several limitations for the *in vivo* study needed to be addressed. Firstly, the sample size was initially small, and for some individuals, only arm samples were available without corresponding buttock samples. We attempted to obtain paired individual samples

for sun-exposed (arm) or sun-protected area (Buttock) for a robust comparison. Unfortunately, this could not be guaranteed for some of the donors. Furthermore, the skin samples received were collected more than 10 years ago, potentially impacting the quality of staining. Some of the samples either did not have an epidermal or dermal layer, which made it impossible to perform a correlation analyses. Moreover, comparing epidermal thickness between different body sites may not be a suitable option due to variations in factors like blood content, which could potentially influence the differences in thickness. Skin samples collected from the inner or outer arm would be a better approach for comparison for more robust results.

Secondly, the number of the samples should have been sufficient for all the senescence markers that were stained *in vitro*, such as P21, Ki-67 and  $\gamma$ H2a.x. However, they were assigned to a different scientist as part of the project. The samples were taken away without any useful data being collected. All these factors led to experimental repetition being impossible.

Regarding quantification, although the use of skin differentiation marker helps in identifying abnormalities within the epidermis, the use of single cell as unit assessment may not be appropriate. Due to unforeseen circumstances, the necessary adjustment could not be made as the raw data is no longer available.

## Chapter VI Addressing the effects of senescent fibroblasts in the full thickness Alvetex 3D skin equivalents

### 6.0 Introduction

Accumulation of senescent cells, especially senescent dermal fibroblasts, has been widely hypothesized as a probable cause of dermal and epidermal ageing (Campisi, 1998; Demaria, Desprez, Campisi, & Velarde, 2015; Fitsiou, Pulido, Campisi, Alimirah, & Demaria, 2021; Ho & Dreesen, 2021; Lee, Choi, Roh, Lee, & Kim, 2021; Toutfaire, Bauwens, & Debaq-Chainiaux, 2017; Velarde & Demaria, 2016; Wang & Dreesen, 2018; Wlaschek, Maity, Makrantonaki, & Scharffetter-Kochanek, 2021). This is in accordance with the fact that senescent cells secrete a wide range of bioactive molecules including cytokines, chemokines, matrix-modifying factors, reactive oxygen species and others termed the Senescence-Associated Secretory Phenotype (SASP) that induce 'ageing-like' bystander effects in neighbouring cells and tissues (Nelson, et al., 2012; Xu, et al., 2018) and with intervention experiments showing postponements of ageing by anti-senescence interventions in many organs (Kirkland & Tchkonja, 2017). However, the specific evidence for senescent fibroblasts causing epidermal ageing is still not very strong (Low, et al., 2021). While very recently reversal of skin ageing effects in mice following high dose senolytic treatment has been reported (Kim, Park, Kweon, & Baek, 2022), this does not address the impact of a specific cell type because senolytic interventions act systemically.

It was challenging in obtaining high-quality human skin samples, in addition to the limitations of 2D monolayer cell culture systems to map the complex structure of the skin, studying the crosstalk between cell types in the skin microenvironment was impossible. Bioengineered 3D skin models are well suited to address this problem from the perspective of multicellular and

multi-layered complexity of human skin *in vitro*, allowing interactions between different cell populations to be studied. They offer a reproducible and scalable approach to studying fundamental skin biology. Importantly, these models offer full control over the type and frequencies of senescent cells that are incorporated. As stated in section 1.5, small number of 3D skin-equivalents have been developed to test the impact of senescent dermal fibroblasts (Diekmann, et al., 2016; Janson, Rietveld, Willemze, & El Ghalbzouri, 2013; Lämmermann, et al., 2018; Weinmüllner, et al., 2020), however, most of these studies have limitations, including a lack of complexity, by foregoing the importance of cellular crosstalk, or physiological relevance, through use of entirely senescent populations. Additionally, results were not unequivocal: in a collagen-based matrix, fibroblasts in H<sub>2</sub>O<sub>2</sub>-or doxorubicin-induced senescence induced hallmarks of intrinsic skin ageing including epidermal thinning, reduction of basal keratinocyte proliferation, impairment of epidermal differentiation and loss of barrier function (Lämmermann, et al., 2018; Weinmüllner, et al., 2020). In a collagen–glycosaminoglycan–chitosan scaffold, senescent fibroblasts (senescence induced by treatment with Mitomycin C) reduced epidermal filaggrin as well as dermal collagen and elastin expression and structure but had no effect on epidermal thickness (Diekmann, et al., 2016). Finally, in a fibroblast-derived matrix in a polyester permeable support (Janson, Rietveld, Willemze, & El Ghalbzouri, 2013), replicatively senescent fibroblasts caused a thinner dermis and minor changes in the epidermal expression of keratin 6 and 10, but no changes in epidermal thickness, keratinocyte proliferation or basement membrane formation.

A main limitation of previous skin equivalents is variability due to the use of complex protocols and of exogenous extracellular matrix (ECM) proteins. We recently developed a robust and unique full-thickness skin equivalent that is highly reproducible due to the use of a consistent scaffold, commercially available cells, and defined low-serum media. The Alvetex® scaffold technology allows human dermal fibroblasts (HDF) to produce their own endogenous ECM proteins within the material, which alleviates the need for exogenous collagen, and fully supports the differentiation and stratification of the epidermis (Costello, et al., 2019; Roger, et al., 2019).

To assess the impact of senescent dermal fibroblasts on the dermal and epidermal compartments, we bioengineered Alvetex-based human full thickness skin models with modifiable frequencies of senescent fibroblasts (ranging from 0-100%) in the dermal model at the point of seeding. Fluorescently labelled fibroblasts were used for a quantitative estimation

of the actual fractions of senescent cells within the skin equivalents and the impact of senescent cell density variation was compared for inter-observer variation. Senescent cells were either treated with 20Gy X-ray radiation or 2uM Doxorubicin for 4 hours to induce senescence phenotypes before seeding into the skin models. The dermal equivalents were allowed to mature for 28 days, followed by the formation of an epidermal layer for an additional 14 days (Section 2.4.2). Epidermal properties were assessed by two independent observers, one of whom was fully blinded to the proportion of senescent HDFn in the sample. Prior to the analysis, the observers reached a consensus on the operationalization of measurements, as outlined in Section 2.7.

This study aimed to comprehend the impact of senescent dermal fibroblasts on the proliferation and differentiation of the epidermis, as well as the morphological parameters of the basal keratinocytes. We hypothesised that an increased frequency of senescent fibroblasts in the dermis would affect the mentioned properties of the epidermis, specifically resulting in an increase in epidermal (keratinocytes) senescence together with a thinning of the epidermal layer. To explore whether the hypothesis is true, multiple biomarkers such including Ki-67, P63, HMGB1, nuclear and basal cell size (Cytokeratin 10 & Cytokeratin 14), as well as measurement of epidermal thickness were conducted to explore the crosstalk between skin layers. To extend our understanding of the specific impact of dermal senescence on the skin layer, HMGB1 staining was also applied in the dermal compartment.

Furthermore, we sought to address the experimental and inter-observer variations within our analyses, in a system where numbers of senescent cells were well controlled.

### 6.1 Full thickness 3D collagen gel and 3D Alvetex skin equivalent

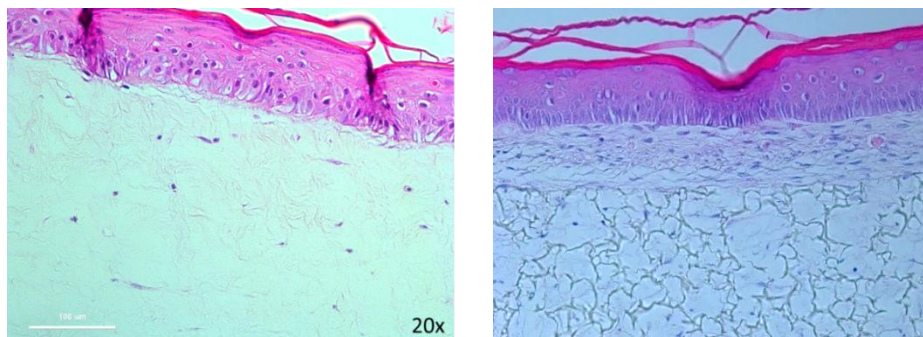


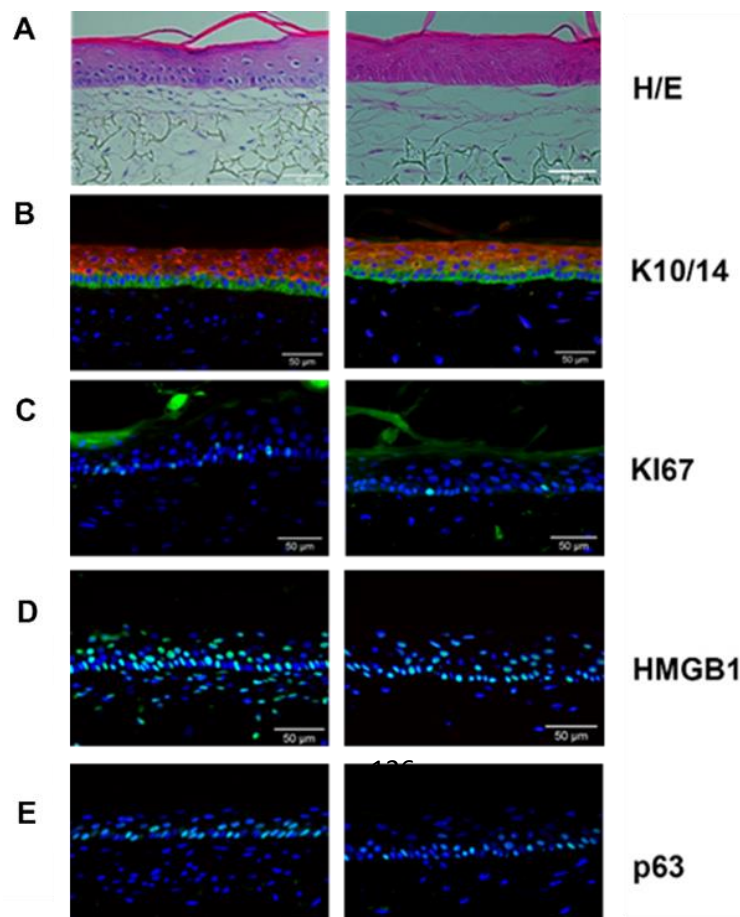
*Figure 50 Full thickness 3D collagen gel and 3D Alvetex skin equivalent.*

The figures show the comparison between full thickness 3D collagen gel skin model (left) and full thickness 3D Alvetex skin model (right).

As a part of a validation process, the full-thickness collagen gel 3D skin model, using only young dermal fibroblast, was repeated for a reproducibility validation. In parallel, full-thickness Alvetex 3D model was created by Dr. Lucy Smith and compared against the collagen gel model to examine the differences in skin structure. Both methods showed a complete epidermis formation with defined keratinocyte sublayers. Alvetex skin models showed better reproducibility. Therefore, the decision was made to proceed further experiments on the Alvetex platform due to extreme shrinkage during the formation of collagen gel 3D model.

## 6.2 Senescent dermal fibroblasts caused basal cells hypertrophy in the epidermis.

To assess the impact of senescent dermal fibroblasts on the dermal and epidermal compartments in the 3D bioengineered skin model, we incorporated different frequencies of senescent fibroblasts (from 0 to 100%) into the dermal model at the point of seeding. Dermal equivalents were matured for 28 days followed by formation of an epidermal layer for 14 days. Epidermal properties were measured by two independent observers, one of which was fully blinded to the fraction of senescent fibroblasts in the sample. Changes in epidermal morphology and phenotypes, such as epidermal thickness (Figure 51A), basal cell size (Figure 51B), basal nuclear size (Figure 51B), ki-67 (Figure 51C), HMGB1 (in basal cells and epidermis) (Figure 51D), and P63 (in basal cells only) (Figure 51E), were measured and compared between observers.

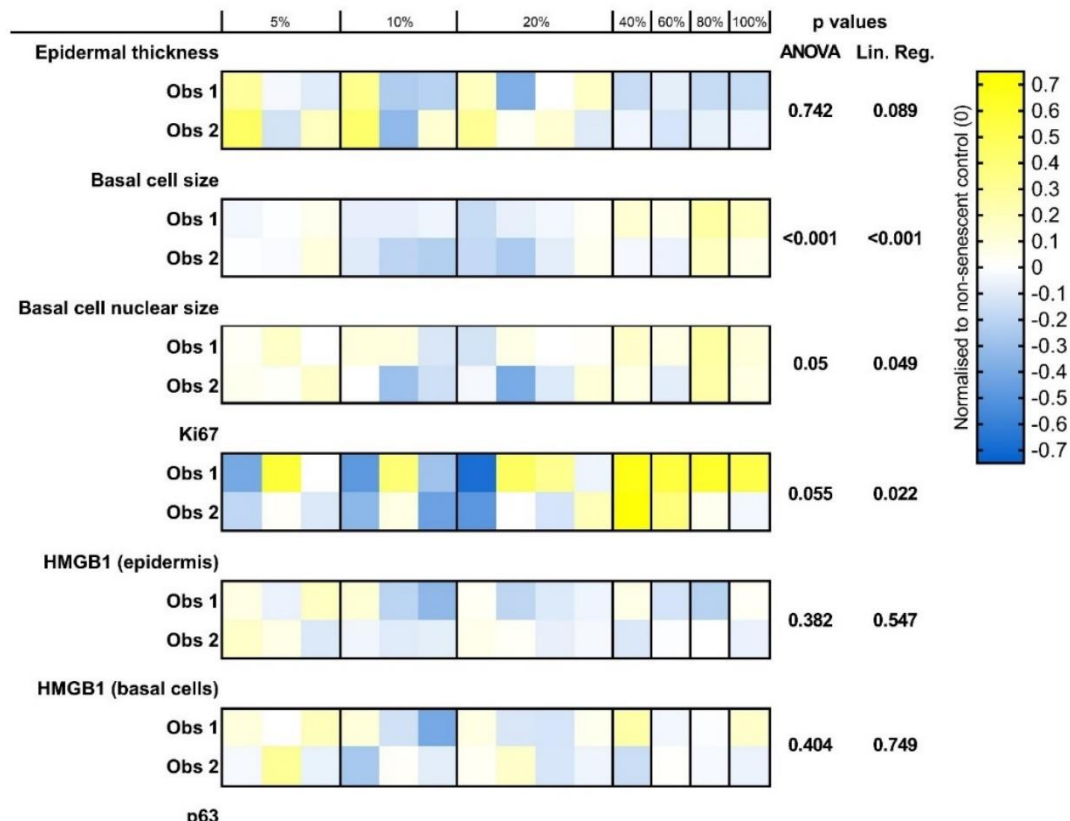


**0%                      100%**  
**senescent HDF**

*Figure 51 Representative immunofluorescence micrographs of full thickness models*

Figures shows the representative immunofluorescence of full thickness models with either 0% or 100% senescent cell seeding density for **A)** Haematoxylin and Eosin, **B)** Cytokeratin-10 (red) and Cytokeratin-14 (green) staining to measure basal cell and nuclear cell size, and **C)** Ki67 **D)** HMGB1 **E)** P63. Magnification bar: 50  $\mu$ m.

Biometric analysis of the epidermis showed a tendency towards epidermal thinning with increase in senescent cell load, but this was not statistically significant (Figure 52A). Qualitatively, there was no evidence for changed epidermal differentiation as judged by co-staining for cytokeratin K10 and K14 (Figure 51B). However, basal cell and nuclear size increased with increasing load of senescent fibroblasts (Figure 52B and C). Cell size histograms did not show the induction of a small number of large cells, but rather revealed a general hypertrophy of all basal keratinocytes together (Figure 52H). Moreover, immunofluorescence assessments of the cell senescence markers including HMGB1, p63 (figure 52 E-G) and LaminB1 (data not shown) were inconclusive showing large inter-experiment and inter-observer variation. Finally, results showed a tendency of induction of proliferation in basal keratinocytes (Ki-67) by high frequencies of senescent dermal fibroblasts (Figure 52D). Together, these data indicate that induction of cell senescence in the epidermis is not a major consequence of dermal senescence in the full thickness Alvetex skin model.





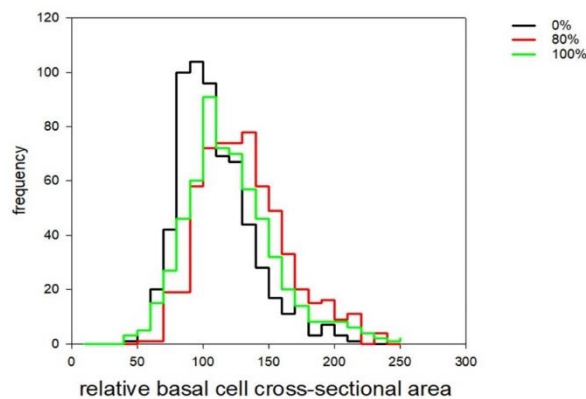


*Figure 52 Effect of increasing frequencies of senescent dermal fibroblasts onto the epidermal compartment measured by two independent observers.*

Samples were stained and measured separately by two individuals, observer 1 (non-blinded) and 2 (blinded). All data were normalized to controls containing only non-senescent HDFs. 5-10% n=3, 20% n=4, 40-100% n=1. **A)** Epidermal thickness, **B)** Basal cell area, **C)** Basal cell nuclear area, **D)** fractions of KI67-positive cells in the epidermis, **E)** fractions of HMGB1-positive cells in the epidermis, **F)** fractions of HMGB1-positive basal cells, **G)** fractions of p63-positive cells in the epidermis. p values were calculated by One-way ANOVA and by linear regression. **H)** Histogram of basal keratinocytes size in full thickness models generated with 0% (black), 80% (red) and 100% (green) senescent cell seeding density. Cell sizes were normalised to the mean size in the 0% model.

2-way ANOVA on the untransformed data indicated significant differences between observers for all parameters with exception of epidermal thickness and Ki-67 positivity (Figure 53). However, when the same analysis was performed on the normalized data (Figure 52), observer effects were cancelled out with the sole exception of p63, while the senescent cell density effects on basal keratinocyte morphology were confirmed (Table 7). This indicated that the major observer variation was due to a systematic bias which was similar in control (non-senescent) and senescent cell experiments and thus cancelled out by normalization for most experiments. The remaining inter-observer variation for the morphological and KI67

measurements was smaller than the experiment-to-experiment variation. However, even after normalisation there was relevant inter-observer variation remaining for the additional immunofluorescence data, which was probably due to differential assignment of signal positivity despite attempted harmonisation of protocols.

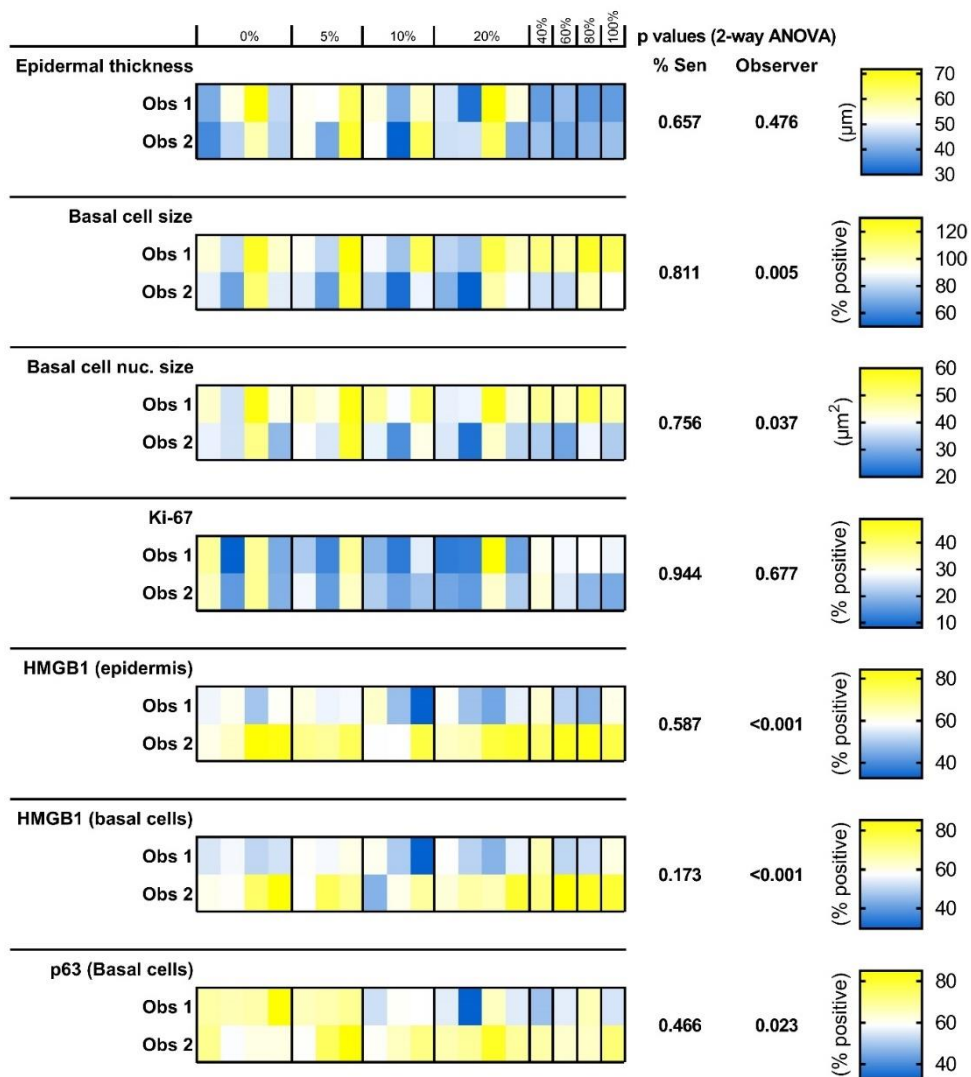


Figure 53 Observer bias in the assessment of increasing frequencies of senescent dermal fibroblasts onto the epidermal compartment.

Samples were stained and measured separately by two individuals, observer 1 (non-blinded) and 2 (blinded). Data are non-normalised. 5-10% n=3, 20% n=4, 40-100% n=1. **A)** Epidermal thickness, **B)** Basal cell area, **C)** Basal cell nuclear area, **D)** fractions of KI67-positive cells in the epidermis, **E)** fractions of HMGB1-positive cells in the epidermis, **F)** fractions of HMGB1-

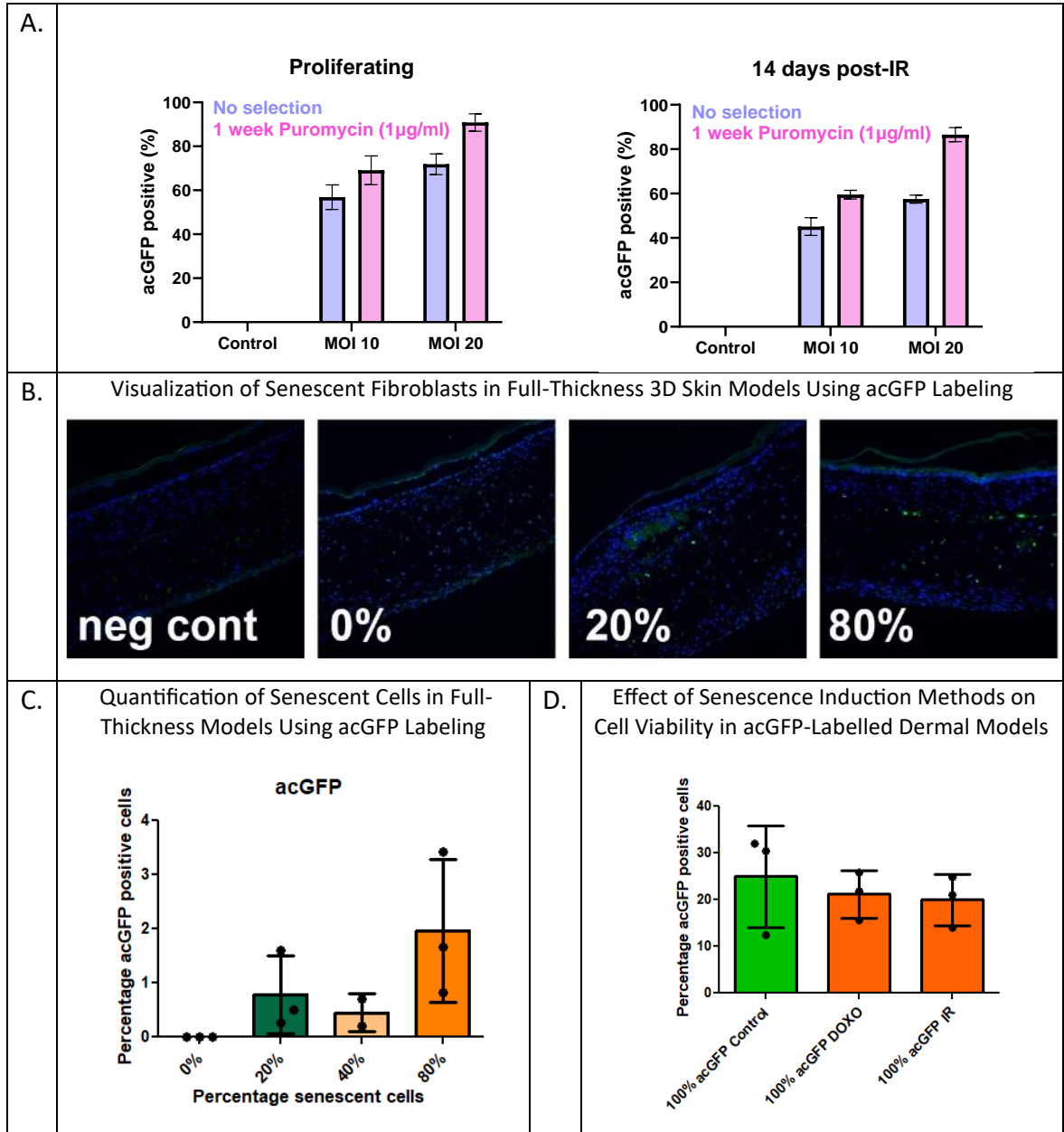
positive basal cells, **G**) fractions of p63-positive cells in the epidermis. p values were calculated by Two-way ANOVA.

### 6.3 Frequencies of senescent fibroblasts in the dermal skin models are low

To fully understand why we observe no evidence of any epidermal response in our model for senescent dermal fibroblast frequencies below a seeding density of 20% (figure 52), we replaced normal senescent dermal fibroblast with acGFP green fluorescing cells to distinguish the number of senescent cells in the 3D skin environment. Early passage human dermal fibroblasts (HDFn) were retrovirally transfected with acGFP, as described in section 2.1. After selection, a clear fluorescence signal was observed in at least 85% of the cells in 2D culture (Figure 53A). Subsequently, we constructed full-thickness 3D skin models with senescent cells seeding densities up to 80%, wherein all the senescent HDFns were labelled with acGFP. Surprisingly, very few acGFP-positive cells were observed through fluorescence microscopy. Even after immunostaining for GFP, the frequency of positive cells remained relatively low, averaging only 2.2% in the 80% senescent acGFP model (Figure 53B and C).

To determine whether this was attributed to low transgene expression or to migration/adherence issues of senescent cells, we created a dermal model with 100% labelled, non-senescent cells (Figure 53D). In this model, only 25% of the cells were seen as positive, indicating significant loss of transgene expression after 28 days in the matrix (Figure 53D). When acGFP cells that had integrated into the model were rendered senescent by either doxorubicin treatment or ionizing radiation, there was no further significant loss of signal (Figure 53D).

Counting the total number of (DAPI+) cells in the dermal models showed an increased vulnerability of acGFP-HDFn as compared to unlabelled cells; only half as many acGFP cells were integrated and retained in the matrix (Figure 53E). Although there was a tendency for reduced total cell numbers following IR or Doxorubicin treatment, this difference was not statistically significant.



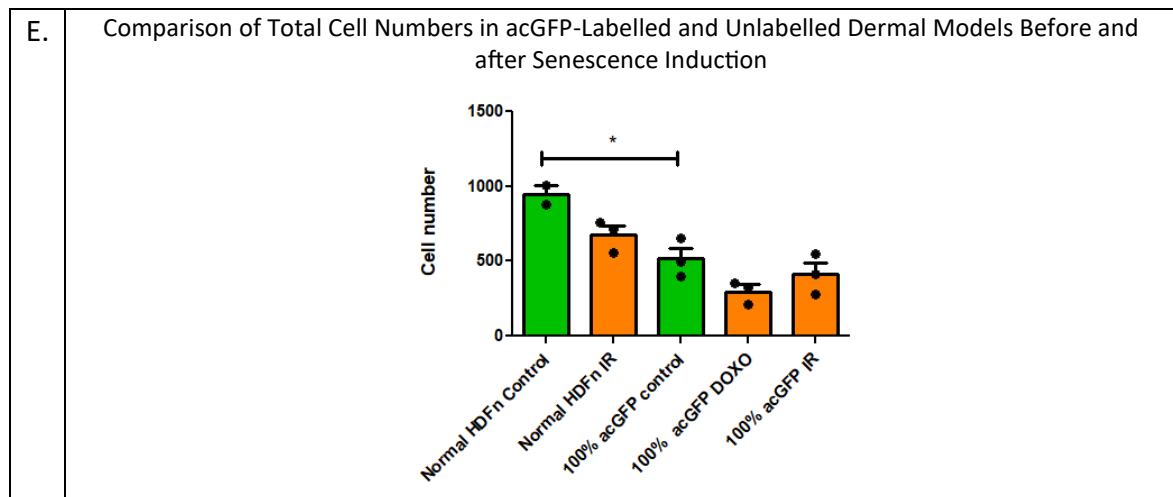


Figure 54 Senescent fibroblast densities within the dermal equivalent.

**A.** Retroviral transduction of human dermal fibroblasts (HDFn) was conducted by Dr. Edward Fielder. Early passage HDFn cells were transduced with acGFP1 using the rLV-EF1a-AcGFP1-Nuc-IRES-Puro-WPRE Vector (Takara bio, #0016VCT). The frequencies of acGFP-positive non-senescent Human Dermal Fibroblasts (HDFs) after transduction at Multiplicity of Infection (MOI) 10 and 20, with and without puromycin selection (left), and at 14 days after induction of senescence by 20 Gray (Gy) ionizing radiation (right). The expression of nuclear located acGFP1 protein was evaluated, with transfection efficacy reaching 90% after selection, and it remained after senescence induction (86%) using 20Gy X-ray irradiation. Analysis was performed using a Leica DMI8 microscope with a GFP cube and manually analysed using the Fiji ImageJ distribution.

**B.** The images illustrate full-thickness 3D skin models with increasing frequencies of senescent fibroblasts within the dermal layer. Starting from the left, the images represent the negative control, followed by conditions with 0%, 20% and 80% senescent frequency. These models were constructed using acGFP-labelled senescent human Dermal Fibroblasts (HDFs), mixed with non-labelled non-senescent HDFs at indicated frequencies before seeding into the matrix. This construction allows the visualization of senescent cells viability within the model. The samples were subsequently stained with GFP antibody (green) and DAPI (blue) for nuclear visualisation.

**C.** The graph shows the number of senescent cells within the full-thickness models, represented as the percentage of acGFP-positive cells across conditions with 0%, 20%, 40%, and 80% senescent frequency. Quantification of acGFP-positive cells from (B) shows no significant differences with a P-value of 0.0977. Each condition consists of 3 biological repeats, except for the 40% ratio of senescent cell models, which only consists of 2 biological repeats. Although the number of acGFP cells increases with the increased senescent cell conditions, very few acGFP-positive cells were observed, averaging 2.2% in the 80% senescent acGFP model, even after immunostaining for GFP. Cell numbers were counted manually using the ImageJ cell counter. Statistical analysis was conducted using one-way ANOVA. Error bars represent standard deviation (SD).

**D.** The graph illustrates dermal models composed entirely of acGFP-labelled cells under various treatment conditions inducing senescence, including 20Gy X-ray irradiation (IR) and Doxorubicin (Doxo) treatment. These conditions are compared against a control condition (untreated) to assess their effect on cell viability within the dermal model. No significant

difference was observed with a P-value of 0.7140, suggesting that different senescence induction methods do not affect cell viability in the model.

E. The graph illustrates the comparison of total cell numbers in acGFP-labelled and unlabelled dermal models before and after senescence induction by either 20Gy X-ray irradiation (IR) or Doxorubicin (Doxo) treatment. Total cell numbers were counted based on DAPI-positive staining. The total cell numbers (per 15,000  $\mu\text{m}^2$ ) in the dermal equivalent were manually measured using Image-J cell counter with 9 images/sample, presented as  $M \pm SD$ . \*\* indicates a statistically significant difference ( $p < 0.01$ , ANOVA). The graph suggests an increased vulnerability of acGFP-HDFn compared to unlabelled cells. Although there was a tendency for reduced total cell numbers following IR or Doxorubicin treatment, this difference was not statistically significant.

## 6.4 Discussion

*Table 7 Summary of two-way-ANOVA p values for untransformed and normalised data.*

This table summarizes the results of two-way ANOVA tests conducted on untransformed and normalized data. The table provides p-values for the effects of the observer, senescence, and their interaction on various parameters. Untransformed column presents the p-values obtained from the two-way ANOVA tests conducted on the original untransformed data. Normalised column presents the p-values obtained from the two-way ANOVA tests conducted on the data that have been normalized. P Observer provides the p-values representing the effect of the observer (inter-observer variability) on the respective parameter. P Senescence provides the p-values representing the effect of senescence on the respective parameter. P Interaction provides the p-values representing the interaction effect between the observer and senescence on the respective parameter.

	Untransformed			Normalised		
	p Observer	p Senescence	p Interaction	p Observer	p Senescence	p Interaction
Epidermal thickness	0.965	0.657	0.998	0.476	0.856	1
Ki-67	0.677	0.944	0.997	0.202	0.136	0.968
Nuclear size (Basal cells)	<0.001	0.656	0.946	0.165	0.072	0.882
Basal cell size	0.004	0.928	1	0.179	0.002	0.684
HMGB1 basal cells	<0.001	0.173	0.647	0.288	0.49	0.655

HMGB1						
Epidermis	<0.001	0.587	0.781	0.657	0.47	0.688
p63(basal cells)	0.023	0.466	0.125	<0.001	0.514	0.686

In general, senescent fibroblasts in the dermal compartment did not induce epidermal changes that are typically observed in intrinsically ageing skin, which include epidermal thinning and compromised keratinocytes differentiation (Low , et al., 2021). This result align with previous study by (Weinmüller, et al., 2020), where epidermal thickness showed a tendency towards thinning with an increased senescent cell load, but it was not statistically significant. The common factor in both studies was the induction of senescence in cells using stressors via H<sub>2</sub>O<sub>2</sub> and Doxorubicin, respectively. This raises the possibility that the use of naturally aged or late-passage fibroblasts might show a more pronounced effect on epidermal thickness. Alternatively, this may imply that senescent fibroblasts may not be the primary factor influencing epidermal thickness in skin ageing. This is supported by 3D model incorporating senescent melanocytes showed a significant epidermal thinning, strongly suggesting that senescent melanocytes might be a major source of senescence-associated signals in the epidermis (Vitorelli, et al., 2019).

An enlargement in both basal cell and nuclear size of keratinocytes was observed as the load of senescent fibroblasts increased. This effect became discernible at senescent fibroblasts seeding frequencies of 20% and higher. Notably, the enlargement of cell size revealed a general hypertrophy of all the basal keratinocytes. These changes might be indicative of induction of bystander senescence in a small number of keratinocytes, as cell and nuclear hypertrophy are well-established markers for cell senescence (Passos & von Zglinicki, 2007; Wallis, et al., 2022).

The immunofluorescence assessment of cell senescence markers, including HMGB1 and p63 yielded inconclusive results due to significant variability between experiments and observers. Both P63 and Ki-67 serve as markers of cell proliferation. However, P63 is predominantly expressed in putative stem cells, thus has been considered as a stem cell marker in keratinocytes. P63 is reported to be a key regulator of epidermal cell proliferation, differentiation, and adhesion (Carroll, et al., 2006; Truong, Kretz, Ridky, Kimmel, & Khavari, 2006). For instance, a complete deletion of p63 in mice resulted in the absence of epidermis

and epidermal-related tissues (Mills, et al., 1999). On the other hand, Ki-67 has been widely used in combination with other senescence markers, as senescent cells permanently exit from the cell cycle, resulting in the absence of Ki-67. We expect to see a reduction in both P63 and Ki-67 expression, as observed in human skin ageing. However, there was a notable tendency for increased proliferation in basal keratinocytes (Ki-67) in high senescent models. A similar trend was observed in a previous study by (Weinmüller, et al., 2020), where approximately 20% increased Ki-67 positivity was observed in the epidermal layer of the senescent skin model. This aligns with previous findings where extracellular vesicles derived from senescent cells promoted the proliferation of mesenchymal stem cells (MSCs) (Weilner, et al., 2016) or keratinocytes (Terlecki-Zaniewicz, et al., 2019). The increase in Ki-67 could possibly be due to the increased presence of senescent cells in the dermal compartment, leading to skin lesions (Soini, et al., 1994). For instance, the cytokines such as IL-4, IL-13, IL-22, and TNF  $\alpha$ ) have been known to induce keratinocyte hyperproliferation (hyperplasia) in the epidermis (Kim, Kim, & Sung, 2022; Bernard, et al., 2012). In our study, we only looked at IL-6 and IL-8 because human dermal fibroblasts from elder donors tend to produce higher amounts of IL-6 and IL-8 compared to younger donors (Wolf, et al., 2012). Therefore, it would be interesting to further characterise the cytokine output through the cytokine assay. As we increased the frequency of senescent fibroblasts cells to 20%, we did not observe any evidence of epidermal response induced by senescent dermal fibroblast in our model. Although the frequency of senescent fibroblasts in the skin of old individuals are expected to be lower than 20%, there is limited data regarding the proportion of senescent fibroblasts in the skin of aged animals or humans. The available senescence markers lack quantitative validation and exhibit significant variations in sensitivity and specificity. For instance, in mouse dermis, frequencies of  $\gamma$ H2AX-positive fibroblasts increased from about 1% in adults to 5% in animals aged 42 months (Wang, et al., 2009). In the dermis of old (>25 years) baboons, about 20% of the fibroblasts were positive for the senescence marker TAF (telomere-associated DNA damage foci) but up to 80% were positive for the heterochromatin marker HIRA, another marker for cell senescence (Herbig, Ferreira, Condel, Carey, & Sedivy, 2006). Frequencies of fibroblasts positive for senescence-associated beta-galactosidase tended to be below a few percent in the dermis of aged mice and humans (Dimri, et al., 1995; Wang, et al., 2009; Waaijer, et al., 2012). Therefore, our findings should still be relatively relevant to skin ageing.



In the context of bioengineered skin equivalents, cell seeding density should be well-controlled by the fractions of senescent fibroblasts seeded. However, when acGFP-fluorescing green senescent fibroblasts were incorporated into the skin model, the number of acGFP-positive was significantly lower than their initial seeding densities. For instance, in a mixed model containing 80% senescent acGFP cells, we would expect a smaller proportion of the senescent cells to be integrated into the model because of their lower migration efficacy or lower general robustness. However, experimentally, only 2% (Figure 2C) was observed which is far lower than expected, suggesting that additional factors contribute to a further 4 to 5-fold reduction in the proportions of senescent HDFs within the matrix. Proliferation of non-senescent cells is a strong candidate, as a fourfold increase in the fraction of non-senescent cells would be achieved by two population doublings over the course of 28 days of maturation of the dermal equivalent, which is not improbable. In other words, in a mixed full-thickness model made of non-transgenic HDFs, the actual fractions of senescent HDFs at the time of keratinocyte overlay may well be up to 10 times lower than their seeding densities.

In conclusion, senescent fibroblasts in the dermal compartment induced hypertrophy but not senescence in basal keratinocytes. They did not reduce keratinocyte proliferation or differentiation and neither did they significantly reduce epidermal thickness. A systematic bias was the main source of inter-observer variation, which could largely be compensated by normalisation to non-senescent controls. Using fluorescently labelled cells, we found that frequencies of senescent fibroblasts in the dermal equivalent were up to 10 times lower than senescent cell seeding densities, however, this did not explain the absence of ageing-like effects in our model. In comparison to published results, we conclude that effects of senescent dermal fibroblasts onto the epidermis are largely matrix dependent.

## Chapter VII General Discussion

Much evidence convincingly proved that cell senescence was a pathophysiologically-relevant cause of age-related deterioration and function loss. Removing senescent cells was shown to postpone age-associated functional decline and deterioration in multiple organ systems, including muscle, liver, lung, bone, the cardiovascular system, and the brain (Robbins, et al., 2021). Transplanting a small number of senescent cells shortened lifespan and led to the onset of symptoms like age-associated diseases but was rescued by the treatment of senolytic in mice (Xu, et al., 2018; Xu, et al., 2017). Similarly, in the skin, there was evidence of senescent cell in all compartments of aged skin *in vivo*; some studies also showed similar results in 3D skin models. In other cases, the application of senolytics or senostatic showed a positive effect in rescuing skin ageing (Low , et al., 2021).

The underlying skin ageing mechanisms strongly resembled the cellular senescence phenotypes (Gorgoulis, et al., 2019; von Zglinicki, Wan, & Miwa, 2021) (see 1.2 & 1.3). However, various studies used different biological models, including *in vivo* (mice, baboon, and human), *in vitro* (keratinocytes, fibroblasts) and 3D skin models. They primarily focused on a specific skin compartment/ cell type. There were difficulties in matching the cause and effect of senescence in the different models to one another. As a result, the available data

were insufficient to draw a conclusion whether the senescent skin cells were the main contributors to skin ageing.

As cancer treatment became a curable disease in a high proportion of patients, cancer survivors who received long-term DNA-damaging cancer therapies such as radiotherapy and chemotherapy tended to show signs of senescence-induced premature ageing. In the worst case, the bystander effects could lead to cancer relapse and even secondary cancers with a poorer prognosis (Jena, Das, Bharadwaj, & Mandal, 2020; Saleh, Tyutyunyk-Massey, & Gewirtz, 2019). Due to the increased cancer survival rate, the incidence of radiation-induced skin injury also rose, with nearly 90% of cancer survivors developing different degrees of skin damage attributed to cancer therapies (Yang, Ren, Guo, Hu, & Fu, 2020). The first experiment aimed to determine whether X-ray radiation caused long-lasting skin damage and whether the senolytics or senostatics could rescue the detrimental effect, as measured by the epidermal thickness in the mice model. I hypothesised that skin thickness reduced with age, and X-ray radiation caused skin damage and led to skin thickening. As expected, this experiment proved that, like humans, mice's epidermis, too, showed a 30% notable attrition of epidermal thickness with age. In contrast, 9 Gy of X-ray radiation caused hypertrophy or hyperplasia in the skin- one of the characteristics of extrinsic skin ageing.

Now that I had confirmed X-ray radiation caused extrinsic skin ageing with skin hypertrophy or hyperplasia, I continued to discover whether senolytic treatment could rescue skin damage from X-ray radiation. So far, only a few studies had tested the effect of senolytics on the skin (see 1.6), with only 1 clinical study showing a reduction of senescence markers in the skin after systemic treatment of Dasatinib and Quercetin (D+Q) (Hickson, et al., 2020). However, the effects on skin ageing after senolytic treatment were still missing, and whether the treatment duration at different times could lead to positive or detrimental effects remained unknown. Thus, to test the hypothesis of whether the anti-senescence intervention could rescue or postpone therapy-induced skin ageing by removing senescent cells, irradiated mouse models treated either with senolytic (Dasatinib+Quercetin (D+Q) or Navitoclax) or senostatic (Metformin) were compared to non-treated groups. The skin samples were collected at different time points to study the effect of drug treatment on epidermal thickness. Our findings showed no significant change in skin morphology after the treatment of senolytics. Early treatment of senostatic (Metformin) showed a trend towards reduction of epidermal hypertrophy. One discrepancy was that the Sham-IR controls for cohort 1 (Figure 14B) had a

mean epidermal thickness of around 6  $\mu\text{m}$ . In contrast, the control mice for cohorts 3, 4 and 5 (Figure 14C) showed mean epidermal thicknesses between 10 and 11  $\mu\text{m}$ . The irradiated mice for cohort 1 had an epidermal thickness of  $9.9 \mu\text{m} \pm 1.1 \mu\text{m}$ , similar to the epidermal thickness in the controls for cohorts 3, 4 and 5. Figure 14A showed a clear difference in the number of hair follicles and subcutaneous glands in the dermis layer. From a technical point of view, it could be due to the angle of incidence on the full-thickness cross-sections when the samples were collected or embedded. Cohort 1 skin samples were collected in 2018; the other cohorts were collected in 2019 and performed by different technicians.

A limitation of this study was that normal mice had a higher density of hair follicles, which may not have been an appropriate model for comparing irradiation responses in human skin. We chose these models due to ongoing experiments investigating the effects of IR-induced premature ageing and the impact of senolytic or senostatic treatment on various organs, including the brain, liver, thymus, testes, and muscles. Thus, skin was collected as a part of the study to correlate with the other organs. In the 1980s, hairless mice replaced normal mice to study the UV responses related to human skin. This was due to hair follicles stem cells are highly radiosensitive, radiation exposure could trigger the hair follicles into an active cycle, thus leading to thicker epidermis in mice (Hansen, Coggle, Wells, & Charles, 1984). In SKH1-HrHr hairless mice, 20 Gy irradiation showed no change in the epidermis morphology, but with the doses increased to 30- and 40 Gy, epidermis thickening associated with irregular cell arrangement was observed 6 days post-irradiation (Jang, et al., 2016).

Due to the significant morphological differences between mammalian models for skin ageing, where mouse epidermis is 2-3 cell layers thick with a higher density of hair follicles and an absence of rete ridges, this difference could introduce some biological relevance issues when compared to the human skin ageing process. To explore this theme, this study also looked at the morphological change in skin ageing between young (20 years old) and old (60 years old) human donor skin samples comprising sun-exposed (arm) and sun-protected (buttock) regions. The aim was to determine the effect of sun exposure on skin ageing. Many studies have shown skin thickening in the sun-exposed region as UV radiation can cause the accumulation of epidermal keratinocytes leading to a thicker epidermis that can protect against UV penetration (Scott, et al., 2012). However, our finding does not agree with the evidence available. Our human skin data showed a trend towards thinning in the epidermis

with age in both sun-protected (buttock) and sun-exposed (arm) skin areas. The sun-protected region showed thicker epidermis compared to sun-exposed region. This could be the result of several risk factors such as lifestyle (Asakura, et al., 2009) or occupation (Lastowiecka-Moras, Bugajska, & Młynarczyk, 2014) of the skin donors. Smoking status was found to correlate with worse skin conditions; at the same time, using topical sunscreen resulted in better skin conditions in both genders, including increased skin spots, texture, and wrinkles (Asakura, et al., 2009). Outdoor workers showed higher photoaging characteristics than the general population in terms of moisture, elasticity, sebum, porosity, smoothness, discolouration, and wrinkles (Lastowiecka-Moras, Bugajska, & Młynarczyk, 2014). Most importantly, it was not comparable between the chosen regions as different skin region has different epidermal thickness that is correlated to blood content especially in the buttock region (Sandby-Møller, Poulsen, & Wulf, 2003). In this case, skin samples collected from the inner or outer arm would be a better approach for comparison for more robust results. Also, due to the difficulty in obtaining quality skin samples, there was lack of samples from the same donors, making it impossible to perform a paired t-test. In addition, the variations in lifestyle conditions may not statistically be accounted for given the low sample counts.

Since there was no clear evidence of senescence and skin morphology in both mice and human skin, it was important to confirm whether senescence phenotypes existed in the samples that I used. Thus, I used different senescence markers to discover the characteristics of senescence markers *in vitro* and *in vivo* in humans. As mentioned, no universal marker can detect the presence of senescent cells. Many have proven the existence of senescent cells in human skin with age (see 1.4). As the skin is a complex organ consisting of multiple cell types, many studies only observed senescence markers in specific models, skin compartment layers, or certain cell types in the skin (Figure 3). With the data currently available, it is not conclusive which or how many markers are required to detect the presence of senescent cells in specific skin compartments. Thus, in this experiment, I utilise as many senescence markers as possible to determine whether senescence phenotypes can vary significantly depending on cell types *in vitro* and *in vivo*. Cells underwent 20 Gy of X-ray irradiation to induce cellular senescence and were compared against young cells. As hypothesised, all the senescence markers, including Ki-67, HMGB1 and LaminB1, significantly reduced in senescent cells *in vitro*. The finding also proved that some senescence markers were indeed cell-type-specific. For instance, P21WAF1/CIP1 was present in dermal fibroblast but not in the keratinocytes; conversely,

P16INK4a was present in keratinocytes but not in dermal fibroblasts. This observation was further supported by a time-course test, which confirmed the finding by observing the changes in senescence phenotype from Day 0 to Day 10 after irradiation and agreed with the notion above. Similar results were shown using a different type of senescence-induced method - H<sub>2</sub>O<sub>2</sub> treatment and observing the changes in senescence phenotypes on Day 7 and Day 10 after treatment. However, the data shows inconsistency of P16INK4a and P21WAF1/CIP1 staining, suggesting they are unsuitable for identifying senescence *in vitro*. Sometimes, the antibodies used for staining may bind non-specifically to other proteins, leading to background staining. To ensure the specificity of staining and minimize false-positive results, BSA blocking agent was used, and negative controls were conducted by omitting the primary antibody. By comparing the staining patterns in the negative controls against those in the experimental samples, nonspecific background staining or false-positive signals can be identified and distinguished from true positive signals, thereby strengthening confidence in the obtained results.

Further validation of the senescence markers could be done by additional approaches such as Western blotting, PCR analysis and ELISA. Western blotting and PCR offer higher sensitivity in detecting protein and gene expression levels, respectively. However, these methods are time-consuming and require specific laboratory equipment. ELISA offers a high-throughput format using multiple well plates. Nonetheless, all these techniques have limitations in visualizing protein expression and localization within cells, capabilities offered by immunofluorescence. Given the complexity of this experiment, which involved a large number of samples and multiple antibodies simultaneously, immunofluorescence was chosen as the preferred method.

For  $\gamma$ H2A.x *in vitro*, although with the combination of Ki-67 to distinguish young and senescent cells,  $\gamma$ H2A.x consistently showed approximately 20% recovery on the 10<sup>th</sup> day after senescence induction in HDFn. As mentioned, non-telomeric DNA damage can be repaired over time but the damage of DNA located within the telomere (TAF) in senescent cells are persistent and less efficient to be repaired or even irreparable (P A Kruk, Kruk, Rampino, & Bohr, 1995; Fumagalli, et al., 2012; Hewitt, et al., 2012) suggesting the staining of telomere-associated DNA damage foci (TAF) distinguished by the colocalization of  $\gamma$ H2A.x, and telomeres (immunoFISH) is more robust in identifying senescent cells. The staining of Sen- $\beta$ -Gal shows increased frequencies in H<sub>2</sub>O<sub>2</sub>-induced senescent HDFn. Enlargement of nuclear

size was observed in all three experiments using IR and H<sub>2</sub>O<sub>2</sub> induced senescent cells. This suggests that the enlargement of nuclear size is the most straightforward assay to determine the senescent cells *in vitro*.

To validate whether the changes of senescence phenotypes *in vitro* are similar to *in vivo*, the same senescence markers were applied in a human tissue sample and compared between sun-exposed (arm) and sun-protected (buttock) regions in young and old donors. Surprisingly, almost none of the senescence markers tested showed any change in skin ageing with age, regardless of the arm or buttock regions. Although p16INK4a increased with age, only a very small frequency of P16INK4a-nuclear-positive cells were detected, accompanied by strong autofluorescence background; p16INK4a might not even be present in the samples. This finding agreed with a study showing similar results *in vivo* where the p16INK4a or p21WAF1/CIP1 increased with age, with only 4% and 6% of total cells found in old donors' epidermis, respectively; no p16INK4a was detected in the dermis with an increase of approximately 20% of p21WAF1/CIP1 with age (Idda, et al., 2020).

There has been controversy regarding the existence of p16INK4a in skin ageing. Some studies argue that p16INK4a is only present in senescent keratinocytes *in vitro* but not *in vivo* (Tinaburri, et al., 2018); some argue that high p16INK4a remained consistently high in replicative, oncogene- and stress-induced senescent keratinocytes (Tinaburri, et al., 2018; Maurelli, et al., 2006; Sasaki, Kajiya, Ozeki, Okabe, & Ikebe, 2014; Miyake, Shimada, Matsumoto, & Okino, 2019; Kim, et al., 2015), and in primary mouse keratinocytes in oncogene- and stress-induced senescence (Ritschka, et al., 2017) and inactivation of P16INK4a immortalised primary human keratinocytes (Maurelli, et al., 2006). In addition, (Wolf, et al., 2012) also found no difference in p16INK4a expression in skin fibroblasts from young and elderly donors. In general, p16INK4a is not robust enough to use as a gold standard in identifying senescent skin ageing *in vivo* and *in vitro*.

As the enlargement of nuclear size was significant *in vitro*, the same method was applied *in vivo*. However, similar to all the other tested markers, the finding is not as hypothesised. Only the buttock samples showed an increase in nuclear size with age in both the epidermis and dermis. Skin differentiation marker Cytokeratin 14 (CK-14) and Cytokeratin 10 (CK-10) was then used to distinguish the sublayers within the epidermis. The nuclear size of basal and suprabasal cells were measured separately, excluding the abnormalities present in the epidermis (Figure 44). The results show that nuclear size in the epidermis were significantly

reduced with age in both arm and buttock samples. This result does not agree with the findings by (Liao, et al., Determination of chronological aging parameters in epidermal keratinocytes by in vivo harmonic generation microscopy, 2013) where basal cells significantly increased with age but not suprabasal cells *in vivo*.

Sen-  $\beta$ -Gal staining in cryosections of human tissue samples was only present in the *stratum corneum* region, absent in the epidermis and dermis, and accompanied by cell melanisation in the *stratum basale* region. This experiment suggested that senescence phenotypes can vary significantly depending on cell types, methodological issues with marker sensitivity or even different time points over senescence phenotype development. When different markers are required to identify senescence, inconsistency of biomarkers application and various combinations of biomarkers can be individually nonspecific (Sharpless & Sherr, 2015).

With our limited tissue samples, with some of them only consisting of the epidermis or dermis, it is impossible to replicate the experiments. Most importantly, the skin tissue received was more than 10 years old; it is reasonable to expect epitope degradation resulting in reduced sensitivity of senescent marker and senescent cells detection, especially Sen-  $\beta$ -Gal. Freshly obtained tissue samples are recommended as  $\beta$ -gal activity staining decreases with cryopreservation time (from 4 to 12 months of storage at  $-80\text{ C}$ ;  $p < 0.05$ ) *in vivo* (Jannone et al., 2020).

To investigate the impact of senescence more accurately on skin ageing, we generated full-thickness 3D skin models with different densities of senescent cells in the dermis. Although no epidermal response was observed in our senescent skin model, even at densities of few percent (corresponding to 20% seeding density), senescent fibroblasts induced a significant SASP. This included an enhanced secretion of pro-inflammatory cytokines and reduction in total collagen deposition (see appendices Figure C & D). These findings align with observations in aged skin (Low , et al., 2021) and in collagen-based 3D skin models containing senescent fibroblasts (Weinmüller, et al., 2020). However, even at higher fractions or as the sole fibroblast species in the dermal equivalent, senescent fibroblasts in an Alvetex matrix did not induce the epidermal changes that are typically observed in intrinsically ageing skin. This included epidermal thinning and compromised keratinocyte differentiation. Additionally, they did not induce keratinocyte senescence in this model. It is possible that senescent dermal fibroblasts might not be robust inducers of ageing changes in the epidermis. For instance, it had been suggested that senescent melanocytes might be a major source of senescence-



associated signals in the epidermis (Victorelli, et al., 2019). Alternatively, stress-induced senescence as applied here might not well recapitulate fibroblast ageing. Again however, incorporation of HDF with stress-induced senescence was sufficient to cause ageing-like changes in the epidermal equivalent in collagen-based models (Weinmüller, et al., 2020).

So far, the development of senescence 3D skin models using the Alvetex scaffold has not been explored, despite its known ability to provide a stable physical 3D microenvironment that enables cells to closely recapitulate their native morphology (Maltman & Przyborski, 2010). While some studies have utilized the Alvetex scaffold for complex experiments such as irritant skin tests (unpublished) and early melanoma invasion (Hill, et al., 2015), the use of primary cells directly from patients has highlighted the issue of donor-to-donor variation, impacting the reproducibility of the models (Hill, et al., 2015). Comparatively, matrix composition appears to be a significant factor influencing the effects of senescent fibroblasts on the epidermis equivalent. For instance, ageing-like epidermal changes were observed in collagen-based skin models containing senescent fibroblasts (Weinmüller, et al., 2020), contrasting with a model based on a permeable polyester matrix where such changes were not evident (Janson, Rietveld, Willemze, & El Ghalbzouri, 2013). This difference could be attributed to the diminished migratory capacity of senescent fibroblasts (Schneider & Mitsui, 1976; Sandeman, Allen, Liu, Faragher, & Lloyd, 2000; Reed, Corsa, Kudravi, McCormick, & Arthur, 2000; Ruiz-Torres, Lozano, Melón, & Carraro, 2003), likely due to cytoskeletal alterations occurring during cellular senescence (Nishio & Inoue, 2005). Actin, a critical component of the cytoskeleton necessary for cellular migration, undergoes significant changes in senescent fibroblasts, with vimentin being produced in place of actin, leading to its down regulation (Nishio & Inoue, 2005). This suggests that matrix-dependency of the effects of senescent fibroblasts in 3D skin models, particularly in collagen gel-based models where cells are mixed and uniformly seeded throughout the gel without undergoing migration.

In the context of experiments, cell seeding frequencies in 3D skin models are well-controlled, as previously used to determine fractions of senescent cells in the models (Weinmüller, et al., 2020). However, in our full thickness 3D skin models, with senescent cell seeding densities up to 80% in which the senescent HDFns were all acGFP- labelled, we observed less than 2% of acGFP-positive cells. This discrepancy may be attributed to the possibility that senescent cells might migrate less well into the matrix and adhere less effectively compared to the non-senescent cells. Consequently, these non-senescent cells could potentially proliferate during

the maturation of the 3D models, resulting in a decrease in the proportion of senescent cells over time relative to the actual seeding frequencies.

Another factor to consider is the use of acGFP-transfected cells. Notably, a significant decline in transgene expression was noted after expression after 28 days in the matrix (Figure 53 D). Additionally, when replacing normal HDFn senescent cells with acGFP- fluorescent green cells, both observers noted a tendency for the viability of acGFP cells to be lower in 2D cell culture compared to normal HDFn cells. This suggests that the transfection process may induce stress in cells, leading to a decrease in viability, and that the Alvetex polystyrene scaffold environment may not be conducive to transfected cells.

Other than that, there were also difficulties in reproducing full-thickness Alvetex-based skin models, especially in the development of the epidermal layer. The earlier repeats of full thickness skin models produced epidermal layer with the expected stratified histology, however, later repeats did not, including in both the control and senescent models. This suggests that the proliferation and differentiation capability of keratinocytes degraded between the first and last experiments.

There are many factors can cause inter-observer variability, such as the microscope used, magnification of the image taken, intensity adjusted for taking images, different focal planes taken on the sample, image file format, photobleaching, inconsistency of the staining across the samples etc. However, these issues could potentially be solved by normalisation to the non-senescent control for each experiment or by shifting immunofluorescence (IF) to immunohistochemistry (IHC) staining as IHC tends to offer stronger signal amplification, leading to more precise determination of 'positive' or negative' of cell staining.

We attempted to measure LaminB1 cell positivity in the epidermis as well as the mean gray value of MMP-1 and collagen-1 in the dermis via the staining of IF. However, LaminB1 staining was generally more variation in the staining patterns (see appendix Figure A). Some cells exhibited a complete perinuclear staining ring of Lamin B1, while some had a partial ring, and some showed staining across the nucleus. This variability made it difficult to determine the criteria for categorizing a cell as 'positive', and it was a challenge to determine the optimal method for quantifying LaminB1 expression within the nucleus. After thorough discussion, both observers decided not to proceed with the quantification of LaminB1, as standardising the measurement was challenging. Moreover, LaminB1 staining tended to show stronger

signal in the epidermis compared to the dermis (see appendix Figure A). As for MMP-1 and Collagen-1 measurement, although both observers came out with a standardised quantification method (see appendix Figure II A), we did not observe change in both Collagen-1 and MMP-1 with increasing senescent densities (see appendix Figure II B). However, the cytokine array data showed the opposite for MMP-1 (see Figure III C).

This suggests that IF staining may not be the most suitable method for the measurement of pro-inflammatory cytokines and collagen content in the dermis. Furthermore, we observed discrepancies between different observers in measuring the same sample, and we suspect that there was a possibility of variations between sections within the same sample. To address this, we opted to analyse the same section. The data showed a similar measurement in both observers, therefore confirming that there were indeed variations between sections from the same sample.

In general, our data revealed the context- and probably matrix-dependency of the effects of senescent fibroblasts in human full thickness skin equivalents. Senescent fibroblasts may drive skin intrinsic ageing in some environments but not others, suggesting that besides interventions that reduce cell senescence also others impacting on properties of the extracellular matrix might have potential to reduce skin ageing. Furthermore, the construction of 3D skin models require further optimisation to achieve reproducibility and consistency methodology before further tests for senescence markers. The construction of a 3D skin model is labour-intensive and time-consuming due to the various types of primary cells used. In addition, the models are strongly donor dependent; thus, it is unavoidable to have technical and biological variances in experimental repeats. Recently, to achieve a better physiological structure and tissue architecture in the 3D skin models, some researchers have begun to introduce more advanced 3D skin model by adding hair follicles (Abaci, et al., 2018), melanocytes (Zoio, Ventura, Leite, & Oliva, 2021; Victorelli, et al., 2019), subcutaneous fat layer (Bellas, Seiberg, Garlick, & Kaplan, 2012), nerves and immune cells (Vidal, et al., 2019). As there is insufficient understanding of how different cell types interact in the skin during the progression to senescence, it is not known whether it is true that melanocytes are the main population of senescent cells in skin ageing (Victorelli, et al., 2019). Could late-passage fibroblast or cells from aged individuals, instead of stress-induced senescence recapitulate aspects of the ageing phenotype *in vitro*? Alternatively, other cell populations such as melanocytes could play a more prominent role in skin ageing. There are many questions that

still need to be clarified and optimisations to be performed. Furthermore, addition of more cell types increases the complexity and difficulty of producing a standardised model. All these suggest that 3D skin model is not yet ready to be further used to study skin ageing and drug tests.

Since 3D skin model is yet ready to be used for further senolytic tests, 2D drugs assay was performed to test the senolytic efficacy in dermal fibroblasts. Overall, only micro-dose of lithium showed a small degree of senolytic activity with the specified dosages of 0.1mM without affecting the proliferating cells. This compound could be the one that contribute to the senolytic effects in the product. However, it is unclear whether it will work the same *in vivo* considering the ADME (i.e., absorption, distribution, metabolism, and excretion) pathways for each of the compounds. The compounds are possibly not metabolised into their active form. For instance, Salidroside is the main bioactive agent of *Rhodiola rosea*. Thus, Salidroside should be more effective and absorbable than *Rhodiola rosea*. Only 1% of salidroside can be extracted from *Rhodiola rosea*, so taking salidroside alone might be a better option. Fisetin has been widely used as senolytic with no evidence of side effects reported. (Yousefzadeh, et al., 2018) has demonstrated that treatment with 15um Fisetin can effectively remove 50% of senescent IMR90 fibroblasts. However, Fisetin has been shown in a similar *in vitro* assay as ours to be senolytic against HUVECS but not IMR90 fibroblasts (Zhu, et al., 2017). I found that Fisetin was more toxic to non-senescent than senescent dermal fibroblasts. It was reported that Ascorbic acid and glycine work synergistically as ascorbic acid improves the absorption of glycine in the intestine (Nekachalova , 1958). Also, both works together to enhance collagen production and wound healing in human dermal fibroblasts (Lee & Boo, 2022). Although Ascorbic acid and glycine have their benefits, but both glycine and ascorbic acid are the standard growth supplement in tissue culture and tissue engineering and have not been shown to possess senolytic effects in standard tissue culture, thus I did not expect to see any senolytic activity from them.

In conclusion, senolytic or senostatic did not improve extrinsic skin ageing characteristic in therapy-induced premature -ageing mice. Natural compounds with reported 'anti-ageing' activity showed no senolytic efficacy against skin fibroblasts. Senescence markers were well detected *in vitro*, but they are not as sensitive in *in vivo* skin samples. Some senescence markers were found to be cell-type specific and can vary over the course of senescence development. However, the enlargement of cell size has shown reliability as a senescence

marker in both *in vitro* and 3D model, potentially *in vivo* if we have better quality of samples. In comparison to published results, 3D skin models revealed effects of senescent dermal fibroblasts onto the epidermis are largely matrix dependent.

## Bibliography

- Abaci, H., Coffman, A., Doucet, Y., Chen, J., Jacków, J., Wang, E., . . . Christiano, A. (2018). Tissue engineering of human hair follicles using a biomimetic developmental approach. *Nature communications*, *9*(1), 5301.
- Ahmed, N. (2005). Advanced glycation endproducts—role in pathology of diabetic complications. *Diabetes Research and Clinical Practice*, 3-21.
- Arai, Y., Watanabe, S., Kimira, M., Shimoi, K., Mochizuki, R., & Kinae, N. (2000). Dietary intakes of flavonols, flavones and isoflavones by Japanese women and the inverse correlation between quercetin intake and plasma LDL cholesterol concentration. *The Journal of nutrition*, *130*(9), 2243–2250.
- Aravintan , A. (2015). Cellular senescence: a hitchhiker's guide. *Human cell*, 51-64.
- Asakura, K., Nishiwaki, Y., Milojevic, A., Michikawa, T., Kikuchi, Y., Nakano, M., . . . Takebayashi, T. (2009). Lifestyle factors and visible skin aging in a population of Japanese elders. *Journal of epidemiology*, *19*(5), 251–259.
- Ashcroft, G., Herrick, S., Tarnuzzer, R., Horan, M., Schultz, G., & Ferguson, M. (1997). Human ageing impairs injury-induced *in vivo* expression of tissue inhibitor of matrix metalloproteinases (TIMP)-1 and -2 proteins and mRNA. *The Journal of pathology*, 169–176.
- Averous, J., & Proud, C. (2006). When translation meets transformation: the mTOR story. *Oncogene*, 6423–6435.
- Azazmeh, N., Assouline, B., Winter, E., Ruppó, S., Nevo, Y., Maly, A., . . . Ben-Porath, I. (2020). Chronic expression of p16INK4a in the epidermis induces Wnt-mediated hyperplasia and promotes tumor initiation. *Nature communications*, 2711.
- Bai, H., Zhang, Z., Li, Y., Song, X., Ma, T., Liu, C., . . . Gao, L. (2020). L-Theanine Reduced the Development of Knee Osteoarthritis in Rats via Its Anti-Inflammation and Anti-Matrix Degradation Actions: In Vivo and In Vitro Study. . *Nutrients*, 1988.
- Baker, D., Wijshake, T., Tchkonja, T., LeBrasseur, N., Childs, B., van de Sluis, B., . . . van Deursen, J. (2011). Clearance of p16Ink4a-positive senescent cells delays ageing-associated disorders. *Nature*, 232–236.

- Beauséjour, C., Krtolica, A., Galimi, F., Narita, M., Lowe, S., Yaswen, P., & Campisi, J. (2003). Reversal of human cellular senescence: roles of the p53 and p16 pathways. *The EMBO journal*, 4212–4222.
- Bellas, E., Seiberg, M., Garlick, J., & Kaplan, D. (2012). In vitro 3D full-thickness skin-equivalent tissue model using silk and collagen biomaterials. *Macromolecular bioscience*, 12(12), 1627–1636.
- Ben-Sahra, I., Howell, J., Asara, J., & Manning, B. (2013). Stimulation of de novo pyrimidine synthesis by growth signaling through mTOR and S6K1. *Science (New York, N.Y.)*, 1323–1328.
- Bernard, F., Morel, F., Camus, M., Pedretti, N., Barrault, C., Garnier, J., & Lecron, J. (2012). Keratinocytes under Fire of Proinflammatory Cytokines: Bona Fide Innate Immune Cells Involved in the Physiopathology of Chronic Atopic Dermatitis and Psoriasis. *Journal of allergy*, 718725.
- Bianchi, M., & Manfredi, A. (2007). High-mobility group box 1 (HMGB1) protein at the crossroads between innate and adaptive immunity. *Immunological reviews*, 35–46.
- Biran, A., Zada, L., Abou Karam, P., Vadai, E., Roitman, L., Ovadya, Y., . . . Krizhanovsky, V. (2017). Quantitative identification of senescent cells in aging and disease. *Aging cell*, 661–671.
- Bishop, C., Bergin, A., Fessart, D., Borgdorff, V., Hatzimasoura, E., Garbe, J., . . . Beach, D. (2010). Primary cilium-dependent and -independent Hedgehog signaling inhibits p16(INK4A). *Molecular cell*, 533–547.
- Bissett, D. (2006). Glucosamine: an ingredient with skin and other benefits. *Journal of cosmetic dermatology*, 309–315.
- Blanpain, C., & Fuchs, E. (2009). Epidermal homeostasis: a balancing act of stem cells in the skin. *Nature reviews. Molecular cell biology*, 207–217.
- Boehlke, C., Kotsis, F., Patel, V., Braeg, S., Voelker, H., Bredt, S., . . . Kuehn, E. (2010). Primary cilia regulate mTORC1 activity and cell size through Lkb1. *Nature cell biology*, 1115–1122.
- Bonta, M., Daina, L., & Mușiu, G. (2013). The process of ageing reflected by histological changes in the skin. *Romanian journal of morphology and embryology = Revue roumaine de morphologie et embryologie*, 797–804.
- Bosset, S., Bonnet-Duquennoy, M., Barré, P., Chalon, A., Lazou, K., Kurfurst, R., . . . Nicolas, J. F. (2003). Decreased expression of keratinocyte beta1 integrins in chronically sun-exposed skin in vivo. *British Journal of Dermatology*, 770-778.
- Branchet, M., Boisnic, S., Frances, C., & Robert, A. (1990). Skin thickness changes in normal aging skin. *Gerontology. Karger Publishers*, 28–35.
- Brennan, M., Bhatti, H., Nerusu, K., Bhagavathula, N., Kang, S., Fisher, G., . . . Voorhees, J. (2007). Matrix Metalloproteinase-1 is the Major Collagenolytic Enzyme Responsible for Collagen Damage in UV-irradiated Human Skin¶. *Photochemistry and Photobiology*, 43-48.
- Brenner, M., & Hearing, V. (2008). The protective role of melanin against UV damage in human skin. *Photochemistry and photobiology*, 539–549.
- Breslin, L., Prosser, S., Cuffe, S., & Morrison, C. (2014). Ciliary abnormalities in senescent human fibroblasts impair proliferative capacity. *Cell cycle*, 2773–2779.
- Bridger, J., Foeger, N., Kill, I., & Herrmann, H. (2007). The nuclear lamina. Both a structural framework and a platform for genome organization. *The FEBS journal*, 1354–1361.

- Briggaman, R. A., & Wheeler, C. E. (1975). The Epidermal-Dermal Junction. *Journal of Investigative Dermatology. Elsevier Masson SAS*, 71–84.
- Bucala, R., & Cerami, A. (1992). Advanced Glycosylation: Chemistry, Biology, and Implications for Diabetes and Aging. *Advances in Pharmacology*, 1-34.
- Burns, T., & Rook, A. (2004). Rook's textbook of dermatology. *Oxford: Blackwell Science*.
- Calamia, V., Ruiz-Romero, C., Rocha, B., Fernández-Puente, P., Mateos, J., Montell, E., . . . Blanco, F. (2010). Pharmacoproteomic study of the effects of chondroitin and glucosamine sulfate on human articular chondrocytes. *Arthritis research & therapy*, R138.
- Cameron, K., Miwa, S., Walker, C., & von Zglinicki, T. (2012). Male mice retain a metabolic memory of improved glucose tolerance induced during adult onset, short-term dietary restriction. *Longev Healthspan*.
- Campisi, J. (1998). The role of cellular senescence in skin aging. *The journal of investigative dermatology*, 1–5.
- Candi, E., Schmidt, R., & Melino, G. (2005). The cornified envelope: A model of cell death in the skin. *Nature Reviews Molecular Cell Biology*, 328–340.
- Carroll, B., Korolchuk, V., & Sarkar, S. (2015). Amino acids and autophagy: cross-talk and co-operation to control cellular homeostasis. *Amino acids*, 2065–2088.
- Carroll, B., Maetzel, D., Maddocks, O., Otten, G., Ratcliff, M., Smith, G., . . . Korolchuk, V. (2016). Control of TSC2-Rheb signaling axis by arginine regulates mTORC1 activity. *eLife*, e11058.
- Carroll, B., Nelson, G., Rabanal-Ruiz, Y., Kucheryavenko, O., Dunhill-Turner, N., Chesterman, C., . . . Korolchuk, V. (2017). Persistent mTORC1 signaling in cell senescence results from defects in amino acid and growth factor sensing. *J Cell Biol.*, 1949–1957.
- Carroll, D., Carroll, J., Leong, C., Cheng, F., Brown, M., Mills, A., & Brugge, J. (2006). p63 regulates an adhesion programme and cell survival in epithelial cells. *Nature cell biology*, 551-561.
- Castillo-Quan, J., Li, L., Kinghorn, K., Ivanov, D., Tain, L., Slack, C., . . . Partridge, L. (2016). Lithium Promotes Longevity through GSK3/NRF2-Dependent Hormesis. *Cell reports*, 15(3), 638–650., 638-650.
- Chang, Z., Huo, L., Li, P., Wu, Y., & Zhang, P. (2015). Ascorbic acid provides protection for human chondrocytes against oxidative stress. *Molecular medicine reports*, 12(5), 7086–7092.
- Charruyer, A., Weisenberger, T., Li, H., Khalifa, A., Schroeder, A., Belzer, A., & Ghadially, R. (2021). Decreased p53 is associated with a decline in asymmetric stem cell self-renewal in aged human epidermis. *Aging cell*, e13310.
- Chen, L., Xiao, W. J., Yan, Q. X., Gong, Z. H., Zhang, S., Zeng, L., . . . Zhou, Y. H. (2020). Protective effects of L-theanine on rats with dextran sulfate sodium-induced inflammatory bowel disease. *Archives of pharmacal research*, 821-862.
- Chen, Q., Espey, M., Krishna, M., Mitchell, J., Corpe, C., Buettner, G., . . . Levine, M. (2005). Pharmacologic ascorbic acid concentrations selectively kill cancer cells: action as a pro-drug to deliver hydrogen peroxide to tissues. *Proceedings of the National Academy of Sciences of the United States of America*, 13604–13609.
- Choi, E. (2019). Aging of the skin barrier. *Clinics in dermatology*, 336–345.

- Chung, C., Lawrence, I., Hoffman, M., Elgindi, D., Nadhan, K., Potnis, M., . . . Sell, C. (2019). Topical rapamycin reduces markers of senescence and aging in human skin: an exploratory, prospective, randomized trial. *GeroScience*, 861–869.
- Chung, H., Suh, E., Han, I., & Oh, E. (2011). Keratinocyte-derived laminin-332 promotes adhesion and migration in melanocytes and melanoma. *The Journal of biological chemistry*, 13438-13447.
- Clément, M., Ramalingam, J., Long, L., & Halliwell, B. (2001). The in vitro cytotoxicity of ascorbate depends on the culture medium used to perform the assay and involves hydrogen peroxide. . *Antioxidants & redox signaling*, 157-163.
- Collado, M., Blasco, M., & Serrano, M. (2007). Cellular senescence in cancer and aging. *Cell*, 223–233.
- Contet-Audonneau, J. L., Jeanmaire, C., & Pauly, G. (1999). A histological study of human wrinkle structures: comparison between sun-exposed areas of the face, with or without wrinkles, and sun-protected areas. *The British journal of dermatology*, 1038-1047.
- Coppé, J., Patil, C., Rodier, F., Sun, Y., Muñoz, D., Goldstein, J., . . . Campisi, J. (2008). Senescence-associated secretory phenotypes reveal cell-nonautonomous functions of oncogenic RAS and the p53 tumor suppressor. *PLoS biology*, 2853–2868.
- Correia-Melo, C., Marques, F., Anderson, R., Hewitt, G., Hewitt, R., Cole, J., . . . Passos, J. (2016). Mitochondria are required for pro-ageing features of the senescent phenotype. *The EMBO journal*, 724–742.
- Costello, L., Fullard, N., Roger, M., Bradbury, S., Dicolandrea, T., Isfort, R., . . . Przyborski, S. (2019). Engineering a Multilayered Skin Equivalent: The Importance of Endogenous Extracellular Matrix Maturation to Provide Robustness and Reproducibility. *Methods in molecular biology (Clifton, N.J.)*, 107–122.
- Cotta-Pereira, G., Guerra Rodrigo, F., & Bittencourt-Sampaio, S. (1976). Oxytalan, Elaunin, And Elastic Fibers In The Human Skin. *Journal of Investigative Dermatology*, 143–148.
- Culetu, A., Fernandez-Gomez, B., Ullate, M., del Castillo, M., & Andlauer, W. (2016). Effect of theanine and polyphenols enriched fractions from decaffeinated tea dust on the formation of Maillard reaction products and sensory attributes of breads. *Food chemistry*, 197(Pt A), 14–23.
- Cybulski, N., & Hall, M. (2009). TOR complex 2: a signaling pathway of its own. *Trends in biochemical sciences*, 620–627.
- d'Adda di Fagagna, F., Reaper, R., Clay-Farrace, L., Fiegler, H., Carr, P., Von Zglinicki, T., . . . Jackson, S. (2003). A DNA damage checkpoint response in telomere-initiated senescence. *Nature*, 194-8.
- Dalle Pezze, P., Nelson, G., Otten, E., Korolchuk, V., Kirkwood, T., von Zglinicki, T., & Shanley, D. (2014). Dynamic modelling of pathways to cellular senescence reveals strategies for targeted interventions. *PLoS computational biology*, e1003728.
- Davalos, A., Kawahara, M., Malhotra, G., Schaum, N., Huang, J., Ved, U., . . . Campisi, J. (2013). p53-dependent release of Alarmin HMGB1 is a central mediator of senescent phenotypes. *The Journal of cell biology*, 613–629.
- de Kossodo, S., Cruz, P., Jr, Dougherty, I., Thompson, P., Silva-Valdez, M., & Beutler, B. (1995). Expression of the tumor necrosis factor gene by dermal fibroblasts in response to ultraviolet irradiation or lipopolysaccharide. *The Journal of investigative dermatology*, 318–322.



- Dechat, T., Pflieger, K., Sengupta, K., Shimi, T., Shumaker, D., Solimando, L., & Goldman, R. (2008). Nuclear lamins: major factors in the structural organization and function of the nucleus and chromatin. *Genes & development*, 832–853.
- Demaria, M., Desprez, P., Campisi, J., & Velarde, M. (2015). Cell Autonomous and Non-Autonomous Effects of Senescent Cells in the Skin. *The Journal of investigative dermatology*, 1722–1726.
- Demetriades, C., Doumpas, N., & Teleman, A. (2014). Regulation of TORC1 in response to amino acid starvation via lysosomal recruitment of TSC2. *Cell*, 786–799.
- Deng, Y., Xiao, W., Chen, L., Liu, Q., Liu, Q., & Gong, Z. (2016). In vivo antioxidative effects of l-theanine in the presence or absence of Escherichia coli-induced oxidative stress. *Journal of Functional Foods*, 527-546.
- Di Micco, R., Sulli, G., Dobrev, M., Liontos, M., Botrugno, O., Gargiulo, G., . . . d'Adda di Fagagna, F. (2011). Interplay between oncogene-induced DNA damage response and heterochromatin in senescence and cancer. *Nature cell biology*, 292-302.
- Dias, T., Bernardino, R., Alves, M., Silva, J., Barros, A., Sousa, M., . . . Oliveira, P. (2019). L-Theanine promotes cultured human Sertoli cells proliferation and modulates glucose metabolism. *European journal of nutrition*, 2961–2970.
- Dibble, C., & Cantley, L. (2015). Regulation of mTORC1 by PI3K signaling. *Trends in cell biology*, 545-555.
- Diekmann, J., Alili, L., Scholz, O., Giesen, M., Holtkötter, O., & Brenneisen, P. (2016). A three-dimensional skin equivalent reflecting some aspects of in vivo aged skin. *Experimental dermatology*, 56–61.
- Dijkhoff, I., Drasler, B., Karakocak, B., Petri-Fink, A., Valacchi, G., Eeman, M., & Rothen-Rutishauser, B. (2020). Impact of airborne particulate matter on skin: a systematic review from epidemiology to in vitro studies. *Particle and fibre toxicology*, 35.
- Dimri, G., Lee, X., Basile, G., Acosta, M., Scott, G., Roskelley, C., . . . Pereira-Smith, O. (1995). A biomarker that identifies senescent human cells in culture and in aging skin in vivo. *Proceedings of the National Academy of Sciences of the United States of America*, 9363-9367.
- Dodig, S., Čepelak, I., & Pavić, I. (2019). Hallmarks of senescence and aging. *Biochemia medica*, 030501.
- Doherty, J., & Baehrecke, E. (2018). Life, death and autophagy. *Nature cell biology*, 1110–1117.
- Dreesen, O., Chojnowski, A., Ong, P., Zhao, T., Common, J., Lunny, D., . . . Colman, A. (2013). Lamin B1 fluctuations have differential effects on cellular proliferation and senescence. *The Journal of cell biology*, 605–617.
- Duncan, K., & Leffell, D. (1997). Preoperative assessment of the elderly patient. *Dermatologic Clinics*, 583-593.
- Duval, K., Grover, H., Han, L., Mou, Y., Pegoraro, A., Fredberg, J., & Chen, Z. (2017). Modeling Physiological Events in 2D vs. 3D Cell Culture. *Physiology (Bethesda, Md.)*, 266–277.
- Eckert, R. L., & Rorke, E. (1989). Molecular biology of keratinocyte differentiation. *Environmental Health Perspectives*, 109–116.
- Edgar, A., & Polak, J. (2000). Molecular cloning of the human and murine 2-amino-3-ketobutyrate coenzyme A ligase cDNAs. *European journal of biochemistry*, 267(6), 1805–1812.

- Enk, C., Sredni, D., Blauvelt, A., & Katz, S. (1995). Induction of IL-10 gene expression in human keratinocytes by UVB exposure in vivo and in vitro. *Journal of immunology*, 4851–4856.
- Erusalimsky, J., & Kurz, D. (2005). Cellular senescence in vivo: its relevance in ageing and cardiovascular disease. *Experimental gerontology*, 634–642.
- Fan, X., Zhou, J., Bi, X., Liang, J., Lu, S., Yan, X., . . . Yin, Z. (2021). L-theanine suppresses the metastasis of prostate cancer by downregulating MMP9 and Snail. *The Journal of nutritional biochemistry*, 108556.
- Farage, M., Miller, K., & Maibach, H. (2008). Intrinsic and extrinsic factors in skin ageing: a review. *Int J Cosmet Sci.*, 87–95.
- Farr, J., Xu, M., Weivoda, M., Monroe, D., Fraser, D., Onken, J., . . . Khosla, S. (2017). Targeting cellular senescence prevents age-related bone loss in mice. *Nature medicine*, 1072–1079.
- Fielder, E., Wan, T., Alimohammadiha, G., Ishaq, A., Low, E., Weigand, B., . . . Miwa, S. (2022). Short senolytic or senostatic interventions rescue progression of radiation-induced frailty and premature ageing in mice. *eLife*, e75492.
- Fielder, E., Weigand, M., Agneessens, J., Griffin, B., Parker, C., Miwa, S., & von Zglinicki, T. (2019). Sublethal whole-body irradiation causes progressive premature frailty in mice. *Mechanisms of ageing and development*, 63–69.
- Fisher, G. J., Kang, S., Varani, J., Bata-Csorgo, Z., Wan, Y., Datta, S., & Voorhees, J. J. (2002). Mechanisms of photoaging and chronological skin aging. *Arch Dermatol.*, 138(11):1462-70.
- Fisher, G., Choi, H., Bata-Csorgo, Z., Shao, Y., Datta, S., Wang, Z., . . . Voorhees, J. (2001). Ultraviolet irradiation increases matrix metalloproteinase-8 protein in human skin in vivo. *The Journal of investigative dermatology*, 219–226.
- Fisher, G., Quan, T., Purohit, T., Shao, Y., Cho, M., He, T., . . . Voorhees, J. (2009). Collagen fragmentation promotes oxidative stress and elevates matrix metalloproteinase-1 in fibroblasts in aged human skin. *The American journal of pathology*, 101–114.
- Fitsiou, E., Pulido, T., Campisi, J., Alimirah, F., & Demaria, M. (2021). Cellular Senescence and the Senescence-Associated Secretory Phenotype as Drivers of Skin Photoaging. *The Journal of investigative dermatology*, 1119–1126.
- Friedman, O. (2005). Changes Associated with the Aging Face. *Facial Plastic Surgery Clinics of North America*, 371–380.
- Fukuyama, K., & Epstein, W. (1975). 'A comparative autoradiographic study of keratohyalin granules containing cystine and histidine. *Journal of Ultrastructure Research*, 314–325.
- Fumagalli, M., Rossiello, F., Clerici, M., Barozzi, S., Cittaro, D., Kaplunov, J., . . . d'Adda di Fagagna, F. (2012). Telomeric DNA damage is irreparable and causes persistent DNA-damage-response activation. *Nature cell biology*, 355–65.
- Ganley, I., Lam, d., Wang, J., Ding, X., Chen, S., & Jiang, X. (2009). ULK1.ATG13.FIP200 complex mediates mTOR signaling and is essential for autophagy. *The Journal of biological chemistry*, 12297–12305.
- Gilchrist, B., Blog, F., & Szabo, G. (1979). Effects of aging and chronic sun exposure on melanocytes in human skin. *The Journal of investigative dermatology*, 141–143.

- Gilhar, A., Ullmann, Y., Karry, R., Shalaginov, R., Assy, B., Serafimovich, S., & Kalish, R. (2004). Aging of human epidermis: reversal of aging changes correlates with reversal of keratinocyte fas expression and apoptosis. *The journals of gerontology. Series A, Biological sciences and medical sciences*, 411-415.
- Gonzaga, E. (2009). Role of UV light in photodamage, skin aging, and skin cancer: importance of photoprotection. *Am J Clin Dermatol*, 19-24.
- Gorgoulis, V., Adams, P., Alimonti, A., Bennett, D., Bischof, O., Campisi, J., . . . Demaria, M. (2019). Cellular Senescence: Defining a Path Forward. *Cell*, 813-827.
- Gorgoulis, V., Adams, P., Alimonti, A., Bennett, D., Bischof, O., Bishop, C., . . . Demaria, M. (2019). Cellular Senescence: Defining a Path Forward. *Cell*, 813-827.
- Grove, G., & Kligman, A. (1983). Age-associated changes in human epidermal cell renewal. *Journal of Gerontology. The Gerontological Society of America*, 137-142.
- Guertin, D. A., & Sabatini, D. M. (2005). An expanding role for mTOR in cancer. *Trends in molecular medicine*, 353-61.
- H Zhang, H. H., Zhang, H., Hoff, H., Marinucci, T., Cristofalo, V., & Sell, C. (2000). Mitogen-independent phosphorylation of S6K1 and decreased ribosomal S6 phosphorylation in senescent human fibroblasts. *Experimental cell research*, 284-292.
- Han, H., Kim, K., Jung, J., An, I., Kim, Y., & An, S. (2018). Anti-apoptotic, antioxidant and anti-aging effects of 6-shogaol on human dermal fibroblasts. *biomedical dermatology*.
- Hansen, L., Coggle, J., Wells, J., & Charles, M. (1984). The influence of the hair cycle on the thickness of mouse skin. *The Anatomical record*, 569-573.
- Hara, K., Maruki, Y., Long, X., Yoshino, K., Oshiro, N., Hidayat, S., . . . Yonezawa, K. (2002). Raptor, a binding partner of target of rapamycin (TOR), mediates TOR action. *Cell*, 177-89.
- Hara, K., Yonezawa, K., Weng, Q., Kozlowski, M., Belham, C., & Avruch, J. (1998). Amino acid sufficiency and mTOR regulate p70 S6 kinase and eIF-4E BP1 through a common effector mechanism. *The Journal of biological chemistry*, 14484-14494.
- Härle-Bachor, C., & Boukamp, P. (1996). Telomerase activity in the regenerative basal layer of the epidermis in human skin and in immortal and carcinoma-derived skin keratinocytes. *Proceedings of the National Academy of Sciences of the United States of America*, 6476-6481.
- Harley, C., Futcher, A., & Greider, C. (1990). Telomeres shorten during ageing of human fibroblasts. *Nature*, 458-460.
- Hashizume, O., Ohnishi, S., Mito, T., Shimizu, A., Ishikawa, K., Nakada, K., . . . Hayashi, J. (2015). Epigenetic regulation of the nuclear-coded GCAT and SHMT2 genes confers human age-associated mitochondrial respiration defects. *Scientific reports*, 5, 10434.
- Hayashi, J., Ohta, S., Kagawa, Y., Kondo, H., Kaneda, H., Yonekawa, H., . . . Miyabayashi, S. (1994). Nuclear but not mitochondrial genome involvement in human age-related mitochondrial dysfunction. Functional integrity of mitochondrial DNA from aged subjects. *The Journal of biological chemistry*, 269(9), 6878-6883.
- Hayflick, L., & Moorhead, P. (1961). The serial cultivation of human diploid cell strains. *Experimental Cell Research*, 585-621.

- He, J., Chen, J., He, Q., Li, S., Jian, L., Xie, F., . . . You, J. (2021). Oral L-theanine administration promotes fat browning and prevents obesity in mice fed high-fat diet associated with the modulation of gut microbiota. *Journal of Functional Foods*, 104476.
- Herbig, U., Ferreira, M., Condel, L., Carey, D., & Sedivy, J. (2006). Cellular senescence in aging primates. *Science (New York, N.Y.)*, 1257.
- Hernandez-Segura, A., Nehme, J., & Demaria, M. (2018). Hallmarks of Cellular Senescence. *Trends in cell biology*, 436–453.
- Hewitt, G., Jurk, D., Marques, F., Correia-Melo, C., Hardy, T., Gackowska, A., . . . Passos, J. (2012). Telomeres are favoured targets of a persistent DNA damage response in ageing and stress-induced senescence. *Nature*, 708.
- Hickson, L., Langhi Prata, L., Bobart, S., Evans, T., Giorgadze, N., Hashmi, S., . . . Kirkland, J. (2020). Corrigendum to 'Senolytics decrease senescent cells in humans: Preliminary report from a clinical trial of Dasatinib plus Quercetin in individuals with diabetic kidney disease. *EBioMedicine*, 446-456.
- Hill, D., Robinson, N., Caley, M., Chen, M., O'Toole, E., Armstrong, J., & Przyborski, S. (2015). A Novel Fully Humanized 3D Skin Equivalent to Model Early Melanoma Invasion. *Molecular cancer therapeutics*, 14(11), 2665–2673.
- Ho, C., & Dreesen, O. (2021). Faces of cellular senescence in skin aging. *Mechanisms of ageing and development*, 111525.
- Holbrook, K. (1989). Biologic structure and function: perspectives on morphologic approaches to the study of the granular layer keratinocyte. *The Journal of investigative dermatology*, 84S–104S.
- Hosokawa, N., Hara, T., Kaizuka, T., Kishi, C., Takamura, A., Miura, Y., . . . Mizushima, N. (2009). Nutrient-dependent mTORC1 association with the ULK1-Atg13-FIP200 complex required for autophagy. *Molecular biology of the cell*, 1981–1991.
- Idda, M., McClusky, W., Lodde, V., Munk, R., Abdelmohsen, K., Rossi, M., & Gorospe, M. (2020). Survey of senescent cell markers with age in human tissues. *Aging*, 12(5), 4052–4066.
- Ikeda, H., Aida, J., Hatamochi, A., Hamasaki, Y., Izumiyama-Shimomura, N., Nakamura, K., . . . Takubo, K. (2014). Quantitative fluorescence in situ hybridization measurement of telomere length in skin with/without sun exposure or actinic keratosis. *Human pathology*, 473-480.
- Ivanov, A., Pawlikowski, J., Manoharan, I., van Tuyn, J., Nelson, D., Rai, T., . . . Adams, P. (2013). Lysosome-mediated processing of chromatin in senescence. *The Journal of cell biology*, 129-143.
- Jacinto, E., Loewith, R., Schmidt, A., Lin, S., Rügge, M., Hall, A., & Hall, M. (2004). Mammalian TOR complex 2 controls the actin cytoskeleton and is rapamycin insensitive. *Nature cell biology*, 1122–1128.
- Jang, W., Shim, S., Wang, T., Yoon, Y., Jang, W., Myung, J., . . . Kim, K. (2016). In vivo characterization of early-stage radiation skin injury in a mouse model by two-photon microscopy. *Scientific Reports*, 6.
- Janson, D., Rietveld, M., Mahé, C., Saintigny, G., & El Ghalbzouri, A. (2017). Differential effect of extracellular matrix derived from papillary and reticular fibroblasts on epidermal development in vitro. *European journal of dermatology : EJD*, 237–246.

- Janson, D., Rietveld, M., Willemze, R., & El Ghalbzouri, A. (2013). Effects of serially passaged fibroblasts on dermal and epidermal morphogenesis in human skin equivalents. *Biogerontology*, 131–140.
- Jeanmaire, C., Danoux, L., & Pauly, G. (2001). Glycation during human dermal intrinsic and actinic ageing: an in vivo and in vitro model study. *The British journal of dermatology*, 10–18.
- Jena, B., Das, C., Bharadwaj, D., & Mandal, M. (2020). Cancer associated fibroblast mediated chemoresistance: A paradigm shift in understanding the mechanism of tumor progression. *Biochimica et biophysica acta. Reviews on cancer*, 1874(2), 188416.
- Jenkins, N., & Grossman, D. (2013). Role of melanin in melanocyte dysregulation of reactive oxygen species. *BioMed research international*, 908797.
- Jenkins, N., Liu, T., Cassidy, P., Leachman, S., Boucher, K., Goodson, A., . . . Grossman, D. (2011). The p16(INK4A) tumor suppressor regulates cellular oxidative stress. *Oncogene*, 265–274.
- Jeon, S., Djian, P., & Green, H. (1998). Inability of keratinocytes lacking their specific transglutaminase to form cross-linked envelopes: absence of envelopes as a simple diagnostic test for lamellar ichthyosis. *Proceedings of the National Academy of Sciences of the United States of America*, 687–690.
- Jeyapalan, J., Ferreira, M., Sedivy, J., & Herbig, U. (2007). Accumulation of senescent cells in mitotic tissue of aging primates. *Mechanisms of ageing and development*, 36–44.
- Johnson, K., Wulff, B., Oberyszyn, T., & Wilgus, T. (2013). Ultraviolet light exposure stimulates HMGB1 release by keratinocytes. *Archives of dermatological research*, 805–815.
- Kammeyer, A., & Luiten, R. M. (2015). Oxidation events and skin aging. *Ageing Res Rev*, 16-29.
- Kang, T., Yevsa, T., Woller, N., Hoenicke, L., Wuestefeld, T., Dauch, D., . . . Zender, L. (2011). Senescence surveillance of pre-malignant hepatocytes limits liver cancer development. *Nature*, 547–551.
- Kapetanovic, I., Muzzio, M., Huang, Z., Thompson, T., & McCormick, D. (2011). Pharmacokinetics, oral bioavailability, and metabolic profile of resveratrol and its dimethylether analog, pterostilbene, in rats. *Cancer chemotherapy and pharmacology*, 593–601.
- Kar, N., & Bellare, J. (2021). Ethanol pre-exposure enhances alcohol-seeking behavior at cellular level by chemoattraction and exhibits bleb-driven cellular stress response in uniform ethanol concentration. *bioRxiv*.
- Kashino, G., Kodama, S., Nakayama, Y., Suzuki, K., Fukase, K., Goto, M., & Watanabe, M. (2003). Relief of oxidative stress by ascorbic acid delays cellular senescence of normal human and Werner syndrome fibroblast cells. *Free radical biology & medicine*, 35(4), 438–443.
- Kawabata, K., Yoshikawa, H., Saruwatari, K., Akazawa, Y., Inoue, T., Kuze, T., . . . Sugiyama, Y. (2011). The presence of N(ε)-(Carboxymethyl) lysine in the human epidermis. *Biochimica et biophysica acta*, 1246–1252.
- Khavkin, J., & Ellis, D. (2011). Ageing Skin: Histology, Physiology and Pathology. *Facial Plastic Surgery Clinics of North America*, 229-234.
- Kim, D., Sarbassov, D., Ali, S., King, J., Latek, R., Erdjument-Bromage, H., . . . Sabatini, D. (2002). mTOR interacts with raptor to form a nutrient-sensitive complex that signals to the cell growth machinery. *Cell*, 163-75.

- Kim, H., Jang, J., Song, M., Kim, G., Park, C., Lee, D., . . . Chung, J. (2022). Attenuation of intrinsic ageing of the skin via elimination of senescent dermal fibroblasts with senolytic drugs. *Journal of the European Academy of Dermatology and Venereology : JEADV*, 1125–1135.
- Kim, J., Nakasaki, M., Todorova, D., Lake, B., Yuan, C., Jamora, C., & Xu, Y. (2014). p53 Induces skin aging by depleting Blimp1+ sebaceous gland cells. *Cell death & disease*, e1141.
- Kim, K., Kim, H., & Sung, G. (2022). An Interleukin-4 and Interleukin-13 Induced Atopic Dermatitis Human Skin Equivalent Model by a Skin-On-A-Chip. *International journal of molecular sciences*, 2116.
- Kim, R., Kang, M., Kim, T., Yang, P., Bae, S., Williams, D., . . . Park, N. (2015). Regulation of p53 during senescence in normal human keratinocytes. *Aging cell*, 14(5), 838–846.
- Kim, T., Park, T., Kweon, Y., & Baek, D. (2022). Age-Dependent Sequential Increase of Senescent Cells in the Skin. *The Journal of investigative dermatology*, 2521–2523.e1.
- Kirkland, J., & Tchkonja, T. (2017). Cellular Senescence: A Translational Perspective. *EBioMedicine*, 21–28.
- Kligman, A. (1979). Perspectives and problems in cutaneous gerontology. *The Journal of investigative dermatology*, 39–46.
- Kligman, L. H. (1989). Photoaging. Manifestations, prevention, and treatment. *Clinics in Geriatric Medicine*, 235–251.
- Kodet, O., Lacina, L., Krejčí, E., Dvořánková, B., Grim, M., Štork, J., . . . Smetana, K. (2015). Melanoma cells influence the differentiation pattern of human epidermal keratinocytes. *Molecular cancer*, 14(1), 1.
- Korolchuk, V., Miwa, S., Carroll, B., & von Zglinicki, T. (2017). Mitochondria in Cell Senescence: Is Mitophagy the Weakest Link? *EBioMedicine*, 7–13.
- Korolchuk, V., Miwa, S., Carroll, B., & von Zglinicki, T. (2017). Mitochondria in Cell Senescence: Is Mitophagy the Weakest Link? *EBioMedicine*, 7–13.
- Kronic, D., Moshir, S., Greulich-Bode, K., Figueroa, R., Cerezo, A., Stammer, H., . . . Boukamp, P. (2009). Tissue context-activated telomerase in human epidermis correlates with little age-dependent telomere loss. *Biochimica et biophysica acta*, 297–308.
- Kueper, T., Grune, T., Prahl, S., Lenz, H., Welge, V., Biernoth, T., . . . Blatt, T. (2007). Vimentin is the specific target in skin glycation. Structural prerequisites, functional consequences, and role in skin aging. *The Journal of biological chemistry*, 23427–23436.
- Kujoth, G., Hiona, A., Pugh, T., Someya, S., Panzer, K., Wohlgemuth, S., . . . Prolla, T. (2005). Mitochondrial DNA mutations, oxidative stress, and apoptosis in mammalian aging. *Science (New York, N.Y.)*.
- Kurz, D., Decary, S., Hong, Y., & Erusalimsky, J. (2000). Senescence-associated (beta)-galactosidase reflects an increase in lysosomal mass during replicative ageing of human endothelial cells. *Journal of cell science*, 3613–3622.
- Kurz, D., Decary, S., Hong, Y., & Erusalimsky, J. (2000). Senescence-associated (beta)-galactosidase reflects an increase in lysosomal mass during replicative ageing of human endothelial cells. *Journal of cell science*, 3613–3622.

- Laberge, R., Sun, Y., Orjalo, A., Patil, C., Freund, A., Zhou, L., . . . Campisi, J. (2016). mTOR regulates the pro-tumorigenic senescence-associated secretory phenotype by promoting IL1A translation. *Nature cell biology*, 1049-1061.
- Lämmermann, I., Terlecki-Zaniewicz, L., Weinmüllner, R., Schosserer, M., Dellago, H., de Matos Branco, A., . . . Grillari, J. (2018). Blocking negative effects of senescence in human skin fibroblasts with a plant extract. *NPJ aging and mechanisms of disease*, 4.
- Lamming, D., & Sabatini, D. (2013). A Central role for mTOR in lipid homeostasis. . *Cell metabolism*, 465–469.
- Langhans, S. (2018). Three-Dimensional in Vitro Cell Culture Models in Drug Discovery and Drug Repositioning. *Frontiers in pharmacology*, 6.
- Laplante, M., & Sabatini, D. (2008). mTOR signaling at a glance. *Journal of cell science*, 3589–3594.
- Laplante, M., & Sabatini, D. (2012). mTOR signaling in growth control and disease. *Cell*, 274–293.
- Laplante, M., & Sabatini, D. (2012). mTOR signaling in growth control and disease. . *Cell*, 274–293.
- Laplante, M., & Sabatini, D. (2013). Regulation of mTORC1 and its impact on gene expression at a glance. . *Journal of cell science*, 1713–1719.
- Largo, R., Alvarez-Soria, M., Díez-Ortego, I., Calvo, E., Sánchez-Pernaute, O., Egido, J., & Herrero-Beaumont, G. (2003). Glucosamine inhibits IL-1beta-induced NFkappaB activation in human osteoarthritic chondrocytes. *Osteoarthritis and cartilage*, 290–298.
- Lastowiecka-Moras, E., Bugajska, J., & Młynarczyk, B. (2014). Occupational exposure to natural UV radiation and premature skin ageing. *International journal of occupational safety and ergonomics : JOSE*, 20(4), 639–645.
- Lee, J., & Boo, Y. (2022). Combination of Glycinamide and Ascorbic Acid Synergistically Promotes Collagen Production and Wound Healing in Human Dermal Fibroblasts. *Biomedicines*, 10(5), 1029.
- Lee, Y., Choi, S., Roh, W., Lee, J., & Kim, T. (2021). Cellular Senescence and Inflammaging in the Skin Microenvironment. *International journal of molecular sciences*, 3849.
- Lewis, D., Travers, J., Machado, C., Somani, A., & Spandau, D. (2011). Reversing the aging stromal phenotype prevents carcinoma initiation. *Aging*, 407–416.
- Li, C., Tong, H., Yan, Q., Tang, S., Han, X., Xiao, W., & Tan, Z. (2016). L-Theanine Improves Immunity by Altering TH2/TH1 Cytokine Balance, Brain Neurotransmitters, and Expression of Phospholipase C in Rat Hearts. *Medical science monitor : international medical journal of experimental and clinical research*, 662-669.
- Li, W., Qin, L., Feng, R., Hu, G., Sun, H., & He, Y. (2019). Emerging senolytic agents derived from natural products. *Mechanisms of ageing and development*, 1-6.
- Li, Y., Li, S., & Lin, C. (2018). Effect of resveratrol and pterostilbene on aging and longevity. *BioFactors (Oxford, England)*, 44(1), 69–82.
- Liao, Y., Chen, S., Chou, S., Wang, P., Tsai, M., & Sun, C. (2013). Determination of chronological aging parameters in epidermal keratinocytes by in vivo harmonic generation microscopy. *Biomedical optics express*, 4(1), 77–88.

- Liao, Y., Chen, S., Chou, S., Wang, P., Tsai, M., & Sun, C. (2013). Determination of chronological aging parameters in epidermal keratinocytes by in vivo harmonic generation microscopy. *Biomedical optics express*, 77–88.
- Liu, J., Sun, Y., Zhang, H., Ji, D., Wu, F., Tian, H., . . . Zhang, G. (2016). Theanine from tea and its semi-synthetic derivative TBrC suppress human cervical cancer growth and migration by inhibiting EGFR/Met-Akt/NF- $\kappa$ B signaling. *European journal of pharmacology*, 297–307.
- Liu, Y., Janssens, G., McIntyre, R., Molenaars, M., Kamble, R., Gao, A., . . . Houtkooper, R. (2019). Glycine promotes longevity in *Caenorhabditis elegans* in a methionine cycle-dependent fashion. *PLoS genetics*, e1007633.
- Lo, H., Lim, Y., Xiong, Z., Martel, N., Ferguson, C., Ariotti, N., . . . Parton, R. (2021). Cavin4 interacts with Bin1 to promote T-tubule formation and stability in developing skeletal muscle. *The Journal of cell biology*, e201905065.
- Locasale, J. (2013). Serine, glycine and one-carbon units: cancer metabolism in full circle. *Nature reviews. Cancer*, 13(8), 572–583.
- Loewith, R., Jacinto, E., Wullschleger, S., Lorberg, A., Crespo, J., Bonenfant, D., . . . Hall, M. (2002). Two TOR complexes, only one of which is rapamycin sensitive, have distinct roles in cell growth control. *Molecular cell*, 457-68.
- Long, X., Ortiz-Vega, S., Lin, Y., & Avruch, J. (2005). Rheb binding to mammalian target of rapamycin (mTOR) is regulated by amino acid sufficiency. *The Journal of biological chemistry*, 23433–23436.
- López-Otín, C., Blasco, M., Partridge, L., Serrano, M., & Kroemer, G. (2013). The hallmarks of aging. *Cell*, 1194–1217.
- Lovell, C., Smolenski, K., Duance, V., Light, N., Young, S., & Dyson, M. (1987). Type I and III collagen content and fibre distribution in normal human skin during ageing. *British Journal of Dermatology*, 419-428.
- Low, E., Smith, L., Costello, L., Przyborski, S., von Zglinicki, T., & Miwa, S. (2021). How good is the evidence that cellular senescence causes skin ageing? *Ageing research reviews*, 71:101456.
- Ma, X., & Blenis, J. (2009). Molecular mechanisms of mTOR-mediated translational control. *Nature reviews*, 307–318.
- Maibach, H., & Waller, J. (2005). Age and skin structure and function, a quantitative approach (I): blood flow, pH, thickness, and ultrasound echogenicity. *Skin Res Technol*, 221-35.
- Makrantonaki, E., & Zouboulis, C. (2007). Molecular Mechanisms of Skin Aging: State of the Art. *Annals of the New York Academy of Sciences*, 40-50.
- Maltman, D., & Przyborski, S. (2010). Developments in three-dimensional cell culture technology aimed at improving the accuracy of in vitro analyses. *Biochemical Society transactions*, 38(4), 1072–1075.
- Martin, J., & Buckwalter, J. (2003). The role of chondrocyte senescence in the pathogenesis of osteoarthritis and in limiting cartilage repair. *The Journal of bone and joint surgery*, 106-110.
- Maurelli, R., Zambruno, G., Guerra, L., Abbruzzese, C., Dimri, G., Gellini, M., . . . Dellambra, E. (2006). Inactivation of p16INK4a (inhibitor of cyclin-dependent kinase 4A) immortalizes primary human keratinocytes by maintaining cells in the stem cell compartment. *FASEB journal* :



official publication of the Federation of American Societies for Experimental Biology, 20(9), 1516–1518.

- Mavrogonatou, E., Papadopoulou, A., Pratsinis, H., & Kletsas, D. (2023). Senescence-associated alterations in the extracellular matrix: deciphering their role in the regulation of cellular function. *American journal of physiology. Cell physiology*, C633–C647.
- McCart, E., Thangapazham, R., Lombardini, E., Mog, S., Panganiban, R., Dickson, K., . . . Day, R. (2017). Accelerated senescence in skin in a murine model of radiation-induced multi-organ injury. *Journal of radiation research*, 58(5), 636–646.
- McColl, G., Killilea, D., Hubbard, A., Vantipalli, M., Melov, S., & Lithgow, G. (2008). Pharmacogenetic analysis of lithium-induced delayed aging in *Caenorhabditis elegans*. *The Journal of biological chemistry*, 350-357.
- McCormack, D., & McFadden, D. (2012). Pterostilbene and cancer: current review. . *The Journal of surgical research*, e53–e61.
- McQuestion, M. (2011). Evidence-based skin care management in radiation therapy: clinical update. *Seminars in oncology nursing*, e1–e17.
- Menon, S., Dibble, C., Talbott, G., Hoxhaj, G., Valvezan, A., Takahashi, H., . . . Manning, B. (2014). Spatial control of the TSC complex integrates insulin and nutrient regulation of mTORC1 at the lysosome. *Cell*, 771–785.
- Merkel, F. (1875). Tastzellen und Tastkörperchen bei den Haustieren und beim Menschen. *Archiv für mikroskopische Anatomie*, 636–652.
- Miller, R., Harrison, D., Astle, C., Bogue, M., Brind, J., Fernandez, E., . . . Strong, R. (2019). Glycine supplementation extends lifespan of male and female mice. *Aging cell*, e12953.
- Mills, A., Zheng, B., Wang, X., Vogel, H., Roop, D., & Bradley, A. (1999). p63 is a p53 homologue required for limb and epidermal morphogenesis. *Nature*, 708–713.
- Mimeault, M., & Batra, S. (2010). Recent advances on skin-resident stem/progenitor cell functions in skin regeneration, aging and cancers and novel anti-aging and cancer therapies. *Journal of cellular and molecular medicine*, 116–134.
- Miyake, T., Shimada, M., Matsumoto, Y., & Okino, A. (2019). DNA Damage Response After Ionizing Radiation Exposure in Skin Keratinocytes Derived from Human-Induced Pluripotent Stem Cells. *International journal of radiation oncology, biology, physics*, 105(1), 193–205.
- Montagna, W., & Carlisle, K. (1979). Structural changes in aging human skin. *The Journal of investigative dermatology*, 47–53.
- Mora Huertas, A., Schmelzer, C., Hoehenwarter, W., Heyroth, F., & Heinz, A. (2016). Molecular-level insights into aging processes of skin elastin. *Biochimie*, 128–129:163–173.
- Moragas, A., Castells, C., & Sans, M. (1993). Mathematical morphologic analysis of aging-related epidermal changes. *Anal Quant Cytol Histol.*, 75–82.
- Nacarelli, T., Azar, A., & Sell, C. (2015). Aberrant mTOR activation in senescence and aging: A mitochondrial stress response? *Experimental gerontology*, 66–70.
- Nair, A., Gopi, S., & Jacob, J. (2021). Bioavailability, pharmacokinetic, pharmacodynamic, and clinical studies of natural products on their antiinflammatory activities. *Inflammation and Natural Products*, 321-358.

- Narita, M., Nunez, S., Heard, E., Narita, M., Lin, A. W., Hearn, S. A., . . . Lowe, S. W. (2003). Rb-mediated heterochromatin formation and silencing of E2F target genes during cellular senescence. *Cell*, 703–716.
- Natarajan, V., Ganju, P., Ramkumar, A., Grover, R., & Gokhale, R. (2014). Multifaceted pathways protect human skin from UV radiation. *Nat. Chem. Biol*, 542-551.
- Nekachalova, I. (1958). The effect of vitamin C on the absorption of glycine and chlorides by the intestine. *Bull Exp Biol Med* 45, 299–302.
- Nelson, G., Wordsworth, J., Wang, C., Jurk, D., Lawless, C., Martin-Ruiz, C., & von Zglinicki, T. (2012). A senescent cell bystander effect: senescence-induced senescence. *Aging cell*, 11(2), 345–349.
- Nishio, K., & Inoue, A. (2005). Senescence-associated alterations of cytoskeleton: extraordinary production of vimentin that anchors cytoplasmic p53 in senescent human fibroblasts. *Histochemistry and cell biology*, 263–273.
- Noureddine, H., Gary-Bobo, G., Alifano, M., Marcos, E., Saker, M., Vienney, N., . . . Adnot, S. (2011). Pulmonary artery smooth muscle cell senescence is a pathogenic mechanism for pulmonary hypertension in chronic lung disease. *Circulation research*, 543-553.
- Ogrodnik, M., Miwa, S., Tchkonja, T., Tiniakos, D., Wilson, C., Lahat, A., . . . Jurk, D. (2017). Cellular senescence drives age-dependent hepatic steatosis. *Nature communications*, 15691.
- Ogrodnik, M., Zhu, Y., Langhi, L., Tchkonja, T., Krüger, P., Fielder, E., . . . Jurk, D. (2019). Obesity-Induced Cellular Senescence Drives Anxiety and Impairs Neurogenesis. *Cell metabolism*, 1061–1077.e8.
- Oh, W., & Jacinto, E. (2011). mTOR complex 2 signaling and functions. *Cell cycle (Georgetown, Tex.)*, 2305–2316.
- Owens, S., Wagner, P., & Vangsness, C. T. (2004). Recent advances in glucosamine and chondroitin supplementation. *The journal of knee surgery*, 185–193.
- P A Kruk, N. J., Kruk, P., Rampino, N., & Bohr, V. (1995). DNA damage and repair in telomeres: relation to aging. *Proceedings of the National Academy of Sciences of the United States of America*, 258–262.
- Pagano, M., Dürst, M., Joswig, S., Draetta, G., & Jansen-Dürr, P. (1992). Binding of the human E2F transcription factor to the retinoblastoma protein but not to cyclin A is abolished in HPV-16-immortalized cells. *Oncogene*, 1681-6.
- Papakonstantinou, E., Roth, M., & Karakiulakis, G. (2012). Hyaluronic acid: A key molecule in skin aging. *Dermato-endocrinology. United States*, 253–258.
- Passos, J., & von Zglinicki, T. (2007). Methods for cell sorting of young and senescent cells. *Methods in molecular biology (Clifton, N.J.)*, 33-44.
- Passos, J., Nelson, G., Wang, C., Richter, T., Simillion, C., Proctor, C., . . . von Zglinicki, T. (2010). Feedback between p21 and reactive oxygen production is necessary for cell senescence. *Molecular systems biology*, 347.
- Passos, J., Saretzki, G., Ahmed, S., Nelson, G., Richter, T., Peters, H., . . . von Zglinicki, T. (2007). Mitochondrial dysfunction accounts for the stochastic heterogeneity in telomere-dependent senescence. *PLoS biology*.

- Piperno, M., Reboul, P., Hellio Le Graverand, M., Peschard, M., Anefeld, M., Richard, M., & Vignon, E. (2000). Glucosamine sulfate modulates dysregulated activities of human osteoarthritic chondrocytes in vitro. *Osteoarthritis and cartilage*, 207–212.
- Quan, T., & Fisher, G. (2015). Role of Age-Associated Alterations of the Dermal Extracellular Matrix Microenvironment in Human Skin Aging: A Mini-Review. *Gerontology*, 427-434.
- Rabanal-Ruiz, Y., & Korolchuk, V. (2018). mTORC1 and Nutrient Homeostasis: The Central Role of the Lysosome. *International journal of molecular sciences*, 818.
- Reed, M., Corsa, A., Kudravi, S., McCormick, R., & Arthur, W. (2000). A deficit in collagenase activity contributes to impaired migration of aged microvascular endothelial cells. *Journal of cellular biochemistry*, 116-126.
- Reginster, J., Deroisy, R., Rovati, L., Lee, R., Lejeune, E., Bruyere, O., . . . Gossett, C. (2001). Long-term effects of glucosamine sulphate on osteoarthritis progression: a randomised, placebo-controlled clinical trial. *Lancet (London, England)*, 251–256.
- Ressler, S., Bartkova, J., Niederegger, H., Bartek, J., Scharffetter-Kochanek, K., Jansen-Dürr, P., & Wlaschek, M. (2006). p16INK4A is a robust in vivo biomarker of cellular aging in human skin. *Aging cell*, 379–389.
- Ricoult, S., & Manning, B. (2013). The multifaceted role of mTORC1 in the control of lipid metabolism. *EMBO reports*, 242–251.
- Ritschka, B., Storer, M., Mas, A., Heinzmann, F., Ortells, M., Morton, J., . . . Keyes, W. (2017). The senescence-associated secretory phenotype induces cellular plasticity and tissue regeneration. *Genes & development*, 31(2), 172–183.
- Rittié, L., & Fisher, G. (2002). UV-light-induced signal cascades and skin aging. *Ageing research reviews*, 705–720.
- Rizza, S., Cardaci, S., Montagna, C., Di Giacomo, G., De Zio, D., Bordi, M., . . . Filomeni, G. (2018). S-nitrosylation drives cell senescence and aging in mammals by controlling mitochondrial dynamics and mitophagy. *Proceedings of the National Academy of Sciences of the United States of America*, E3388–E3397.
- Robbins, P., Jurk, D., Khosla, S., Kirkland, J., LeBrasseur, N., Miller, J., . . . Niedernhofer, L. (2021). Senolytic Drugs: Reducing Senescent Cell Viability to Extend Health Span. *Annual review of pharmacology and toxicology*, 779–803.
- Robitaille, A., Christen, S., Shimobayashi, M., Cornu, M., Fava, L., Moes, S., . . . Hall, M. (2013). Quantitative phosphoproteomics reveal mTORC1 activates de novo pyrimidine synthesis. *Science (New York, N.Y.)*, 1320–1323.
- Roger, M., Fullard, N., Costello, L., Bradbury, S., Markiewicz, E., O'Reilly, S., . . . Przyborski, S. (2019). Bioengineering the microanatomy of human skin. *Journal of anatomy*, 234(4), 438–455.
- Rorteau, J., Chevalier, F., Fromy, B., & Lamartine, J. (2020). Functional integrity of aging skin, from cutaneous biology to anti-aging strategies. *Med Sci*, 1155-1162.
- Rübe, C., Bäumer, C., Schuler, N., Isermann, A., Schmal, Z., Glanemann, M., . . . Scherthan, H. (2021). Human skin aging is associated with increased expression of the histone variant H2A.J in the epidermis. *NPJ aging and mechanisms of disease*, 7.

- Rübe, C., Bäumer, C., Schuler, N., Isermann, A., Schmal, Z., Glanemann, M., . . . Scherthan, H. (2021). Human skin aging is associated with increased expression of the histone variant H2A.J in the epidermis. *NPJ aging and mechanisms of disease*, 7.
- Ruiz-Torres, A., Lozano, R., Melón, J., & Carraro, R. (2003). Age-dependent decline of in vitro migration (basal and stimulated by IGF-1 or insulin) of human vascular smooth muscle cells. *The journals of gerontology*, B1074–B1077.
- Saeed, M., Khan, M., Kamboh, A., Alagawany, M., Khafaga, A., Noreldin, A., . . . Chao, S. (2020). L-theanine: an astounding sui generis amino acid in poultry nutrition. *Poultry science*, 5625–5636.
- Salama, R., Sadaie, M., Hoare, M., & Narita, M. (2014). Cellular senescence and its effector programs. *Genes & development*, 99–114.
- Saleh, T., Tyutyunyk-Massey, L., & Gewirtz, D. (2019). Tumor Cell Escape from Therapy-Induced Senescence as a Model of Disease Recurrence after Dormancy. *Cancer research*, 79(6), 1044–1046.
- Salvo, N., Barnes, E., van Draanen, J., Stacey, E., Mitera, G., Breen, D., . . . De Angelis, C. (2010). Prophylaxis and management of acute radiation-induced skin reactions: a systematic review of the literature. *Current oncology*, 94–112.
- Sancak, Y., Bar-Peled, L., Zoncu, R., Markhard, A., Nada, S., & Sabatini, D. (2010). Ragulator-Rag complex targets mTORC1 to the lysosomal surface and is necessary for its activation by amino acids. *Cell*, 290-303.
- Sandby-Møller, J., Poulsen, T., & Wulf, H. (2003). Epidermal thickness at different body sites: relationship to age, gender, pigmentation, blood content, skin type and smoking habits. *Acta dermato-venereologica*, 410–413.
- Sandeman, S., Allen, M., Liu, C., Faragher, R., & Lloyd, A. (2000). Human keratocyte migration into collagen gels declines with in vitro ageing. *Mechanisms of ageing and development*, 149–157.
- Sarbassov, D., Ali, S., Kim, D., Guertin, D., Latek, R., Erdjument-Bromage, H., . . . Sabatini, D. (2004). Rictor, a novel binding partner of mTOR, defines a rapamycin-insensitive and raptor-independent pathway that regulates the cytoskeleton. *Current biology*, 1296–1302.
- Sasaki, M., Kajiya, H., Ozeki, S., Okabe, K., & Ikebe, T. (2014). Reactive oxygen species promotes cellular senescence in normal human epidermal keratinocytes through epigenetic regulation of p16(INK4a). *Biochemical and biophysical research communications*, 452(3), 622–628.
- Sauermann, K., Clemann, S., Jaspers, S., Gambichler, T., Altmeyer, P., Hoffmann, K., & Ennen, J. (2002). Age related changes of human skin investigated with histometric measurements by confocal laser scanning microscopy in vivo. *Skin research and technology : official journal of International Society for Bioengineering and the Skin (ISBS) [and] International Society for Digital Imaging of Skin (ISDIS) [and] International Society for Skin Imaging (ISSI)*, 52–56.
- Schneider, E., & Mitsui, Y. (1976). The relationship between in vitro cellular aging and in vivo human age. *Proceedings of the National Academy of Sciences of the United States of America*, 3584–3588.
- Schrauzer, G. (2002). Lithium: occurrence, dietary intakes, nutritional essentiality. *Journal of the American College of Nutrition*, 14-21.
- Scientific evidence behind Novos' best-in-class longevity formulas*. (2022).

- Scott, T., Christian, P., Kesler, M., Donohue, K., Shelton, B., Wakamatsu, K., . . . D'Orazio, J. (2012). Pigment-independent cAMP-mediated epidermal thickening protects against cutaneous UV injury by keratinocyte proliferation. *Experimental dermatology*, 771–777.
- Severino, J., Allen, R., Balin, S., Balin, A., & Cristofalo, V. (2000). Is beta-galactosidase staining a marker of senescence in vitro and in vivo? *Experimental cell research*, 162–171.
- Sharma, E., Joshi, R., & Gulati, A. (2018). L-Theanine: An astounding sui generis integrant in tea. *Food chemistry*, 242, 601–610.
- Sharpless, N., & Sherr, C. (2015). Forging a signature of in vivo senescence. *Nature reviews. Cancer*, 15(7), 397–408.
- Shuster, S., Black, M. M., & McVitie, E. (1975). The influence of age and sex on skin thickness, skin collagen and density. *The British journal of dermatology*, 639–643.
- Si, Z., Sun, L., & Wang, X. (2021). Evidence and perspectives of cell senescence in neurodegenerative diseases. *Biomedicine & pharmacotherapy = Biomedecine & pharmacotherapie*, 111327.
- Soini, Y., Kamel, D., Pääkkö, P., Lehto, V., Oikarinen, A., & Vähäkangas, K. (1994). Aberrant accumulation of p53 associates with Ki67 and mitotic count in benign skin lesions. *The British journal of dermatology*, 514–520.
- Streilein, J., & Bergstresser, P. (1984). 'Langerhans Cells: Antigen Presenting Cells of the Epidermis. *Immunobiology*, 285–300.
- Sun, M., Liao, J., Jing, Z., Gao, H., Shen, B., Xu, Y., & Fang, W. (2022). Effects of polyol excipient stability during storage and use on the quality of biopharmaceutical formulations. *Journal of pharmaceutical analysis*, 774–782.
- Takahara, M., Kang, K., Liu, L., Yoshida, Y., McCormick, T., & Cooper, K. (2003). iC3b arrests monocytic cell differentiation into CD1c-expressing dendritic cell precursors: a mechanism for transiently decreased dendritic cells in vivo after human skin injury by ultraviolet B. *The Journal of investigative dermatology*, 802–809.
- Takeshima, M., Miyazaki, I., Murakami, S., Kita, T., & Asanuma, M. (2016). L-Theanine protects against excess dopamine-induced neurotoxicity in the presence of astrocytes. *Journal of clinical biochemistry and nutrition*, 93–99.
- Teng, W., Huang, P., Wang, H., Tseng, C., & Yen, F. (2021). Pterostilbene Attenuates Particulate Matter-Induced Oxidative Stress, Inflammation and Aging in Keratinocytes. *Antioxidants (Basel, Switzerland)*, 1552.
- Terlecki-Zaniewicz, L., Pils, V., Bobbili, M., Lämmermann, I., Perrotta, I., Grillenberger, T., . . . Grillari, J. (2019). Extracellular Vesicles in Human Skin: Cross-Talk from Senescent Fibroblasts to Keratinocytes by miRNAs. *The Journal of investigative dermatology*, 2425–2436.e5.
- Tinaburri, L., D'Errico, M., Sileno, S., Maurelli, R., Degan, P., Magenta, A., & Dellambra, E. (2018). miR-200a Modulates the Expression of the DNA Repair Protein OGG1 Playing a Role in Aging of Primary Human Keratinocytes. *Oxidative medicine and cellular longevity*, 9147326.
- Toutfaire, M., Bauwens, E., & Debacq-Chainiaux, F. (2017). The impact of cellular senescence in skin ageing: A notion of mosaic and therapeutic strategies. *Biochemical pharmacology*, 1-12.

- Trifunovic, A., Wredenberg, A., Falkenberg, M., Spelbrink, J., Rovio, A., Bruder, C., . . . Larsson, N. (2004). Premature ageing in mice expressing defective mitochondrial DNA polymerase. *Nature*, 417–423.
- Truong, A., Kretz, M., Ridky, T., Kimmel, R., & Khavari, P. (2006). p63 regulates proliferation and differentiation of developmentally mature keratinocytes. *Genes & development*, 3185–3197.
- Tsai, C., Wang, M., Chang, K., Soung, H., Yang, C., & Tseng, H. (2019). Possible nitric oxide mechanism involved in the protective effect of L-theanine on haloperidol-induced orofacial dyskinesia. *The Chinese journal of physiology*, 17–26.
- Uetaki, M., Tabata, S., Nakasuka, F., Soga, T., & Tomita, M. (2015). Metabolomic alterations in human cancer cells by vitamin C-induced oxidative stress. *Scientific reports*, 13896.
- Valentijn, F., Falke, L., Nguyen, T., & Goldschmeding, R. (2018). Cellular senescence in the aging and diseased kidney. *Journal of cell communication and signaling*, 69–82.
- Varani, J., Warner, R. L., Gharaee-Kermani, M., Phan, S. H., Kang, S., Chung, J., . . . Voorhees, J. J. (2000). Vitamin A Antagonizes Decreased Cell Growth and Elevated Collagen-Degrading Matrix Metalloproteinases and Stimulates Collagen Accumulation in Naturally Aged Human Skin. *Journal of Investigative Dermatology*, 480-486.
- Varani, J., Warner, R., Gharaee-Kermani, M., Phan, S., Kang, S., Chung, J., . . . Voorhees, J. (2000). Vitamin A antagonizes decreased cell growth and elevated collagen-degrading matrix metalloproteinases and stimulates collagen accumulation in naturally aged human skin. *The Journal of investigative dermatology*, 480–486.
- Velarde, M., & Demaria, M. (2016). Targeting Senescent Cells: Possible Implications for Delaying Skin Aging: A Mini-Review. *Gerontology*, 513–518.
- Verdier-Sévrain, S., & Bonté, F. (2007). Skin hydration: a review on its molecular mechanisms. *Journal of cosmetic dermatology*, 75–82.
- Veysey, E., & Finlay, A. (2010). Aging and the Skin. *Brocklehurst's Textbook of Geriatric Medicine and Gerontology (7th Edition)*, 133–137.
- Vitorelli, S., Lagnado, A., Halim, J., Moore, W., Talbot, D., Barrett, K., . . . Passos, J. (2019). Senescent human melanocytes drive skin ageing via paracrine telomere dysfunction. *The EMBO journal*, e101982.
- Vidal, S., Tamamoto, K., Nguyen, H., Abbott, R., Cairns, D., & Kaplan, D. (2019). 3D biomaterial matrix to support long term, full thickness, immuno-competent human skin equivalents with nervous system components. *Biomaterials*, 198, 194–203.
- Viel, T., Chinta, S., Rane, A., Chamoli, M., Buck, H., & Andersen, J. (2020). Microdose lithium reduces cellular senescence in human astrocytes - a potential pharmacotherapy for COVID-19? *Aging*, 12(11), 10035–10040.
- von Zglinicki, T. (2000). Role of oxidative stress in telomere length regulation and replicative senescence. *Annals of the New York Academy of Sciences*, 99-110.
- von Zglinicki, T., Wan, T., & Miwa, S. (2021). Senescence in Post-Mitotic Cells: A Driver of Aging? *Antioxidants & redox signaling*, 308–323.
- Waaiker, M., Gunn, D., Adams, P., Pawlikowski, J., Griffiths, C., van Heemst, D., . . . Maier, A. (2016). P16INK4a Positive Cells in Human Skin Are Indicative of Local Elastic Fiber Morphology, Facial

- Wrinkling, and Perceived Age. *The journals of gerontology. Series A, Biological sciences and medical sciences*, 1022–1028.
- Waaijer, M., Parish, W., Strongitharm, B., van Heemst, D., Slagboom, P., de Craen, A., . . . Maier, A. (2012). The number of p16INK4a positive cells in human skin reflects biological age. *Aging cell*, 722–725.
- Wakame, K., Komatsu, K., Nakata, A., Sato, K., Takaguri, A., Masutomi, H., . . . Uchiyama, H. (2017). Transcriptome Analysis of Skin from SMP30/GNL Knockout Mice Reveals the Effect of Ascorbic Acid Deficiency on Skin and Hair. *In vivo (Athens, Greece)*, 31(4), 599–607.
- Wallis, R., Milligan, D., Hughes, B., Mizen, H., López-Domínguez, J., Eduputa, U., . . . Bishop, C. (2022). Senescence-associated morphological profiles (SAMPs): an image-based phenotypic profiling method for evaluating the inter and intra model heterogeneity of senescence. *Aging*, 4220–4246.
- Wang, A., & Dreesen, O. (2018). Biomarkers of Cellular Senescence and Skin Aging. *Frontiers in genetics*, 247.
- Wang, A., Ong, P., Chojnowski, A., Clavel, C., & Dreesen, O. (2017). Loss of lamin B1 is a biomarker to quantify cellular senescence in photoaged skin. *Scientific reports*, 15678.
- Wang, C., Jurk, D., Maddick, M., Nelson, G., Martin-Ruiz, C., & von Zglinicki, T. (2009). DNA damage response and cellular senescence in tissues of aging mice. *Aging cell*, 311–323.
- Wang, D., Gao, Q., Zhao, G., Kan, Z., Wang, X., Wang, H., . . . Ho, C. (2018). Protective Effect and Mechanism of Theanine on Lipopolysaccharide-Induced Inflammation and Acute Liver Injury in Mice. *Journal of agricultural and food chemistry*, 7674-7683.
- Wang, E. (1995). Senescent human fibroblasts resist programmed cell death, and failure to suppress bcl2 is involved. *Cancer research*, 2284-92.
- Wang, S., Livingston, M., Su, Y., & Dong, Z. (2015). Reciprocal regulation of cilia and autophagy via the MTOR and proteasome pathways. *Autophagy*, 607–616.
- Weilner, S., Schraml, E., Wieser, M., Messner, P., Schneider, K., Wassermann, K., . . . Grillari, J. (2016). Secreted microvesicular miR-31 inhibits osteogenic differentiation of mesenchymal stem cells. *Aging cell*, 744–754.
- Weinmüller, R., Zbiral, B., Becirovic, A., Stelzer, E., Nagelreiter, F., Schosserer, M., . . . Grillari, J. (2020). Organotypic human skin culture models constructed with senescent fibroblasts show hallmarks of skin aging. *NPJ aging and mechanisms of disease*.
- Wiley, C., Velarde, M., Lecot, P., Liu, S., Sarnoski, E., Freund, A., . . . Campisi, J. (2016). Mitochondrial Dysfunction Induces Senescence with a Distinct Secretory Phenotype. *Cell metabolism*, 303-14.
- Wlaschek, M., Maity, P., Makrantonaki, E., & Scharffetter-Kochanek, K. (2021). Connective Tissue and Fibroblast Senescence in Skin Aging. *The Journal of investigative dermatology*, 985–992.
- Wlaschek, M., Tantcheva-Poór, I., Naderi, L., Ma, W., Schneider, L. A., Razi-Wolf, Z., . . . Scharffetter-Kochanek, K. (2001). Solar UV irradiation and dermal photoaging. *Journal of photochemistry and photobiology. B, Biology*, 41–51.

- Wolf, J., Weinberger, B., Arnold, C., Maier, A., Westendorp, R., & Grubeck-Loebenstien, B. (2012). The effect of chronological age on the inflammatory response of human fibroblasts. *Experimental gerontology*, 749–753.
- Wu, P., Lyu, J., Liu, Y., Chien, T., Hsu, H., Wen, K., & Chiang, H. (2017). Fisetin Regulates Nrf2 Expression and the Inflammation-Related Signaling Pathway to Prevent UVB-Induced Skin Damage in Hairless Mice. *International journal of molecular sciences*.
- Wullschleger, S., Loewith, R., & Hall, M. (2006). TOR signaling in growth and metabolism. *Cell*, 471–84.
- Xia, W., Hammerberg, C., Li, Y., He, T., Quan, T., Voorhees, J., & Fisher, G. (2013). Expression of catalytically active matrix metalloproteinase-1 in dermal fibroblasts induces collagen fragmentation and functional alterations that resemble aged human skin. *Aging cell*, 661–671.
- Xiao, T., Chen, Y., Song, C., Xu, S., Lin, S., Li, M., . . . Gu, H. (2021). Possible treatment for UVB-induced skin injury: Anti-inflammatory and cytoprotective role of metformin in UVB-irradiated keratinocytes. *Journal of dermatological science*, 25–35.
- Xu, M., Bradley, E., Weivoda, M., Hwang, S., Pirtskhalava, T., Decklever, T., . . . Kirkland, J. (2017). Transplanted Senescent Cells Induce an Osteoarthritis-Like Condition in Mice. *The journals of gerontology. Series A, Biological sciences and medical sciences*, 780–785.
- Xu, M., Pirtskhalava, T., Farr, J., Weigand, B., Palmer, A., Weivoda, M., . . . Kirkland, J. (2018). Senolytics improve physical function and increase lifespan in old age. *Nature medicine*, 1246–1256.
- Yamada, S., & Maruyama, I. (2007). HMGB1, a novel inflammatory cytokine. *Clinica chimica acta; international journal of clinical chemistry*, 36–42.
- Yang, M., Teng, S., Ma, C., Yu, Y., Wang, P., & Yi, C. (2018). Ascorbic acid inhibits senescence in mesenchymal stem cells through ROS and AKT/mTOR signaling. *Cytotechnology*, 70(5), 1301–1313.
- Yang, X., Ren, H., Guo, X., Hu, C., & Fu, J. (2020). Radiation-induced skin injury: pathogenesis, treatment, and management. *Aging*, 12(22), 23379–23393.
- Yasui, T., Yonetsu, M., Tanaka, R., Fukushima, S., Yamashita, T., Ogura, Y., . . . Araki, T. (2012). In vivo observation of age-related structural changes of dermal collagen in human facial skin using collagen-sensitive second harmonic generation microscope equipped with 1250-nm mode-locked. *Journal of Biomedical Optics*.
- Yosef, R., Pilpel, N., Tokarsky-Amiel, R., Biran, A., Ovadya, Y., Cohen, S., . . . Krizhanovsky, V. (2016). Directed elimination of senescent cells by inhibition of BCL-W and BCL-XL. *Nature communications*, 11190.
- Yoshida, Y., Kang, K., Berger, M., Chen, G., Gilliam, A., Moser, A., . . . Cooper, K. (1998). Monocyte induction of IL-10 and down-regulation of IL-12 by iC3b deposited in ultraviolet-exposed human skin. *Journal of immunology*, 5873–5879.
- Yousefzadeh, M., Zhu, Y., McGowan, S., Angelini, L., Fuhrmann-Stroissnigg, H., Xu, M., . . . Niedernhofer, L. (2018). Fisetin is a senotherapeutic that extends health and lifespan. *EBioMedicine*, 36, 18–2.
- Zarse, K., Terao, T., Tian, J., Iwata, N., Ishii, N., & Ristow, M. (2011). Low-dose lithium uptake promotes longevity in humans and metazoans. *European journal of nutrition*, 387–389.



- Zhu, Y., Doornebal, E., Pirtskhalava, T., Giorgadze, N., Wentworth, M., Fuhrmann-Stroissnigg, H., . . . Kirkland, J. (2017). New agents that target senescent cells: the flavone, fisetin, and the BCL-XL inhibitors, A1331852 and A1155463. *Aging*, 955–963.
- Zhu, Y., Tchkonina, T., Pirtskhalava, T., Gower, A., Ding, H., Giorgadze, N., . . . Kirkland, J. (2015). The Achilles' heel of senescent cells: from transcriptome to senolytic drugs. *Aging Cell*, 644-658.
- Zhuang, W., Yue, L., Dang, X., Chen, F., Gong, Y., Lin, X., & Luo, Y. (2019). Rosenroot (Rhodiola): Potential Applications in Aging-related Diseases. *Aging and disease*, 10(1), 134–146.
- Zoio, P., Ventura, S., Leite, M., & Oliva, A. (2021). Pigmented Full-Thickness Human Skin Model Based on a Fibroblast-Derived Matrix for Long-Term Studies. *Tissue engineering. Part C, Methods*, 27(7), 433–443.
- Zouboulis, C., & Makrantonaki, E. (2011). Clinical aspects and molecular diagnostics of skin aging. *Clinics in Dermatology*, 3-14.

## Appendices

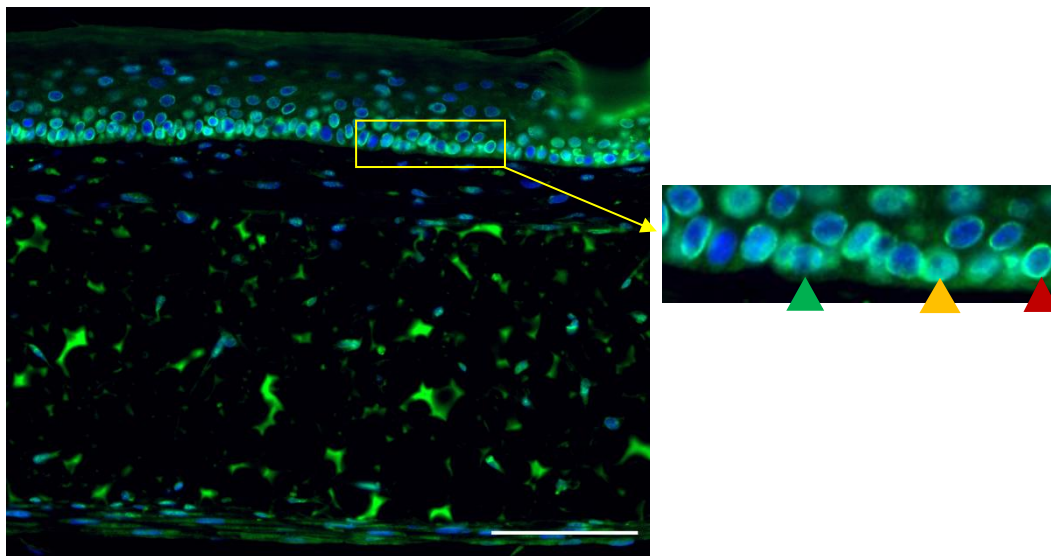
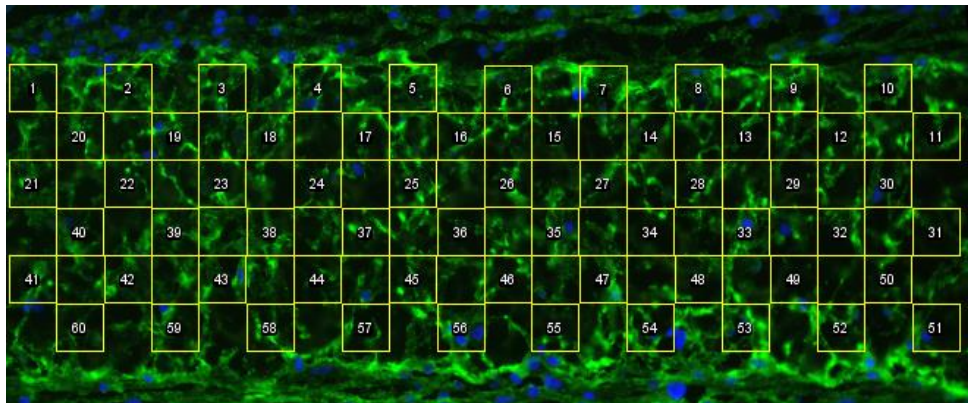


*Figure 1 Example of the variation in the staining patterns of LaminB1 of 3D full thickness skin equivalent*

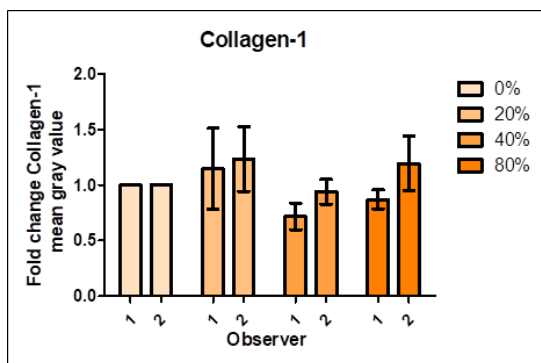
Figure above provides an example of the variation in the staining patterns of LaminB1 within a 3D full-thickness skin equivalent. LaminB1 staining exhibited diverse patterns, with some cells showing a complete staining ring of Lamin B1 (indicated by the red arrow), while others displayed a partial ring (indicated by the green arrow), and some exhibited staining across the nucleus (indicated by the yellow

arrow). Additionally, a stronger signal was observed in the epidermis compared to the dermis. Magnification bar: 100µm.

A



B



C

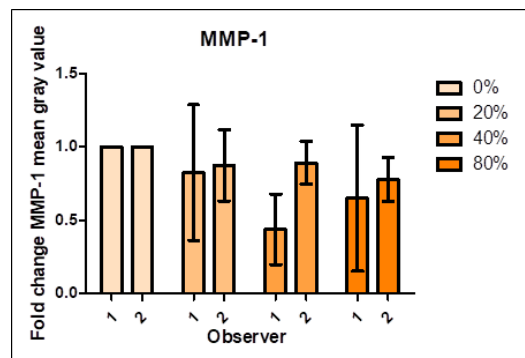


Figure II Example of MMP-1 and Collagen-1 measurement via IF staining

**A)** 3D skin samples were subjected to fluorescent staining with MMP-1 and Collagen-1 markers, represented in green fluorescence, and subsequently counterstained with nuclear DAPI, indicated in blue. Images were captured using a 20x objective on a DMI8 microscope. For quantitative analysis, an array of approximately 50x 1000  $\mu\text{m}^2$  square Regions of Interest (ROIs) was placed at one ROI apart and overlaid on the green channel. The mean grey value of each of these squares was measured and presented as fold change, allowing for the assessment of marker expression levels. **B and C)** Samples were stained and measured separately by two individuals, observer 1 (non-blinded) and 2 (blinded). All data were normalized to controls containing only non-senescent HDFs. 0% n=3, 20% n=3, 40% n=2, 80% n=3. **B)** Collagen-1, Observer p-value 0.099, senescent seeding density p-value 0.102. **C)** MMP-1, observer p-value 0.227, senescent seeding density p-value 0.271. p values were calculated by Two-way ANOVA.

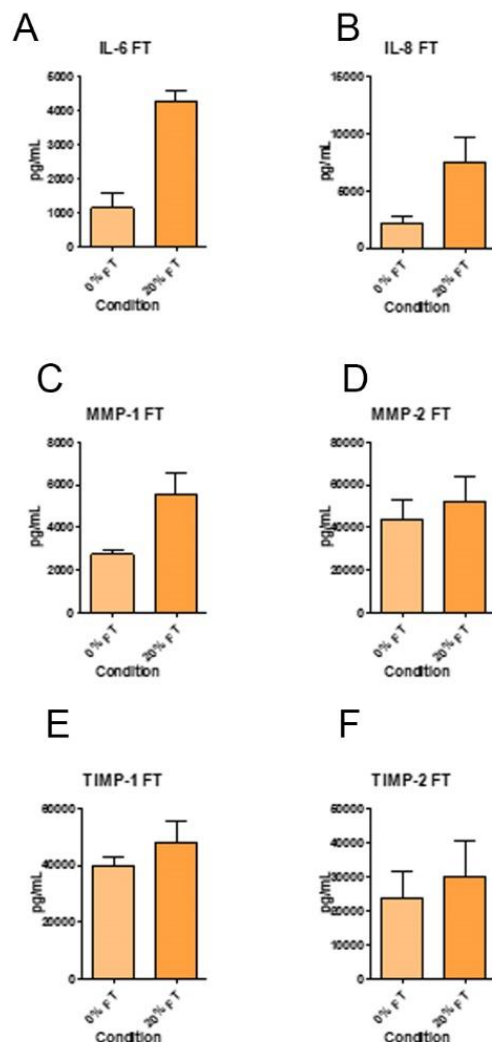


Figure III Concentrations of SASP components in the supernatant of 3D full thickness skin equivalents generated with no or 20% senescent HDF as measured by cytokine array.

A) IL-6, B) IL-8, C) MMP-1, D) MMP-2, E) TIMP-1, F) TIMP-2. Data are M±SEM, n=3 independent experiments. \*\*\* indicates p<0.001, \*\* indicates p<0.01, \* indicates p<0.05, ns indicates p>0.05

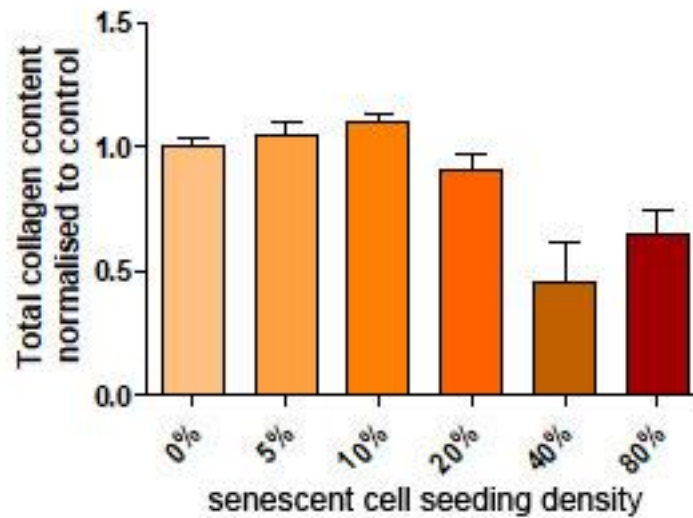


Figure IV Total collagen content in the dermal equivalent in 3D skin models measured using the QuickZyme Total Collagen assay.

Data are normalised to the control models. M±SEM, n ≥ 3 models per condition. \*\*\* indicates p<0.001, \*\* indicates p<0.01, One way ANOVA.

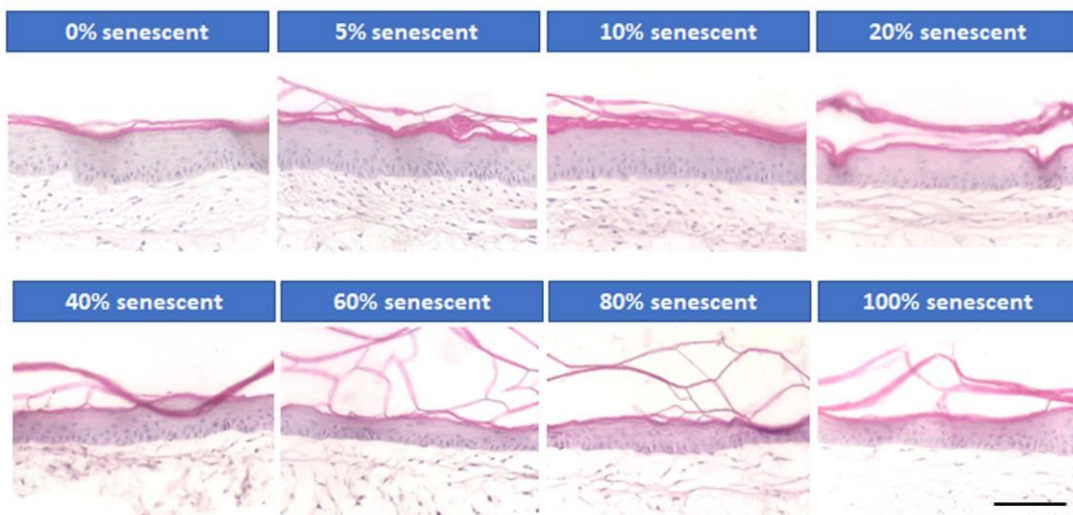
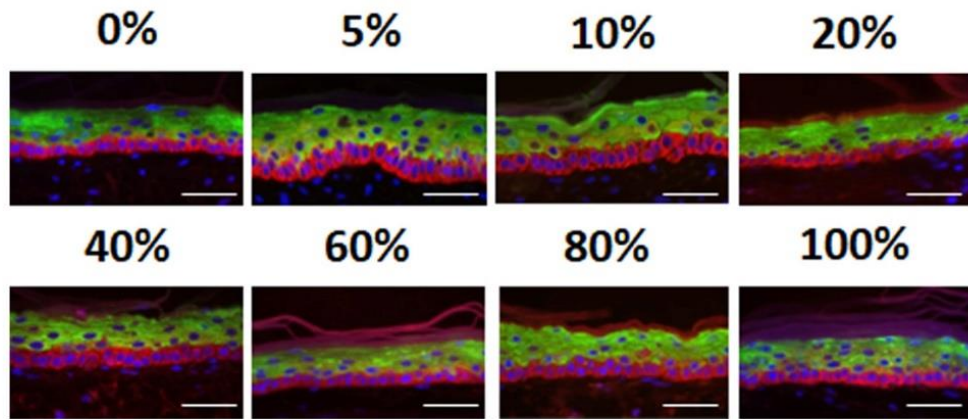


Figure V H/E images of full thickness 3D skin models

Senescent cell seeding densities are indicated on top of the micrographs. Magnification bar: 100 μm.



*Figure VI 1K10/K14 micrographs of full thickness 3D skin models.*

*Senescent cell seeding densities are indicated on top of the micrographs. Magnification bar: 50 mm.*